

SANDIA REPORT

SAND97-0796 • UC-721

Unlimited Release

Printed August 1997

A Summary of the Sources of Input Parameter Values for the Waste Isolation Pilot Plant Final Porosity Surface Calculations

B. M. Butcher

Prepared by
Sandia National Laboratories
Albuquerque, New Mexico 87185 and Livermore, California 94550

Sandia is a multiprogram laboratory operated by Sandia
Corporation, a Lockheed Martin Company, for the United States
Department of Energy under Contract DE-AC04-94AL85000.

Approved for public release; distribution is unlimited.



Sandia National Laboratories

Issued by Sandia National Laboratories, operated for the United States Department of Energy by Sandia Corporation.

NOTICE: This report was prepared as an account of work sponsored by an agency of the United States Government. Neither the United States Government nor any agency thereof, nor any of their employees, nor any of their contractors, subcontractors, or their employees, makes any warranty, express or implied, or assumes any legal liability or responsibility for the accuracy, completeness, or usefulness of any information, apparatus, product, or process disclosed, or represents that its use would not infringe privately owned rights. Reference herein to any specific commercial product, process, or service by trade name, trademark, manufacturer, or otherwise, does not necessarily constitute or imply its endorsement, recommendation, or favoring by the United States Government, any agency thereof or any of their contractors or subcontractors. The views and opinions expressed herein do not necessarily state or reflect those of the United States Government, any agency thereof or any of their contractors.

Printed in the United States of America. This report has been reproduced directly from the best available copy.

Available to DOE and DOE contractors from
Office of Scientific and Technical Information
PO Box 62
Oak Ridge, TN 37831

Prices available from (615) 576-8401, FTS 626-8401

Available to the public from
National Technical Information Service
US Department of Commerce
5285 Port Royal Rd
Springfield, VA 22161

NTIS price codes
Printed copy: A08
Microfiche copy: A01

SAND97-0796
Unlimited Release
Printed June 1997

Distribution
Category UC-721

A Summary of the Sources of Input Parameter Values for the Waste Isolation Pilot Plant Final Porosity Surface Calculations

B. M. Butcher

WIPP Disposal Room Systems Department
Nuclear Waste Management Center
Sandia National Laboratories
P.O. Box 5800
Albuquerque, NM 87185-1341

ABSTRACT

A summary of the input parameter values used in final predictions of closure and waste densification in the Waste Isolation Pilot Plant disposal room is presented, along with supporting references. These predictions are referred to as the final porosity surface data and will be used for WIPP performance calculations supporting the Compliance Certification Application to be submitted to the U.S. Environmental Protection Agency. The report includes tables that list all of the input parameter values, references citing their source, and in some cases references to more complete descriptions of considerations leading to the selection of values.

TABLE OF CONTENTS

1.0 INTRODUCTION	1
1.1 Background.....	1
2.0 DISPOSAL ROOM GEOMETRY	3
3.0 MATERIAL PROPERTIES	11
3.1 Halite	11
3.2 Anhydrite	11
3.3 Waste	11
3.4 Gas Generation.....	19
4.0 SUMMARY	21
5.0 REFERENCES	22
APPENDIX A: UNPUBLISHED REFERENCES.....	A-1
APPENDIX B: SUPPORTING JUSTIFICATION MEMORANDA.....	B-1
APPENDIX C: DOCUMENTATION OF CALCULATIONS	C-1
APPENDIX D: MESH COORDINATES AND CONNECTIVITY.....	D-1

LIST OF TABLES

Table 1: Final Porosity Surface Calculation Input Parameters: Dimensions	4
Table 2: Final Porosity Surface Calculation Input Parameters - Computational Configuration and Stratigraphy	5
Table 3: Final Porosity Surface Calculation Input Parameters - Halite Constitutive Parameters ...	12
Table 4: Final Porosity Surface Calculation Input Parameters - Anhydrite Properties	15
Table 5: Final Porosity Surface Calculation Input Parameters - Waste Composition Assumptions	16
Table 6: Final Porosity Surface Calculation Input Parameters: Waste Densities; Porosity	17
Table 7: Final Porosity Surface Calculation Input Parameters - Waste Mechanical Properties	18
Table 8: Pressure-Volumetric Strain Data Used in the Volumetric-Plasticity Model for the Waste Drums	18
Table 9: Final Porosity Surface Calculation Input Parameters - Gas Generation Assumptions	20

LIST OF FIGURES

1	Simplified stratigraphic model used for the disposal room analyses	7
2	Mesh discretization and boundary conditions used for the disposal room analyses	9

1.0 INTRODUCTION

This report provides information and supporting references on the input parameter values used in final predictions of closure and waste densification in the Waste Isolation Pilot Plant (WIPP) disposal room. These predictions are referred to as the final porosity surface data and will be used for WIPP performance calculations supporting the Compliance Certification Application (CCA) to be submitted to the Environmental Protection Agency. The planning document under which these data were acquired was Butcher (1995), and the WIPP primary source document for the parameter values used for the WIPP CCA was Butcher (1996).

The objective of the report is to establish traceability (the sources) of the parameter values. This is accomplished through a series of tables that list all of the input parameter values and related information used in calculating the final porosity surface results. A reference citing the source of each parameter value accompanies each entry, and in some cases a reference to a more complete description of considerations leading to their selection is provided. Many of these citations refer to a memorandum from D. Munson to M.S. Tierney defining the mechanical parameter values for the rock formation surrounding the disposal room, data which are also used for other rock mechanics thermal/structural calculations related to borehole closure and seal design. A copy of the memorandum is reproduced in Appendix A, along with other principal references not available in the published literature. Other less extensive documentation related to parameter selection is included in the memoranda reproduced in Appendix B; documentation of several calculations is reproduced in Appendix C, and the finite-element mesh coordinates and connectivity for the final porosity surface calculations are given in Appendix D.

The information presented in this report also supports two other documents. The first of these reports describes the evolution of the disposal room model to its present state of development (Butcher, 1997). The second describes the version of the disposal room conceptual model used to generate the final porosity surface data and how the calculations were performed (Stone, 1997a).

1.1 Background

The WIPP is a United States Department of Energy research and development facility designed to demonstrate the safe management, storage, and long-term disposal of contact-handled transuranic (CH-TRU) and remote-handled transuranic (RH-TRU) waste generated by defense activities of the United States. The repository is located in southeastern New Mexico in bedded salt deposits 655 m below the surface.

The ability of salt to deform with time, fill voids, and create an impermeable barrier around the waste was one of the principal reasons for locating the WIPP repository in a bedded salt formation. The "closure" process is a complex and interdependent series of events starting after a region within a repository is excavated and filled with waste (Butcher, 1997). Immediately upon excavation, the equilibrium state of the rock surrounding the repository is disturbed, and the rock begins to deform and return to equilibrium. Eventually, as mechanical equilibrium is reestablished,

subsidence ceases, and the waste and backfill have undergone as much compaction by the weight of the rock above the repository (overburden) as is possible. Prediction of the extent of closure for WIPP performance assessment is required because the amount determines the density of the waste at any given time, thus controlling flow of brine and gases through the waste and its capacity for storing fluids. Permeability and storage volume of the waste are dependent on the extent of closure, and in turn determine the extent of migration of radioactive and hazardous species. The conceptual model of these processes is collectively referred to as the disposal room model.

Closure calculations were made with the finite-element computer code SANTOS (Version 2.00 on the CRAY-J916/UNICOS 8.04 system configuration) (Stone, 1997b). These calculations compute the porosity of the waste and its surroundings as a function of time. Computation of repository closure has been a particularly challenging structural engineering problem because the rock surrounding the repository continually deforms with time. Not only is the deformation of the salt inelastic, but it also involves larger deformations than are customarily addressed with conventional structural deformation codes. In addition, the formation surrounding the repository is far from homogeneous in composition, containing various parting planes and interbeds with different properties than the salt.

Deformation of the waste is also nonlinear, with large strains, and its response is complicated by the presence of gas. These complex characteristics of the materials comprising the repository and its surroundings require the use of highly specialized constitutive models that have been built into the SANTOS code over a number of years (Stone, 1997a).

2.0 DISPOSAL ROOM GEOMETRY

The basic unit of the disposal room model encompasses an excavated room 3.96 m high by 10.06 m wide by 91.44 m in length, with an initial room free volume of 3644 m³ plus the surroundings. The current disposal assumption is that a maximum of 6804 drums of uniformly distributed unprocessed waste will be stored in the disposal room in 7-pack units. There are 972 of these units stacked three high on the disposal room floor. Unlike previous calculations, which included a crushed salt layer around the waste and in the space between the drums, the final porosity surface analysis considered a disposal room without backfill. The volume occupied by the waste and the drums was 1728 m³. Parameter values for the room geometry in the final porosity surface calculations are given in Table 1.

A two-dimensional plane strain model was used for the SANTOS analyses. The discretized model represents the room as one of an infinite number of rooms located at the repository horizon. Making use of symmetry, only half of the room needed to be modeled. The left and right boundaries are planes of symmetry. The basic half-symmetry disposal room dimensions are 3.96 m high by 5.03 m wide (Tables 1 and 2).

The idealized stratigraphy for the WIPP underground used in the geomechanical model is the stratigraphy defined by Munson (see memorandum in Appendix A). This stratigraphy is shown in Figure 3 of Stone (1997a). A difficulty with this abstraction is that it is more detailed than can conveniently be incorporated into the numerical analysis. To circumvent this problem, recent work by Osnes and Labreche (see memorandum in Appendix A) has examined the differences in room closure obtained by assuming different simplifying abstractions of the stratigraphy. Closure results assuming the full stratigraphic model of Munson, which consisted of 12 clay seams and 7 anhydrite layers, was compared with analysis results using smaller combinations of clay seams and marker beds. In preparing for the current analyses, Stone performed a set of calculations (see memorandum in Appendix A), that identified a simple stratigraphic model that captured most of the room closure and room porosity results seen in the more complex stratigraphic models. The stratigraphic model used in the current work (Table 2 and Figure 1) is composed mainly of argillaceous salt with a clean salt layer above the disposal room between Clay G and Clay I, anhydrite MB 139, and a thin layer located in the clean salt layer identified as anhydrite. Based on the study by Stone, no clay seams were included in the model.

The assumed storage volume configuration for the waste differs from past calculations because there is no backfill: the space between the drums is empty. Since modeling the extreme detail of the 7-pack packing and the space between drums for the entire room was beyond the capability of the numerical technique, an assumption about the waste configuration was required in order to have an accurate continuum representing the waste response. The space between the drums was eliminated by assuming that each waste drum deformed laterally from a cylindrical cross-section to a close-packed configuration with its neighbors during the early phases of closure. The justification for this assumption was that little force is required to laterally deform a drum. As the distance between the walls decreases, the drums are assumed to be pushed together

Table 1: Final Porosity Surface Calculation Input Parameters: Dimensions

Description	Value	Reference	Comments
Room Geometry			
Room Height	13 ft (3.96 m)	Sandia WIPP Project, (1992) p. 3-5	
Room Width	33 ft (10.06 m)	Sandia WIPP Project, (1992) p. 3-5	
Room Length	300 ft (91.44 m)	Sandia WIPP Project, (1992) p. 3-5	
Initial Room Volume	3644 m ³		Height x width x length (use feet and convert)
Number of Drums/Room	6804	Sandia WIPP Project, (1992) p. 3-11	
Number of 7-Packs/Room	972	Calculated from 6804 drums	
Drum External Volume	0.2539 m ³	Sandia WIPP Project, (1992) Table 3.1-2, p. 3-10	
Waste Volume	1728 m ³		(6804 drums) x (external drum volume)
Waste Height	2.676 m	Sandia WIPP Project, (1992) Fig. 3.1-3, p. 3-12	
Nominal Waste Width with Voids Between Drums	8.6 m	Stone, (1997a) Eq. 2, p. 9	Calculated from Sandia WIPP Project, 1992, Fig. 3.3-3, p. 3-12.
Nominal Waste Length with Voids Between Drums	89.1 m	Stone, (1997a) Eq. 2, p. 9	Calculated from Sandia WIPP Project, 1992, Fig. 3.3-3, p. 3-12.
Width of Waste Continuum	7.35 m	Stone, (1997a) Eq. 2, p. 9	
Height of Waste Continuum	2.676 m	Sandia WIPP Project, (1992) Fig. 3.1-3, p. 3-12	
Length of Waste Continuum	87.85 m	Stone, (1997a) Eq. 2, p. 9	

Table 2: Final Porosity Surface Calculation Input Parameters - Computational Configuration and Stratigraphy

Description	Value	Reference	Comments
Boundary Distances			
Pillar Thickness	100 ft (30.5 m)	Sandia WIPP Project (1992) p. 3-5	
Half Room Width	5.03 m		(Room Width)/2
Distance from the Center of the Room to the Center of the Pillar	20.27 m		(Room Width + Pillar Width)/2 computed in feet and then converted to meters.
Relative Elevation of Clay G, (Anhydrite B)	0 m	Munson (see memo in App. A) Fig. 2.5.1, p. 24/ 24	As of 2/15/96 this reference represents the latest representation of local stratigraphy for numerical calculations.
Relative Elevation Top Boundary	52.87 m	Munson (see memo in App. A) Fig. 2.5.1, p. 24/ 24	
Relative Elevation Bottom Boundary	-54.19 m	Munson (see memo in App. A) Fig. 2.5.1, p. 24/ 24	
Disposal Room Floor	-6.39 m	Justification for this value is provided in a memorandum from C. M. Stone, March 4, 1996 (see App. B).	
Disposal Room Ceiling	-2.43 m	Justification for this value is provided in a memorandum from C. M. Stone, March 4, 1996 (see App. B).	
Local Rock Stratigraphy			
Argillaceous Salt	-54.19 m to -8.63 m	Taken from Munson (see memo in App. A) Fig. 2.5.1, p. 24/ 24. See Stone (see memo in App. A), Fig. 1, p. 3.	Figure 1
Anhydrite MB 139 Lower Boundary	-8.63 m	Munson (see memo in App. A) Fig. 2.5.1, p. 24/ 24	
Anhydrite MB 139 Interbed	-8.63 m to -7.77 m	Munson (see memo in App. A) Fig. 2.5.1, p. 24/ 24	

Table 2 (continued) Final Porosity Surface Calculation Input Parameters - Computational Configuration and Stratigraphy

Description	Value	Reference	Comments
Local Rock Stratigraphy - (continued)			Figure 1
Anhydrite MB 139 Upper Boundary	-7.77 m	Munson (see memo in App. A) Fig. 2.5.1, p. 24/ 24	
Argillaceous Salt	-7.77 m to 0.00 m	Taken from Munson (see memo in App. A) Fig. 2.5.1, p. 24/ 24. See Stone (App. A) Fig. 1, p. 3.	
Clay G (anhydrite “b”)	0.00 m	Munson, (see memo in App. A) Fig. 2.5.1, page 24/ 24	
Clean Salt	0.0 m to 4.27 m	Taken from Munson (see memo in App. A) Fig. 2.5.1, p. 24/ 24. See Stone (App. A), Fig. 1, p. 3.	
Clay I (Upper Boundary of Clean Salt)	4.27 m	Munson (see memo in App. A) Fig. 2.5.1, p. 24/ 24	
Argillaceous Salt	4.27 m to 52.87 m	Taken from Munson (see memo in App. A) Fig. 2.5.1, p. 24/ 24. See Stone (App. A), Fig. 1, p. 3.	
Traction on Upper Mesh Boundary	13.57 MPa compression	Munson, (see memo in App. A) Fig. 2.5.1, page 24/ 24	
Traction on Lower Mesh Boundary	15.97 MPa	Munson (see memo in App. A) Fig. 2.5.1, p. 24/ 24, Sec. 2.5.4, p. 22/ 24	
Mesh Configuration Coordinates	See App. D		

at very low stress levels, eliminating space between them. These stress levels were considered to have a negligible effect on later consolidation of the waste. The consequence of this assumption is elimination of any resistance of the waste to lateral closure until all the space is eliminated, which would imply a greater than expected rate of closure at early times. Thus, this assumption leads to an overly severe performance assessment because it implies a faster buildup of gas pressure,

DEPTH WITH RESPECT
TO REFERENCE
STRATIGRAPHY ZERO (m)

13.57 MPa

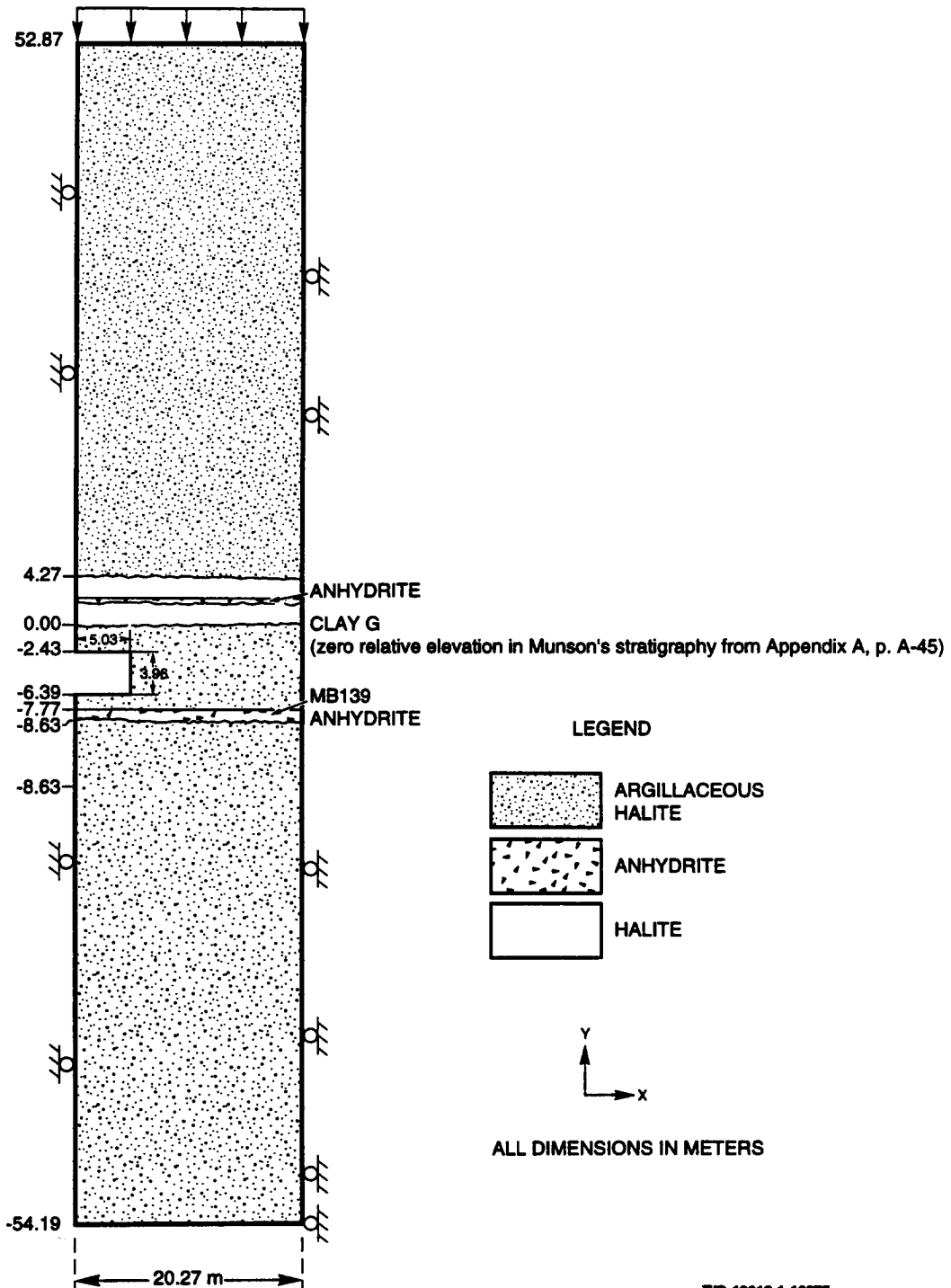
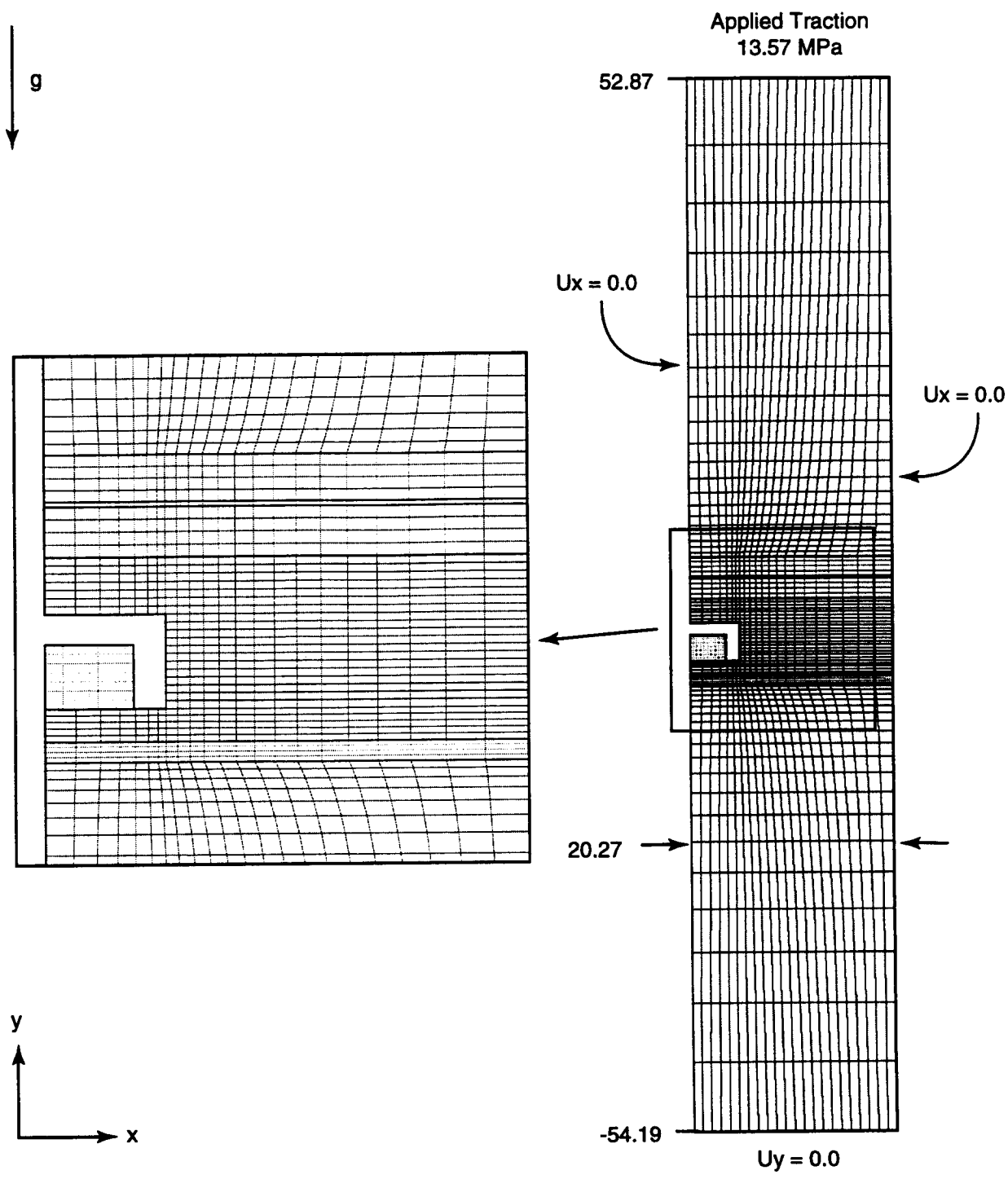


Figure 1. Simplified stratigraphic model used for the disposal room analyses.

which is the driver for releases of radionuclides. Based on the no lateral resistance assumption, the waste was assumed to occupy a modified continuum width of 7.35 m and a length of 87.85 m (Table 1), as defined by Equation 2 in Stone (1997a). The height of the waste during this collapse was assumed to remain unchanged.

Applying the assumptions defined in the previous paragraphs of this section, the mesh discretization and boundary conditions for the final porosity surface analysis are shown in Figure 2, which is identical to Figure 4 in Stone (1997a). The coordinates and connectivity of the meshes in this figure are given in Appendix D of this report.



TRI-6348-44-0

Figure 2. Mesh discretization and boundary conditions used for the disposal room analyses.

This page intentionally left blank

3.0 MATERIAL PROPERTIES

3.1 Halite

A combined transient-secondary creep constitutive model for rock salt attributed to Munson and Dawson (1982) and described by Munson et al. (1989) was used for the clean and argillaceous salt. The material properties (Munson, see Appendix A) are described in Table 3.

3.2 Anhydrite

The anhydrite layer beneath the disposal room is expected to experience inelastic material behavior. The MB 139 anhydrite layer is considered to be isotropic and elastic until yield occurs. Once the yield stress is reached, plastic strain begins to accumulate, according to the Drucker-Prager criterion (Stone, 1997a, Equation 10). The elastic properties and the Drucker-Prager constants C and a for the anhydrite are given in Table 4.

3.3 Waste

The waste properties depend on the waste inventory. The transuranic waste is a combination of metals, sorbents, cellulose, rubber and plastics, and sludges. The waste is modeled as an average mixture of these components, which changes in properties as the respective amounts of each component change in the inventory projections. The waste inventory assumptions and property values used for the final porosity surface calculations and their origins are given in Tables 5 and 6. The initial average waste density is 559.5 kg/m^3 ; the average solid density is 1757 kg/m^3 , which corresponds to an initial average waste porosity of 0.681. The volume of solids in a single disposal room is 551.2 m^3 , and the initial average porosity of the undeformed disposal room (waste + void volume = 3644 m^3) is 0.849.

The stress-strain behavior of the waste was represented by a volumetric plasticity model (Stone, 1997b) with a piecewise linear function defining the relationship between the mean stress and the volumetric strain. Values for the elastic constants and plasticity model parameters are given in Table 7, and the piecewise linear data for the average stress-strain behavior of the waste are given in Table 8.

Table 3: Final Porosity Surface Calculation Input Parameters - Halite Constitutive Parameters

Description	Value	Reference	Comments
Halite Constitutive Parameters			
Elastic Properties (Both Clean and Argillaceous Salt)			
G	12,400 GPa	Munson (see memo in App. A) Sec. 2.5.1, p. 1/ 24	As of 2/15/96 this reference represents the latest values for the mutlimechanism deformation model and the traceability of their origin. The method of converting input elastic constants to the elastic parameters TWOMU and BULK MODULUS used in SANTOS is described in the memorandum from C. M. Stone, March 4, 1996, p. 3 (App. B).
E	31,000 GPa	Munson (see memo in App. A) Sec. 2.5.1, p. 1/ 24	
n	0.25	Munson (see memo in App. A) Sec. 2.5.1, p. 1/ 24	The method of converting input elastic constants to the elastic parameters TWOMU and BULK MODULUS used in SANTOS is described in the memorandum from C. M. Stone, March 4, 1996, p. 3 (App. B).
Clean Salt Creep Properties			
A ₁	8.386E22 /sec	Munson (see memo in App. A) Sec. 2.5.1, p. 1/ 24	
Q ₁	25,000 Cal/mole	Munson (see memo in App. A) Sec. 2.5.1, p. 1/ 24	
n ₁	5.5	Munson (see memo in App. A) Sec. 2.5.1, p. 1/ 24	
B ₁	6.086E6 /sec	Munson (see memo in App. A) Sec. 2.5.1, p. 1/ 24	
A ₂	9.672E12 /sec	Munson (see memo in App. A) Sec. 2.5.1, p. 1/ 24	
Q ₂	10,000 cal/mole	Munson (see memo in App. A) Sec. 2.5.1, p. 1/ 24	

**Table 3 (continued) Final Porosity Surface Calculation Input Parameters - Halite
Constitutive Parameters**

Description	Value	Reference	Comments
Clean Salt Creep Properties - continued			
n_2	5.0	Munson (see memo in App. A) Sec. 2.5.1, p. 1/ 24	
B_2	3.034E-2	Munson (see memo in App. A) Sec. 2.5.1, p. 1/ 24	
S_0	20.57 MPa	Munson (see memo in App. A) Sec. 2.5.1, p. 1/ 24	
q	5,335	Munson (see memo in App. A) Sec. 2.5.1, p. 1/ 24	
m	3.0	Munson (see memo in App. A) Sec. 2.5.1, p. 1/ 24	
K_0	6.275	Munson (see memo in App. A) Sec. 2.5.1, p. 1/ 24	
c	9.198E-3 /K	Munson (see memo in App. A) Sec. 2.5.1, p. 1/ 24	
a	-17.37	Munson (see memo in App. A) Sec. 2.5.1, p. 1/ 24	
b	-7.738	Munson (see memo in App. A) Sec. 2.5.1, p. 1/ 24	
d	0.58	Munson et al. (1989) Table 2-2, p. 41.	
Argillaceous Salt Creep Properties			
A_1	1.407E23 /sec	Munson, (see memo in App. A) Sec. 2.5.1, page 3/ 24	
Q_1	25,000 cal/mole	Munson (see memo in App. A) Sec. 2.5.1, p. 3/ 24	
n_1	5.5	Munson (see memo in App. A) Sec. 2.5.1, p. 3/ 24	
B_1	8.998E6 /sec	Munson (see memo in App. A) Sec. 2.5.1, p. 3/ 24	

**Table 3 (continued) Final Porosity Surface Calculation Input Parameters - Halite
Constitutive Parameters**

Description	Value	Reference	Comments
Argillaceous Salt Creep Properties - continued			
A ₂	1.314E13 /sec	Munson (see memo in App. A) Sec. 2.5.1, p. 3/ 24	
Q ₂	10,000 cal/mole	Munson (see memo in App. A) Sec. 2.5.1, p. 3/ 24	
n ₂	5.0	Munson (see memo in App. A) Sec. 2.5.1, p. 3/ 24	
B ₂	4.289E-2 /sec	Munson (see memo in App. A) Sec. 2.5.1, p. 3/ 24	
S ₀	20.57 MPa	Munson (see memo in App. A) Sec. 2.5.1, p. 3/ 24	
q	5,335	Munson (see memo in App. A) Sec. 2.5.1, p. 4/ 24	
m	3.0	Munson (see memo in App. A) Sec. 2.5.1, p. 4/ 24	
K ₀	2.470E6	Munson (see memo in App. A) Sec. 2.5.1, p. 4/ 24	
c	9.198E-3 /K	Munson (see memo in App. A) Sec. 2.5.1, p. 4/ 24	
a _w	-14.96	Munson (see memo in App. A) Sec. 2.5.1, p. 4/ 24	
b _w	-7.738	Munson (see memo in App. A) Sec. 2.5.1, p. 4/ 24	
d	0.58	Munson et al. (1989) Table 2-2, p. 41.	

Table 4: Final Porosity Surface Calculation Input Parameters - Anhydrite Properties

Description	Value	Reference	Comments
Anhydrite Properties			
Young's Modulus	75.1	Munson (see memo in App. A) Sec. 2.5.2, p. 18/ 24	As of 2/15/96 this reference represents the latest values for nonsalt materials adjacent to the repository and the traceability of their origin. The method of converting input elastic constants to the elastic parameters TWOMU and BULK MODULUS used in SANTOS is described in the memorandum from C. M. Stone, March 4, 1996, p. 3 (App. B).
Poisson's Ratio	0.35	Munson (see memo in App. A) Sec. 2.5.2, p. 18/ 24	The method of converting input elastic constants to the elastic parameters TWOMU and BULK MODULUS used in SANTOS is described in the memorandum from C. M. Stone, March 4, 1996, p. 3 (App. B).
C	1.35 MPa	Munson (see memo in App. A) Sec. 2.5.2, p. 19/ 24	The method of converting these input constants to the anhydrite model parameters used in SANTOS is described in the memorandum from C. M. Stone, March 4, 1996, p. 2 (App. B).
a	0.45	Munson (see memo in App. A) Sec. 2.5.2, p. 19/ 24	The method of converting these input constants to the anhydrite model parameters used in SANTOS is described in the memorandum from C. M. Stone, March 4, 1996, p. 2 (App. B).

Table 5: Final Porosity Surface Calculation Input Parameters - Waste Composition Assumptions

Description	Value	Reference	Comments
Waste Composition Assumptions:		Baseline Inventory Report (BIR) 1995, Rev. 1. Hereafter referred to as BIR.	Justification for use of this version of the inventory provided in a memorandum of record by B. M. Butcher, March 11, 1996 (App. B).
Metallic	122 kg/m ³	BIR (1995) Rev. 1, Table 5-1, p. 5-4.	
Sorbents	40 kg/m ³	BIR (1995) Rev. 1, Table 5-1, p. 5-4.	Minor change from 40 kg/m ³ in draft copy to 39 kg/m ³ in final document neglected. The final document was issued after the calculations were initiated.
Cellulose	170 kg/m ³	BIR (1995) Rev. 1, Table 5-1, p. 5-4.	
Rubber and Plastics	84 kg/m ³	BIR (1995) Rev. 1, Table 5-1, p. 5-4.	
Sludges	143.5 kg/m ³	BIR (1995) Rev. 1, Table 5-1, p. 5-4.	Minor change from 143.5 kg/m ³ in draft copy to 144.1 kg/m ³ in final document neglected
Initial Waste Density	559.5 kg/m ³		Sum of waste component densities : 122 + 40 + 170 + 84 + 143.5

Table 6: Final Porosity Surface Calculation Input Parameters: Waste Densities; Porosity

Description	Value	Reference	Comments
Solid Densities			
Metallic	7830 kg/m ³	Butcher et al. (1991) p. 1, paragraph 5	Values between 7830 kg/m ³ and 7860 kg/m ³ are quoted for iron in the literature. Any value within this range is considered acceptable.
Sorbents	3000 kg/m ³	Butcher et al. (1991) p. 9, Table 2-2	Portland cement considered representative
Cellulose	1100 kg/m ³	Butcher et al. (1991) p. 14, paragraph 4	Computed for the composition of mixture 3 (Table 2-1) using solid density values in Table 2-2.
Rubber and Plastics	1200 kg/m ³	Butcher et al. (1991) p. 40, paragraph 1	Computed for the composition of mixture 6 (Table 2-1) using handbook solid density values for PVC and polyethylene.
Sludges	2200 kg/m ³	Butcher et al. (1991) p. 67, paragraph 2.	Estimated from the composition of mixture 13 (Table 2-1) using solid density values in Table 2-2.
Waste Solid Density	1757 kg/m ³	Calculation documented in App. C.	
Waste Volume Fraction			
Metallic	0.218		(Metals waste density)/(initial waste density)
Sorbents	0.071		(Sorbents waste density)/(initial waste density)
Cellulose	0.304		(Cellulose waste density)/(initial waste density)
Rubber and Plastics	0.150		(Rubber and plastics waste density)/(initial waste density)
Sludges	0.256		(Sludge waste density)/(initial waste density)
Initial Waste Porosity	0.681		1 - (initial waste density/waste solid density)
Initial Solid Volume	551.2 m ³		(1 - waste porosity) x (waste volume)
Initial Room Porosity	0.849		1 - (Initial solid volume)/(initial room volume)

Table 7: Final Porosity Surface Calculation Input Parameters - Waste Mechanical Properties

Description	Value	Reference	Comments
Waste Mechanical Compaction Properties			
Pressure-Volume Strain Data	See Table 9		
G	333 MPa	Weatherby et al. (1991) p. 922	
K	222 MPa	Weatherby et al. (1991) p. 922	
a ₀	1.0 MPa	Weatherby et al. (1991) p. 922	The method for determining this value is provided in a memorandum from C. M. Stone, March 4, 1996, p. 1 (App. B).
a ₁	3.0	Weatherby et al. (1991) p. 922	The method for determining this value is provided in a memorandum from C. M. Stone, March 4, 1996, p. 1 (App. B).
a ₂	0.	Weatherby et al. (1991) p. 922	The method for determining this value is provided in a memorandum from C. M. Stone, March 4, 1996, p. 1 (App. B).

Table 8: Pressure-Volumetric Strain Data Used in the Volumetric-Plasticity Model for the Waste Drums

Pressure (MPa)	$\ln(r / r_0)$
1.53	0.510
2.03	0.631
2.53	0.719
3.03	0.786
3.53	0.838
4.03	0.881
4.93	0.942
12.0	1.14

3.4 Gas Generation

The current practice for calculating gas pressures in SANTOS closure calculations is to either assume gas generation rates or a lookup table of gas production (Brown and Weatherby, 1993, p. A-7). Given an assumed number of moles of gas within the repository as a function of time, the void volume available for storage at a given time is computed and used to compute the gas pressure using the ideal gas law (Brown and Weatherby, 1993, p. A-7).

The porosity surface approach is required because a fully coupled analysis of closure based on detailed descriptions of salt creep, waste consolidation, brine flow in or out of the waste, gas production, and gas migration away from the waste into the interbeds is not technically feasible. As a consequence, a two-step process has been developed. This porosity surface approach begins by computing the extent of closure for various assumed gas contents with the SANTOS code. The method of coupling closure with the coupled fluid flow interactions related to gas production is to determine porosities for actual waste contents by interpolation of these data in the WIPP performance assessment code BRAGFLO (WIPP PA Department, 1993, pp. 4-18 to 4-23). Inherent in this process is the assumption that the porosity - gas pressure values for a given amount of gas are independent of the previous gas generation history. Thus, the closure data provided by SANTOS can be thought of as representing a surface, with any gas generation history computed by BRAGFLO constrained to fall in this surface. The reader is referred to Butcher (1997) for validation of these concepts.

Since exact histories of gas generation are not known for the closure calculations, an arbitrary set of gas generation conditions must be selected that spans all gas generation potentials likely to be encountered. The reason for this requirement is to avoid any uncertainty that might occur if gas production predictions from BRAGFLO fell outside the closure data. That is, extrapolation of conditions outside the range of the data is considered unacceptable. Bounds for assumed gas production for SANTOS were that (1) no gas is generated or (2) all the potential gas-generating materials are consumed. The gas generation rates for SANTOS were the fastest rates possible, those for waste completely immersed in brine. The consequences of any slower rates can be obtained by interpolation between curves. To preserve a link with reality, the gas generation input parameter values for SANTOS calculations were approximately the same as values used in past performance assessments. Because the gas generation histories used in SANTOS calculations are simply a device used to introduce a given amount of gas in the waste at various times, we did not need to update our assumptions to be consistent with all the changes in the nature of reaction products, generation rates, and variations in waste inventory that are required for the CCA.

The gas generation histories assumed for the final porosity surface calculations (Table 9) are representative of waste inundated with brine, a worst case because inundated rates are greater than rates for waste that is not immersed in brine. Gas from two sources is considered: anoxic corrosion and microbial activity. The estimated anoxic corrosion gas production from Beraún and Davies (1992) is 1050 moles/drum with a production rate of 1 mole/drum/year (Table 9) and that from microbial activity is 550 moles/drum with a production rate of 1 mole/drum/year (Table 9). This means that for the baseline case, microbial activity ceases at 550 years while anoxic

corrosion will continue until 1050 years after emplacement. The amount of gas generated in the disposal room is based on 6804 unprocessed waste drums per room.

To simulate different gas amounts within the room at any given time, the baseline gas production was multiplied by a factor f which varies between 0 and 2.0 (Stone, 1997a). Values of f selected for the calculations were $f = 0, 0.025, 0.05, 0.1, 0.2, 0.4, 0.5, 0.6, 0.8, 0.8, 1.0, 1.2, 1.6$ and 2.0. The condition $f = 0$ represents the state of the repository when no gas is produced, and the condition $f = 2$ represents two times the maximum expected rate of gas production. The factor of 2 is used to guarantee that data are available to BRAGFLO for all gas generation scenarios imaginable.

Table 9: Final Porosity Surface Calculation Input Parameters - Gas Generation Assumptions

Description	Value	Reference	Comments
Input Parameters Gas Parameters			
Corrosion Gas Production Rate	1 mole/year/drum	Brush (1991) Table 1, p. A-35	Inundated best-value production rate
Corrosion Gas Potential	1050 moles/drum	Beraún and Davies (1992), p. A-11	Justification for use of this value is provided in a memorandum of record by B. M. Butcher, March 18, 1996 (App. B).
Microbial Gas Production Rate	1 mole/year/drum	Brush (1991) Table 1, p. A-35	Inundated best-value production rate
Microbial Gas Potential	550 moles/drum	Beraún and Davies (1992) p. A-11	Justification for use of this value is provided in a memorandum of record by B. M. Butcher, March 18, 1996 (App. B).
Scaling factor f	0, 0.025, 0.05, 0.1, 0.2, 0.4, 0.5, 0.6, 0.8, 1.0, 1.2, 1.6, 2.0	Analyst's choice	
Gas Constant R	8.23 (m ³ Pa)/(g-mole K)	Physical constant	
Gas Temperature	300 K	Common repository assumption	Nominal value sufficient; see discussion of gas generation in memorandum of record by B. M. Butcher, March 18, 1996 (App. B).

4.0 SUMMARY

The input parameter values used in final predictions of closure and waste densification in the Waste Isolation Pilot Plant disposal room and supporting references are summarized in this report. The closure predictions are referred to as the final porosity surface data and will be used for WIPP performance calculations supporting the Compliance Certification Application to be submitted to the U.S. Environmental Protection Agency. This report includes tables that list all of the input parameter values, references citing their source, and in some cases references to more complete descriptions of considerations leading to the selection of values.

5.0 REFERENCES

- Baseline Inventory Report (BIR). 1995. *Waste Isolation Pilot Plant Transuranic Waste Baseline Inventory Report*. WIPP Technical Assistance Contractor, Report CAO-94-1005, Revision 1. [Carlsbad, NM]: WIPP Technical Assistance Contractor for U.S. Department of Energy.
- Beraún, R., and P. B. Davies. 1992. "Appendix A: Baseline Design Input Data Base to be Used During Calculations Effort to be Performed by Division 1514 in Determining the Mechanical Creep Closure Behavior of Waste Disposal Rooms in Bedded Salt," in *Preliminary Performance Assessment for the Waste Isolation Pilot Plant, December 1992. Volume 3: Model Parameters*. Sandia WIPP Project. SAND92-0700/3. Albuquerque, NM: Sandia National Laboratories. A-7 through A-13.
- Brown, W. T., and J. R. Weatherby. 1993. "Appendix A: Influence of Gas Generation Potential and Gas Generation Rate on the Performance of CH-TRU Disposal Rooms," in *A Summary of the Models Used for the Mechanical Response of Disposal Rooms in the Waste Isolation Pilot Plant with Regard to Compliance with 40 CFR 191, Subpart B*. B.M. Butcher and F.T. Mendenhall. SAND92-0427. Albuquerque, NM: Sandia National Laboratories. A-5 through A-25.
- Brush, L. H. 1991. "Appendix A: Current Estimates of Gas Production Rates, Gas Production Potentials, and Expected Chemical Conditions Relevant to Radionuclide Chemistry for the Long-Term WIPP Performance Assessment," *Preliminary Comparison with 40 CFR Part 191, Subpart B for the Waste Isolation Pilot Plant, December 1991. Volume 3: Reference Data*. Eds. R. P. Rechard, A. C. Peterson, J. D. Schreiber, H. J. Iuzzolino, M. S. Tierney, and J. S. Sandha. SAND91-0893/3. Albuquerque, NM: Sandia National Laboratories. A-27 through A-41.
- Butcher, B. M. 1995. "Sandia National Laboratories Waste Isolation Pilot Plant Analysis Plan: Final Porosity Surface Calculations, WBS 1.1.01.2.3, Rev. 1, Effective date 11/6/95." (Copy on file in the Sandia WIPP Central Files, Sandia National Laboratories, Albuquerque, NM as WPO#29792.)
- Butcher, B. M. 1996. "Principal Investigator Documentation Package for Final Porosity Surface Data." Albuquerque, NM: Sandia National Laboratories. (Copy on file in the Sandia WIPP Central Files, Sandia National Laboratories, Albuquerque, NM as WPO#35697.)
- Butcher, B. M. 1997. *Waste Isolation Pilot Plant Disposal Room Model*. SAND97-0794. Albuquerque, NM: Sandia National Laboratories.
- Butcher, B. M., T. W. Thompson, R. G. VanBuskirk, and N. C. Patti. 1991. *Mechanical Compaction of Waste Isolation Pilot Plant Simulated Waste*. SAND90-1206. Albuquerque, NM: Sandia National Laboratories.

- Munson, D. E., and P. R. Dawson. 1982. "A Work Hardening/Recovery Model of Transient Creep of Salt During Stress Loading and Unloading," in *Issues in Rock Mechanics, Proceedings of the 23rd U.S. Symposium on Rock Mechanics, Berkeley, CA, August 25-27, 1982*. Eds. R.E. Goodman and F.E. Heuze. New York, NY: American Institute of Mining, Metallurgical and Petroleum Engineers. Vol. 23, pp. 299-306. Also published as SAND82-0962 and SAND82-0810J. Albuquerque, NM: Sandia National Laboratories.
- Munson, D. E., A. F. Fossum, and P. E. Senseny. 1989. "Approach to First Principles Model Prediction of Measured WIPP In Situ Room Closure in Salt," in *Rock Mechanics as a Guide for Efficient Utilization of Natural Resources, Proceedings of the 30th US Symposium on Rock Mechanics, West Virginia University, Morgantown, WV, June 19-22, 1989*. Ed. A.W. Khair. Brookfield, VT: A.A. Balkema. 673-680. Also published as SAND88-2535. Albuquerque, NM: Sandia National Laboratories.
- Sandia WIPP Project. 1992. *Preliminary Performance Assessment for the Waste Isolation Pilot Plant, December 1992. Volume 3: Model Parameters*. SAND92-0700/3. Albuquerque, NM: Sandia National Laboratories.
- Stone, C. M. 1997a. *Final Disposal Room Structural Response Calculations*. SAND97-0795. Albuquerque, NM: Sandia National Laboratories.
- Stone, C. M. 1997b. *SANTOS³ A Two-Dimensional Finite Element Program for the Quasistatic, Large Deformation, Inelastic Response of Solids*. SAND90-0543. Albuquerque, NM: Sandia National Laboratories.
- Weatherby, J. R., W. T. Brown, and B. M. Butcher. 1991. "The Closure of WIPP Disposal Rooms Filled with Various Waste and Backfill Combinations," in *Rock Mechanics as a Multidisciplinary Science, Proceedings of the 32nd U.S. Symposium, University of Oklahoma, Norman, OK, July 10-12, 1991*. Ed. J. C. Roegiers. Brookfield, VT: A. A. Balkema. 919-928. Also published as SAND90-2399C. Albuquerque, NM: Sandia National Laboratories.
- WIPP PA (Performance Assessment) Department. 1993. *Preliminary Performance Assessment for the Waste Isolation Pilot Plant, December 1992. Volume 4: Uncertainty and Sensitivity Analyses for 40 CFR 191, Subpart B*. SAND92-0700/4. Albuquerque, NM: Sandia National Laboratories.

This page intentionally left blank

Appendix A: Unpublished References

B. M. Butcher, “Waste Compressibility Curve Predictions.” Sandia National Laboratories Memorandum of Record, February 16, 1995. A-3

D. E. Munson, “Mechanical Parameters for Update of Reference Data Report.” Sandia National Laboratories Memorandum to M. S. Tierney, September 26, 1995..... A-22

J. D. Osnes and D. A. Labreche, “The Effect of Clay Seams and Anhydrite Layers on the Closure of Waste Isolation Pilot Plant Disposal Rooms and Guidelines for Simplifying the Modeled Stratigraphy.” RE/SPEC External Memorandum RS(RCO)-390/7-95/58, August 29, 1995. A-47

C.M. Stone, “Proposed Model for the Final Porosity Surface Calculations.” Sandia National Laboratories Memorandum to B. M. Butcher, October 27, 1995.A-106

Appendix A errata

Page	Reference	Corrections
A-4	Luker et al., 1991	Correct the spelling of the word “Science”
A-24, A-26	2.5.1 Fossum et al., 1994	Brookfield is in Vermont
A-24, A-27	2.5.1 Fossum et al., 1988 2.5.7 " " " "	Brookfield is in Vermont " " " "
A-24, A-27	2.5.8 Munson and Dawson, 1982	Dawson’s middle initial is R
A-25, A-27	2.5.13 Munson et al., 1992	Brookfield is in Vermont
A-26 A-43	2.5.2 Munson et al., 1989 2.5.1 " " " "	Insert “WIPP” after “Measured” in title " " " " " "
A-28, A-29	2.5.15 Chan et al., 1995	Bodner’s initials are S.R. Journal ref. is Vol. 5, no. 3, pp. 292-314 (July 1996)
A-38	2.5.25 Stone et al., 1985	SAND number should be 84-2618
A-39, A-42, A-43	2.5.26 Yang, 1981	Correct the spelling of "Thermophysical". This chapter is on file in the Sandia WIPP Central Files as WPO#43754
A-45	2.5.30 Munson et al., 1987	Insert a closing parenthesis after “1987” and add the following to the end of this title: Waste Isolation Pilot Plant (WIPP), Thermal/Structure Interactions Program
A-80	Callahan et al., 1990	This report is dated August 28, 1989. It is available from the National Technical Information Service (NTIS), Springfield, VA as DE90000681/XAB and DE90000682/XAB. This report is called out in Sections 3.0 and 3.3 of this memo.

A-81	Osnes and Brandshaug, 1980	The published proceedings is titled, <i>Underground Rock Engineering, 13th Canadian Rock Mechanics Symposium, Toronto, Canada, May 28-29, 1980</i> . Series: Special Volume - Canadian Institute of Mining and Metallurgy; 22. Montreal: Canadian Institute of Mining and Metallurgy. pp. 193-197. Copy of proceedings paper is on file in the Sandia WIPP Central Files as WPO#44095.
A-81	Stone, 1992	This memo has been reprinted in pages E-41 through E-61 of SAND94-0890, which is available from the National Technical Information Service as DE95016749/XAB. The word "Behavior" should be inserted after the word "Closure."
A-82	Zienkiewicz et al., 1968	The final author's first initial is "I." This journal article is on file in the Sandia WIPP Central Files as WPO#43859.
A-117	Citation 5. Munson et al., 1989	Fossum's middle initial is "F."
A-117	Citation 8. Beraun and Davies	Insert phrase "to be Performed" after word "Effort."
A-118	Citation 9. Butcher et al.	The final version of this document, "Systems Prioritization Method—Iteration 2 Baseline Position Paper: Disposal Room and Cuttings Model," is dated March 28, 1995 and is on file in the Sandia WIPP Central Files as WPO#28729 (Vol. 1) and WPO#28733 (Vol. 2). This document is not available from the National Technical Information Service.

p. A-102 The references should appear in the following order: Beraún, R., and P.B. Davies. 1991; Butcher, B.M. 1995; Butcher, B.M. et al. 1991; Krieg, R.D. 1984; Munson, D.E. 1992; Munson, D.E. et al. 1989; 92 PA V3 1992; Sjaardema, G.D. and R.D. Krieg. 1987

In addition, the following references should be added:

Baseline Inventory Report (BIR). 1995. *Waste Isolation Pilot Plant Transuranic Waste Baseline Inventory Report*. CAO-94-1005, Revision 1. [Carlsbad, NM]: WIPP Technical Assistance Contractor for U.S. Department of Energy.

Bechtel, Inc. 1986. "WIPP Design Validation Final Report." DOE/WIPP-86-010. Prepared for the U.S. Department of Energy. San Francisco, CA: Bechtel National, Inc.

Butcher, B.M., and F.T. Mendenhall. 1993. *A Summary of the Models Used for the Mechanical Response of Disposal Rooms in the Waste Isolation Pilot Plant with Regard to Compliance with 40 CFR 191, Subpart B*. SAND92-0427. Albuquerque, NM: Sandia National Laboratories.

Krieg, 1984 is on file in the SWCF as WPO# 36331. This rough draft is also available in the Sandia National Laboratories' Technical Library as SC-DR-72-0883. This rough draft is titled, "A Simple Constitutive Description for Cellular Concrete."

Sandia National Laboratories

Albuquerque, New Mexico 87185-1342

date: February 16, 1995

to: Memorandum of Record

[Note: All calculations described in this memorandum were performed by B. M. Butcher.]

B. M. Butcher

from: B. M. Butcher, 6348, MS 1341

subject: Waste Compressibility Curve Predictions

This memorandum of record describes the suggested method for defining the average waste compressibility curve for the repository. In this case, the starting point for the calculations is the Draft Baseline Inventory Report, Document CAO-94-1005, Rev. 1, issued February, 1995, Table 6-1, titled WIPP CH_TRU Waste Material Parameter disposal Inventory. A copy of this table is in Appendix A of this memo.

The listing of the QBASIC computer code COMPRESS.BAS used to compute the average compressibility curve is given in Appendix B. The basis for this calculation is the mixture theory approach and the compressibility data for the individual waste components described in Butcher, et al (1991) and Luker, et al (1991). Any effects because of containers (drums) are not included, because the containers offer very little resistance to collapse. A lookup file for the compressibility of sludge type wastes is also needed for the calculation and is included in the Appendix B listings. Input to program COMPRESS in order of insertion is:

- The output file name xxxxxxxx, as in C:\xxxxxxx.DAT must be specified. An example for xxxxxxxx might be RESULTS\COMP\BIR295, which would produce the BIR295.DAT file in directory RESULTS, subdirectory COMP.
- The average amounts of iron based, aluminum based and other metals in the inventory (3 values) must be specified. Reference to Table 6-1 indicates that these numbers would be 83 Kg/m³, 12 Kg/m³, and 27 Kg/m³.
- The average solid density of the metals in g/cm³ is required. This value is a judgment call because the composition of "other metals", which would include lead, copper, tantalum, etc., is not defined in Table 6-1. Normally, if the composition were known, this quantity could be computed as described in Butcher et. al (1991). Values for the solid density of iron would be 7.83 g/cm³, the solid density of aluminum based metals would be 2.7 g/cm³, and an appropriate average density would be used for the other metals, maybe something of the order of 9 g/cm³ depending on the composition. In the absence of this information a value of 7.83 g/cm³, the value for iron, was used for the calculation described in this memorandum. Justification for the use of this value is that (1) iron based metals are the principal components of the metals waste, (2) the low solid density of the aluminum tends to offset the higher density of the "other metals," yielding an average density close to that of iron, and (3) sensitivity calculations in which the average solid density of metals value was varied showed that the dependence of the compaction curve on the exact value of this parameter was small.

- The average amounts of plastics and rubber (2 values) must be defined. Reference to Table 6-1 indicates that these numbers would be 63 Kg/m³ and 21 Kg/m³.
- The average amount of cellulose (1 value) must be defined. Reference to Table 6-1 indicates that this number would be 170 Kg/m³.
- The average amount of sorbents (defined as other organics)(1 value) must be defined. Reference to Table 6-1 indicates that this number would be 40 Kg/m³. In the COMPRESS program sorbents can be characterized as either dry portland cement (C), vermiculite (V), or Oil Dri (OD).
- The average amounts of sludges and soils (3 values) must be defined. Soils are considered more like sludges than like the other waste components (such as cellulose), and can be lumped with the sludges because they represent a very small portion of this category. Should the amount of soils increase in the future, a separate curve for their compactibility should be introduced into the calculation. Reference to Table 6-1 indicates that these numbers would be 130 Kg/m³ for inorganic sludge, 7.8 Kg/m³ for organic sludge, and 5.7 Kg/m³ for soils.

Given these parameters, the program is used to compute the average compressibility curve. A copy of this data file is given in Appendix B. The results in the attached figure show that even though recent waste composition values have changed substantially from previous values, the average compressibility curve using the new inventory data differs very little from the curve used for the 1992 Preliminary Performance Assessment (Butcher, et. al, 1991, Figure 4-1), probably because of compensating changes.

References :

Butcher, B. M., R. G. VanBuskirk*, N. C. Patti*, and T. W. Thompson, 1991. "Mechanical Compaction of WIPP Simulated Waste," SAND90-1206, Sandia National Laboratories, Albuquerque, NM; See also Luker, R. S., Thompson, T. W., and Butcher, B. M., 1991. "Compaction and Permeability of Simulated Waste." In Rock Mechanics as a Multidisciplinary Science, Proceedings of the 32nd U. S. Symposium, Roegiers (ed.), A. A. Balkema, Rotterdam, pp 693-702.

Luker, R. S., Thompson, T. W., and Butcher, B. M., 1991. "Compaction and Permeability of Simulated Waste." In Rock Mechanics as a Multidisciplinary Science, Proceedings of the 32nd U. S. Symposium, Roegiers (ed.), A. A. Balkema, Rotterdam, pp 693-702.

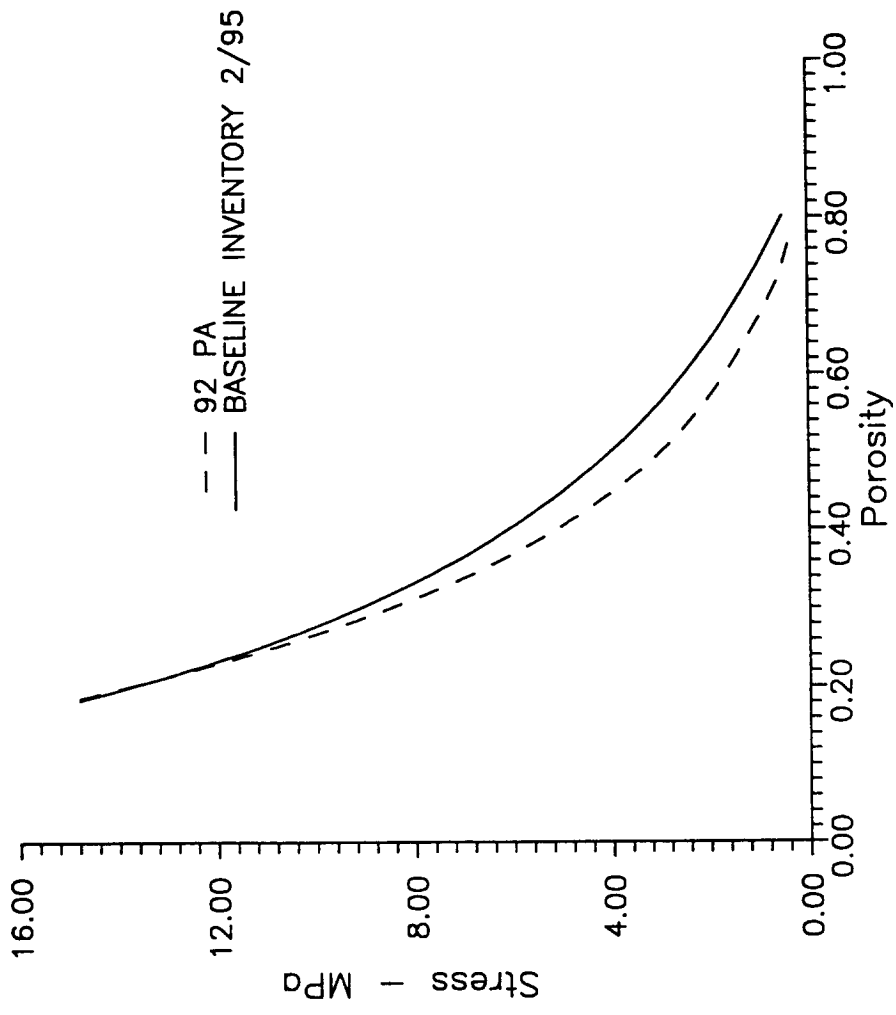
Copy to:

~~MS 1342 B. M. Butcher (day file) (6348)~~

MS 1342 J. T. Holmes (6348)

MS 1330 SWCF(DRM) (WBS 1.1.1.2.3) (6352)
D. Lebreche (RE/SPEC)

Figure 1: A Comparison of the 12/92 PA Average Repository
Compaction Curve With a More Recent Curve Based in Baseline
Inventory Report Parameters



File c: graph compact2 newcurv1

Appendix A: Table 6-1 from the Draft Baseline Inventory Report,
Document CAO-94-1005. Rev. 1, issued February, 1995

Table 6-1

WIPP CH-TRU Waste Material Parameter Disposal Inventory

	Materials	(Kg/m3)		
		Maximum	Average	Minimum
Inorganics	Iron Based	1.7E+03	8.3E+01	0.0E+00
	Aluminum Based	1.0E+03	1.2E+01	0.0E+00
	Other Metals	1.4E+03	2.7E+01	0.0E+00
	Other Inorganics	2.1E+03	4.0E+01	0.0E+00
	Organics	Cellulose	9.6E+02	1.7E+02
	Rubber	6.8E+02	2.1E+01	0.0E+00
	Plastics	8.9E+02	6.3E+01	0.0E+00
Solidified Materials	Inorganic	2.2E+03	1.3E+02	0.0E+00
	Organic	1.4E+03	7.8E+00	0.0E+00
Soils		1.6E+03	5.7E+00	0.0E+00
Container Materials				
	Steel		1.4E+02	
	Plastic/ Liners		3.3E+01	

Appendix B:

- Listing of data file SLUDGE.DAT for the compressibility of sludges
- Listing of data file BIRREV1.DAT for the average compressibility of waste
 - Listing of program COMPRESS output
 - QA CONFIRMATION OF RESULTS

Additional Explanation of the Section "QA Confirmation of Results"

This section is a numerical check of the code COMPRESS to ensure that the calculated porosities are correct. The code listing shows that the output command on line 900 for indices K prints the stress [STRESS(K)], the density of the metal waste [RHOM(K)], the density of the plastic waste [RHOP(K)], the density of the cellulose [RHOC(K)], the density of the sorbent [RHOS(K)], and the density of the sludge [RHOSL(K)] corresponding to the value of STRESS. Output from line 950 includes the specific volume of the waste [VOL(K)] (1/density), the void volume corresponding to VOL, [VVOL(K)], the porosity [P(K)], and the waste density [RH(K)] corresponding to the value for STRESS. Values of these parameters at a stress of 2002.16 psi (K = 63) are highlighted on page A-17.

The MATHCAD calculation following the program listing is an independent hand calculation of the parameter values at 2002.16 psi (13.80 MPa). The parameter *rhom* in the hand calculation corresponds to RHOM of the COMPRESS output, *rhop* corresponds to RHOP, *rhoc* corresponds to RHOC, etc. The hand calculation parameter *vt* corresponds to VOL and the parameter *vvt* corresponds to VVOL. Comparison of the highlighted computer output at 2002.16 psi with the hand-calculated values shows that the values are identical within roundoff error, confirming the COMPRESS calculation. The hand calculated values were also used to calculate the porosity *por*, which corresponds to the COMPRESS parameter value P(63). These values are also in agreement. Finally, the conversion of the stress in psi to stress in MPa is checked in the hand calculation and found to be in agreement with the COMPRESS value, completing the verification.

Sheet1

File	SLUDGE	2/16/95
density g/cc		stress - psi
1.5	0	1
1.53	0	75
1.55828	0.060019	149.576
1.56528	0.062796	170.501
1.57939	0.065582	199.564
1.59177	0.068369	232.053
1.60281	0.071116	263.725
1.61266	0.073901	292.033
1.62225	0.076688	323.903
1.63173	0.079475	356.767
1.64042	0.082225	387.358
1.64972	0.085012	418.571
1.65815	0.087795	450.93
1.66624	0.090572	480.134
1.67423	0.093363	510.277
1.68238	0.096114	542.351
1.69084	0.0989	572.877
1.70137	0.101687	603.088
1.71392	0.104482	635.756
1.72029	0.107224	665.846
1.73443	0.110014	696.41
1.74671	0.112797	729.206
1.75268	0.115575	759.819
1.75902	0.118353	791.797
1.76576	0.121147	821.167
1.77235	0.123904	853.236
1.77883	0.12669	883.57
1.78531	0.129477	915.037
1.79207	0.132231	947.167
1.79864	0.135018	976.693
1.80521	0.137805	1007.25
1.81135	0.140587	1038.42
1.81741	0.143356	1070.09
1.82335	0.146144	1101.76
1.82918	0.148924	1133.77
1.83477	0.151666	1163.57
1.83999	0.154447	1194.43
1.8455	0.157225	1226.08
1.85108	0.160002	1255.83
1.85637	0.16278	1286.73
1.86167	0.165558	1318.94
1.86667	0.168335	1349.14
1.87198	0.171145	1381.34
1.87688	0.173914	1411.22
1.88189	0.176696	1443.35
1.88679	0.179478	1472.84
1.89164	0.182256	1503.58
1.89646	0.185033	1536.01

Sheet1

1.90099	0.187815	1567.19
1.90558	0.190588	1596.98
1.91006	0.193361	1628.9
1.91451	0.196135	1660.49
1.91893	0.198908	1691.53
1.9232	0.201676	1721.33
1.92736	0.204453	1751.69
1.93161	0.20724	1784.15
1.9358	0.210013	1814.13
1.93998	0.212786	1845.92
1.9441	0.215563	1876.93
1.94818	0.218341	1909.08
1.95213	0.221119	1938.95
1.95609	0.223896	1970.24
1.96	0.22667	2002.16

Sheet1

WASTE STRESS MPa	COMPACTION POROSITY
0.5171025	0.8006011
1.031282	0.7395592
1.175553	0.7237282
1.375934	0.7024797
1.599936	0.67979
1.818305	0.6587131
2.01348	0.6408958
2.233214	0.6220217
2.459801	0.6036918
2.670717	0.5875416
2.885921	0.5718592
3.109027	0.5564186
3.31038	0.5430908
3.518207	0.5299146
3.739347	0.5164916
3.949815	0.5042071
4.158111	0.4924215
4.383347	0.4800999
4.590808	0.469373
4.801538	0.45852
5.027657	0.4473844
5.238724	0.4375826
5.459203	0.4276801
5.6617	0.41883
5.882806	0.4095016
6.09195	0.4009367
6.308906	0.3923278
6.530432	0.3837928
6.734005	0.3761524
6.944686	0.3684704
7.159595	0.3608786
7.377949	0.3533862
7.596305	0.3461036
7.817004	0.3389504
8.022466	0.332452
8.235237	0.3259226
8.453453	0.3193853
8.658571	0.3133651
8.871617	0.3072904
9.093696	0.3011253
9.301916	0.29548
9.523925	0.2896025
9.729939	0.2842753
9.951465	0.2786932
10.15479	0.2736635
10.36673	0.2685496
10.59033	0.2632942
10.8053	0.2583605

Sheet1

11.0107	0.2537278
11.23078	0.2488981
11.44858	0.2442196
11.66259	0.2397153
11.86805	0.2354757
12.07738	0.2312546
12.30118	0.2268475
12.50788	0.2228396
12.72707	0.2186917
12.94087	0.2147223
13.16253	0.2107019
13.36848	0.2070263
13.58421	0.203261
13.80429	0.199503
14.8	0.1825007

```

1 REM PROGRAM COMPRESS 2/16/95
2 REM Derived from Program WASTEAD3: 11/14/89
3 REM Given a tabular description of the compression of the sludge
  REM category: C:\DATA\RESULTS\COMP\SLUDGE.DAT, this program is used
  REM to compute its compressibility curve. Creep corrections are included.
5 REM Densities are in g/cc, stress is in psi, but results are in MPa
10 DIM STRESS(200), RHOM(200), RHOP(200), RHOC(200), RHOS(200)
  DIM RHOSL(200), VOL(200), VVOL(200), P(200), RH(200)
20 S1$ = "C:\\"
30 PRINT "ENTER OUTPUT FILE NAME"
40 INPUT S2$
50 S4$ = ".DAT"
60 S3$ = S1$ + S2$ + S4$
70 PRINT "FILE NAME IS", S3$
90 S6$ = S3$
100 PRINT "OUTPUT FILE IS", S6$
  O OPEN "O", #2, S6$
  REM FM IS THE WEIGHT FRACTION OF METALS WASTE
  REM FP IS THE WEIGHT FRACTION OF PLASTICS WASTE
  REM FC IS THE WEIGHT FRACTION OF CELLULOSICS WASTE
  REM FS IS THE WEIGHT FRACTION OF SORBENTS WASTE
  REM SORBENTS ARE CLASSIFIED AS "OTHER ORGANICS"
  REM FSL IS THE WEIGHT FRACTION OF SLUDGE WASTE
  REM SOILS ARE LUMPED IN WITH SLUDGE WASTE
  REM RMSD IS THE SOLID DENSITY OF THE METAL WASTE: define in g/cc
  REM RPSD IS THE SOLID DENSITY OF PLASTICS: 1.2 g/cc unless changed
  REM RCSL IS THE SOLID DENSITY OF CELLULOSICS: 1.1 g/cc unless changed
  REM RSCSD IS THE SOLID DENSITY OF CEMENT: 3.0 g/cc unless changed
  REM RSVSD IS THE SOLID DENSITY OF VERMICULITE: 2.9 unless changed
  REM RSODSD IS THE SOLID DENSITY OF OIL DRY: 2.6 unless changed
  REM RSLSD IS THE SOLID DENSITY OF SLUDGES: 2.2 unless changed
230 PRINT "ENTER THE AVE WEIGHT FRACTION OF METALS: IRON, ALUMINUM, AND OTHER"
240 INPUT FM1, FM2, FM3
  FM = FM1 + FM2 + FM3
250 PRINT "THE SOLID DENSITY OF THE METAL WASTE IS?"
260 INPUT RMSD
270 PRINT "ENTER THE AVERAGE WEIGHT OF PLASTICS: PLASTICS + RUBBER"
280 INPUT FP1, FP2
  FP = FP1 + FP2
290 RPSD = 1.2
300 PRINT "ENTER THE AVERAGE WEIGHT OF WASTE - CELLULOSICS"
310 INPUT FC
  RCSL = 1.1
320 PRINT "ENTER THE AVERAGE WEIGHT OF WASTE - SORBENTS"
340 INPUT FS
350 PRINT "IS THIS COMPONENT CEMENT (C), VERMICULITE (V) OR OIL DRI (OD)?"
360 INPUT SORB$
370 RSCSD = 3!
380 RSVSD = 2.9
390 RSODSD = 2.6
400 PRINT "ENTER THE AVERAGE WEIGHT OF SLUDGE: INORGANIC; ORGANIC, SOILS"
410 INPUT FSL1, FSL2, FSL3
  FSL = FSL1 + FSL2 + FSL3
420 RSLSD = 2.2
430 FT = FM + FP + FC + FS + FSL
  PRINT "TOTAL WEIGHT OF WASTE IS ", FT
  INPUT PAUSE
  FM = FM / FT
  PRINT "THE MASS FRACTION OF METALS IS ", FM
  INPUT PAUSE

```

```

FP = FP / FT
PRINT "THE MASS FRACTION OF PLASTICS IS ", FP
INPUT PAUSE
FC = FC / FT
PRINT "THE MASS FRACTION OF COMBUSITBLES IS ", FC
INPUT PAUSE
FS = FS / FT
PRINT "THE MASS FRACTION OF SORBENTS IS ", FS
INPUT PAUSE
FSL = FSL / FT
PRINT "THE MASS FRACTION OF SLUDGES IS ", FSL
INPUT PAUSE
FT = FM + FP + FC + FS + FSL
440 IF FT = 1 THEN 470
450 PRINT "WEIGHT FRACTIONS ADD UP TO ", FT
460 GOTO 230
    REM SLUDGE CURVE IS IN TABULAR FORM
470 OPEN "I", #1, "C:\DATA\RESULTS\COMP\SLUDGE.DAT"
480 FOR K = 1 TO 63
490 INPUT #1, RHOSL(K), D, STRESS(K)
491 REM PRINT RHOSL(K), STRESS(K)
500 IF FM = 0 THEN 550
    REM DEFINE METAL DENSTIY AT GIVEN STRESS STRESS(K)
    REM EQUATIONS ARE FROM SAND REPORT
510 RHOM(K) = RMSD / 10240 * (STRESS(K) + 1800)
520 VM = FM / RHOM(K)
530 VV = (1 - RHOM(K) / RMSD) * VM + VV
540 V = VM + V
550 IF FP = 0 THEN 620
    REM DEFINE PLASTICS DENSITY AT GIVEN STRESS
560 TEMP1 = LOG(STRESS(K) / 3115) / 4.179
570 IF TEMP1 < -1 THEN 961
580 RHOP(K) = RPSD * (1 + TEMP1)
581 IF STRESS(K) < 254 THEN RHOP(K) = RPSD * (1 - (890 - STRESS(K)) / 1060)
582 IF STRESS(K) < 0 THEN RHOP(K) = .16 * RPSD
590 VP = FP / RHOP(K)
600 VV = (1 - RHOP(K) / RPSD) * VP + VV
610 V = VP + V
620 IF FC = 0 THEN 670
    REM DEFINE DENSITY OF COMBUSTIBLES AT GIVEN STRESS
630 RHOC(K) = RCSD * (1 - EXP(-(STRESS(K) + 103) / 1167))
640 VC = FC / RHOC(K)
    VV = (1 - RHOC(K) / RCSD) * VC + VV
650 V = VC + V
670 IF FS = 0 THEN 850
    REM DEFINE THE DENSITY OF SORBENTS (OTHER ORGANICS)
680 IF SORB$ = "C" THEN 710
690 IF SORB$ = "V" THEN 760
700 IF SORB$ = "OD" THEN 810
710 RHOS(K) = RSCSD * (1 + LOG(STRESS(K) / 2280000!) / 21.9)
711 IF STRESS(K) < 233 THEN RHOS(K) = RSCSD * (1 - (2350 - STRESS(K)) / 5110)
712 IF STRESS(K) < 0 THEN RHOS(K) = RSCSD * .46
720 VS = FS / RHOS(K)
730 VV = (1 - RHOS(K) / RSCSD) * VS + VV
740 V = VS + V
    J GOTO 850
760 RHOS(K) = LOG(STRESS(K) / 60.2) / 1.432
770 VS = FS / RHOS(K)
780 VV = (1 - RHOS(K) / RSVSD) * VS + VV
790 V = VS + V

```

```

800 GOTO 850
810 RHOS(K) = LOG(STRESS(K) / .467) / 7.27
820 VS = FS / RHOS(K)
830 VV = (1 - RHOS(K) / RSODSD) * VS + VV
840 V = VS + V
850 IF FSL = 0 THEN 900
      REM DEFINE THE DENSITY OF SLUDGE WASTE - INCLUDING SOILS
870 VSL = FSL / RHOSL(K)
880 VV = (1 - RHOSL(K) / RSLSD) * VSL + VV
890 V = VSL + V
900 PRINT "LINE 900", STRESS(K), RHOM(K), RHOP(K), RHOC(K), RHOS(K), RHOSL(K)
910 RH(K) = 1 / V
920 VOL(K) = V
930 VVOL(K) = VV
940 P(K) = VV / V
      PORE = P(K)
      POREM = P(K - 1)
      STMPA = STRESS(K) * .0068947#
      STMPAM = STRESS(K - 1) * .0068947#
950 PRINT "LINE 950", K, VOL(K), VVOL(K), P(K), RH(K)
960 WRITE #2, STMPA, P(K)
      PRINT STMPA, P(K)
961 V = 0
962 VV = 0
970 NEXT K
      REM EXTRAPOLATE TO 14.8 MPa"
      SLOPE = (PORE - POREM) / (STMPA - STMPAM)
      PKM = (14.8 - STMPA) * SLOPE + PORE
      WRITE #2, 14.8, PKM
      PRINT 14.8, PKM
980 END

```

NotACall PROGRAM CHECK
2/26/95

Baseline Inventory Report Results BINV295 File

i := 1 ..10

iron - i = 1
aluminum - 2
other metals - 3

sorbents - i = 4

cellulose - i = 5
rubber - 6
plastics - 7

sludges
(organic) - i = 8
sludges
(inorganic) - = 9

"soils - i = 10

A := 83 A := 12 A := 27 A := 40 A := 170 A := 21
1 2 3 4 5 6

A := 63 A := 130 A := 7.8 A := 5.7
7 8 9 10

ΣA = 559.5

$$RM := \frac{A_1 + A_2 + A_3}{\Sigma A} \quad RM = 0.218$$

$$RS := \frac{A_4}{\Sigma A} \quad RS = 0.071$$

$$RCEL := \frac{A_5}{\Sigma A} \quad RCEL = 0.304$$

$$RPLA := \frac{A_6 + A_7}{\Sigma A} \quad RPLA = 0.15$$

$$RC := \frac{A_5 + A_6 + A_7}{\Sigma A} \quad RC = 0.454$$

$$RSL := \frac{A_8 + A_9 + A_{10}}{\Sigma A} \quad RSL = 0.256$$

$$RM + RS + RC + RSL = 1$$

 Calculate a point - assume a stress of 2002.16 psi
 corresponding to a sludge density of 1.96 g/cc

Assume a solid metal density of 7.83 g/cc
 plastics density of 1.2 g/c
 cellulosics density of 1.1 g/cc
 sorbent density (cement) of 3.0 g/cc
 sludge density of 2.2 g/cc
 S := 2002.16

Metals density, void volume, volume

$$rhom := 7.83 \cdot \frac{S + 1800}{10240} \quad rhom = 2.907$$

$$vm := \frac{RM}{rhom} \quad vm = 0.075$$

$$vvm := \left[1 - \frac{rhom}{7.83} \right] \cdot vm \quad vvm = 0.047$$

Plastics density, void volume, volume

$$rhop := \frac{\ln \left[\frac{S}{3115} \right]}{4.179} \quad rhop = -0.106$$

$$rhop := 1.2 \cdot (1 + rhop) \quad rhop = 1.073$$

$$vp := \frac{RPLA}{rhop} \quad vp = 0.14$$

$$vvp := \left[1 - \frac{rhop}{1.2} \right] \cdot vp \quad vvp = 0.015$$

Cellulosics density, void volume, volume

$$rhoc := 1.1 \cdot \left[1 - \exp \left[\frac{-(S + 103)}{1167} \right] \right] \quad rhoc = 0.919$$

$$vc := \frac{RCEL}{rhoc} \quad vc = 0.331$$

$$vvc := \left[1 - \frac{rhoc}{1.1} \right] \cdot vc \quad vvc = 0.054$$

Sorbents density, void volume, volume

$$\text{rhosb} := 3 \cdot \left[1 + \frac{\ln \left[\frac{S}{2280000} \right]}{21.9} \right] \quad \text{rhosb} = 2.036$$

$$\text{vsb} := \frac{RS}{\text{rhosb}} \quad \text{vsb} = 0.035$$

$$\text{vvsb} := \left[1 - \frac{\text{rhosb}}{3} \right] \cdot \text{vsb} \quad \text{vvsb} = 0.011$$

Sludge density, void volume, volume

$$\text{rhosl} := 1.96$$

$$\text{vsl} := \frac{RSL}{\text{rhosl}} \quad \text{vsl} = 0.131$$

$$\text{vvsl} := \left[1 - \frac{\text{rhosl}}{2.2} \right] \cdot \text{vsl} \quad \text{vvsl} = 0.014$$

Totals

$$\text{vt} := \text{vm} + \text{vp} + \text{vc} + \text{vsb} + \text{vsl} \quad \text{vt} = 0.712$$

$$\text{vvt} := \text{vvm} + \text{vvp} + \text{vvc} + \text{vvsb} + \text{vvsl} \quad \text{vvt} = 0.142$$

$$\text{por} := \frac{\text{vvt}}{\text{vt}} \quad \text{por} = 0.2$$

$$S := S \cdot .0068947 \quad S = 13.804$$

$$\begin{aligned} \text{rhom} &= 2.907 \\ \text{rhop} &= 1.073 \\ \text{rhoc} &= 0.919 \\ \text{rhosb} &= 2.036 \\ \text{rhosl} &= 1.96 \end{aligned}$$

2/26/95

1.378665				
12.94087	.2147223			
LINE 900	1909.08	2.836142	1.059409	.9038425
.02941	1.94818			
LINE 950	60	.7216447	.1520519	.2107019
1.385723				
13.16253	.2107019			
LINE 900	1938.95	2.858982	1.063867	.9087995
2.031536	1.95213			
LINE 950	61	.7182997	.148707	.2070263
1.392177				
13.36848	.2070263			
LINE 900	1970.24	2.882908	1.068464	.9138579
2.033729	1.95609			
LINE 950	62	.714905	.1453123	.203261
.398787				
13.58421	.203261			
LINE 900	2002.16	<i>Printed</i> 2.907376	<i>Printed</i> 1.073079	<i>Printed</i> .9188803
2.035981 <i>Scan</i>	1.95609 <i>Printed</i>	<i>Volume</i> 7.115489	<i>total volume</i> 14.19561	<i>pages</i> .199503
LINE 950	63			
1.405385				
13.80429 <i>stars</i>	.199503			
14.8	.1825007			

Press any key to continue

Side Calculation 2/28/95 - Show the correspondence between the constant for cement sorbent in SAND 90-1206, Section 2.4.4.1, in units of MPa, and that used in the COMPRESS program, which is in units of psi.

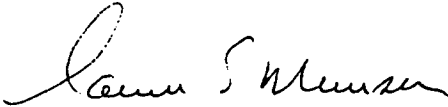
$$\rho := 3.0 \cdot \left[1 + \frac{\ln \left[\frac{13.80429}{15700} \right]}{21.9} \right]$$

$$\rho = 2.036$$

$$\frac{15700}{0.0068947} = 2.277 \cdot 10^6$$

date: 09/26/95

to: M.S. Tierney, 6741 (1328)

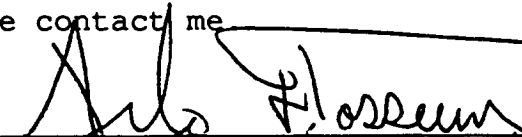

from: D.E. Munson, 6121 (1322)

subject: Mechanical Parameters for Update of Reference Data Report

I have attached the best current set of mechanical parameters for use in the Reference Data Report update (essentially an update to the PA 92, Volume 3). These parameters are those in current use for thermal/structural calculations in the Rock Mechanics Program of the WIPP Project. The parameters are for the Multimechanism Deformation Coupled Fracture (MDCF) Model, which, in the absence of fracture, reduces to the previously given Multimechanism Deformation (M-D) Model. The parameter set for the model includes both clean and argillaceous salt. The parameter set, together with the respective constitutive descriptions, are permissible for the purposes of performance assessment. I have also included a set of parameters consistent with the Reduced Modulus (R-M) steady state creep model which has been used in the past. Although no longer recommended for future WIPP calculations, use of the R-M model historical calculations is permitted provided they are adequately verified for the specific calculation against the more precise M-D model which includes both steady state and transient creep.

These parameters will be updated as necessary in subsequent inputs to the Compliance Application process. Specifically, both a healing kinetics and a damage-permeability relationship will be incorporated into the MDCF model.

If you have any questions, please contact me

Reviewed: 
A. F. Fossum, 1517 9/25/95

Reviewed: 
J. R. Tillerson, 6121 9/25/95

Copy to:
0443 A. F. Fossum, 1517
1322 J. R. Tillerson, 6121
1395 M. Marietta, 6707
SWCF-A:1.1.3.4.5:PA:TSI/PROP:rock mechanics model parameters

2.5 Mechanical Parameters for Material in Salado Formation

2.5.1 Halite and Argillaceous Halite

Elastic Constants (Halite and Argillaceous Halite)

Parameter*	Nominal	Range	Units	Distribution	Source
Shear Modulus, μ	12.4		GPa		2.5.1
Young's Modulus, E	31.0		GPa		2.5.1
Poisson's Ratio, ν	0.25				2.5.1

Source(s): 2.5.1. Munson, D. E., A. F. Fossum, and P. E. Senseny. 1989. Advances in Resolution of Discrepancies between Predicted and Measured In Situ Room Closures. SAND88-2948. Albuquerque, NM: Sandia National Laboratories.

* Note that any two independent elastic constants are sufficient to define the mechanical response, with all the others simply derived from the two given values.

Creep Constants - MDCF Model (Halite)

Parameter	Nominal	Range**	Units	Distribution**	Source
A ₁	8.386 E22		/s		2.5.2
Q ₁	25		Kcal/mol		2.5.2
n ₁	5.5				2.5.2
B ₁	6.086 E06		/s		2.5.2
A ₂	9.672 E12		/s		2.5.2
Q ₂	10		Kcal/mol		2.5.2
n ₂	5.0				2.5.2
B ₂	3.034 E-2		/s		2.5.2
σ_0	20.57		MPa		2.5.2
q	5.335 E03				2.5.2
m	3.0				2.5.2
K ₀	6.275 E05				2.5.2

c	9.198 E-3	/T	2.5.2
α_w	-17.37		2.5.2
β_w	-7.738		2.5.2
α_r	-2.69		2.5.3
β_r	-1.00		2.5.3
R	1.987	cal/mol-deg	2.5.4

**Distribution functions for the halite (clean salt) parameters have been determined [2.5.1]; however, the evaluation procedure is complicated and the results cannot be presented in tabular form.

- Source(s) :
- 2.5.1. Fossum, A. F., T. W. Pfeifle, K. D. Mellegard, and D. E. Munson. 1994. Probability Distributions for Parameters of the Munson-Dawson Salt Creep Model. Proc. 1st N. Am. Rock Mechanics Symp. Brookfield, MA: pp. 715-722.
 - 2.5.2. Munson, D. E., A. F. Fossum, and P. E. Senseny. 1989. Advances in Resolution of Discrepancies between Predicted and Measured, In Situ Room Closures. SAND88-2948. Albuquerque, NM: Sandia National Laboratories.
 - 2.5.3. WIPP Project. 1992. Preliminary Performance Assessment for the Waste Isolation Pilot Plant, December 1992, Volume 3: Model Parameters. SAND92-0700/3. Albuquerque, NM: Sandia National Laboratories. pp. A109-A123.
 - 2.5.4. Munson, D. E., and P. R. Dawson. 1979. Constitutive Model for the Low Temperature Creep of Salt (with Application to WIPP). Sand79-1853. Albuquerque, NM: Sandia National Laboratories.
 - 2.5.5. Fossum, A. F., and D. E. Munson. 1995. Reliability Assessment of Underground Shaft Closure. Proc. 10th Eng. Mech. Conf. New York, NY: ASCE. pp. 345-348.
 - 2.5.6. Munson, D. E. 1979. Preliminary Deformation-Mechanism Map for Salt (with Application to WIPP). SAND79-0076. Albuquerque, MN: Sandia National Laboratories.
 - 2.5.7. Fossum, A. F., G. D. Callahan, L. L. Van Sambeek, and P. E. Senseny. 1988. How Should One-Dimensional Laboratory Equations be Cast into Three-Dimensional Form? Proc. 29th U. S. Symp. on Rock Mech. Brookfield, MA: Balkema. pp. 35-41.
 - 2.5.8. Munson, D. E., and P. E. Dawson. 1982. A Transient Creep Model for Salt during Stress Loading

- and Unloading. SAND82-0962. Albuquerque, NM: Sandia National Laboratories.
- 2.5.9. Mellegard, K. D., G. D. Callahan, and P. E. Senseny. 1992. Multiaxial Creep of Natural Rock Salt. SAND91-7083. Albuquerque, NM: Sandia National Laboratories.
- 2.5.10. Callahan, G. D., A. F. Fossum, and D. K. Svalstad. 1986. Documentation of SPECTROM-32: a Finite Element Thermomechanical Stress Analysis Program. RSI-0269. Rapid City, SD: RE/SPEC Inc.
- 2.5.11. Biffle, J. H. 1993. JAC3D-A Three-Dimensional Finite Element Computer Program for the Nonlinear Quasistatic Response of Solids with the Conjugate Gradient Method. SAND87-1305. Albuquerque, NM: Sandia National Laboratories.
- 2.5.12. Munson, D. E., and K. L. DeVries. 1991. Development and Validation of a Predictive Technology for Creep Closure of Underground Rooms in Salt. Proc. 7th International Congress on Rock Mechanics. Rotterdam, The Netherlands: A. A. Balkema. pp. 127-134. [SAND90-1147].
- 2.5.13. Munson, D. E., K. L. DeVries, D. M. Schiermeister, W. F. DeYonge, and R. L. Jones. 1992. Measured and Calculated Closures of Open and Brine Filled Shafts and Deep Vertical Boreholes in Salt. Proc. 33rd U. S. Symp. on Rock Mechanics. Brookfield, MA: A. A. Balkema. pp. 439-448.
- 2.5.14. Munson, D. E., J. R. Weatherby, and K. L. DeVries. 1993. Two- and Three-Dimensional Calculations of Scaled In Situ Tests using the M-D Model of Salt Creep. Int'l J. Rock Mech. Min. Sci. & Geomech. Abstr. 30. pp. 1345-1350.

Creep Constants - MDCF Model (Argillaceous Halite)

Parameter	Nominal	Range**	Units	Distribution**	Source
A ₁	1.407 E23		/s		2.5.2
Q ₁	25		Kcal/mol		2.5.2
n ₁	5.5				2.5.2
B ₁	8.998 E06		/s		2.5.2
A ₂	1.314 E13		/s		2.5.2
Q ₂	10		Kcal/mol		2.5.2
n ₂	5.0				2.5.2
B ₂	4.289 E-2		/s		2.5.2
σ ₀	20.57		MPa		2.5.2

q	5.335 E03		2.5.2
m	3.0		2.5.2
K ₀	2.470 E06		2.5.2
c	9.198 E-3	/T	2.5.2
α_w	-14.96		2.5.2
β_w	-7.738		2.5.2
α_r	-2.69		2.5.3
β_r	-1.00		2.5.3
R	1.987	cal/mol-deg	2.5.4

**Distribution functions for the argillaceous salt parameters have been determined [2.5.5]; however, the evaluation procedure is complicated and the results cannot be presented in tabular form.

- Source(s):
- 2.5.1. Fossum, A. F., T. W. Pfeifle, K. D. Mellegard, and D. E. Munson. 1994. Probability Distributions for Parameters of the Munson-Dawson Salt Creep Model. Proc. 1st N. Am. Rock Mechanics Symp. Brookfield, MA: pp. 715-722.
 - 2.5.2. Munson, D. E., A. F. Fossum, and P. E. Senseny. 1989. Advances in Resolution of Discrepancies between Predicted and Measured In Situ Room Closures. SAND88-2948. Albuquerque, NM: Sandia National Laboratories.
 - 2.5.3. WIPP Project. 1992. Preliminary Performance Assessment for the Waste Isolation Pilot Plant, December 1992, Volume 3: Model Parameters. SAND92-0700/3. Albuquerque, NM: Sandia National Laboratories. pp. A109-A123.
 - 2.5.4. Munson, D. E., and P. R. Dawson. 1979. Constitutive Model for the Low Temperature Creep of Salt (with Application to WIPP). Sand79-1853. Albuquerque, NM: Sandia National Laboratories.
 - 2.5.5. Fossum, A. F., and D. E. Munson. 1995. Reliability Assessment of Underground Shaft Closure. Proc. 10th Eng. Mech. Conf. New York, NY: ASCE. pp. 345-348.
 - 2.5.6. Munson, D. E. 1979. Preliminary Deformation-Mechanism Map for Salt (with Application to WIPP). SAND79-0076. Albuquerque, MN: Sandia National Laboratories.
 - 2.5.7. Fossum, A. F., G. D. Callahan, L. L. Van Sambeek, and P. E. Senseny. 1988. How Should One-Dimensional Laboratory Equations be Cast into Three-

- Dimensional Form? Proc. 29th U. S. Symp. on Rock Mech. Brookfield, MA: Balkema. pp. 35-41.
- 2.5.8. Munson, D. E., and P. E. Dawson. 1982. A Transient Creep Model for Salt during Stress Loading and Unloading. SAND82-0962. Albuquerque, NM: Sandia National Laboratories.
- 2.5.9. Mellegard, K. D., G. D. Callahan, and P. E. Senseny. 1992. Multiaxial Creep of Natural Rock Salt. SAND91-7083. Albuquerque, NM: Sandia National Laboratories.
- 2.5.10. Callahan, G. D., A. F. Fossum, and D. K. Svalstad. 1986. Documentation of SPECTROM-32: a Finite Element Thermomechanical Stress Analysis Program. RSI-0269. Rapid City, SD: RE/SPEC Inc.
- 2.5.11. Biffle, J. H. 1993. JAC3D-A Three-Dimensional Finite Element Computer Program for the Nonlinear Quasistatic Response of Solids with the Conjugate Gradient Method. SAND87-1305. Albuquerque, NM: Sandia National Laboratories.
- 2.5.12. Munson, D. E., and K. L. DeVries. 1991. Development and Validation of a Predictive Technology for Creep Closure of Underground Rooms in Salt. Proc. 7th International Congress on Rock Mechanics. Rotterdam, The Netherlands: A. A. Balkema. pp. 127-134. [SAND90-1147].
- 2.5.13. Munson, D. E., K. L. DeVries, D. M. Schiermeister, W. F. DeYonge, and R. L. Jones. 1992. Measured and Calculated Closures of Open and Brine Filled Shafts and Deep Vertical Boreholes in Salt. Proc. 33rd U. S. Symp. on Rock Mechanics. Brookfield, MA: A. A. Balkema. pp. 439-448.
- 2.5.14. Munson, D. E., J. R. Weatherby, and K. L. DeVries. 1993. Two- and Three-Dimensional Calculations of Scaled In Situ Tests using the M-D Model of Salt Creep. Int'l J. Rock Mech. Min. Sci. & Geomech. Abstr. 30. pp. 1345-1350.

Fracture Constants - MDCF Model (Halite)

Parameter	Median	Range	Units	Distribution	Source
x_1	6				2.5.15
x_2	9				2.5.15
x_{3s}	5.5				2.5.15
x_{3t}	40				2.5.15
x_4	3				2.5.15
χ_s ($\sigma > \sigma_0$)	231.0		MPa		2.5.15
χ_s ($\sigma \leq \sigma_0$)	351.1		MPa		2.5.15

χ_t	15.15	MPa	2.5.15
x_6	0.75		2.5.15
x_7	1.0	MPa	2.5.15
x_8	0.1		2.5.15
c_0	5 E04		2.5.15
c_2	850		2.5.15
c_3	10		2.5.15
c_4	6		2.5.15
c_5	25	Mpa	2.5.15
t_0	1	s	2.5.15
n_3	3		2.5.15
ω_0	≥ 1 E-4		2.5.15

Source (s) 2.5.15. Chan, K. S., D. E. Munson, A. F. Fossum, and S. F. Bodner. 1995. Inelastic Flow Behavior of Argillaceous Salt. Int'l J. Damage Mechanics (in press). [SAND94-3017].

2.5.16. Chan, K. S., S. R. Bodner, A. F. Fossum, and D. E. Munson. 1992. A Constitutive Model for Inelastic Flow and Damage Evolution in Solids under Triaxial Compression. Mech. Mat. 14.: Elsevier. pp. 1-14.

2.5.17. Chan, K. S., N. S. Brodsky, A. F. Fossum, S. R. Bodner, and D. E. Munson. 1994. Damage-Induced Nonassociated Inelastic Flow in Rock Salt. Int'l J. of Plasticity. 10 : Elsevier Science. pp. 623-642.

2.5.18. Chan, K. S., A. F. Fossum, S. R. Bodner, and D. E. Munson. 1995. Constitutive Representation of Damage Healing in WIPP Salt. Proc. 35th U. S. Symp. on Rock Mechanics. Rotterdam: Balkema. pp. 485-490.

2.5.19. Fossum, A. F., N. S. Brodsky, K. S. Chan, and D. E. Munson. 1993. Experimental Evaluation of a Constitutive Model for Inelastic Flow and Damage Evolution in Solids Subjected to Triaxial Compression. Int'l J. Rock Mech. Min. Sci. & Geomech. Abstr. 30: pp. 1341-1344.

2.5.20. Chan, K. S., K. L DeVries, S. R. Bodner, A. F. Fossum, and D. E. Munson. 1995. A Damage Mechanics Approach to Life Prediction for a Salt Structure. Proc. ICES '95, (Computational Mechanics '95). Berlin: Springer. pp. 1140-1145.

2.5.21. Munson, D. E., D. J. Holcomb, K. L. DeVries, N. S. Brodsky, and K. S. Chan. 1995. Correlation of Theoretical Calculations and Experimental Measurements of Damage Around a Shaft in Salt. Proc. 35th U. S. Symp. on Rock Mechanics. Rotterdam: Balkema. pp. 491-496.

Fracture Constants - MDCF Model (Argillaceous Halite)

Parameter	Nominal	Range	Units	Distribution	Source
x ₁	6				2.5.15
x ₂	9				2.5.15
x _{3s}	5.5				2.5.15
x _{3t}	40				2.5.15
x ₄	3				2.5.15
χ _s (σ > σ ₀)	231.0		MPa		2.5.15
χ _s (σ ≤ σ ₀)	351.1		MPa		2.5.15
χ _t	15.15		MPa		2.5.15
x ₆	0.75				2.5.15
x ₇	1.0		MPa		2.5.15
x ₈	0.1				2.5.15
c ₀	5 E4				2.5.15
c ₂	850				2.5.15
c ₃	10				2.5.15
c ₄	6				2.5.15
c ₅	25		Mpa		2.5.15
t ₀	1		s		2.5.15
n ₃	3				2.5.15
ω ₀	≥1 E-4				2.5.15
p ₁ (ρ _a > 0.0)	20.6				2.5.15

Source(s) 2.5.15. Chan, K. S., D. E. Munson, A. F. Fossum, and S. F. Bodner. 1995. Inelastic Flow Behavior of Argillaceous Salt. Int'l J. Damage Mechanics (in press, SAND94-3017).
 2.5.16. Chan, K. S., S. R. Bodner, A. F. Fossum, and D. E. Munson. 1992. A Constitutive Model for Inelastic Flow and Damage Evolution in Solids under Triaxial Compression. Mech. Mat. 14.: Elsevier. pp. 1-14.
 2.5.17. Chan, K. S., N. S. Brodsky, A. F. Fossum, S. R. Bodner, and D. E. Munson. 1994. Damage-Induced Nonassociated Inelastic Flow in Rock Salt. Int'l J. of Plasticity. 10 : Elsevier Science. pp. 623-642.
 2.5.18. Chan, K. S., A. F. Fossum, S. R. Bodner, and D. E. Munson. 1995. Constitutive Representation of Damage Healing in WIPP Salt. Proc. 35th U. S. Symp. on Rock Mechanics. Rotterdam: Balkema. pp. 485-490.
 2.5.19. Fossum, A. F., N. S. Brodsky, K. S. Chan, and

D. E. Munson. 1993. Experimental Evaluation of a Constitutive Model for Inelastic Flow and Damage Evolution in Solids Subjected to Triaxial Compression. Int'l J. Rock Mech. Min. Sci. & Geomech. Abstr. 30: pp. 1341-1344.

2.5.20. Chan, K. S., K. L DeVries, S. R. Bodner, A. F. Fossum, and D. E. Munson. 1995. A Damage Mechanics Approach to Life Prediction for a Salt Structure. Proc. ICES '95, (Computational Mechanics '95). Berlin: Springer. pp. 1140-1145.

2.5.21. Munson, D. E., D. J. Holcomb, K. L. DeVries, N. S. Brodsky, and K. S. Chan. 1995. Correlation of Theoretical Calculations and Experimental Measurements of Damage Around a Shaft in Salt. Proc. 35th U. S. Symp. on Rock Mechanics. Rotterdam: Balkema. pp. 491-496.

Discussion:

The constitutive model for salt creep and fracture now recommended for use in WIPP structural calculations is the most recent formulation of the Multimechanism Deformation Coupled Fracture (MDCF) model [2.4.15]. This MDCF model is to be used in those cases where the occurrence of damage or microfractures is important, such as in the damaged rock zone (DRZ). However, in those cases where only the continuum creep process is important and the damage contribution of the MDCF model can be suppressed, the MDCF model reduces identically to that of the original extended Multimechanism Deformation (M-D) model of creep [2.5.1]. Thus, previous calculations with the extended M-D model are included within the framework of the now recommended MDCF model.

The clean and argillaceous salt (halite) material parameters for creep and fracture given above are the nominal or engineering values, as obtained through fitting of data in a consistent manner and as governed by theoretical guidance and restrictions. These parameter values are consistent with, but not identical to, the median and mean values of distribution functions obtained, where possible, from the data. The determination of distribution functions from sparse creep databases has been accomplished for both clean [2.5.1] and argillaceous [2.5.5] salt. The remainder of the material parameters are nominal or engineering values.

The current creep and fracture model incorporates and is an extension of the Modified Multimechanism Deformation (M-D) steady state creep model, with workhardening/recovery transients, proposed in PA 92 [2.5.3] for WIPP structural calculations. The fracture aspect of the MDCF model [2.5.15] now permits the tertiary, or accelerated, creep transient response to be modeled in addition to the steady state with workhardening/recovery transients. The MDCF

model is based on the mechanism maps for creep [2.5.6] and fracture [2.5.16] as they pertain to the temperature, stress, and pressure conditions of the potential WIPP repository. From the mechanism maps, the individual mechanisms that can be expected to contribute to the WIPP storage room creep response are (1) a high stress dislocation slip, (2) a mechanistically undefined but empirically specified, low temperature, low stress creep, and (3) a high temperature, low stress dislocation climb creep. The three fracture mechanisms are (1) low stress, stress rupture, (2) high stress, brittle intergranular fracture, and (3) low confining pressure, cleavage fracture. In the MDCF model [2.5.15], the creep strains add directly to the fracture induced strains to give the overall total creep strain. Coupling occurs because the formation of damage (microfractures) reduces the effective load bearing area and hence increases the effective stress driving the creep process. Further coupling occurs because the evolution of the damage depends upon the transient creep strain rate [2.5.17].

This coupled creep and damage induced flow behavior can be described in terms of the generalized kinetic equation [2.5.7, 2.5.18]

$$\dot{\epsilon}_{ij}^I = \frac{\partial \sigma_{eq}^c}{\partial \sigma_{ij}} \dot{\epsilon}_{eq}^c + \frac{\partial \sigma_{eq}^{\omega_s}}{\partial \sigma_{ij}} \dot{\epsilon}_{eq}^{\omega_s} + \frac{\partial \sigma_{eq}^{\omega_f}}{\partial \sigma_{ij}} \dot{\epsilon}_{eq}^{\omega_f} + \frac{\partial \sigma_{eq}^h}{\partial \sigma_{ij}} \dot{\epsilon}_{eq}^h \quad (1)$$

where $\dot{\epsilon}_{ij}^I$ is the total inelastic strain rate and σ_{eq}^c , $\sigma_{eq}^{\omega_s}$, and $\sigma_{eq}^{\omega_f}$ are the power-conjugate equivalent stress measures for dislocation creep, shear damage, and tensile damage, respectively. The $\dot{\epsilon}_{eq}^c$,

$\dot{\epsilon}_{eq}^{\omega_s}$, and $\dot{\epsilon}_{eq}^{\omega_f}$ are the conjugate equivalent inelastic strain rates.

The last term in Eq. 1 concerns the healing aspects of damage. Although experimental [2.5.19] and constitutive modeling [2.5.18] efforts to define the healing response have been completed, the results have not yet been incorporated into the numerical codes and will not be discussed further in this document.

Continuum Creep: The creep portion of Eq. 1 is treated first. Here, we follow directly the development given by Munson et al. [2.5.1] and PA 92 [2.5.3] for the extended M-D model, but make the straightforward modifications to the stress terms necessary for the MDCF model [2.5.15]. The kinetic equation for representing the creep rate, $\dot{\epsilon}_{eq}^c$, resulting from dislocation mechanisms is given by

$$\dot{\epsilon}_{eq}^c = F \sum_{i=1}^3 \dot{\epsilon}_{si} \quad (2)$$

where F is the function representing transient behavior and the summation of $\dot{\epsilon}_{s_i}$ is the sum of the steady state creep rates of the three thermally activated mechanisms from the mechanism map that are controlling for the stress and temperature conditions of the WIPP repository.

The steady state creep rates of the individual mechanisms are [2.5.1]

$$\dot{\epsilon}_{s_1} = A_1 e^{-Q_1/RT} \left(\frac{\sigma_{eq}^c}{\mu(1-\omega)} \right)^{n_1} \quad (3a)$$

$$\dot{\epsilon}_{s_2} = A_2 e^{-Q_2/RT} \left(\frac{\sigma_{eq}^c}{\mu(1-\omega)} \right)^{n_2} \quad (3b)$$

$$\dot{\epsilon}_{s_3} = H \left(B_1 e^{-Q_1/RT} + B_2 e^{-Q_2/RT} \right) \sinh \left[\frac{q \left(\frac{\sigma_{eq}^c}{(1-\omega)} - \sigma_0 \right)}{\mu} \right] \quad (3c)$$

where the A_i 's and B_i 's are constants; Q_i 's are the activation energies; T is the absolute temperature; R is the universal gas constant; μ is the shear modulus; n_i 's are the stress exponents; q is a stress constant; and σ_0 is the stress limit of the dislocation slip mechanism. H is the Heaviside function with an argument of $[(\sigma_{eq}^c/(1-\omega)) - \sigma_0]$. The damage, ω , is coupled into these rate equations through a term in the denominator of the stress term which represents the decrease in load bearing area with damage [2.5.15]. The dislocation climb mechanism, designated by subscript 1, dominates at low stress and high temperature. The undefined mechanism, designated by subscript 2, although it has no associated micromechanical model, is well defined empirically on the basis of laboratory testing and dominates at low stress and temperatures. This mechanism is also the most likely controlling mechanism over most of the range of the WIPP underground conditions. The glide mechanism, denoted by subscript 3, is dominant at high stress for all temperatures.

The transient function, F , has been developed by considering the change in strain rate with strain, during either workhardening or recovery, as the transient strain evolves to a steady state condition. The transient response is described in terms of an

internal variable, ζ , whose value increases in workhardening and decreases in recovery to the transient strain limit, ε_i^* . Thus, the transient function is composed of a workhardening branch, an equilibrium branch, and a recovery branch [2.5.8], and is given by

$$F = \begin{cases} \exp\left[\Delta\left(1-\frac{\zeta}{\varepsilon_i^*}\right)\right]^2, & \zeta \leq \varepsilon_i^* \\ 1, & \zeta = \varepsilon_i^* \\ \exp\left[-\delta\left(1-\frac{\zeta}{\varepsilon_i^*}\right)\right]^2, & \zeta \geq \varepsilon_i^* \end{cases} \quad (4)$$

where Δ and δ represent the workhardening and recovery parameters, respectively, and ζ is the internal state variable. Temperature dependence of the transient strain limit, ε_i^* , is represented by

$$\varepsilon_i^* = K_0 e^{cT} \left[\frac{\sigma_{eq}^c}{\mu(1-\omega)} \right]^m \quad (5)$$

where K_0 , c , and m are constants. The evolution rate of the internal state variable, ζ , is governed by

$$\dot{\zeta} = (F-1)\dot{\varepsilon}_s \quad (6)$$

which diminishes to zero as the steady state condition is achieved.

The conjugate equivalent stress measure, σ_{eq}^c , for non-dilatant continuum creep flow resulting from dislocation mechanisms is the Tresca equivalent stress,

$$\sigma_{eq}^c = |\sigma_1 - \sigma_3| \quad (7)$$

where σ_1 and σ_3 are the maximum and minimum principal stresses, respectively. The Tresca equivalent stress measure is preferred over the von Mises measure because experimental creep measurements of the flow surface and inelastic strain rate vector are in better agreement with the former measure [2.5.9].

Note that Eqs. 2-7 represent the continuum creep part of the

MDCF model and, when ω is zero, reduces to the M-D model presented in PA 92 [2.5.3]. The ω appearing in Eqs. 2-7 is the Kachanov damage variable and when represented by an appropriate evolutionary equation describes the effect on continuum creep caused by an increase in stress through a reduction of load bearing area.

Initially, the continuum creep behavior as given by the extended M-D model was incorporated into both a two-dimensional finite element code, SPECTROM-32 [2.5.10], and a three-dimensional finite element code, JAC-3D [2.5.11]. These codes and the model have been used to simulate, with success, the measured room closure of a number of large scale in situ tests, in both two-dimensional [2.5.12, 2.5.13] and three-dimensional [2.5.14] geometries.

As indicated in the tables, the distribution functions of the critical parameters have been determined for clean [2.5.2] and argillaceous salt [2.5.5]. These distribution functions were used further with Fast Probability Integration methods to demonstrate the calculation of distribution functions for shaft closure.

Fracture: The fracture processes are considered as separate mechanisms, distinct from those of dislocation mechanism induced, nondilatant strain. However, the mechanisms are coupled in the process of salt deformation and the strains attributed to the dislocation induced strain and the fracture induced strain are additive. In the fracture process, microfractures, envisioned to preexist or to be induced during salt creep, are considered to exhibit sliding by shear during creep at low or zero confining pressure, resulting in a deviatoric strain rate. Furthermore, some of the sliding microfractures may develop wing-tip cracks, whose opening leads to a dilational strain rate. Thus, fracture response of salt exhibits both deviatoric and dilational characteristics. Opening of the cracks is logically a pressure dependent process, which causes the damage induced inelastic flow to depend upon the pressure [2.5.15, 2.5.16].

The kinetic equation of damage induced inelastic flow is given by [2.5.15, 2.5.17]

$$\dot{\epsilon}_{ed}^{\omega_i} = F \omega_i \dot{\epsilon}_s^{\omega_i} \quad (8)$$

where $i = s$ or t for shear or tensile damage, respectively, and

$$F \omega_s = F \exp\left(\frac{c_4(\sigma_{eq}^c - c_5)}{\sigma_0}\right) \quad (9a)$$

and

$$F\omega_t = F \exp\left(\frac{c_4(\sigma_{eq}^{\omega_i} - c_5)}{\sigma_0}\right) \quad (9b)$$

are the transient functions for shear and tensile damage induced flow, respectively. The kinetic equations for the flow, $\dot{\epsilon}_s^{\omega_i}$, during steady state creep are

$$\dot{\epsilon}_s^{\omega_i} = c_1 \omega_0 e^{c_3 \omega} \left[\sinh\left(\frac{c_2 \sigma_{eq}^{\omega_i} H(\sigma_{eq}^{\omega_i})}{(1-\omega)(1-\rho_a)}\right) \right]^{n_3} \quad (10a)$$

with $i = s$ or t , for shear and tensile damage, respectively, and

$$c_1 = c_0 (B_1 e^{-Q_1/RT} + B_2 e^{-Q_2/RT}) \quad (10b)$$

where c_0 , c_2 , c_3 , c_4 , c_5 and n_3 are material constants. The initial damage, ω_0 , is either an assumed small value (0.0001 is used) or the actual initial value of the damage variable, ω . The B_i 's and Q_i 's are the constants for the dislocation slip mechanism. This form of kinetic equations allows $\dot{\epsilon}_s^{\omega_i}$ to exhibit a transient

behavior by virtue of the transient function, $F\omega_i$, which is directly coupled to the transient function, F , for creep.

Damage development is described by the damage evolution equation [2.5.15]

$$\dot{\omega} = \frac{x_4}{t_0} \left[\ln\left(\frac{1}{\omega}\right) \right]^{-\frac{x_4+1}{x_4}} \left\{ \left[\frac{\sigma_{eq}^{\omega_i} H(\sigma_{eq}^{\omega_i})}{(1-\rho_a)\chi_s} \right]^{x_5} + \left[\frac{\sigma_{eq}^{\omega_i} H(\sigma_{eq}^{\omega_i})}{(1-\rho_a)\chi_t} \right]^{x_5} \right\} - h(\omega, T, I_1) \quad (11)$$

where x_{3i} , x_4 , x_5 , χ_i (with $i = s$ or t for shear or tensile damage, respectively) are material constants, t_0 is a reference time, and $h(\omega, T, I_1)$ is the damage healing function whose exact form remains to be determined. While the last term of Eq. 11 is not treated in this memo because it is not yet ready for inclusion in the model, the appropriate form of $h(\omega, T, I_1)$ for WIPP salt has been a subject of experimental [2.5.19] and theoretical [2.5.18] investigations.

The use of the scalar damage variable, ω , for representing creep damage due to sliding of microfractures is valid as long as the microfractures are randomly oriented. Thus, shear induced damage may be reasonably described in terms of a scalar quantity.

On the other hand, wing tip cracks typically develop and align with a preferential direction parallel to the minimum compressive stress. Such a flow anisotropy is not normally utilized in the modeling, even though a method has been developed for its treatment [2.5.15]. This special treatment is not considered further, here.

The damage evolution of Eq. 11 is generally integrated with respect to time after loading. This requires some initial value of damage. Thus, ω_0 is assumed equal to 0.0001, if there is no actual damage, or is taken as the actual amount of preexisting damage, if there is initial damage. For creep under constant triaxial compression or extension and with no initial damage (or healing), integration of Eq. 11 gives

$$\omega = \exp \left[- \left(\frac{\lambda_s^{x_2} t_0}{[\sigma_{eq}^{\omega_s} H(\sigma_{eq}^{\omega_s})]^{x_2} t} \right)^{x_4} \right] \quad (12)$$

at some elapsed time, t , after loading.

The conjugate equivalent stress measure, $\sigma_{eq}^{\omega_s}$, for the shear form of damage, as required in the kinetic equation, Eq. 10a, and in the damage evolution equation, Eq. 11, is given by

$$\sigma_{eq}^{\omega_s} = |\sigma_1 - \sigma_3| - f x_2 x_7 \operatorname{sgn}(I_1 - \sigma_1) \left[\frac{I_1 - \sigma_1}{3 x_7 \operatorname{sgn}(I_1 - \sigma_1)} \right]^{x_4} \quad (13)$$

where I_1 is the first invariant of the Cauchy stress, the x_i 's are material constants, and the σ_i 's are principal stresses. Here $\operatorname{sgn}()$ is the signum function. The influence of the argillaceous particles in the salt matrix is to act as local sites of stress concentration which effectively lower the confining pressure. Additional microfractures can then form at the sites. This is represented as a linear approximation to a more detailed function [2.5.15], as

$$f = 1 - p_1 \rho_a \quad (14)$$

where p_1 is a material constant and ρ_a is the argillaceous content by volume.

Because the damage induced inelastic flow was found to be nonassociated [2.5.17], a different conjugate equivalent stress measure, $[\sigma_{eq}^{\omega_s}]_f$, is used in conjunction with Eq. 1 to obtain the flow law. Thus, the nonassociated flow for shear induced damage

is given by

$$[\sigma_{eq}^{w_i}]_f = |\sigma_1 - \sigma_3| - \frac{x_2 x_3}{3} [I_1 - \sigma_1] \quad (15)$$

where x_8 is a constant.

The conjugate equivalent stress measure, $\sigma_{eq}^{w_i}$, for the tensile form of damage is given by

$$\sigma_{eq}^{w_i} = -x_1 \sigma_3 H(-\sigma_3) \quad (16)$$

where x_1 is a material constant and H is the Heaviside function with a least principal stress argument, σ_3 , which is a tensile stress.

The fracture aspects have been incorporated into the finite element codes, SPECTROM 32 [2.5.10] and JAC3D [2.5.11]. The MDCF model has been used to simulate the formation of the damaged rock zone (DRZ) around a typical storage room [2.5.20]. This simulation also predicts, rather crudely, the life to failure of the room. The model has also been used to predict the formation of the DRZ around the air intake shaft for comparison to measured ultrasonic quantities indicative of damage [2.5.21].

Elastic Constants - R-M Model (Halite and Argillaceous Halite)

Parameter*	Nominal	Range	Units	Distribution	Source
Shear Modulus, μ	0.992		GPa		2.5.22
Young's Modulus, E	2.480		GPa		2.5.22
Bulk Modulus, K	1.656		GPa		2.5.22
Poisson's Ratio, ν	0.25				2.5.23

Source(s): 2.5.22. Morgan, H. S., C. M. Stone, and R. D. Krieg. 1985. The Use of Field Data to Evaluate and Improve Drift Response Model for the Waste Isolation Pilot Plant (WIPP). Proc. 26th U. S. Symp. on Rock Mechanics. Boston, MA: Balkema. pp. 769-776.
 2.5.23. Krieg, R. D. 1984. Reference Stratigraphy and Rock Properties for the Waste Isolation Pilot Plant (WIPP) Project. SAND83-1908. Albuquerque, NM: Sandia National Laboratories.

*Note that any two independent elastic constants are sufficient to define the response, with all the others simply derived from

the two given values.

Creep Constants - R-M Model (Clean Halite)

Parameter	Nominal	Range	Units	Distribution	Source
A	1.66 E14		/s		2.5.24
Q	12		Kcal/mol		2.5.23
n	4.9				2.5.23

Source(s): 2.5.23. Krieg, R. D. 1984. Reference Stratigraphy and Rock Properties for the Waste Isolation Pilot Plant (WIPP) Project. SAND83-1908. Albuquerque, NM: Sandia National Laboratories.
2.5.24. Ehgartner, B. L. and D. E. Munson. 1992. This parameter is derived from values of D, u, and n found in Krieg [2.5.23]. Albuquerque, NM: Sandia National Laboratories.
2.5.25. Stone, C. M., R. D. Krieg, and Z. E. Beisinger. 1985. SANCHO - A Finite Element, Computer Program for the Quasistatic, Large Deformation, Inelastic Response of Two-Dimensional Solids. SAND84-1618. Albuquerque, NM: Sandia National Laboratories.

Creep Constants - R-M Model (Argillaceous Halite)

Parameter	Nominal	Range	Units	Distribution	Source
A	4.99 E14		/s		2.5.24
Q	12		Kcal/mol		2.5.23
n	4.9				2.5.23

Source(s): 2.5.23. Krieg, R. D. 1984. Reference Stratigraphy and Rock Properties for the Waste Isolation Pilot Plant (WIPP) Project. SAND83-1908. Albuquerque, NM: Sandia National Laboratories.
2.5.24. Ehgartner, B. L. and D. E. Munson. 1992. This parameter is derived from values of D, u, and n found in Krieg [2.5.23]. Albuquerque, NM: Sandia National Laboratories.
2.5.25. Stone, C. M., R. D. Krieg, and Z. E. Beisinger. 1985. SANCHO - A Finite Element, Computer Program for the Quasistatic, Large Deformation, Inelastic Response of Two-Dimensional Solids. SAND84-1618. Albuquerque, NM: Sandia National Laboratories.

Discussion:

As is apparent, the Reduced Modulus (R-M) model was developed by an reduction of the elastic moduli of salt [2.5.22]. The elastic constants for this model are obtained by dividing the normal elastic constants by a factor of 12.5, which was obtained by backfitting in situ closure data of the South Drift. Because the reduced moduli values are not within the accepted range of the experimental uncertainty, the reduction is artificial.

The R-M model is based entirely on steady state creep as described by a function of the form of Eq. 3b, which is equivalent to assuming a single thermally activated controlling mechanism. However, evaluation of the parameters of the equation utilized all of the experimental creep data available at the time from both the unknown and climb mechanism regimes of the deformation mechanism map as used in the development of the modified M-D model. As a consequence, the constants do not match those of the steady state portion of the modified M-D model for the unknown mechanism. Because of the use of a single function, the subscripts on the parameters have been dropped.

The general model from which the R-M model was initially taken [2.5.23] also provided for a first order kinetics transient response. The transient part of the model has not been used in WIPP calculations and will not be presented here.

Typically, the R-M model has been used most frequently in conjunction with the SANCHO finite element code [2.5.25]. However, it can be used equally with other finite element codes. In all calculations with the R-M model to date, a von Mises flow criterion has been used.

Thermal Properties (Halite and Argillaceous Halite)

Parameter	Nominal	Range	Units	Distribution	Source
Specific Heat	862.8		J/kg-deg		2.5.26
Coef. Lin. Exp.	45.0 E-6		/deg		2.5.27
λ_{300}	5.40		W/m-deg		2.5.27
γ	1.14				2.5.27
Source(s):	2.5.26. Yang, J. M. 1981. Physical Properties Data for Rock Salt: Chapter 4 - Thermalphysical Properties, NBS Monograph 167. Washington, D.C.: National Bureau of Standards. pp. 205-221. 2.5.27. Sweet, J. N., and J. E. McCreight. 1980. Thermal Conductivity of Rocksalt and Other Geologic Materials for the Site of the Proposed Waste				

Isolation Pilot Plant. SAND79-1665. Albuquerque, NM: Sandia National Laboratories.
 2.5.28. Munson, D. E., and H. S. Morgan. 1986. Methodology for Performing Parallel Design Calculations (Nuclear Waste Repository Application) SAND85-0324. Albuquerque, NM: Sandia National Laboratories.

Discussion:

Thermal conductivity is determined from the equation [2.5.28]

$$\lambda = \lambda_{300} \left(\frac{300}{T} \right)^7 \quad (17)$$

where the temperature, T, is in degrees Kelvin.

2.5.2 Non-Salt Materials

Elastic Constants (Anhydrite)

Parameter*	Nominal	Range	Units	Distribution	Source
Shear Modulus, μ	27.8		GPa		2.5.28
Young's Modulus, E	75.1		GPa		2.5.28
Bulk Modulus, K	83.4		GPa		2.5.28
Poisson's Ratio, ν	0.35				2.5.28

Source(s): 2.5.28. Munson, D. E., and H. S. Morgan. 1986. Methodology for Performing Parallel Design Calculations (Nuclear Waste Repository Application) SAND85-0324. Albuquerque, NM: Sandia National Laboratories.

*Note that any two independent elastic constants are sufficient to define the response, with all the others simply derived from the two given values.

Elastic Constants (Polyhalite)

Parameter*	Nominal	Range	Units	Distribution	Source
Shear Modulus, μ	20.3		GPa		2.5.28

Young's Modulus, E	55.3	GPa	2.5.28
Bulk Modulus, K	65.8	GPa	2.5.28
Poisson's Ratio, v	0.36		2.5.28

Source(s): 2.5.28. Munson, D. E., and H. S. Morgan. 1986. Methodology for Performing Parallel Design Calculations (Nuclear Waste Repository Application). SAND85-0324. Albuquerque, NM: Sandia National Laboratories.

*Note that any two independent elastic constants are sufficient to define the response, with all the others simply derived from the two given values.

Plasticity Parameters - Drucker-Prager Yield Model (Anhydrite)

Parameter	Nominal	Range	Units	Distribution	Source
a	0.45				2.5.28
C	1.35		MPa		2.5.28

Source(s): 2.5.28. Munson, D. E., and H. S. Morgan. 1986. Methodology for Performing Parallel Design Calculations (Nuclear Waste Repository Application). SAND85-0324. Albuquerque, NM: Sandia National Laboratories.

Plasticity Parameters - Drucker-Prager Yield Model (Polyhalite)

Parameter	Nominal	Range	Units	Distribution	Source
a	0.473				2.5.28
C	1.42		MPa		2.5.28
B					

Source(s): 2.5.28. Munson, D. E., and H. S. Morgan. 1986. Methodology for Performing Parallel Design Calculations (Nuclear Waste Repository Application). SAND85-0324. Albuquerque, NM: Sandia National Laboratories.

Discussion:

The Drucker-Prager model is an elastic, perfectly plastic model which has a pressure dependent yield. Typically it is given as

$$\sqrt{J_2} = C - aI_1 \quad (18)$$

where $\sqrt{J_2}$ is the square root of the second invariant of the deviatoric Cauchy stress and I_1 is the first invariant of the Cauchy stress.

Although the Drucker-Prager model has been used extensively to represent anhydrite and polyhalite, the exact nature of the flow of these materials is under further study. In most of the analyses, the mechanical response of the polyhalite can be assumed to be elastic because the polyhalite beds are at large distances from the WIPP horizon. The anhydrite beds however may be very close to the excavations, as in the case of MB139, and it is necessary to determine if the bed material will yield under the condition of the analysis before it may be assumed to be elastic.

Thermal Properties (Anhydrite)

Parameter	Nominal	Range	Units	Distribution	Source
Specific Heat	733.3		J/kg-deg		2.5.26
Coef. Lin. Exp.	20.0 E-6		/deg		2.5.29
λ_{300}	4.70		W/m-deg		2.5.29
γ	1.15				2.5.29
Source(s):	2.5.26. Yang, J. M. 1981. Physical Properties Data for Rock Salt: Chapter 4 - Thermalphysical Properties, NBS Monograph 167. Washington, D.C.: National Bureau of Standards. pp. 205-221. 2.5.27. Sweet, J. N., and J. E. McCreight. 1980. Thermal Conductivity of Rocksalt and Other Geologic Materials for the Site of the Proposed Waste Isolation Pilot Plant. SAND79-1665. Albuquerque, NM: Sandia National Laboratories. 2.5.28. Munson, D. E., and H. S. Morgan. 1986. Methodology for Performing Parallel Design Calculations (Nuclear Waste Repository Application). SAND85-0324. Albuquerque, NM: Sandia National Laboratories. 2.5.29. Moss, M., and G. M. Haseman, 1981. Thermal Conductivity of Polyhalite and Anhydrite from the Site of the Proposed Waste Isolation Pilot Plant. SAND81-0856. Albuquerque, NM: Sandia National Laboratories.				

Discussion:

The thermal conductivity is determined from Eq. 17 [2/5/28], as given previously.

Thermal Properties (Polyhalite)

Parameter	Nominal	Range	Units	Distribution	Source
Specific Heat	890.0		J/kg-deg		2.5.26
Coef. Lin. Exp.	24.0 E-6		/deg		2.5.29
λ_{300}	0.35		W/m-deg		2.5.29
γ	1.14				2.5.29
Source(s):	2.5.26. Yang, J. M. 1981. Physical Properties Data for Rock Salt: Chapter 4 - Thermalphysical Properties, NBS Monograph 167. Washington, D.C.: National Bureau of Standards. pp. 205-221. 2.5.27. Sweet, J. N., and J. E. McCreight. 1980. Thermal Conductivity of Rocksalt and Other Geologic Materials for the Site of the Proposed Waste Isolation Pilot Plant. SAND79-1665. Albuquerque, NM: Sandia National Laboratories. 2.5.28. Munson, D. E., and H. S. Morgan. 1986. Methodology for Performing Parallel Design Calculations (Nuclear Waste Repository Application). SAND85-0324. Albuquerque, NM: Sandia National Laboratories. 2.5.29. Moss, M., and G. M. Haseman, 1981. Thermal Conductivity of Polyhalite and Anhydrite from the Site of the Proposed Waste Isolation Pilot Plant. SAND81-0856. Albuquerque, NM: Sandia National Laboratories.				

Discussion:

The thermal conductivity is determined from Eq. 17 [2.5.28], as given previously.

2.5.3 Interbed Mechanical Response Parameter

Parameter	Nominal	Range	Units	Distribution	Source
Coef. Friction	0.2				2.5.1
Source(s):	2.5.1. Munson, D. E., A. F. Fossum, and P. E. Senseny. 1989. Advances in Resolution of Discrepancies				

between Predicted and Measured In Situ Room Closures. SAND88-2948. Albuquerque, NM: Sandia National Laboratories.

Discussion:

The very thin interbeds that occur in the stratigraphy (as given later in Figure 2.5-1) between the major layers of salt, argillaceous salt, anhydrite, and polyhalite. These interbeds consist of either anhydrite or clay, or mixtures of these components. In structural calculations, it is not possible to model these thin interbeds as discrete layers. As a consequence, they are handled as slip planes in the numerical codes. These slip planes have a coefficient of friction assigned to them which appears to be correct based on underground observations.

2.5.4 Non-Material Input Parameters

Initial Overburden Weight (Averaged)

Parameter	Nominal	Range	Units	Distribution	Source
Weight, G	22710		Pa/m		2.5.23
Source(s):	2.5.23. Krieg, R. D. 1984. Reference Stratigraphy and Rock Properties for the Waste Isolation Pilot Plant (WIPP) Project. SAND83-1908. Albuquerque, NM: Sandia National Laboratories.				

Discussion:

The lithostatic overburden pressure, P at any depth, H, is given by [2.5.23]

$$P = GH \tag{19}$$

This function uses parameters based on the integrated densities of the overburden as determined from neutron logs [2.5.23]. For the nominal facility depth of 650.45 m below ground surface, the lithostatic pressure is 14.77 MPa. The lithostatic pressure can be adjusted in an appropriate manner for any other horizon.

Initial Rock Temperature at Facility Horizon

Parameter	Nominal	Range	Units	Distribution	Source
Temperature, T ₀	26.8	+/-0.5	C		2.5.30
Source(s):	2.5.30. Munson, D. E., R. L. Jones, D. L. Hoag, and J. R. Ball. 1987. Heated Axisymmetric Pillar Test (Room H): In Situ Data Report (February 1985 - April 1987. SAND87-2488. Albuquerque, NM: Sandia National Laboratories.				

Discussion:

The temperature was obtained from a single thermocouple placed deep in the formation, laterally away from the excavation of the Room H entry.

Local Stratigraphy for Thermal/Structural Numerical Calculations

Parameter	Nominal	Range	Units	Distribution	Source
Stratigraphy	As given in Figure 2.5-1				2.5.1
Source(s):	2.5.1. Munson, D. E., A. F. Fossum, and P. E. Senseny. 1989. Advances in Resolution of Discrepancies between Predicted and Measured In Situ Room Closures. SAND88-2948. Albuquerque, NM: Sandia National Laboratories.				

Discussion:

The recommended calculational stratigraphy is that given by Munson et al. [2.5.1]. This is shown in Figure 2.5-1 and has a local vertical zero referenced to the anhydrite "b" (Clay G). The location of a excavated storage room at the WIPP repository horizon is also shown. The extent of the given stratigraphy is sufficient for calculations involving single rooms, but must be checked for adequacy of extent before larger simulations are made.

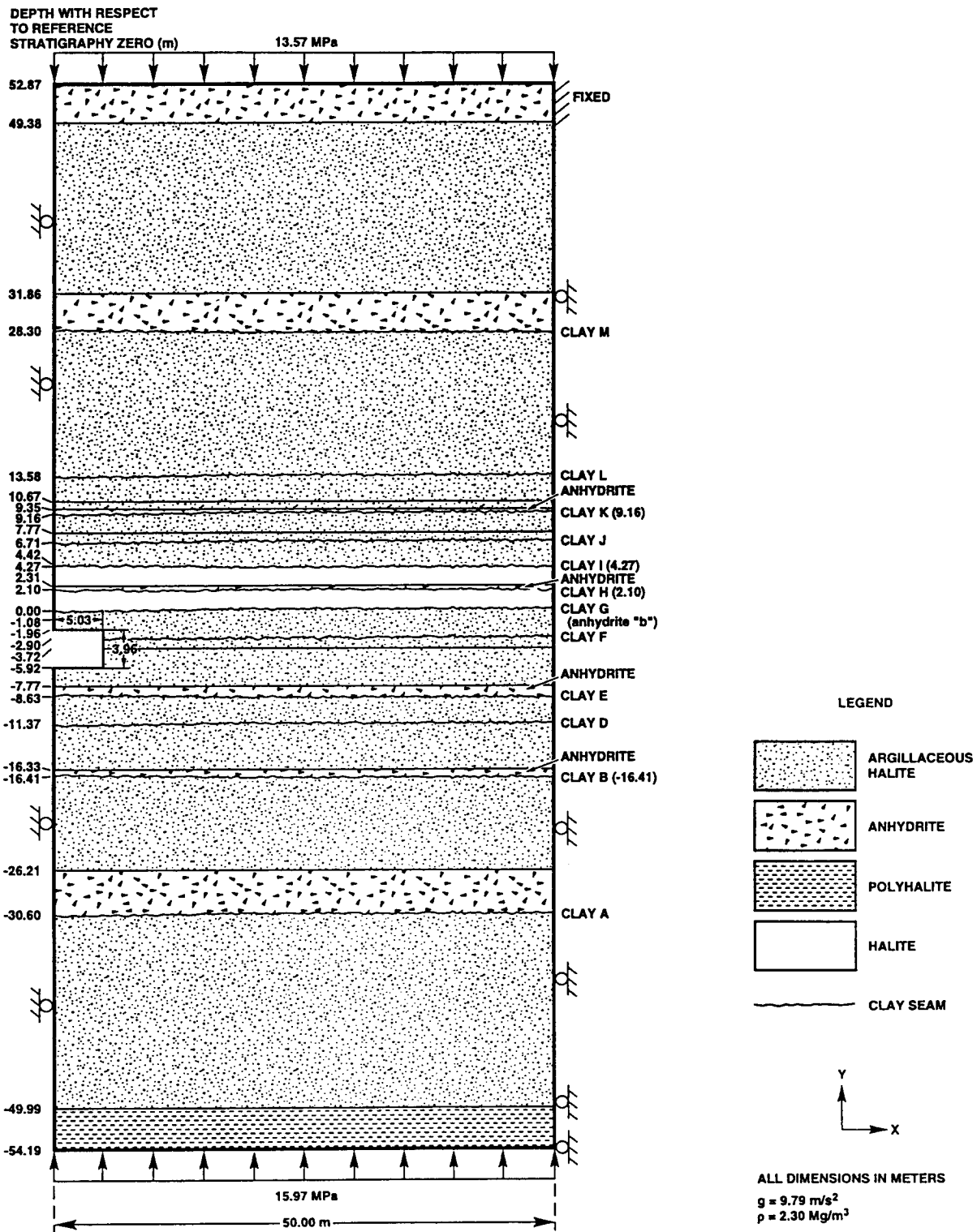


Figure 2.5-1. Local Stratigraphy for Numerical Calculations.

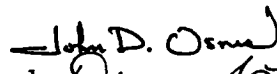


Rapid City, South Dakota • Albuquerque, New Mexico
 Pierre, South Dakota • Minneapolis, Minnesota

External Memorandum

To: Dr. B. M. Butcher
 Sandia National Laboratories
 Department 6748
 Mail Stop 1341
 P. O. Box 5800
 Albuquerque, NM 87185-5800

cc: C390 TR 2: Model Modification

From: Dr. John D. Osnes 
 Mr. Duane A. Labreche 
 RE/SPEC Inc.
 P.O. Box 725
 Rapid City, SD 57709-0725

Date: August 29, 1995

Subject: The Effect of Clay Seams and Anhydrite Layers on the Closure of Waste Isolation Pilot Plant Disposal Rooms and Guidelines for Simplifying the Modeled Stratigraphy

1.0 INTRODUCTION

This memorandum documents the results of a numerical study of the effects that clay seams and associated marker beds have on the calculated porosity of Waste Isolation Pilot Plant (WIPP) disposal rooms. In addition, it makes recommendations for simplifying the stratigraphy in future calculations of the disposal room porosity. The Disposal Room Model (DRM) simulates the creep closure of a WIPP disposal room after transuranic (TRU) waste and crushed-salt backfill have been emplaced. The input to the mathematical representations of the DRM consists of parameters that describe the geologic materials surrounding a room, the waste and backfill emplaced in a room, and the gas generation process that results from waste decomposition and corrosion. The output of the DRM simulations consists of stress and displacement fields as a function of time for all materials represented in the problem. From the standpoint of repository system performance assessment, the most important results of DRM simulations are predictions of the void space (porosity) in the room. The interrelationship between void space, time, and gas quantity has been termed a *porosity surface*, the development of which requires multiple DRM simulations and substantial computer resources.

Recently, a Sandia memorandum [Butcher and Holmes, 1995] was issued reaffirming the standardized set of input parameters for the DRM. One of the "parameters" is a definition of the local WIPP stratigraphy for use in disposal room modeling. The recommended stratigraphy contains 12 clay seams and 8 marker beds interspersed between layers of argillaceous and clean halite. All of the clay seams and several of the marker beds are relatively thin and from a volume-of-rock perspective, appear to be unimportant. Indeed, almost all of the previous calculations of room porosity (e.g., Weatherby et al. [1991a]; Weatherby et al. [1991b]; Callahan and DeVries [1991]; Stone [1992]; and Labreche et al. [1993]) have been based on "all-salt" models in which the clay seams and marker beds have been omitted.

When considered in light of the additional detail and effort required in the development and solution of a numerical model, the tactic of omitting most, if not all, of the thin layers from the geologic model is understandable. However, the discontinuities in stiffness and strength introduced by these thin layers make them potentially too important to ignore for some aspects of rock behavior without investigating the consequences. Butcher and Holmes [1995] anticipated that simplifications of the stratigraphy probably can be made without adversely affecting the results of DRM simulations, and they concluded by stating that an addendum will be issued to provide guidelines for simplifying the local WIPP stratigraphy for DRM simulations. The objective of this study is to investigate the consequences of simplifying the stratigraphy in calculations of disposal room closure and particularly in room porosity calculations.

A brief description of the problem is provided in Section 2.0. The modeling approach is described in Section 3.0. Section 4.0 contains the results of the numerical simulations in terms of room closures and porosities. A critical review of these results and their implications for the calculation of porosity surfaces are presented in Section 5.0. References cited in this memorandum are listed in Section 6.0. Figures showing the room closures and porosities predicted for each of the stratigraphic variations considered in this study are provided in Attachment A. Attachment B contains a copy of Butcher and Holmes [1995].

2.0 PROBLEM DESCRIPTION

In general terms, the DRM is a mechanical simulation of the creep closure of an infinite array of disposal rooms, each filled with 6,804 drums of TRU waste covered with crushed-salt backfill to within 0.711 m of the roof of the room. Specifications for the DRM are clearly defined in Butcher and Holmes [1995], a copy of which is attached to this memorandum (Attachment B). Consequently, only specific conditions that require clarification or that deviate from the problem description in Butcher and Holmes [1995] are presented in the following subsections.

2.1 STRATIGRAPHIC VARIATIONS

The objective of this study is to assess the effects of simplifying the reference DRM stratigraphy on calculations of room closure and porosity. Consequently, the major deviations from the specifications in Butcher and Holmes [1995] are in the stratigraphy, particularly in the number of clay seams represented in the model. Figure 1 shows the Revised Reference Stratigraphy for DRM simulations that is defined in Butcher and Holmes [1995]. This stratigraphy contains 12 clay seams (A, B, D, E, F, G, H, I, J, K, L, and M, from bottom to top) and 8 marker beds (MB134, MB136, MB138, Anhydrite A, MB139, Anhydrite C, MB140, and MB141, from top to bottom) interspersed between layers of argillaceous and clean halite. The Revised Reference Stratigraphy is taken from Munson et al. [1989] and is reaffirmed in Munson [1992]; it differs from the WIPP Reference Stratigraphy given by Krieg [1984] primarily in the definitions of the argillaceous and clean halite layers.

The Revised Reference Stratigraphy illustrated in Figure 1 is the baseline from which simplifications to the stratigraphy are derived and subsequently assessed with respect to their effect on calculations of room closure and porosity. Most of these simplifications are in the number of clay seams represented in the DRM. In total, seven variations on the Revised Reference Stratigraphy are analyzed in this study. These variations are summarized in Table 1 and are discussed below.

The baseline model is referred to as the "12-Clay Model" because it contains all 12 of the clay seams defined in the Revised Reference Stratigraphy, as well as all of the other stratigraphic details *except Anhydrite C*. Anhydrite C, which lies 10 m below the floor of the disposal room, is omitted from the 12-Clay Model because it is very thin (0.08 m). Krieg [1984] omitted Anhydrite B, which is 0.06-m thick and is less than 2.5 m above the disposal room roof (immediately above Clay G), because "it is too thin to be structurally sound." This omission of Anhydrite B from structural models of WIPP rooms has been maintained in subsequent definitions of the stratigraphy, including the Revised Reference Stratigraphy. Consequently, omitting Anhydrite C from the 12-Clay Model appears justifiable considering its thickness is comparable to the thickness of Anhydrite B and it is located substantially further from the disposal room.

It is assumed *a priori* that the influence of a clay seam on room closure and porosity diminishes with increasing distance between the clay seam and the disposal room. Consequently, the simplifications to the Revised Reference Stratigraphy generally involve eliminating the clay seams furthest from the room to progressively reduce the number of clay seams in the model. In this manner, the 7-Clay, 5-Clay, and 3-Clay Models are derived from the 12-Clay Model, with only the three clay seams (E, F, and G) nearest the disposal room remaining in the 3-Clay Model. The 7 marker beds (omitting Anhydrite C) and the argillaceous and clean halite layers in the 12-Clay Model are all represented in the 7-Clay, 5-Clay, and 3-Clay Models.

RSI-390-95-002

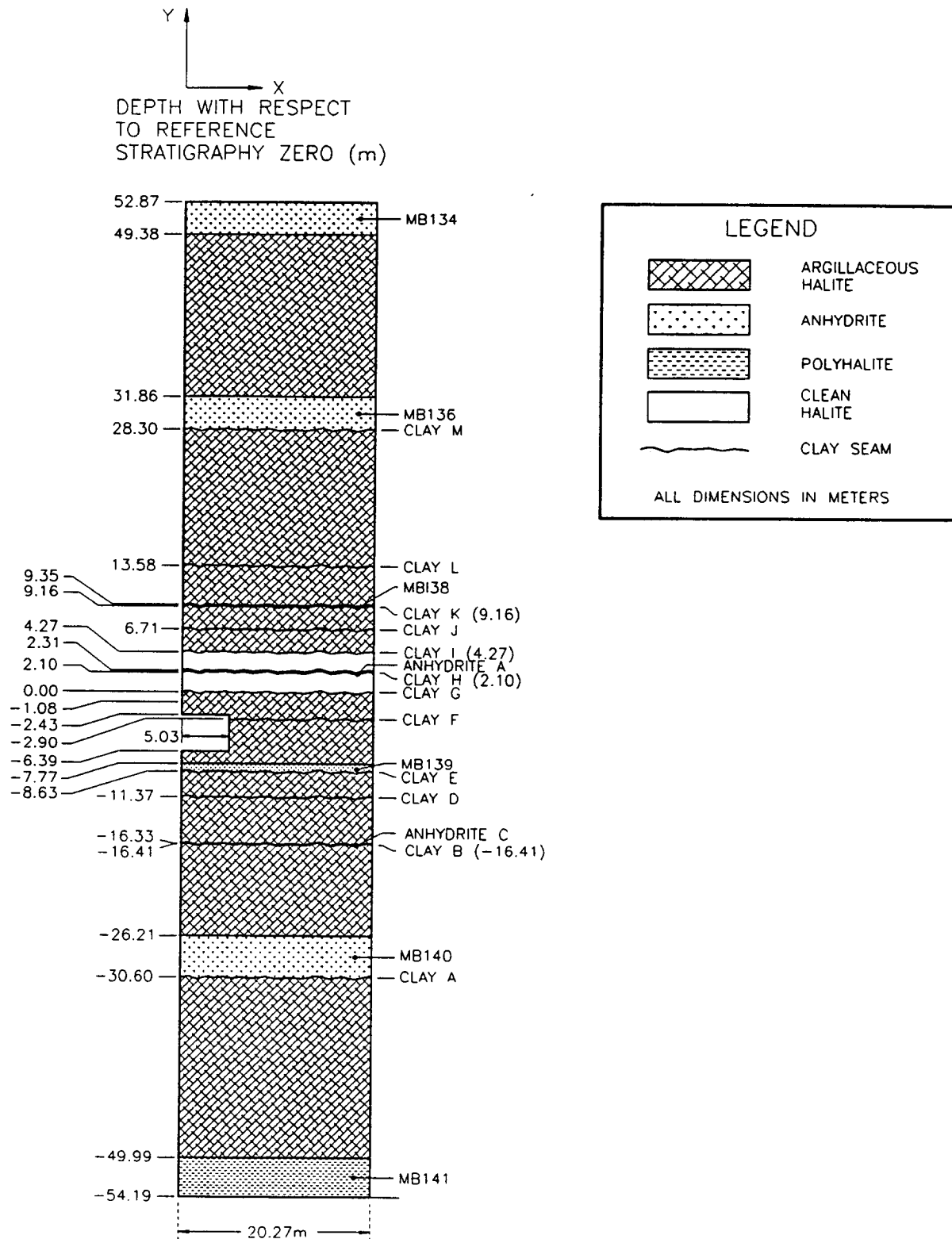


Figure 1. Revised Reference Stratigraphy for Disposal Room Models (after Butcher and Holmes [1995]).

Table 1. Variations From Revised Reference Stratigraphy [Butcher and Holmes, 1995] Modeled in Current Study

Stratigraphic Unit	Materials ^(a) in Stratigraphic Model						
	12-Clay	7-Clay	5-Clay	3-Clay	PA Profile	All-Salt	Clean-Salt
MB134	An	An	An	An	aH	aH	cH
MB136	An	An	An	An	aH	aH	cH
Clay M	CS	aH	aH	aH	aH	aH	cH
Clay L	CS	aH	aH	aH	aH	aH	cH
MB138	An	An	An	An	An	aH	cH
Clay K	CS	CS	CS	aH	CS	aH	cH
Clay J	CS	CS	aH	aH	aH	aH	cH
Clay I	CS	CS	cH	cH	cH	cH	cH
Anhydrite A	An	An	An	An	An	cH	cH
Clay H	CS	CS	CS	cH	CS	cH	cH
Clay G	CS	CS	CS	CS	aH	aH	cH
Clay F	CS	CS	CS	CS	aH	aH	cH
MB139	An	An	An	An	An	aH	cH
Clay E	CS	CS	CS	CS	CS	aH	cH
Clay D	CS	aH	aH	aH	aH	aH	cH
Anhydrite C	aH	aH	aH	aH	aH	aH	cH
Clay B	CS	aH	aH	aH	aH	aH	cH
MB140	An	An	An	An	aH	aH	cH
Clay A	CS	aH	aH	aH	aH	aH	cH
MB141	pH	pH	pH	pH	aH	aH	cH
Argillaceous Halite	aH	aH	aH	aH	aH	aH	cH
Clean Halite	cH	cH	cH	cH	cH	cH	cH

(a) CS = Clay Seam; An = Anhydrite; aH = Argillaceous Halite; cH = Clean Halite; pH = Polyhalite

A different simplification of the stratigraphy has been used in the flow and transport models used to assess the undisturbed performance of the WIPP repository and shaft system [WIPP Performance Assessment Department, 1993]. In these models, only the three marker beds closest to a disposal room (MB138, Anhydrite A, and MB139) were represented. Using a similar stratigraphy for mechanical models of the disposal room is desirable so that all of the disposal room models used in future WIPP performance assessments are consistent. Consequently, in this study, another variation on the Revised Reference Stratigraphy is modeled in which only MB138, Anhydrite A, and MB139 and the clay seams beneath them (E, H, and K) are represented. This variation on the stratigraphy is designated the "PA Profile" and is compared to the other stratigraphic models in Table 1. Like the 3-Clay Model, the PA Profile contains three clay seams but they are not the clay seams closest to the disposal room.

Almost all of the previous calculations of room porosity (e.g., Weatherby et al. [1991a]; Weatherby et al. [1991b]; Callahan and DeVries [1991]; Stone [1992]; and Labreche et al. [1993]) have been based on "all-salt" models in which the clay seams and marker beds were omitted. Actually, even the differentiation between clean and argillaceous halite was eliminated in these models, and the salt was modeled using the creep parameters for clean halite even though the vast majority of the salt in the Revised Reference Stratigraphy is classified as argillaceous halite. Consequently, these all-salt models are the extreme simplifications of the Revised Reference Stratigraphy.

Unfortunately, the room closures and porosities calculated previously with all-salt models are not likely to be directly comparable to calculations based on the DRM specifications in Butcher and Holmes [1995] because aspects *other than stratigraphy* also are substantially different in these models. Among the obvious differences are model geometry (quarter-room versus half-room), compaction characteristics of the TRU waste, and gas generation rates. To independently assess the effects of omitting all of the clay seams and marker beds and the effects of other differences from previous disposal room models, *two* additional variations on the Revised Reference Stratigraphy are evaluated in this study. In the "All-Salt Model," all of the clay seams and marker beds are omitted, but the clean and argillaceous halite layers in the Revised Reference Stratigraphy are preserved. Hence, most of the All-Salt Model is composed of argillaceous halite. In the second variation, designated the "Clean-Salt Model," not only are the clay seams and marker beds omitted, but all of the salt is modeled using the creep parameters for *clean halite*. This model bears the most similarity to previous models used for room closure and porosity calculations. Nevertheless, there are distinct differences in the model geometry, TRU waste characteristics, and gas generation rate between the Clean-Salt Model and the models used in previous analyses.

2.2 DISPOSAL ROOM LOCATION

In Butcher and Holmes [1995], there is an inconsistency between the stratigraphic elevations specified in the narrative description and the elevations illustrated in the

accompanying figure (which is reproduced in Figure 1 of this memorandum). In the figure, the local or reference zero for the stratigraphy is located at Clay G and the top of MB139 is 7.77 m below Clay G. According to the narrative description of the stratigraphy, the elevation of Clay G is 387.07 m above mean sea level (amsl) and the elevation of the top of MB139 is 379.11 m amsl. Hence, the reported elevation difference between Clay G and the top of MB139 is 7.96 m, not 7.77 m as illustrated in the figure. The absolute elevations are taken from Figure 2.2-2 of Sandia WIPP Project [1992], which is cited as "after Munson et al., 1989." However, none of these elevations, when taken relative to Clay G, agree exactly with the cited reference, which is the source of the illustration of the stratigraphy in Butcher and Holmes [1995]. This internal inconsistency within Butcher and Holmes [1995] will have to be resolved in future revisions. *In the disposal room models in the current study, the distance between Clay G and the top of MB139 is taken to be 7.77 m, the distance illustrated in the figure of the Revised Reference Stratigraphy in Butcher and Holmes [1995] and reproduced in Figure 1 of this memorandum.*

The most critical aspect of the inconsistency in the distance between Clay G and the top of MB139 is that the horizon of the disposal room is specified with respect to these stratigraphic units in Butcher and Holmes [1995]. In the reference, a disposal room is not illustrated in the figure showing the Revised Reference Stratigraphy (the location of experimental Room G is shown instead). The location of the repository floor is specified in the narrative description of the stratigraphy as 6.58 m below Clay G and 1.38 m above the top of MB139. This specification is consistent with a distance of 7.96 m between Clay G and the top of MB139. However, it is not consistent with the distance of 7.77 m that is indicated in the Revised Reference Stratigraphy figure and that is modeled in the current study. The specified distances from the room floor to Clay G and to the top of MB139 cannot both be satisfied in this 7.77-m interval. *Consequently, the specified distance of 1.38 m between the room floor and the top of MB139 is used in this study, as illustrated in Figure 1.* This location of the room with respect to MB139 is consistent with the recent disposal room analyses by DeVries [1994] and Labreche [1995]. However, it places the room floor 6.39 m below Clay G, instead of 6.58 m as specified in Butcher and Holmes [1995].

2.3 DIMENSIONS OF TRU WASTE REGION

Butcher and Holmes [1995] provide a tabulation of the volumes of the disposal room contents and a figure illustrating the dimensions of the room and its contents. However, there is an inconsistency between the tabulated volume of the TRU waste (1,727.5 m³) and the dimensions of the TRU waste region (9.06-m wide by 2.676-m high by 89.10-m long) illustrated in the figure. The tabulated volume is derived from the number of drums per disposal room (6,804) multiplied by the external volume of each drum (0.2539 m³); whereas the dimensions are based on the exterior of the region composed of seven-packs of drums in a disposal room. These exterior dimensions include the space between drums that may be filled with either air or crushed-salt backfill, depending on how and when the backfill is emplaced.

The compaction characteristics specified for TRU waste in Butcher and Holmes [1995] are based on the assumed distribution of the contents of individual drums; they do not account for the behavior of either air or crushed-salt backfill between the drums as they are emplaced in a disposal room. *Consequently, it is assumed that representing the volume of the drums and their contents is more important in simulating the disposal room closure than representing the exterior dimensions of the region that contains the drums, as well as the air or backfill between them.* Based on this assumption, the tabulated volume of the TRU waste (1,727.5 m³) given in Butcher and Holmes [1995] is used to derive the height of the TRU waste region in the two-dimensional models in this study. This volume is divided by the disposal room length (91.44 m) and the width of any section across six seven-packs (8.60 m) to yield a height of 2.20 m.

The TRU waste height of 2.20 m that is used in the disposal room models in this study is 0.476 m less than the height of seven-packs of drums stacked three high in a room. In the disposal room models, the additional headspace is modeled as being filled with crushed-salt. This modeling approach reproduces the volume of the crushed-salt backfill in a disposal room *if the space between the drums is indeed backfilled in the WIPP repository.*

2.4 CONSTITUTIVE MODEL FOR ANHYDRITE

Elastic properties for the anhydrite and polyhalite that comprise the marker beds are specified in Butcher and Holmes [1995]. Although plasticity parameters are not provided, Butcher and Holmes [1995] do note that "the analyst is not required to use an elastic model" for these materials. A preliminary simulation of the 12-Clay Model revealed that an elastic model of the anhydrite marker beds would not yield realistic results. As shown by Figure 2, tensile stresses in excess of 150 MPa were predicted in the anhydrite marker beds near the room (MB138, Anhydrite A, and MB139) within 3 years of excavation of the room. Geologic materials generally have tensile strengths less than 3 MPa, and no geologic material, including anhydrite, can withstand tensile stresses of this magnitude without fracturing.

Krieg [1984] provides plasticity parameters for Drucker-Prager and Mohr-Coulomb representations of the brittle failure of anhydrite and polyhalite; Munson [1992] reiterates these same parameter values for the Drucker-Prager model. However, both the Drucker-Prager and Mohr-Coulomb constitutive models are more representative of the shear failure of geologic materials; whereas the preliminary simulation of the 12-Clay Model indicated that a tensile mode of failure is more likely in the anhydrite marker beds near the disposal room. *Consequently, a limited-tension material model [Zienkiewicz et al., 1968; Osnes and Brandshaug, 1980] that simulates tensile failure was specified for all of the anhydrite marker beds.* The tensile strength of the anhydrite was assumed to be 1 MPa. The only marker bed composed of polyhalite is MB141, and tensile stresses were not predicted in this marker bed in any of the simulations. Consequently, an elastic model was considered adequate to represent the response of polyhalite.

RSI-390-95-005

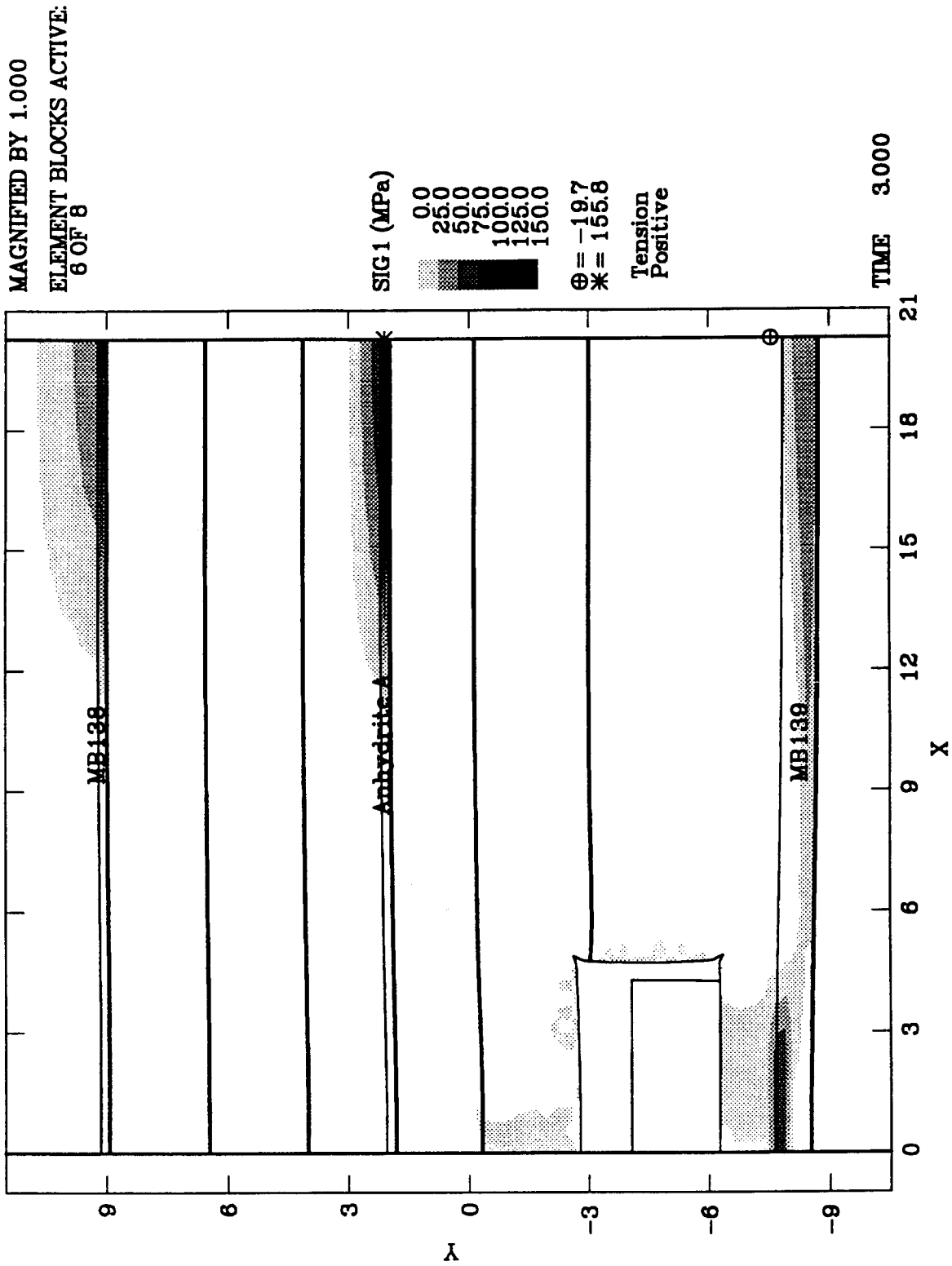


Figure 2. Least-Compressive Principal Stress Predicted in a Preliminary Simulation of the 12-Clay Model in Which the Anhydrite was Modeled as an Elastic Material.

In the limited-tension material model, the material behaves elastically at stress states in which the least-compressive principal stress is more compressive than the tensile strength of the material. Tensile stresses are limited to values less than or equal to the tensile strength by plastic deformation that redistributes stress to surrounding materials. Modeling the anhydrite marker beds as limited-tension materials reduces the amount of tension they can support, in turn making them more flexible as they bend in response to room closure. The effect of this enhanced flexibility is readily apparent in Figure 3 which compares the vertical room closures predicted in preliminary simulations of the 12-Clay Model with the anhydrite marker beds modeled as elastic and as limited-tension materials. In both simulations, the disposal room was not backfilled with crushed salt, so room closure was not restrained by consolidation of the backfill.

2.5 GAS GENERATION RATE

Although waste decomposition and corrosion are likely to generate gas in WIPP disposal rooms, gas generation is not represented in the DRM simulations in the current study. Gas generation and the associated pressurization of the disposal rooms limit the closure of the rooms. Neglecting gas generation in this study serves to isolate and amplify the effects of the stratigraphic variations on calculations of room closure and porosity.

3.0 MODELING APPROACH

The various models of the stratigraphy described in Section 2.1 were analyzed using the finite-strain formulation in Version 4.06 of the finite element program SPECTROM-32 [Callahan, 1994; Callahan et al., 1990]. Special modeling methodologies were required to simulate the sequence of room excavation and waste and backfill emplacement, and to represent the clay seams. The results of the finite element analyses were assessed and compared in terms of vertical and horizontal room closures and room porosity as functions of time. The finite element model, the special modeling methodologies, and the methods for calculating room closure and porosity are described in the following subsections.

3.1 FINITE ELEMENT MODEL

The same finite element mesh was used to represent all of the stratigraphic variations considered in this study. Figure 4 shows the finite element mesh, which consists of 3,333 nodes in 1,056 eight-noded quadrilateral elements. To simulate the various models of the stratigraphy, the geologic material assigned to the layers of elements corresponding to each stratigraphic unit was changed according to the specifications in Table 1.

RSI-390-95-003

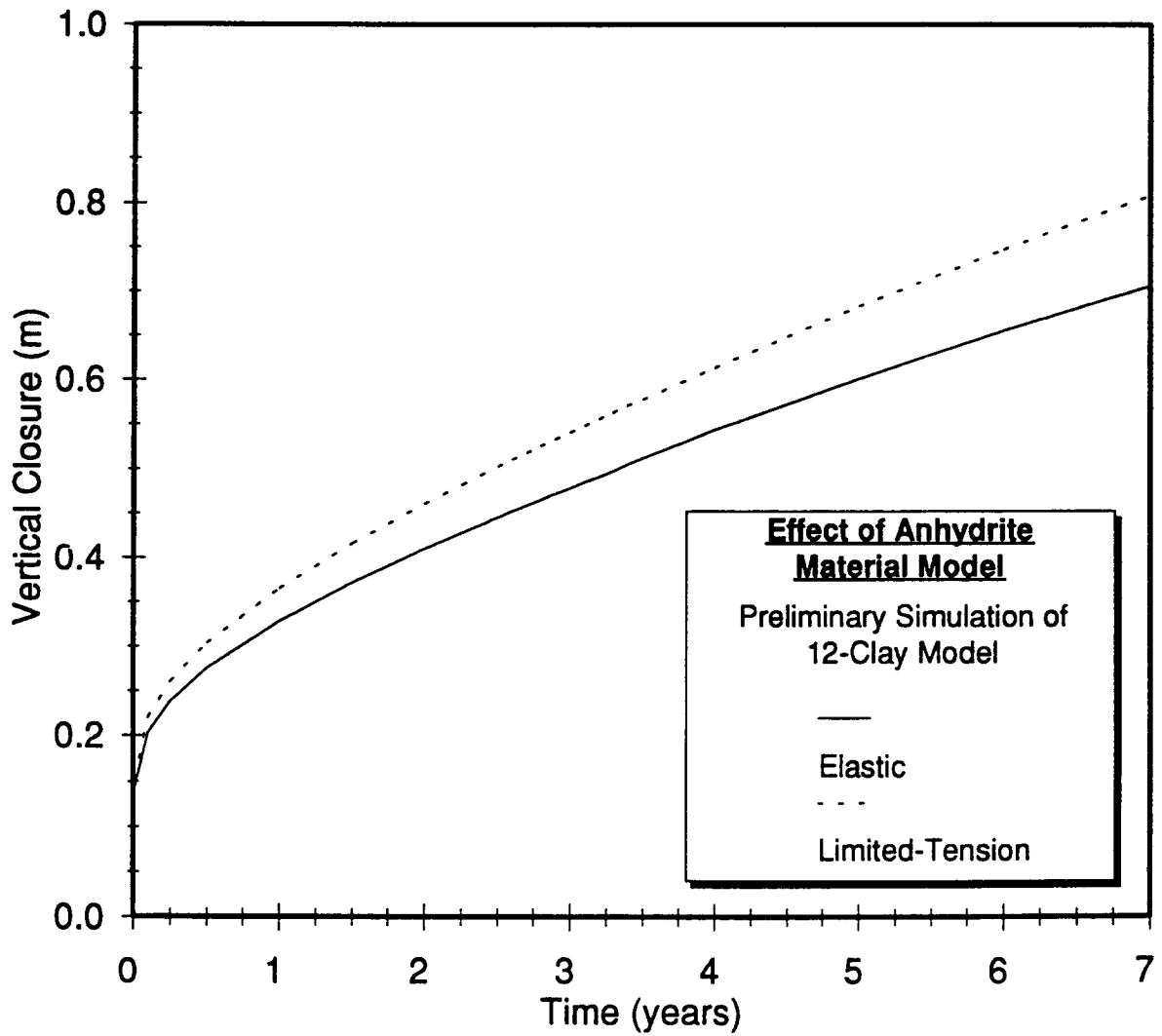


Figure 3. Comparison of Vertical Room Closures Predicted in Preliminary Simulations of the 12-Clay Model in Which the Anhydrite Was Modeled as an Elastic or a Limited-Tension Material.

RSI-390-95-006

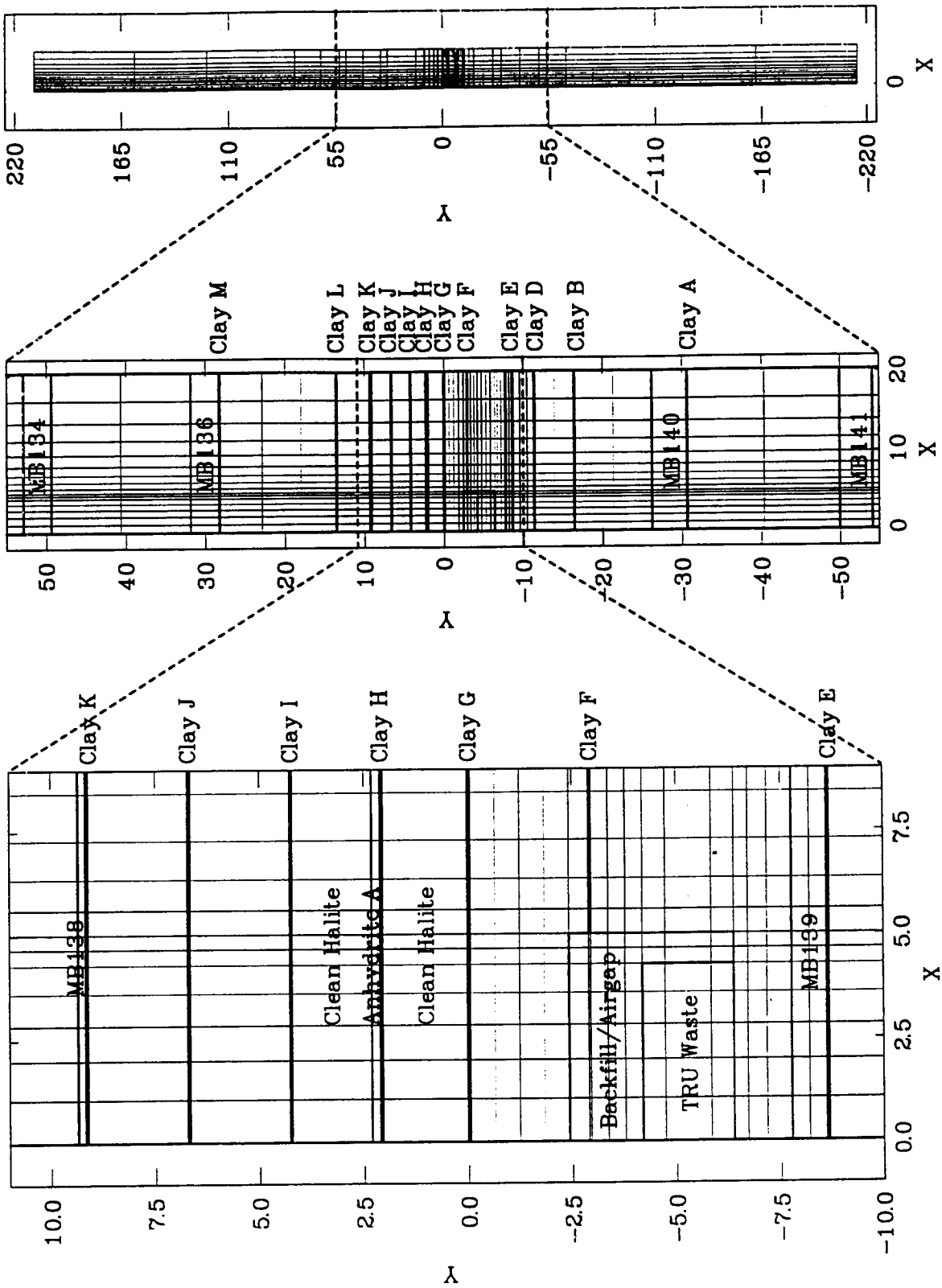


Figure 4. Finite Element Mesh Used to Simulate a Disposal Room in all Variations of the Revised Reference Stratigraphy (Unlabeled Blocks are Argillaceous Halite).

The two-dimensional, plane-strain model represents a vertical cross section that is perpendicular to the long axes of an infinite array of parallel disposal rooms. Vertical planes of symmetry through the room mid-plane and the pillar mid-plane bound the model on the left and right, respectively. Based on the symmetry conditions, horizontal displacement was not permitted along these boundaries.

The vertical extent of the finite element model extends approximately 160 m above and below the 107-m high section of the Revised Reference Stratigraphy that was defined in Butcher and Holmes [1995] and that is shown in Figure 1. This extension was deemed necessary because the simulated time period was uncertain at the outset of this study, and 10,000-year simulations were considered a possibility. Over such a lengthy simulation period, it is likely that the response of the disposal room would be significantly effected by boundary conditions specified at boundaries located only 50 m above and below the disposal room. Butcher and Holmes [1995] do not specify the vertical extent of disposal room models for precisely this reason; they state that, "The analyst should choose a model height appropriate for the problem and the simulation code being used, a height which does not adversely influence the results of interest."

The objective of extending the finite element model beyond the limits of the Revised Reference Stratigraphy was to eliminate boundary effects on the disposal room response over the simulated period of time. The effects of the material properties specified in the 160-m extensions to the Revised Reference Stratigraphy were assumed to be secondary to the boundary effects. Consequently, stratigraphy representative of the WIPP site was not specified in these extensions. Instead, the extensions were assigned the material properties of the predominate rock type in the stratigraphic variation being modeled. This rock type was argillaceous halite in all of the variations except the Clean-Salt Model, which was composed entirely of clean halite.

Vertical displacement was not allowed along the bottom boundary of the finite element model. A vertical traction of 10.03 MPa was specified along the top boundary. Butcher and Holmes [1995] specify an initial, isotropic stress state that varies linearly with depth based on an average density of 2,300 kg/m³, a gravitational acceleration of 9.79 m/s², and a compressive stress of 13.57 MPa at the top of MB134. This specification yields an initial compressive stress of 15.97 MPa at the bottom of MB141. The conditions specified along the top and bottom boundaries of the finite element model, in conjunction with the density and gravitational acceleration values, yield the specified compressive stresses at the top of MB134 and the bottom of MB141. A uniform temperature of 27°C was specified throughout the finite element model [Butcher and Holmes, 1995].

Although 10,000-year simulations were a possibility at the outset of the study, the simulation period was nonetheless a variable to be determined during the course of the study. The simulations of most of the stratigraphic models were terminated when the calculated room porosities approached zero. At least 250 years were simulated for all of the stratigraphic

models; the simulation of the baseline 12-Clay Model was taken to 1,000 years. The restart capabilities of SPECTROM-32 were utilized to perform the simulations incrementally and to continue them as needed.

3.2 SIMULATION OF EXCAVATION AND WASTE AND BACKFILL EMPLACEMENT

The room detail given in Figure 4 shows the regions used to represent the TRU waste and the crushed-salt backfill. The symmetric half of the room that is simulated in the finite element model is 5.03-m wide by 3.96-m high. As shown in Figure 4, the corners of the room are represented as being right angles. The half of the TRU waste region represented in the model is 4.30-m wide by 2.20-m high and is located in the lower left corner of the half-room. The backfill/airgap region surrounds the TRU waste region and extends to the rib and the roof of the room.

In reality, there will be periods of time between excavating a disposal room, emplacing TRU waste in it, and backfilling it with crushed salt. The lengths of these intervals have not been defined and probably are insignificant relative to simulation periods of 100's or 1,000's of years. When the room is backfilled, the backfill cannot be emplaced to the roof of the room. Butcher and Holmes [1995] specify an airgap of 0.711 m between the top of the backfill and the roof. This airgap will decrease and eventually disappear as the room closes. Closure of the airgap cannot be explicitly simulated with Version 4.06 of SPECTROM-32 because it does not have an algorithm for simulating the contact between two surfaces. An alternative that has been used in previous infinitesimal-strain simulations is to represent the airgap with elements composed of extremely compressible material (like air). When the volume of each airgap element decreases to a small fraction of its original volume, the element's material is changed to crushed salt. However, this approach is not reliable in finite-strain simulations because the elements tend to collapse before the requisite volume reduction is achieved.

In the DRM simulations performed in this study, excavation of the room was immediately followed by emplacement of TRU waste in the waste region. The weight of the TRU waste provides a small load on the floor of the room beneath the TRU waste region. To simulate the closure of the airgap, the backfill/airgap region was not filled with crushed salt until the area of this region decreased by 3.58 m^2 (the room half-width of 5.03 m multiplied by the airgap thickness of 0.711 m). This approach is based on the assumption that the backfill provides negligible resistance to closure of the room until the airgap completely closes.

To precisely determine the time for backfilling, a preliminary simulation of each stratigraphic model would have been required. The closure of the backfill/airgap region as a function of time after excavation could have been calculated from these preliminary simulations. However, performing seven preliminary simulations would have consumed a substantial amount of computer time when it was likely that the variation in the resultant backfill times would be

minimal. Consequently, only a preliminary simulation of the 12-Clay Model was performed initially.

In the preliminary simulation of the 12-Clay Model, the area of the backfill/airgap region decreased by 3.58 m² at approximately 3.24 years after excavation. *Based on this simulation, backfilling of the remaining area of the backfill /airgap region was simulated at 3.24 years after excavation in all of the stratigraphic models except the All-Salt and Clean-Salt Models.* Additional preliminary simulations of the All-Salt and Clean-Salt Models had to be performed to more precisely determine the backfill times for these models (1.45 years and 4.21 years, respectively). As indicated by Table 2, analysis of the final simulations confirmed that the area of the backfill/airgap region decreased by approximately 3.58 m² at the time of backfilling in all of the stratigraphic models.

Table 2. Decrease in the Area of the Backfill/Airgap Region at the Time of Backfilling

Stratigraphic Model	Backfill Time (years after excavation)	Decrease in Area at Backfill Time (m²)
12-Clay	3.24	3.47
7-Clay	3.24	3.45
5-Clay	3.24	3.42
3-Clay	3.24	3.11
PA Profile	3.24	3.31
All-Salt	1.45	3.51
Clean-Salt	4.21	3.51

3.3 REPRESENTATION OF THE CLAY SEAMS

Butcher and Holmes [1995] describe the clay seams as frictional interfaces with a friction coefficient of 0.2 (friction angle of 11.31°). They were simulated in this study using the "frictional slideline" component model in SPECTROM-32 [Callahan et al., 1990]. This component model provides the capability to simulate a thin region within a host material that has a shear resistance which is proportional to the normal stress across the region. The thin region behaves like the host material when the shear stress parallel to the region does not exceed the shear resistance. When the shear resistance is exceeded, the material in the region deforms perfectly plastically, straining without further increases in shear stress. The clay seams in this study

were represented by 0.05-m thick elements composed of either argillaceous or clean halite with the frictional slideline model specified concurrently in these elements.

3.4 CALCULATION OF ROOM CLOSURE AND POROSITY

In Section 4.0, the results of the finite element simulations are assessed and compared in terms of vertical and horizontal room closures and room porosity as functions of time. The vertical and horizontal closures provide quantitative measures of the deformed shape of the disposal room. The vertical closure is equal to the relative vertical displacement between the centers of the roof and floor; from symmetry, the horizontal closure is equal to twice the horizontal displacement of the midheight of the rib. These quantities are relatively easy to calculate and are unambiguous. The calculation of the porosities of the room and its contents is more involved, and the remainder of this subsection is devoted to describing the calculational methods used in previous studies and in the current study.

The porosity (also called the void fraction) is defined as the percentage or fraction of the total volume of a porous region that is composed of voids. The remainder of the porous region is composed of solids, so the void volume can be calculated by subtracting the volume of the solids in the region from the total volume. In the DRM, there are two distinct porous regions (the backfill and the TRU waste) which have substantially different initial porosities (39.25 percent and 68.1 percent, respectively, based on the DRM specifications in Butcher and Holmes [1995]). Hence, the porosities of these two regions generally are calculated independently; the volume-averaged porosity of the disposal room can then be calculated from the porosities of the backfill and TRU waste and their corresponding volumes.

Generally, the compressibility of the solid volume in a porous region is negligible compared to the compressibility of the void volume. Consequently, it was assumed in porosity calculations in previous DRM analyses that the volume of the solids is constant and that the change in the volume of the region is entirely due to the change in the void volume. However, for a number of reasons, this assumption is not valid in the current study because it results in the calculation of negative TRU waste porosities, which are physically impossible. Therefore, the underlying assumption had to be modified and the calculational method changed accordingly. The previous methodology, the rationale for changing it, and the revised methodology are described in the following subsections.

3.4.1 Previous Method for Calculating Porosities

In previous calculations of porosities from DRM simulations (e.g., Labreche et al. [1993]; DeVries [1994]; and Labreche [1995]), it was assumed that the solids in the backfill and TRU waste regions are essentially incompressible. In turn, the solid volume in each region was assumed to be constant. Based on this assumption and the definition of porosity, the porosities of these regions were calculated according to the following equations:

$$\phi_{BF}(t) = 1 - \frac{V_{BF,s}}{V_{BF}(t)} \quad (1)$$

$$\phi_{TW}(t) = 1 - \frac{V_{TW,s}}{V_{TW}(t)} \quad (2)$$

where:

- $\phi_{BF}(t)$ = Backfill porosity at time t
- $V_{BF,s}$ = Volume of the solids in the backfill
- $V_{BF}(t)$ = Volume of the backfill region at time t
- $\phi_{TW}(t)$ = TRU waste porosity at time t
- $V_{TW,s}$ = Volume of the solids in the TRU waste
- $V_{TW}(t)$ = Volume of the TRU waste region at time t .

Since the void volume is the product of the porosity and the total volume, it is straightforward to show that the volume-averaged porosity of the disposal room can be calculated from the porosities and total volumes of the backfill and TRU waste as follows:

$$\phi_{Room}(t) = \frac{\phi_{BF}(t) V_{BF}(t) + \phi_{TW}(t) V_{TW}(t)}{V_{BF}(t) + V_{TW}(t)} \quad (3)$$

Calculating porosities according to Equations 1 and 2 requires the volume of the solids in each region and the total volume of each region as a function of time. The solid volumes are easily calculated by rearranging Equations 1 and 2 and substituting the specified values of the initial porosities into them, as shown below:

$$V_{BF,s} = (1 - \phi_{BF,o}) V_{BF,o} \quad (4)$$

$$V_{TW,s} = (1 - \phi_{TW,o}) V_{TW,o} \quad (5)$$

where:

- $\phi_{BF,o}$ = Initial backfill porosity
- $V_{BF,o}$ = Initial volume of the backfill regions
- $\phi_{TW,o}$ = Initial TRU waste porosity
- $V_{TW,o}$ = Initial volume of the TRU waste region.

In previous DRM analyses, the volumes of the backfill and TRU waste regions as functions of time were simply calculated from the deformed outlines of these regions. This approach was satisfactory because the volumes of the regions were always greater than the volumes of the

solids in them, which is consistent with the assumption that the compressibilities of the solid volumes are negligible.

3.4.2 Problems with the Previous Method

It should be noted in Equations 1 and 2 that if the volume of a region becomes less than the (initial) volume of the solids in the region, a negative porosity is calculated, which is physically impossible. The fact that negative porosities were not calculated in previous analyses is largely because nonzero gas generation rates were simulated in most of these analyses and the resultant gas pressures kept the room contents from completely consolidating. In analyses in which gas generation was not considered, negative porosities were not calculated, in part because of the shorter time periods simulated (generally less than 250 years), and in part because the specified compaction characteristics yielded smaller compressibilities as the porosities approached zero than the characteristics specified in Butcher and Holmes [1995] yield.

In the current study, a gas generation rate of zero is modeled and time periods of at least 250 years are simulated for all of the stratigraphic models. In addition, the initial porosity and the compaction characteristics specified in Butcher and Holmes [1995] for TRU waste are different from the values specified for previous studies. The combination of all of these factors resulted in the calculation of negative porosity values for the TRU waste region when the methodology used in previous DRM analyses was employed.

The effects of the differences in the TRU waste characteristics are graphically illustrated in Figure 5. This figure compares the compaction function specified in Butcher and Holmes [1995] to the compaction function specified previously [Sandia WIPP Project, 1992]. Both compaction functions are stated in terms of natural (true) volumetric strain as a function of mean stress. From these compaction functions and the specifications of the initial porosity of TRU waste, the TRU waste porosity as a function of mean stress can be calculated using the following equation:

$$\phi = 1 - (1 - \phi_0) \exp(\epsilon_v) \quad (6)$$

where:

- ϕ = Porosity
- ϕ_0 = Initial porosity
- ϵ_v = Natural volumetric strain (compression positive).

The resultant porosity functions also are shown in Figure 5. As indicated by Equation 6, the porosity not only depends on the volumetric strain but also on the initial porosity. The initial porosity specified in Sandia WIPP Project [1992] was 74.0 percent; whereas Butcher and Holmes [1995] specified an initial porosity of 68.1 percent.

RSI-390-95-004

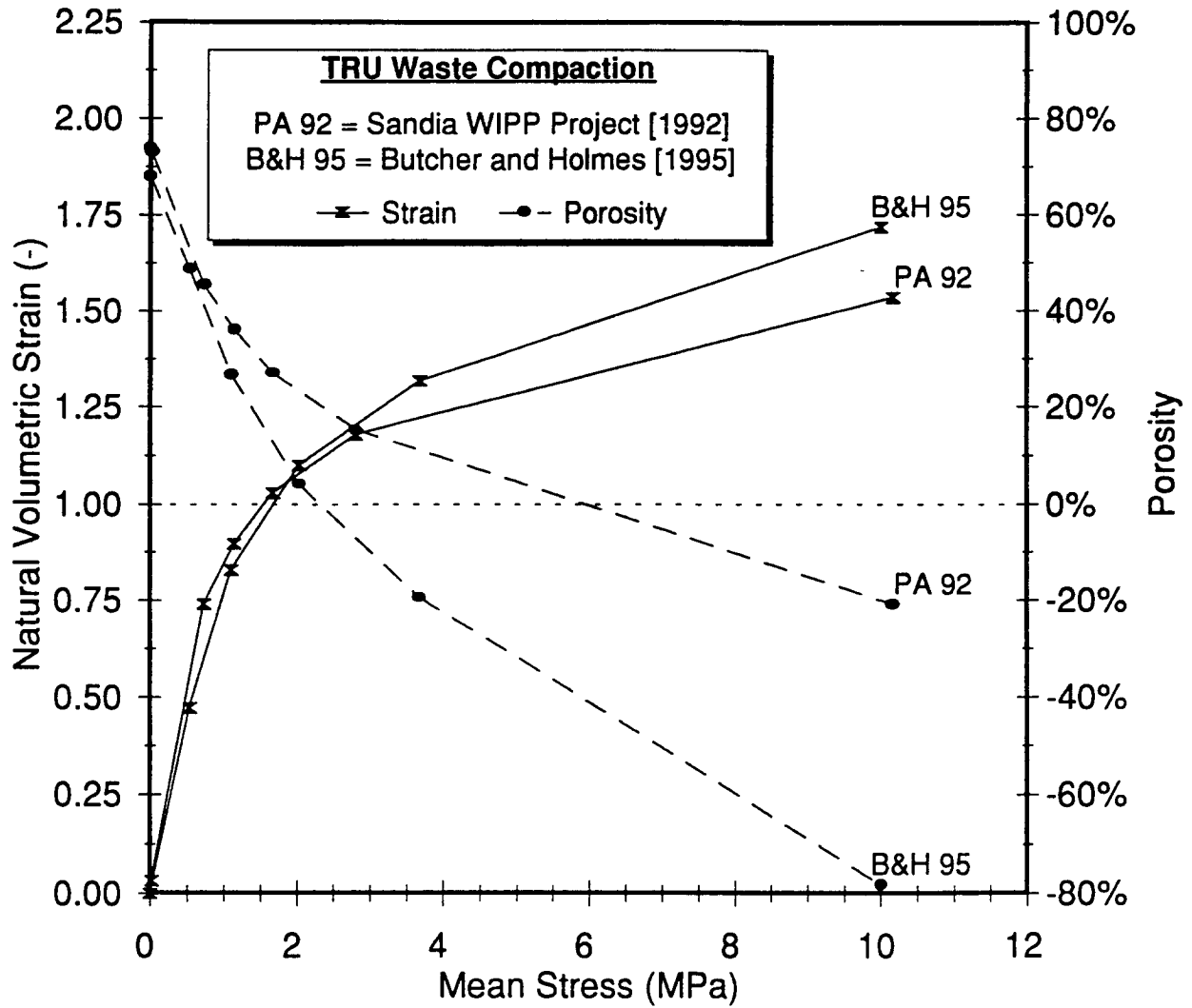


Figure 5. Comparison of the Compaction Characteristics Specified for TRU Waste in Butcher and Holmes [1995] and in Sandia WIPP Project [1992].

In terms of volumetric strains, the TRU waste compaction functions shown in Figure 5 are very similar at mean stresses less than 3 MPa; beyond that they deviate significantly from each other, especially considering that the differences in the resultant porosities are exponential functions of the differences in the volumetric strains. In addition to the differences in the compaction functions, the differences in the initial porosities yield significant differences in the TRU waste porosities at mean stresses greater than 1 MPa. *The cumulative effect of the differences in the compaction functions and the initial porosities is that the porosities calculated from the Butcher and Holmes [1995] specifications become negative at mean stresses greater than 2.5 MPa and the porosities calculated according to the Sandia WIPP Project [1992] specifications do not become negative until the mean stress exceeds 6 MPa.*

Equation 6 is derived from the fundamental definitions of porosity and natural volumetric strain and is based on the assumption that the solids are incompressible. Assuming that the compaction functions shown in Figure 5 are representative of the volumetric response of TRU waste, these functions indicate that the solids in TRU waste are relatively compressible, at least when compared to geologic materials such as halite. Since the underlying assumption of incompressibility is not satisfied, the methodology for calculating porosities had to be revised in the current study.

3.4.3 Revised Method for Calculating Porosities

The negative porosities calculated at mean stresses greater than 2.5 MPa indicate that the volume of the solids cannot be assumed to be constant, as was done in previous calculations of porosity. However, it seems reasonable to presume that as long as there is void space in a subregion of the TRU waste, the compressibility of the solids *in that subregion* is negligible compared to the compressibility of the voids. Consequently, in calculating the porosities in this study, it is assumed that the volume of the solids in a subregion is constant until the porosity in the subregion approaches zero. By definition, the volume of the solids is equal to the volume of the subregion when the porosity is zero (no void space), and this volume can be less than the initial volume of the solids in the subregion because of the compressibility of the solids. This concept of the compaction of a porous material implies that the solid volume is constant in subregions with nonzero porosities while the solid volume is equal to the subregion volume in subregions that have fully compacted to zero porosity.

This concept is implemented in the revised method for calculating porosities by modifying Equations 1 and 2 so that the volumes of the solids in each region, as well as the volumes of the regions themselves, vary with time. The modified equations are shown below:

$$\phi_{\text{BF}}(t) = 1 - \frac{V_{\text{BF},s}(t)}{V_{\text{BF}}(t)} \quad (7)$$

$$\phi_{\text{TW}}(t) = 1 - \frac{V_{\text{TW},s}(t)}{V_{\text{TW}}(t)} \quad (8)$$

where:

$$\begin{aligned} V_{\text{BF},s}(t) &= \text{Volume of the solids in the backfill at time } t \\ V_{\text{TW},s}(t) &= \text{Volume of the solids in the TRU waste at time } t. \end{aligned}$$

As in previous DRM analyses, the volumes of the backfill and TRU waste regions as functions of time ($V_{\text{BF}}(t)$ and $V_{\text{TW}}(t)$) are calculated from the deformed outlines of the regions.

The solid volumes in the backfill and TRU waste regions are simply the sums of the solid volumes in all of the subregions that comprise the respective regions. In calculations of porosities from finite element simulations, the subregions are conveniently defined by the finite elements that compose the backfill and TRU waste regions. Therefore, the volumes of the solids are calculated according to the following summations over the elements in each region:

$$V_{\text{BF},s}(t) = \sum_{e_{\text{BF}}} V_{s,e}(t) \quad (9)$$

$$V_{\text{TW},s}(t) = \sum_{e_{\text{TW}}} V_{s,e}(t) \quad (10)$$

where:

$$\begin{aligned} V_{s,e}(t) &= \text{Volume of the solids in element } e \text{ at time } t \\ e_{\text{BF}} &= \text{Elements in the backfill region} \\ e_{\text{TW}} &= \text{Elements in the TRU waste region.} \end{aligned}$$

The volume of the solids in each element (subregion) depends on whether or not the material in the element has fully compacted to zero porosity. Once the element has fully compacted to zero porosity, then the volume of the solids in the element at any time thereafter must be identically equal to the volume of the element because there is no void space left in the element. In an element that has not fully compacted, it is assumed that the compressibility of the solids is negligible compared to the compressibility of the void space. Neglecting the compressibility of the solids in such an element implies that the initial volume of the solids in the element is maintained until the element fully compacts to zero porosity. These conditions for calculating the solid volume in each element as a function of time are expressed algebraically as follows:

$$V_{s,e}(t) = \begin{cases} V_e(t), & \text{if } V_e(t') \leq V_{s,e}(0) \text{ at any } t' \leq t \text{ (fully compacted)} \\ V_{s,e}(0), & \text{otherwise} \end{cases} \quad (11)$$

where:

$$V_{s,e}(0) = (1 - \phi_{o,e}) V_{o,e} \quad (12)$$

and:

$$\begin{aligned}V_e(t) &= \text{Volume of element } e \text{ at time } t \\V_{s,e}(0) &= \text{Initial volume of the solids in element } e \\ \phi_{o,e} &= \text{Initial porosity of element } e \\V_{o,e} &= \text{Initial volume of element } e.\end{aligned}$$

The elemental volumes required in Equations 11 and 12 are calculated from the initial and deformed shapes of the elements.

As indicated by the preceding pairs of equations, the porosities of both the crushed-salt backfill and the TRU waste are calculated using the revised methodology in the current study. This is simply a matter of consistency because the constitutive model for crushed salt is implemented in **SPECTROM-32** in such a way that a crushed-salt element is transformed to solid salt as the porosity of the element approaches zero. Consequently, the volume of a crushed-salt element is never less than or equal to the initial volume of the solids in it (i.e., the condition in Equation 11 is never satisfied). In turn, the revised methodology yields exactly the same backfill porosities as the method used in previous DRM analyses. In the current study as in previous analyses, the volume-averaged porosity of the room is calculated according to Equation 3 from the porosities and volumes of the backfill and TRU waste regions.

4.0 SIMULATION RESULTS

The results of the simulations of the stratigraphic models defined in Table 1 are compared in this section. Only comparisons of room closures and porosities are made because these are the responses of interest in this study of the effects of simplifying the modeled stratigraphy. Figures showing the closures and porosities predicted as functions of time by each model are provided in Attachment A. Closure and porosity values at 10, 50, 100, 250, 500, and 1,000 years also are given on these figures.

The vertical and horizontal closures predicted by the stratigraphic models considered in this study are compared in Figures 6 and 7, respectively. Note that the time axes of these and all figures in this section are shifted so that zero is the time at which airgap closure was predicted and backfilling of the remaining area was simulated. As indicated by Table 2, the airgap closure time and the coincident backfill time varied slightly among the All-Salt, the Clean-Salt, and the other models. Subtracting the backfill time from the simulation time yields comparisons that begin with comparable values of closure and porosity. (The time axes of the figures in Attachment A are *not* shifted because those figures show the results for individual stratigraphic models.)

RSI-390-95-007

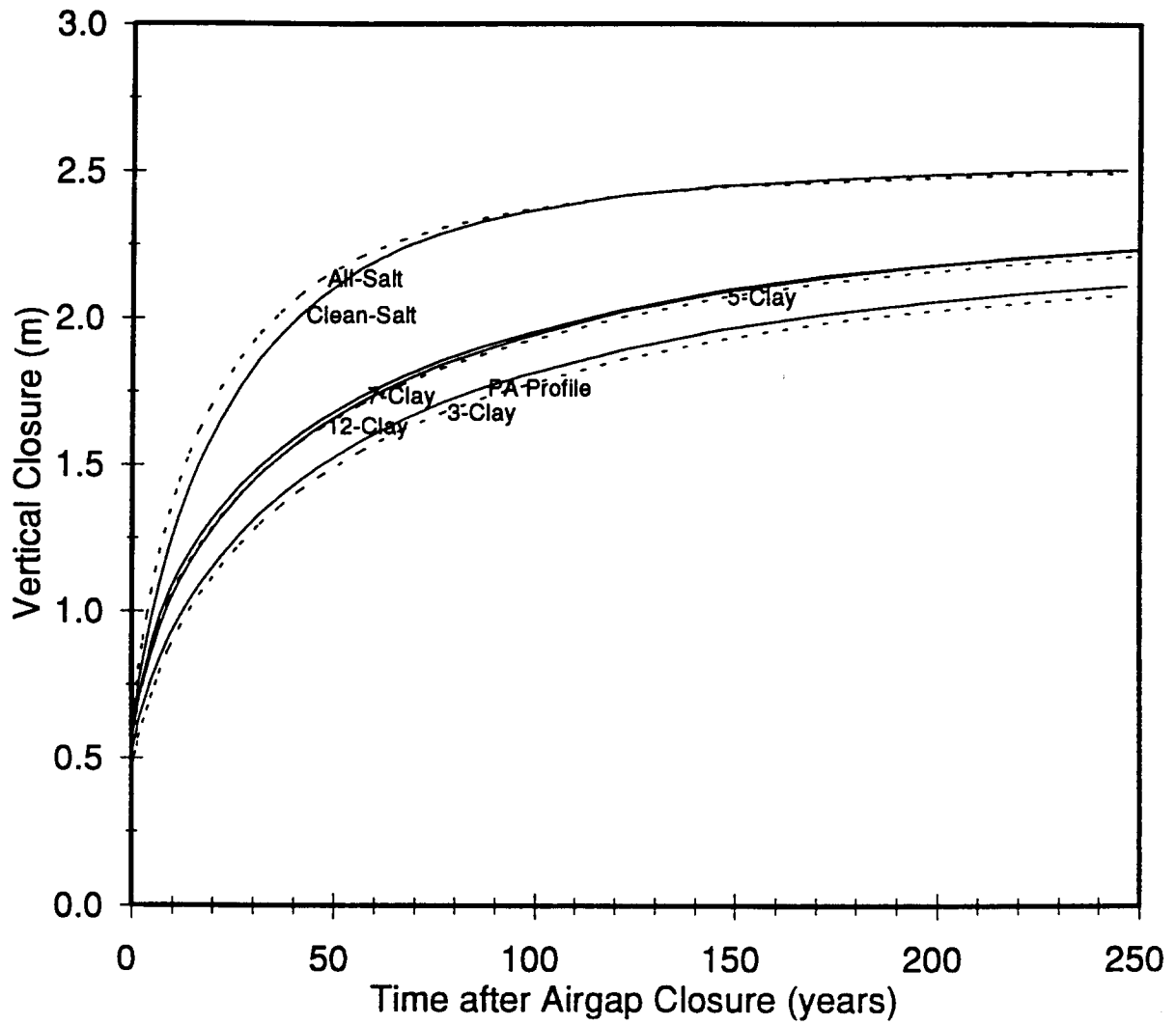


Figure 6. Comparison of the Vertical Closures of the Disposal Room Predicted by Each of the Stratigraphic Models.

RSI-390-95-008

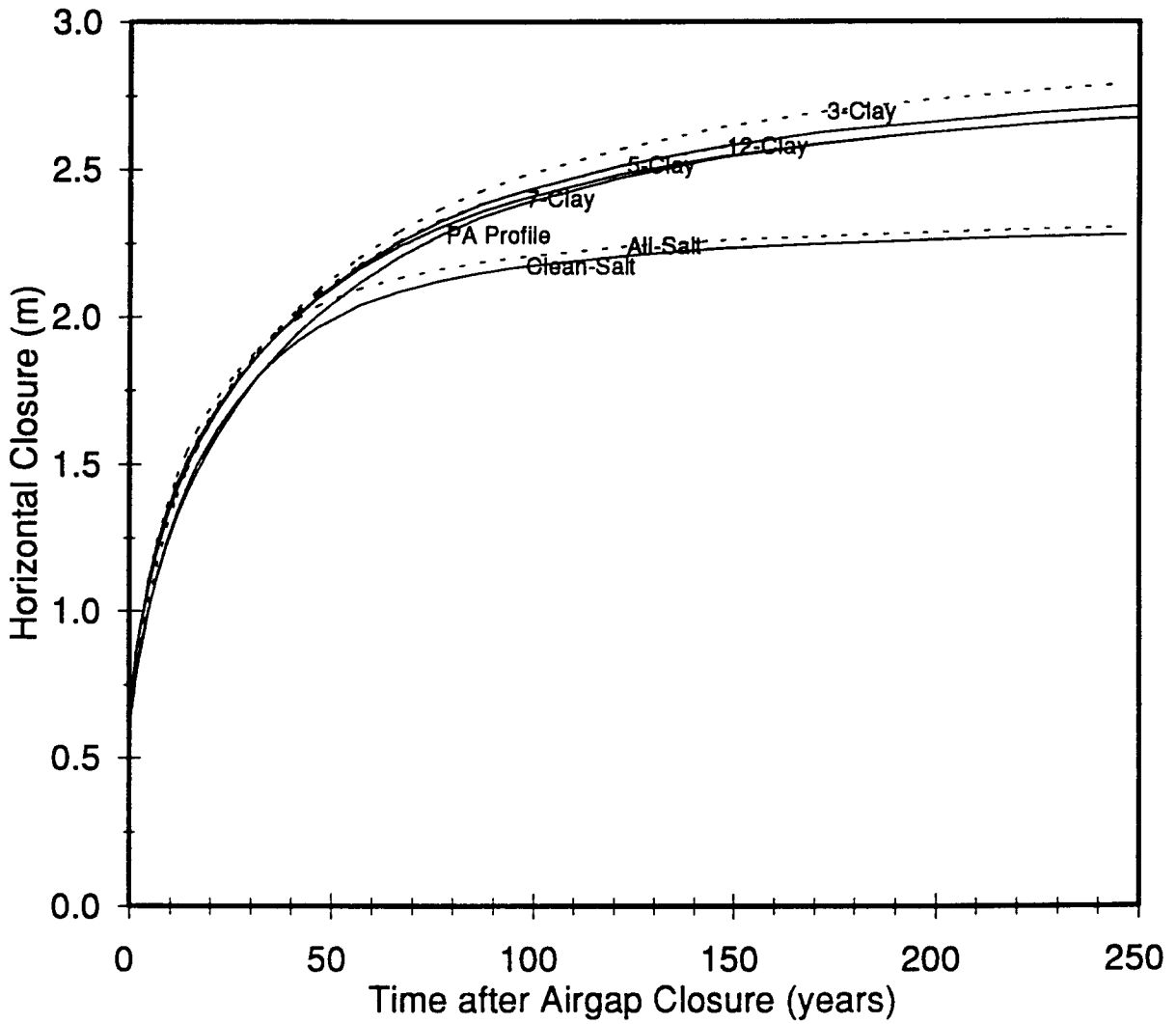


Figure 7. Comparison of the Horizontal Closures of the Disposal Room Predicted by Each of the Stratigraphic Models.

In Figures 6 and 7, the vertical and horizontal closure predictions for all of the models in which clay seams and marker beds were represented fall in narrow bands. In addition, the horizontal closures predicted for these models exceed the vertical closures at all times, with differences of about 0.5 m at 250 years. The closure results for the All-Salt and Clean-Salt Models, in which clay seams and marker beds were not represented, are discernibly different from the results for the other stratigraphic models. At 250 years, these two models predict vertical closures that are about 0.3 m more and horizontal closures that are about 0.4 m less than the corresponding closures predicted by the other models. Further, unlike the predictions of the other models, the horizontal closures are smaller than the vertical closures at all times in the All-Salt and Clean-Salt Models.

The differences between the closure predictions are accentuated in Figures 8 and 9 by comparing the closures predicted by each stratigraphic model to the closures predicted by the 12-Clay Model. The 12-Clay Model was considered the baseline model for this comparison because all of the stratigraphic units in the Revised Reference Stratigraphy, except Anhydrite C, are represented in the 12-Clay Model; the other stratigraphic models represent additional simplifications to the Revised Reference Stratigraphy. The vertical and horizontal closures predicted by the 7-Clay and 5-Clay Models are essentially the same as the closures predicted by the 12-Clay Model, differing by less than 0.05 m at all times. Simplifying the stratigraphy further to the 3-Clay and PA Profile Models yielded somewhat greater deviations from the 12-Clay Model predictions. Nevertheless, the maximum difference between the vertical closures predicted by these two models and the 12-Clay Model is only 0.17 m; the maximum difference in the horizontal closure predictions is even smaller (less than 0.1 m). To provide perspective for the magnitudes of these differences, Figure 3 indicates that modeling the anhydrite marker beds as either elastic or limited-tension materials in the 12-Clay Model yields a difference in vertical closure of 0.1 m at only 7 years after excavation and this difference is clearly increasing with time. Hence, the differences in the closures predicted by the 3-Clay, PA Profile, and 12-Clay Models are relatively insignificant compared to the effects of other modeling considerations.

Figures 8 and 9 clearly illustrate the magnitudes of the differences between the closures predicted by the All-Salt and Clean-Salt Models and the closures predicted by the other stratigraphic models. The differences in vertical closure at 50 years are particularly significant when one considers that the 12-Clay Model predicted a room height at the centerline of 2.33 m whereas the All-Salt and Clean-Salt Models predicted heights of only 1.80 m and 1.90 m. The close agreement between the closures predicted by the All-Salt and Clean-Salt Models is somewhat surprising because the All-Salt Model is composed predominately of argillaceous halite which creeps appreciably faster than the clean halite that comprises the entirety of the Clean-Salt Model.

The room porosities calculated from the simulations of the various stratigraphic models are compared in Figure 10. The differences in the room porosities relative to the porosities

RSI-390-95-009

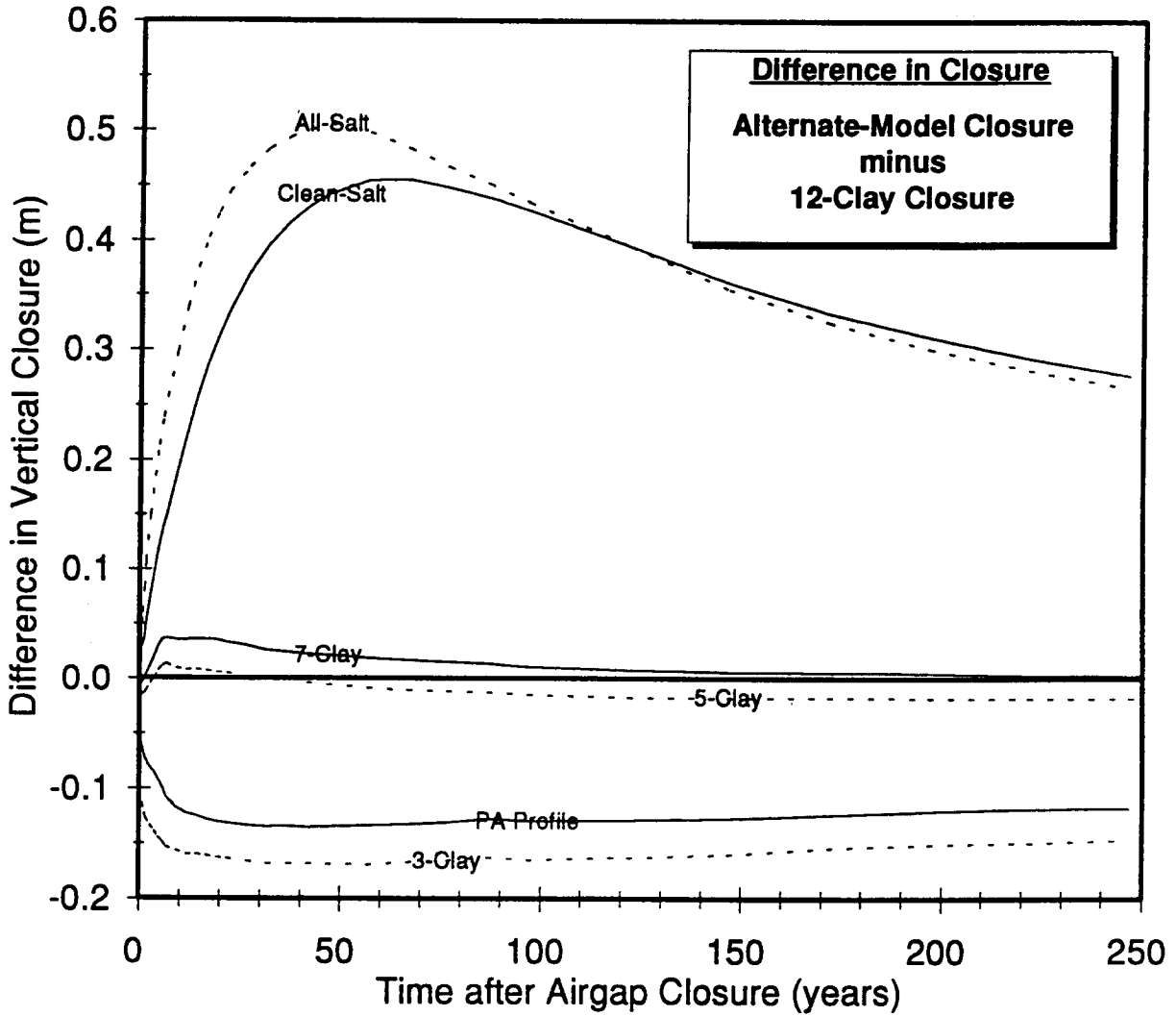


Figure 8. Differences Between the Vertical Closures of the Disposal Room Predicted by Each of the Stratigraphic Models and the 12-Clay Model.

RSI-390-95-010

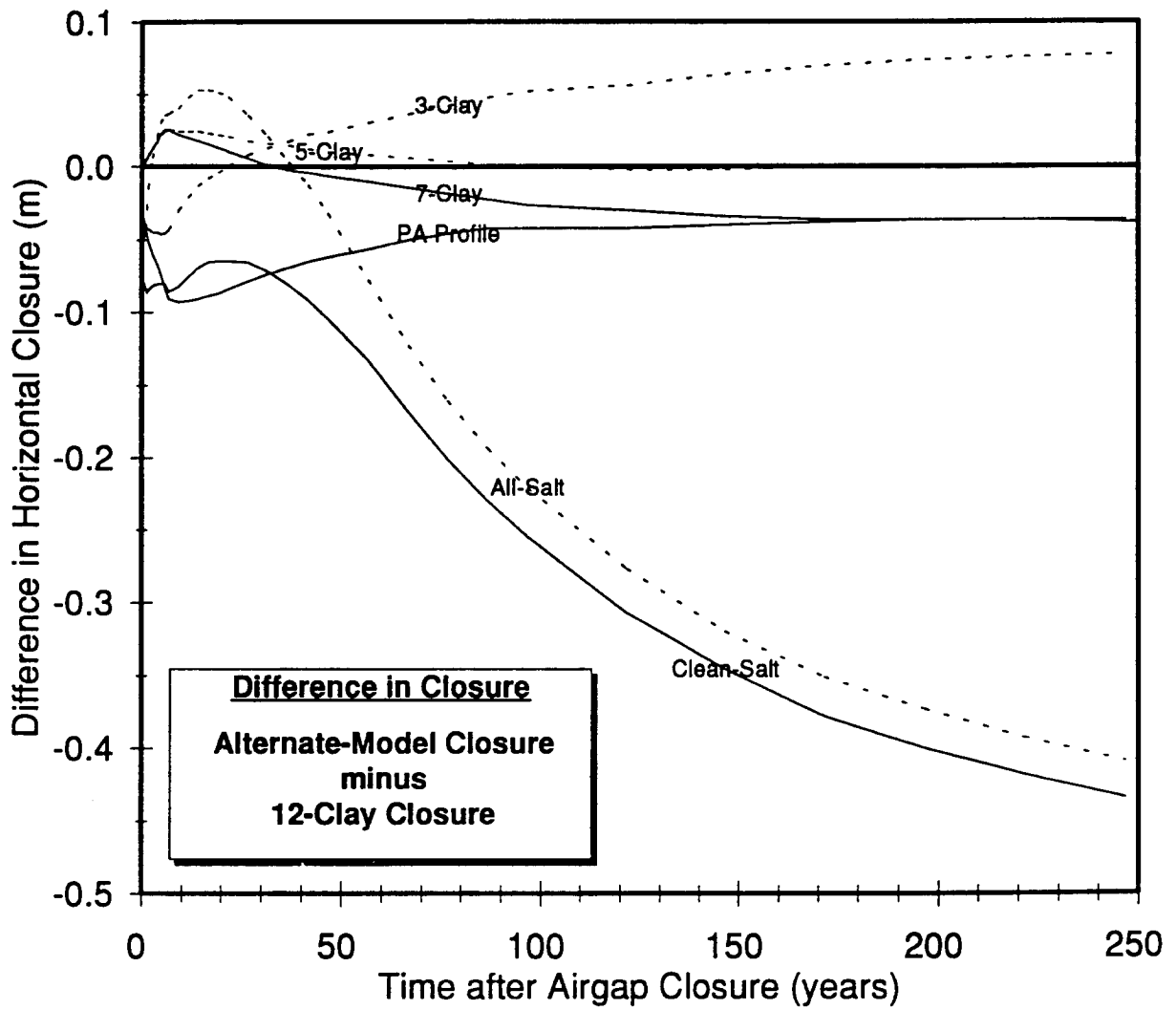


Figure 9. Differences Between the Horizontal Closures of the Disposal Room Predicted by Each of the Stratigraphic Models and the 12-Clay Model.

RSI-390-95-011

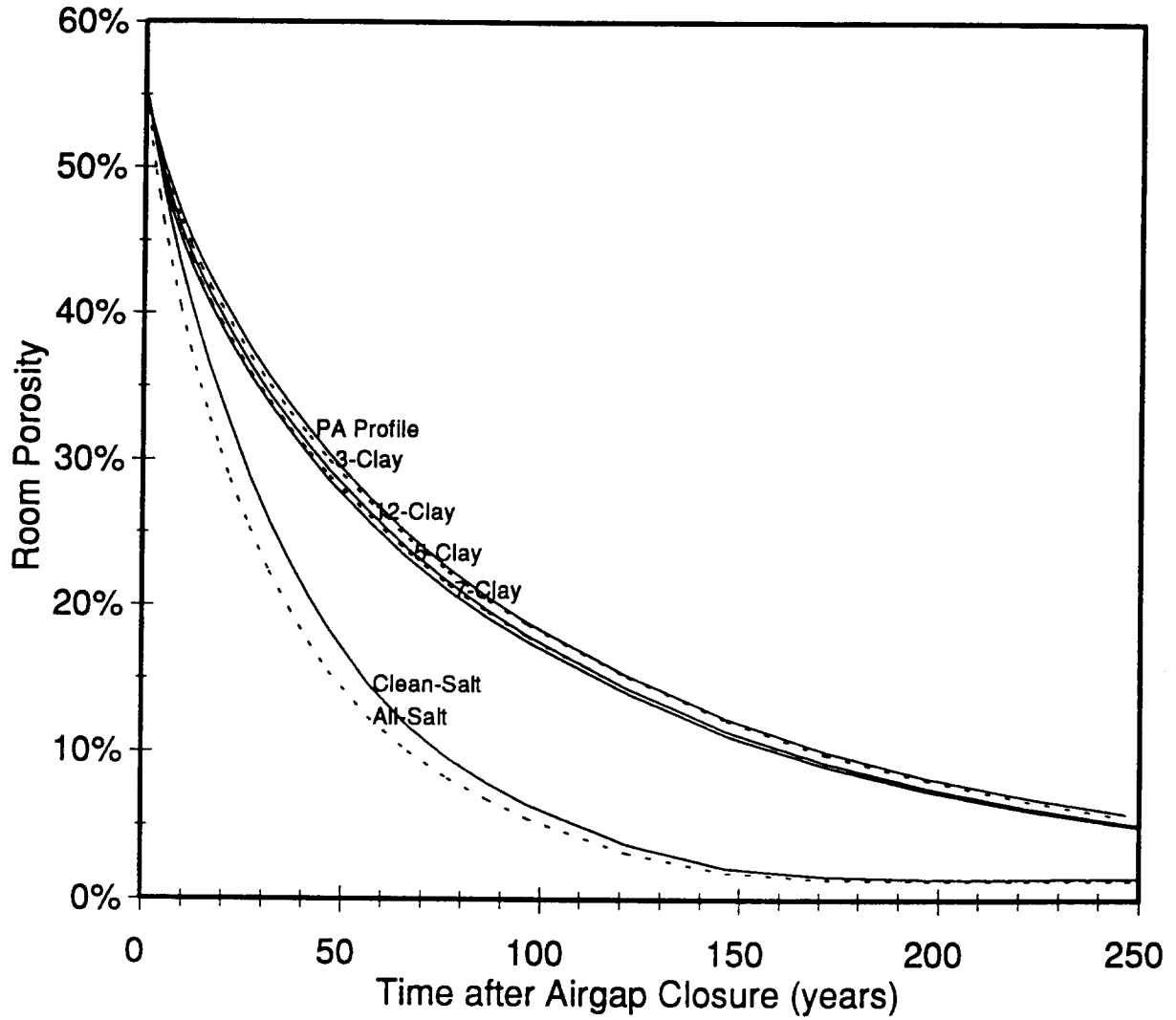


Figure 10. Comparison of the Room Porosities Calculated From the Simulations of Each of the Stratigraphic Models.

calculated from the 12-Clay simulation are shown in Figure 11. Like the room closures, the room porosities calculated from all of the models except the All-Salt and Clean-Salt Models fall in a narrow band; whereas the porosities calculated from the All-Salt and Clean-Salt simulations are appreciably different from the porosities calculated from the other models in which clay seams and marker beds were represented. Of the latter group of models, the porosities calculated from the PA Profile simulation deviate the most from the 12-Clay simulation, but the maximum difference is only 1.2 percent. The porosities calculated from the 5-Clay simulation deviate the least from the 12-Clay simulation, although the porosities calculated from the 5-Clay and 7-Clay simulations are essentially the same and differ from each other by less than 0.4 percent.

The porosities calculated from the All-Salt and Clean-Salt simulations are appreciably smaller than the porosities calculated from all of the other stratigraphic models at all times less than 250 years. The maximum differences from the porosities calculated from the 12-Clay simulation are approximately 14 and 12 percent, respectively. The maximum differences occur at about 50 years when the room porosity calculated from the 12-Clay simulation is 29 percent. The consolidation of the room contents is essentially complete at 200 years in the All-Salt and Clean-Salt simulations; whereas the room contents continue to consolidate through about 500 years in the 12-Clay simulation.

Room porosities are needed in simulations of repository performance assessment because the gas pressure that drives fluid transport depends on the volume of the void space and the amount of gas in the room. According to the ideal gas law, the pressure produced by a given amount of gas is inversely proportional to the void volume in the room, which is the product of the room porosity and the room volume. Consequently, even though gas generation was not simulated in this study, a crude indication of the relative effects of the differences in room porosity on gas pressure can be obtained from the ratios between the void volumes calculated from the various simulations in this study. This simplistic approach neglects the fact that gas generation and the associated gas pressure reduces the room closure and increases the room porosity relative to values determined in this study without gas generation.

Figure 12 shows the void volume ratios calculated by dividing the void volumes from the 12-Clay simulation by the corresponding void volumes from the simulations of the other stratigraphic models. The ratios for all of the models except the All-Salt and Clean-Salt Models are so narrowly grouped that they are regraphed at an expanded scale in Figure 13 for clarification. Because of the inverse relationship between gas pressure and void volume, ratios greater than unity in these figures indicate that the pressures that would be produced by the same amounts of gas would be greater in the alternate stratigraphic model than in the 12-Clay Model. Clearly, disposal room simulations based on the All-Salt and Clean-Salt Models would yield substantially higher gas pressures than simulations based on any of the other stratigraphic models *if the higher gas pressures did not result in correspondingly larger room porosities and void volumes.*

RSI-390-95-012

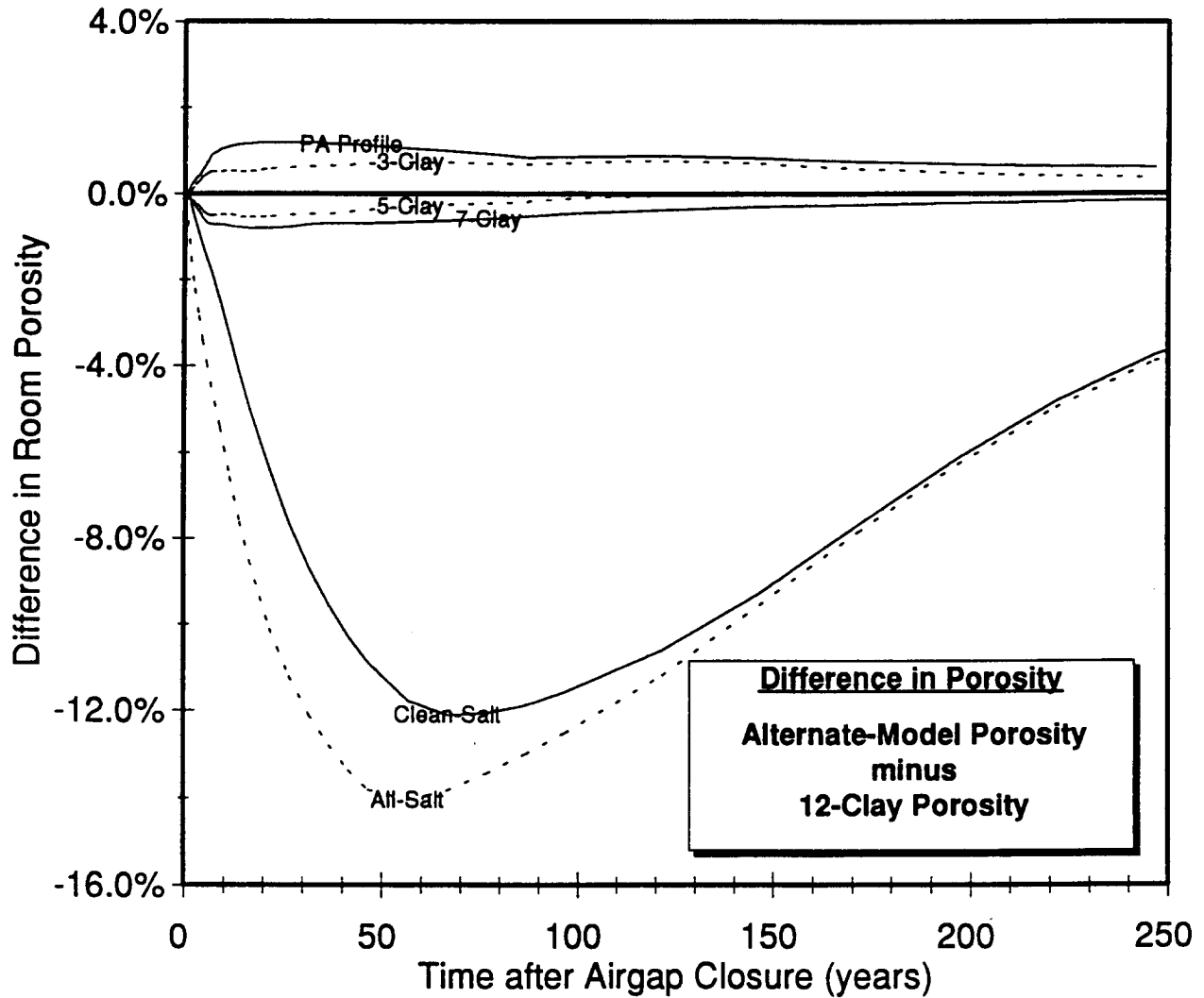


Figure 11. Differences Between the Room Porosities Calculated From the 12-Clay Simulation and the Room Porosities Calculate From the Simulations of the Other Stratigraphic Models.

RSI-390-95-013

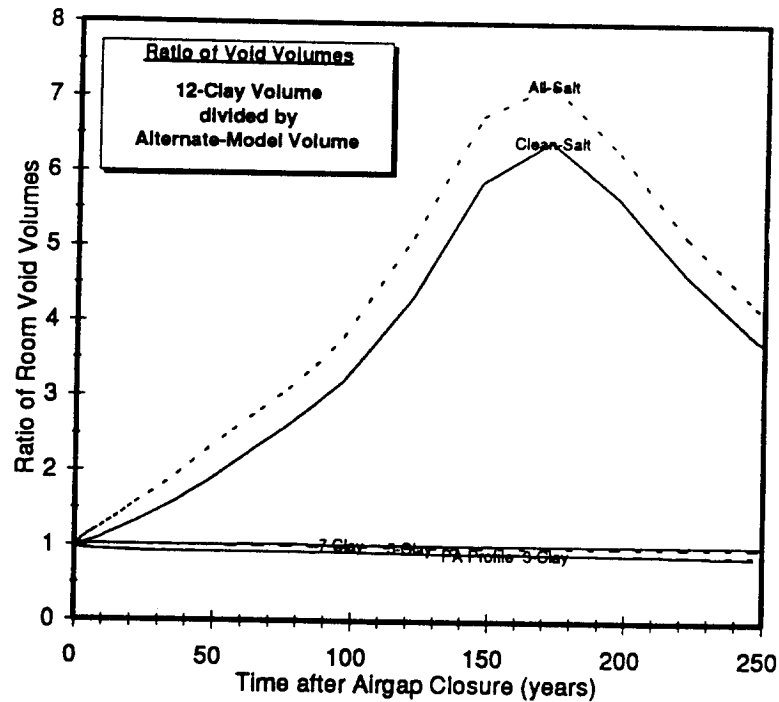


Figure 12. Ratios Between the Room Void Volumes Calculated From the 12-Clay Simulation and the Room Void Volumes Calculated From the Simulations of the Other Stratigraphic Models.

RSI-390-95-028

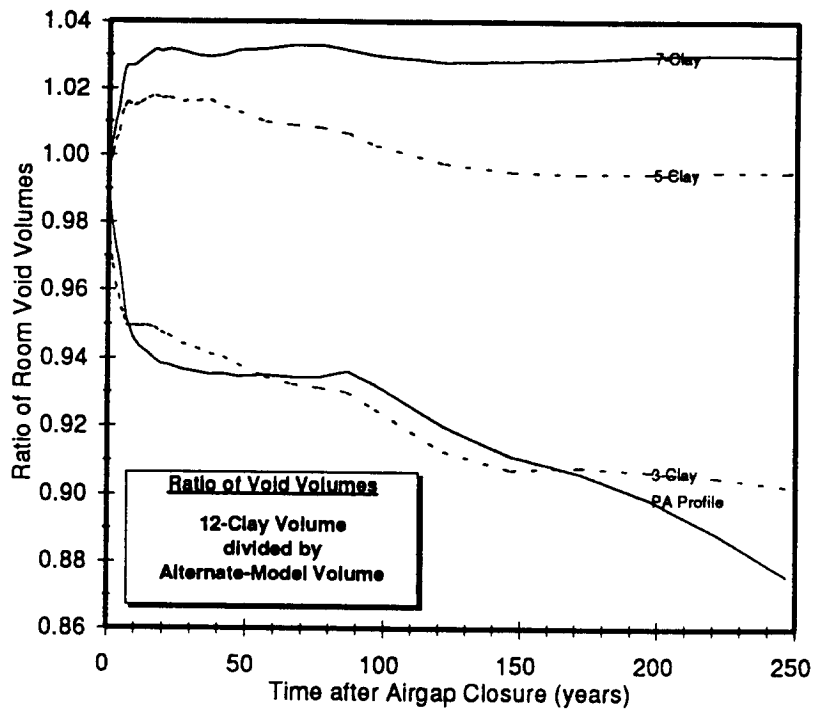


Figure 13. Ratios Between Room Void Volumes Calculated From the 12-Clay Simulation and the Room Void Volumes Calculated From the Simulations of the Other Clay-Seam Models.

5.0 SUMMARY AND CONCLUSIONS

The objective of this study was to investigate the effects of simplifying the Revised Reference Stratigraphy defined in Butcher and Holmes [1995] on simulations of the mechanical response of WIPP disposal rooms. The simplification of principal interest was the number of clay seams represented in the disposal room model, and the only responses considered were room closure and porosity. The Revised Reference Stratigraphy contains 12 clay seams and 8 marker beds interspersed between layers of argillaceous and clean halite. A symmetric half of a WIPP disposal room and pillar in an infinite array of disposal rooms was simulated in 7 variations of the Revised Reference Stratigraphy using the finite-strain modeling capability in Version 4.06 of the finite element program SPECTROM-32.

The 7 stratigraphic models simulated in this study were designated the 12-Clay, 7-Clay, 5-Clay, 3-Clay, PA Profile, All-Salt, and Clean-Salt Models. The stratigraphy represented in each of these models is defined in Table 1. The 12-Clay Model was considered the baseline model because all of the stratigraphic units in the Revised Reference Stratigraphy except the 0.08-m thick Anhydrite C layer were represented in the 12-Clay Model. Additional simplifications to the Revised Reference Stratigraphy were simulated in the other 6 stratigraphic models. The 7 marker beds represented in the 12-Clay Model also were represented in the 7-Clay, 5-Clay, and 3-Clay Models, but progressively fewer clay seams were simulated in each of these models. Three clay seams also were simulated in the PA Profile Model, but the only other stratigraphic units represented in this model were the 3 marker beds directly above these clay seams and the clean halite layer above the room. None of the marker beds or clay seams were simulated in the All-Salt Model, although the clean halite layer was represented. Hence, the All-Salt Model was composed predominately of argillaceous halite. The Clean-Salt Model was composed entirely of clean halite. Although this model has little resemblance to the Revised Reference Stratigraphy, it was simulated because most of the previous calculations of disposal room closure and porosity were based on models composed of only clean halite.

The room closures and porosities calculated from the 12-Clay, 7-Clay, and 5-Clay simulations were essentially the same throughout the 500-year period of consolidation of the room contents. The horizontal and vertical closures predicted by the 7-Clay and 5-Clay Models differed from the corresponding closures predicted by the 12-Clay Model by less than 0.05 m; the room porosities differed by less than 0.8 percent. Further simplifying the stratigraphy to the 3-Clay and PA Profile Models produced slightly larger deviations from the 12-Clay results, yielding maximum differences in vertical closure, horizontal closure, and room porosity of 0.17 m, 0.08 m, and 1.2 percent, respectively, through 250 years. Nevertheless, these differences probably are insignificant compared to differences that would be caused by other changes in the models such as mesh refinement, time-step control, and convergence tolerances.

The room closures and porosities calculated from the All-Salt and Clean-Salt simulations were very similar to each other, but they differed appreciably from the results calculated from

the other stratigraphic models. Both of these models overpredicted the room closure, and in turn, underpredicted the room porosity. The Clean-Salt Model generally yielded vertical closures and room porosities that were closer to the results of the 12-Clay Model, with maximum differences of 0.46 m and 12.1 percent, respectively, through 250 years; the All-Salt Model predicted horizontal closures that were slightly closer to the predictions of the 12-Clay Model with a maximum difference of 0.41 m.

With respect to calculations of room closure and porosity, the results of this study clearly indicate that inclusion of the nonsalt units in the Revised Reference Stratigraphy in disposal room models yields appreciable reductions in vertical room closure and increases in room porosities compared to predictions based on models without the marker beds and clay seams. The results are relatively insensitive to the number of clay seams represented in the model, but they are far more sensitive to whether or not the 3 marker beds nearest the room (MB139, Anhydrite A, and MB138) are modeled. This conclusion is supported by the results of the PA Profile Model which contains only these 3 marker beds and the clay seam below each of them. The room closures and porosities calculated from the PA Profile Model closely agree with the results of the 3-Clay Model that contains 7 marker beds and 3 clay seams (of which only Clay E is represented in both models). Conversely, the results of the PA Profile Model differ substantially from the closures and porosities calculated from the All-Salt Model, which has the same stratigraphy as the PA Profile Model with the 3 marker beds and clay seams removed.

Overall, the stratigraphy represented in the PA Profile Model appears to be adequate for calculations of room porosity. Using this model for room porosity calculations has the added advantage of being consistent with the models used for flow and transport simulations in repository performance assessment. It must be emphasized that these conclusions regarding stratigraphy in disposal room models are strictly applicable to room closure and porosity calculations, the responses focused upon in this study. Prediction of other mechanical responses such as stresses in the disturbed rock zone around the room may require inclusion of additional stratigraphic details. It also should be noted that the effects of gas generation were not investigated in this study. Representing at least the stratigraphy in the PA Profile Model clearly yields appreciable differences in the room closures and porosities calculated from simulations in which gas generation is not modeled. These differences may be muted to some extent in simulations with nonzero gas generation rates because gas generation and the associated pressurization of the disposal rooms limit the closure of the rooms. The relationship between the effects of stratigraphy and gas generation cannot be assessed without further investigation.

Preliminary simulations of the 12-Clay Model indicated that the material model used to represent the anhydrite marker beds is at least as important in room closure and porosity calculations as whether or not the marker beds are represented at all. When the marker beds were represented as elastic materials, unrealistically large tensile stresses (in excess of 150 MPa) were predicted in the marker beds near the disposal room. When the tensile stresses were

limited to a maximum of 1 MPa by using a limited-tension model to represent the anhydrite marker beds, the marker beds were substantially more flexible as they bent in response to room closure. As a result, the vertical room closure at 7 years after excavation increased by 0.1 m in the preliminary simulations of the 12-Clay Model, and this difference was increasing with time.

As a final note with respect to disposal room modeling and porosity calculation, this study revealed that the TRU waste characteristics specified in Butcher and Holmes [1995] yield substantially different waste porosities as a function of mean stress than the characteristics used in previous analyses. The cumulative effect of the changes to the TRU waste characteristics is that the porosities calculated from the Butcher and Holmes [1995] specifications become negative at mean stresses greater 2.5 MPa if it is assumed that the solids are incompressible. This physically impossible response is apt to be predicted in long-term simulations of disposal rooms without gas generation, such as made in this study. Negative porosities were precluded in this study by assuming that the compressibility of the solids can be neglected only until the porosity approaches zero and by modifying the calculational method accordingly. As a result, the porosities of the TRU waste region approached zero and never became negative. Nonetheless, the validity and applicability of the TRU waste characteristics should be investigated further.

6.0 REFERENCES

Butcher, B. M. and J. T. Holmes, 1995. *Completion of Milestone DR015, Definition of Closure Analysis Input Parameters, Due March 31, 1995*, Internal Memorandum to L. Shephard and M. Tierney, Sandia National Laboratories, Albuquerque, NM, March 31.

Callahan, G. D., 1994. *SPECTROM-32: A Finite Element Thermomechanical Stress Analysis Program, Version 4.06*, prepared by RE/SPEC Inc., Rapid City, SD, RSI-0531, for Sandia National Laboratories, Albuquerque, NM.

Callahan, G. D. and K. L. DeVries, 1991. *Analyses of Backfilled Transuranic Wastes Disposal Rooms*, SAND91-7052, Sandia National Laboratories, Albuquerque, NM.

Callahan, G. D., A. F. Fossum, and D. K. Svalstad, 1990. *Documentation of SPECTROM-32: A Finite Element Thermomechanical Stress Analysis Program*, DOE/CH/10378-2, prepared by RE/SPEC Inc., Rapid City, SD, for U. S. Department of Energy, Chicago Operations Office, Argonne, IL, Vol. 1 and 2.

DeVries, K. L., 1994. *Analysis of a WIPP Disposal Room Located in the Reference Stratigraphy Using the Finite Strain Formulation and the M-D Constitutive Model (Sandia National Laboratories Contract AB-5908)*, External Memorandum RSI(RCO)-262/10-94/39, RE/SPEC Inc., Rapid City, SD, November 2.

Krieg, R. D., 1984. *Reference Stratigraphy and Rock Properties for the Waste Isolation Pilot Plant (WIPP) Project*, SAND83-1908, Sandia National Laboratories, Albuquerque, NM.

Labreche, D. A., 1995. *Comparison of SPECTROM-32 and SANTOS Results: Analysis of a WIPP Disposal Room Located in a Layered Stratigraphy (SNL Contract AK-7653)*, External Memorandum RSI(ALO)-390/07-95/641, RE/SPEC Inc., Albuquerque, NM, August 3.

Labreche, D. A., G. D. Callahan, K. L. DeVries, and J. D. Osnes, 1993. *Comparison of Two Geomechanical Analysis Codes for WIPP Disposal Room Modeling: SANCHO and SPECTROM-32*, RSI-0461, prepared by RE/SPEC Inc., Rapid City, SD, for Sandia National Laboratories, Albuquerque, NM.

Munson, D. E., 1992. *Mechanical Parameters for Volume 3, SAND92-0700*, Internal Memorandum to M. S. Tierney, Sandia National Laboratories, Albuquerque, NM, October 26, (in *Preliminary Performance Assessment for the Waste Isolation Pilot Plant, December 1992, Volume 3: Model Parameters*, SAND92-0700/3, Appendix A, pp. A-107 to A-124, Sandia National Laboratories, Albuquerque, NM).

Munson, D. E., A. F. Fossum, and P. E. Senseny, 1989. *Advances in Resolution of Discrepancies Between Predicted and Measured In Situ WIPP Room Closures*, SAND88-2948, Sandia National Laboratories, Albuquerque, NM.

Osnes, J. D. and T. Brandshaug, 1980. "Application of 'No Tension' Analysis to Fissure Development in Plutonic Rock Above a Nuclear Waste Vault," *13th Canadian Rock Mechanics Symposium Special Volume*, Toronto, Ontario.

Sandia WIPP Project, 1992. *Preliminary Performance Assessment for the Waste Isolation Pilot Plant, December 1992, Volume 3: Model Parameters*, SAND92-0700/3, Sandia National Laboratories, Albuquerque, NM.

Stone, C. M., 1992. *Creep Closure of Waste Disposal Rooms in Bedded Salt Due to Gas Generation Produced by Several Alternatives of the Engineered Alternatives Task Force*, Internal Memorandum to B. M. Butcher, Sandia National Laboratories, Albuquerque, NM.

Weatherby, J. R., J. G. Argüello, B. M. Butcher, and C. M. Stone, 1991a. "The Structural Response of a WIPP Disposal Room with Internal Gas Generation," *Proceedings, 32nd U. S. Symposium on Rock Mechanics, July 10–12, University of Oklahoma, Norman, OK, A. A. Balkema, Rotterdam, Netherlands*, pp. 929–937.

Weatherby, J. R., W. T. Brown, and B. M. Butcher, 1991b. "The Closure of WIPP Disposal Rooms Filled with Various Waste and Backfill Combinations," *Proceedings, 32nd U. S. Symposium on Rock Mechanics, July 10–12, University of Oklahoma, Norman, OK, A. A. Balkema, Rotterdam, Netherlands*, pp. 919–928.

WIPP Performance Assessment Department, 1993. *Preliminary Performance Assessment for the Waste Isolation Pilot Plant, December 1992, Volume 4: Uncertainty and Sensitivity Analyses for 40 CFR 191, Subpart B, SAND92-0700/4, Sandia National Laboratories, Albuquerque, NM.*

Zienkiewicz, O. C., B. E. Valliappan, and J. P. King, 1968. "Stress Analysis of Rock as a 'No Tension' Material," *Geotechnique*, Vol. 18, pp. 56–66.

JDO:sdc

ATTACHMENT A

**ROOM CLOSURES AND POROSITIES
PREDICTED BY EACH STRATIGRAPHIC MODEL**

RSI-390-95-014

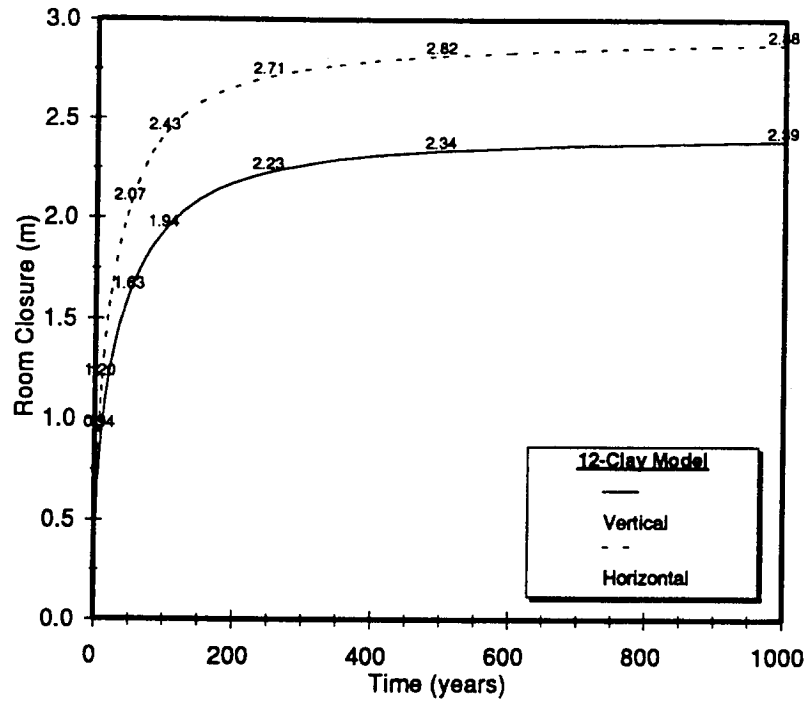


Figure A-1. Vertical and Horizontal Room Closures Predicted by the 12-Clay Model.

RSI-390-95-015

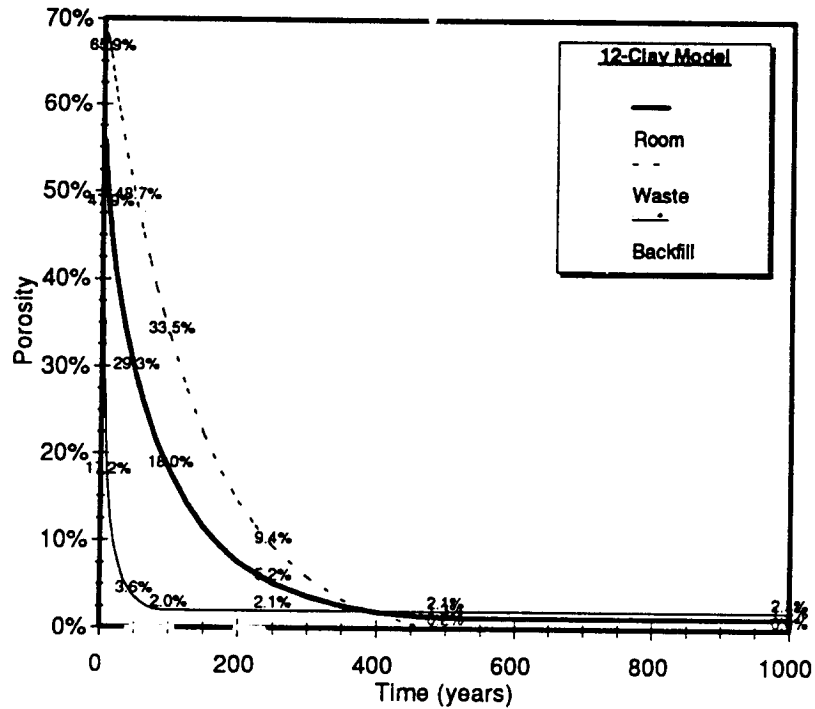


Figure A-2. Backfill, Waste, and TRU Waste Porosities Predicted by the 12-Clay Model.

RSI-390-95-016

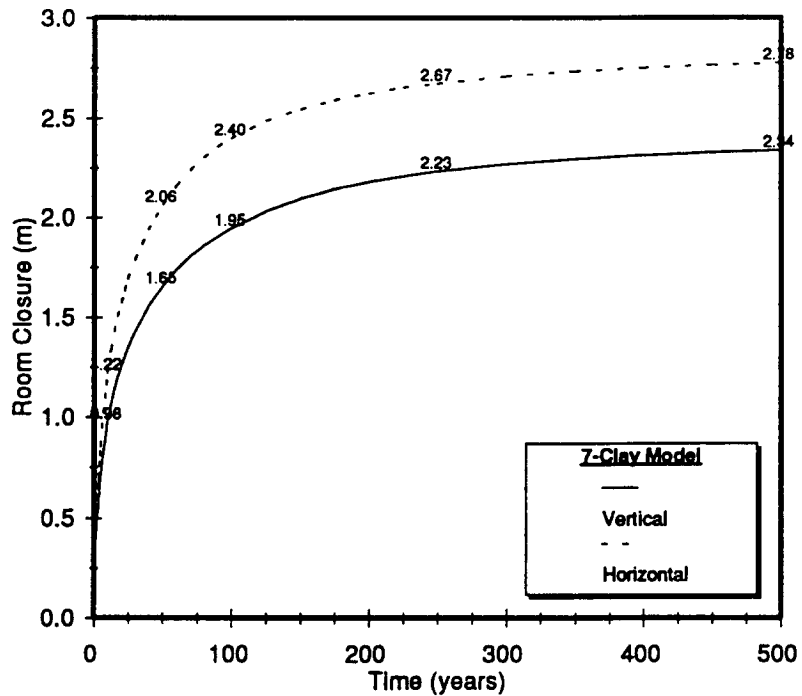


Figure A-3. Vertical and Horizontal Room Closures Predicted by the 7-Clay Model.

RSI-390-95-017

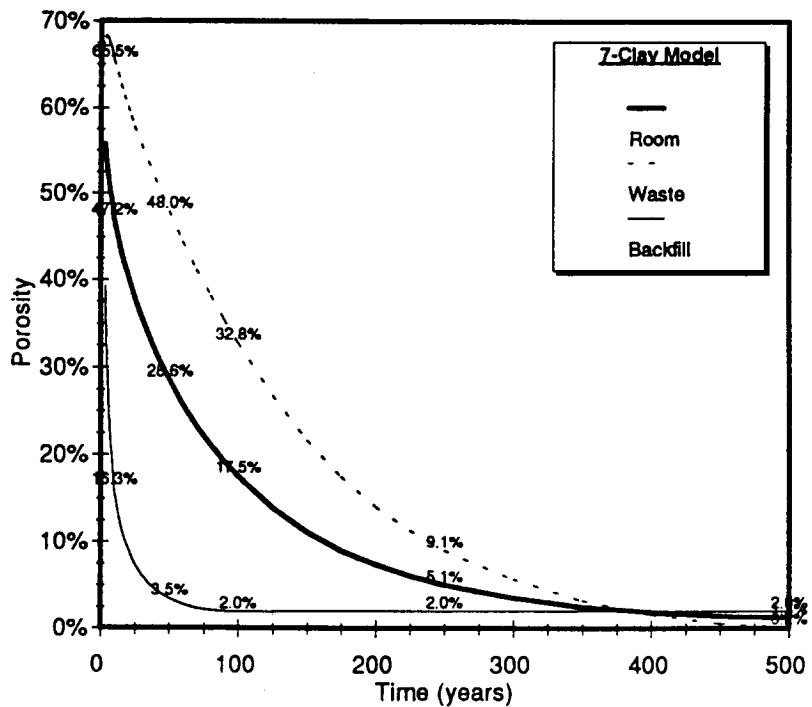


Figure A-4. Backfill, Waste, and TRU Waste Porosities Predicted by the 7-Clay Model.

RSI-390-95-018

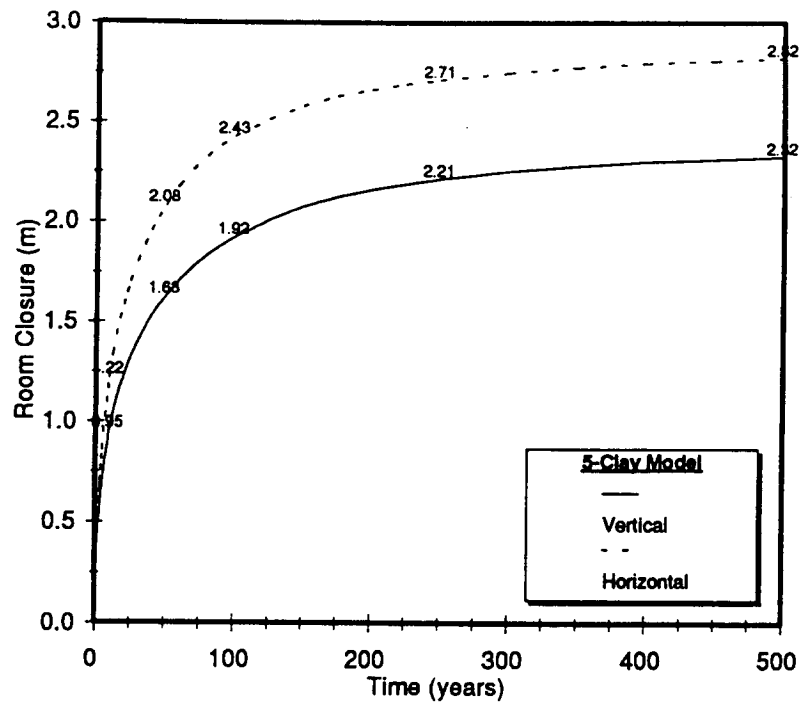


Figure A-5. Vertical and Horizontal Room Closures Predicted by the 5-Clay Model.

RSI-390-95-019

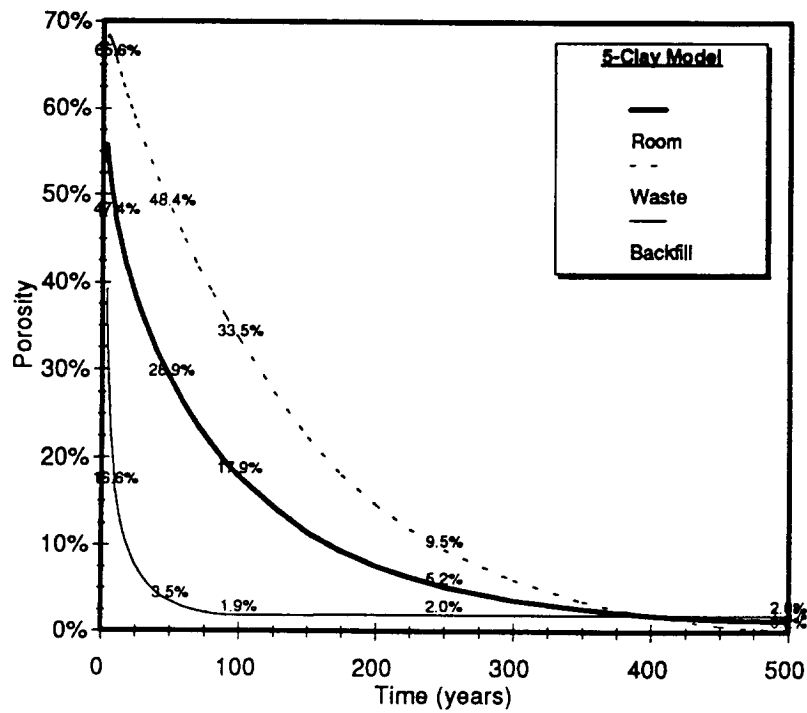


Figure A-6. Backfill, Waste, and TRU Waste Porosities Predicted by the 5-Clay Model.

RSI-390-95-020

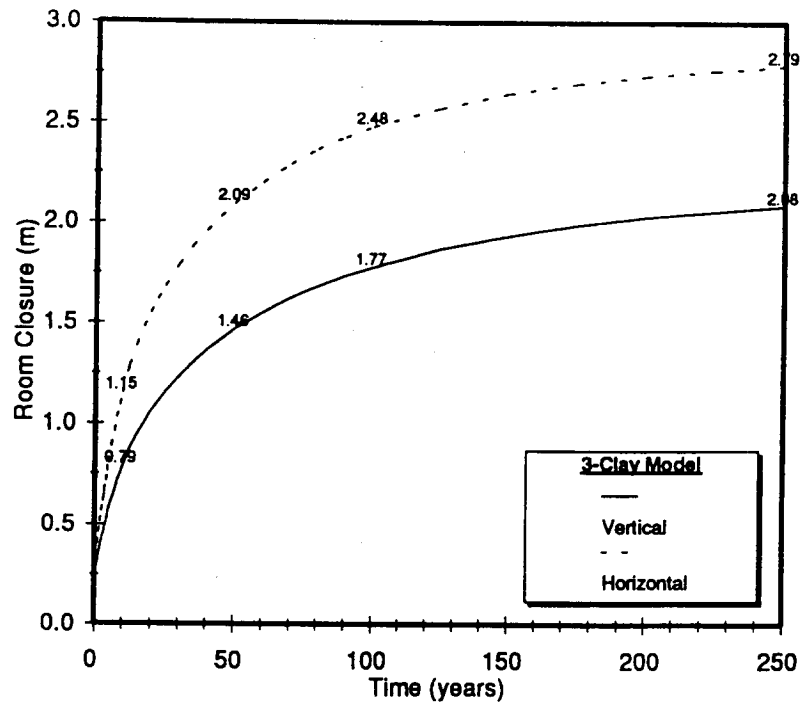


Figure A-7. Vertical and Horizontal Room Closures Predicted by the 3-Clay Model.

RSI-390-95-021

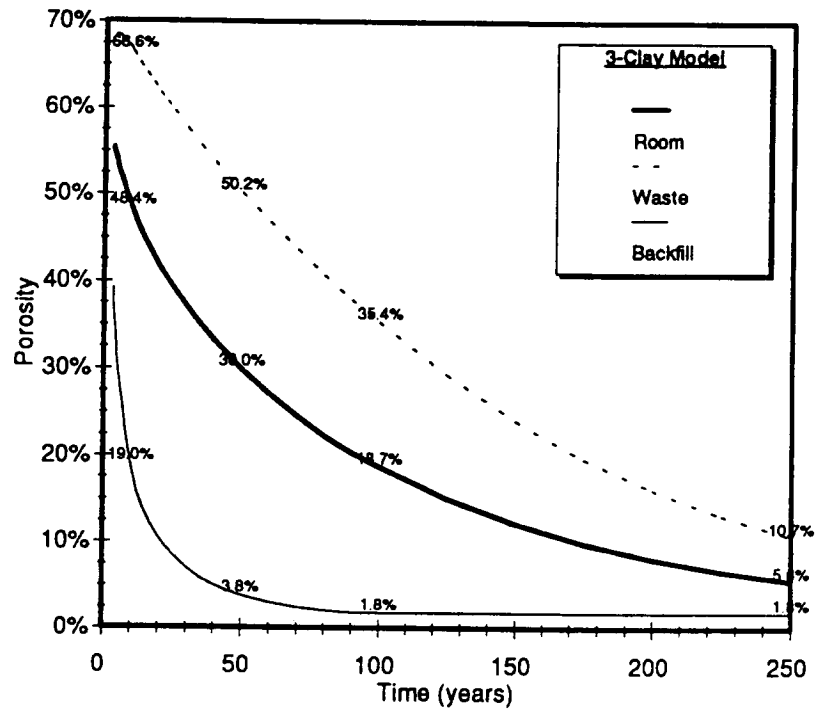


Figure A-8. Backfill, Waste, and TRU Waste Porosities Predicted by the 3-Clay Model.

RSI-390-95-022

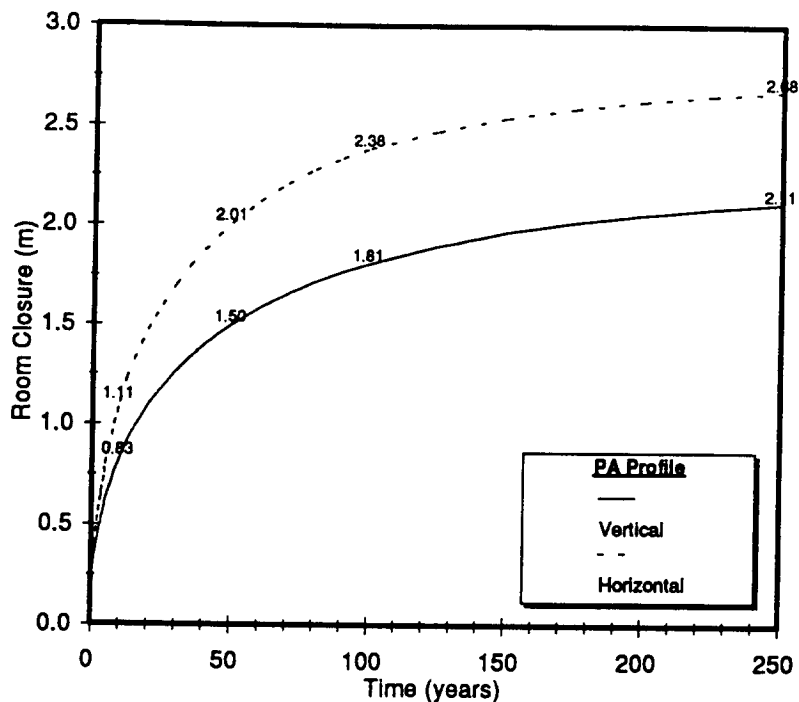


Figure A-9. Vertical and Horizontal Room Closures Predicted by the PA Profile Model.

RSI-390-95-023

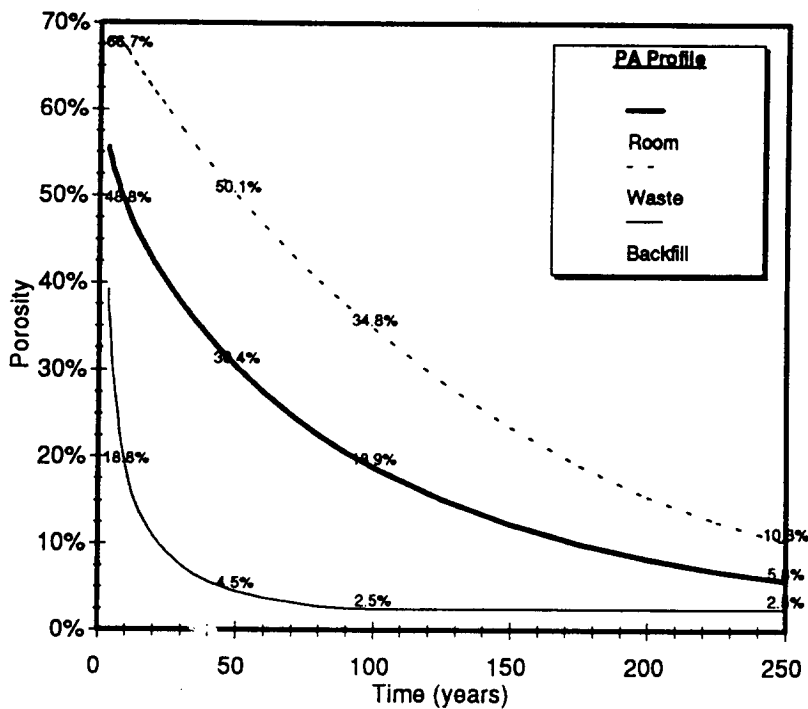


Figure A-10. Backfill, Waste, and TRU Waste Porosities Predicted by the PA Profile Model.

RSI-390-95-024

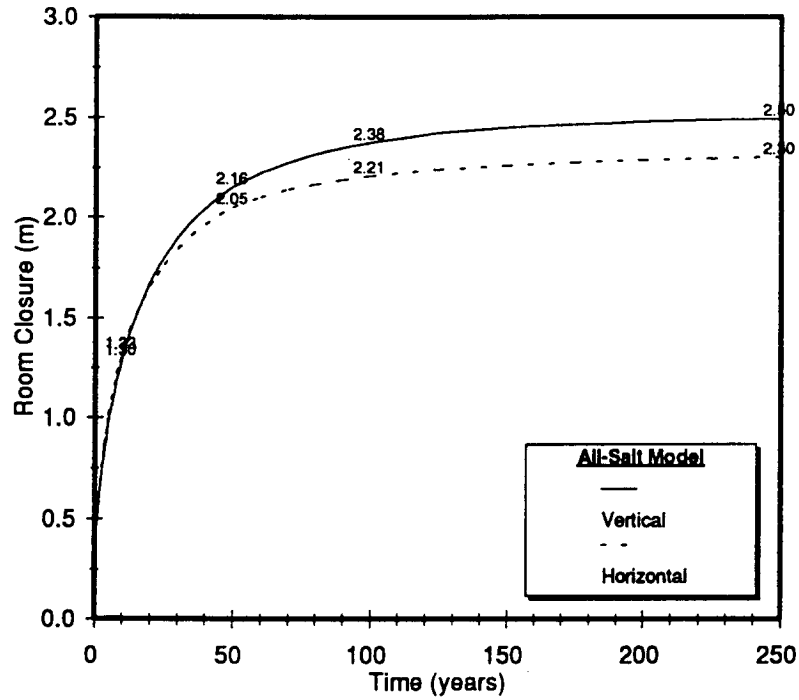


Figure A-11. Vertical and Horizontal Room Closures Predicted by the All-Salt Model.

RSI-390-95-025

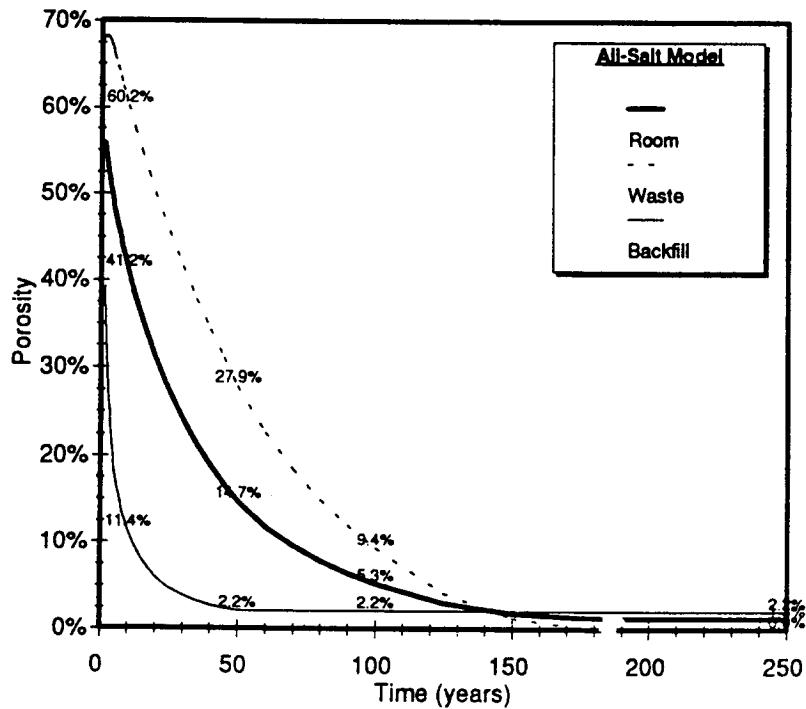


Figure A-12. Backfill, Waste, and TRU Waste Porosities Predicted by the All-Salt Model.

RSI-390-95-026

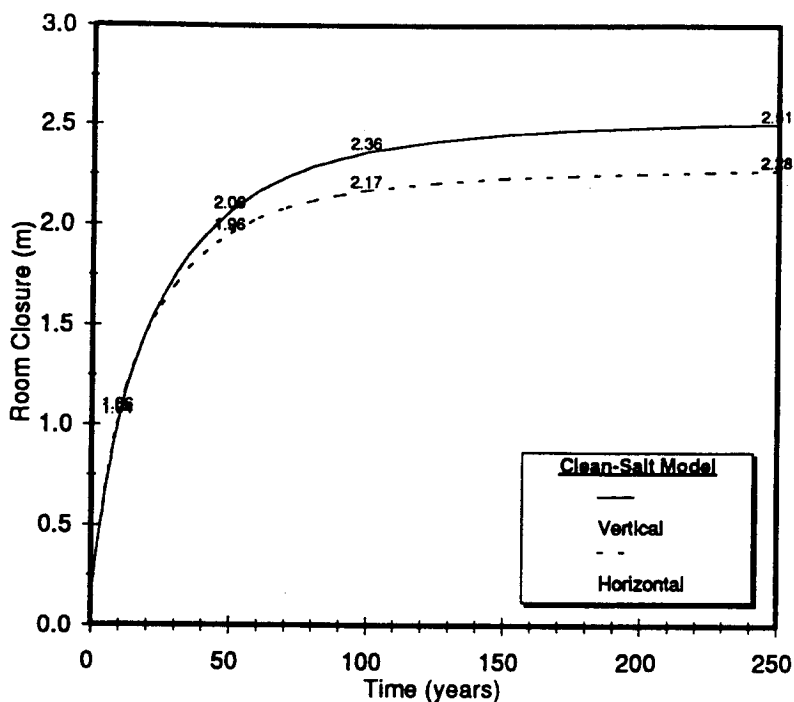


Figure A-13. Vertical and Horizontal Room Closures Predicted by the Clean-Salt Model.

RSI-390-95-027

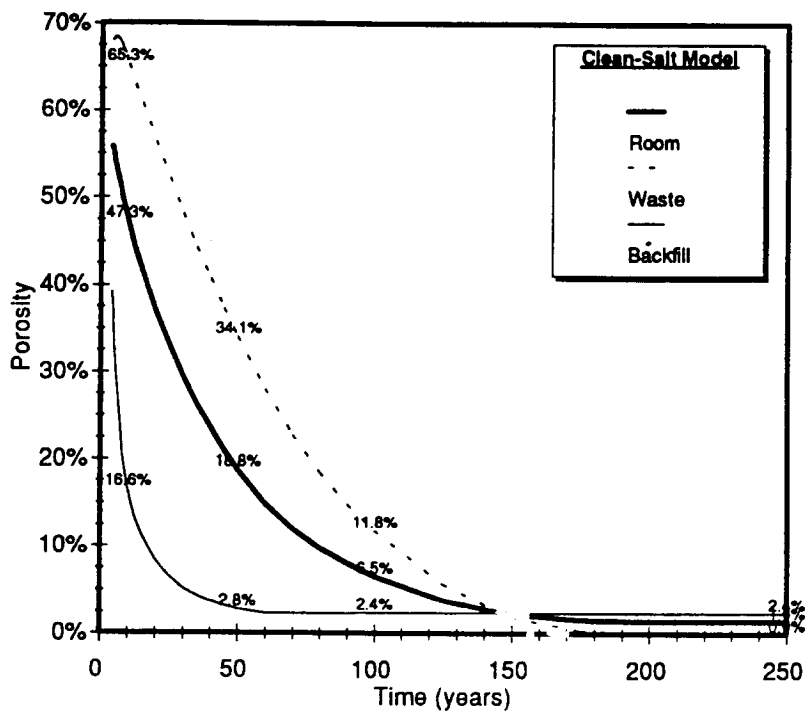


Figure A-14. Backfill, Waste, and TRU Waste Porosities Predicted by the Clean-Salt Model.

ATTACHMENT B

**DEFINITION OF CLOSURE ANALYSIS INPUT PARAMETERS
[BUTCHER AND HOLMES, 1995]**

Sandia National Laboratories

Albuquerque, New Mexico 87185-1341

date: March 31, 1995

to: Les Shephard, 6701, MS 1395, Martin Tierney, 6741, MS 1328


from: Barry Butcher, John Holmes, 6748, MS 1341

subject: Completion of milestone DR015, definition of closure analysis input parameters, due March 31, 1995

A task to review and update closure analysis input parameters has been completed. These values are listed in the attachment, and should be used for all future porosity surface calculations. This same memo and the attachment are also being transmitted to our QA representative, in order to request guidance about what QA procedures are required to qualify the information for compliance calculations.

Copy to:

MS 0443 C. M. Stone (1517)
MS 0443 J. G. Arguello, Jr (1517)
MS 1322 D. E. Munson (6121)
MS 1330 SWCF(DRM) (WBS 1.1.1.2.3) (6352)
MS 1341 B. M. Butcher (6748) day file
MS 1341 A. L. Stevens (6706)
MS 1341 Wyla Green (6706)
MS 1341 Dyan Foss (6706)
Duane Lebreche, RE/SPEC

Copy without attachment to:

MS 1395 P. E. Brewer (6700)
MS 1335 S. A. Goldstein (6705)
MS 1328 D. R. Anderson (1328)
MS 1395 D. Brewer (6352)
MS 1330 G. M. Pullen (6352)
MS 1330 M. Alkis (6352)
MS 1330 D. Armijo (6352)

Parameter Summary for the WIPP Disposal Room Model

Part 1

Model Geometry, Initial Stress, Boundary Conditions and Miscellaneous Constants

A. Dimensions of the WIPP Disposal Room

The nominal room dimensions are listed in the reference (92PAV3) as 13 ft high, 33 ft wide, and 300 ft long; the values cited in the table are conversions (0.3048 m/ft) from these values. The air gap is specified in Bechtel (1986) as 28 in; the value cited in the table is a conversion from this value with the three significant digits as shown in the reference (Figure 3.1-3). The baseline room dimensions are shown in an idealized geometry Figure 1.

Table 1.1 Geometry of the Baseline Disposal Room

Parameter	Units	Value	Reference		
			Document	Section	Figure
Height	m	3.96	92PAV3	3.1.1	
Width	m	10.06	92PAV3	3.1.1	
Length	m	91.44	92PAV3	3.1.1	
Air Gap	m	0.711	92PAV3	3.1.6	F 3.1-3

B. Contents of the Baseline WIPP Disposal Room

The contents of the baseline room model assumes an idealized arrangement of 972 7-Pack units, a total of 6804 drums. The room volume is the value specified in Beraún and Davies (1991). The volume of TRU Waste is the product of the number of drums in a room and the external volume of a drum, 0.2539 m³ (92PAV3, Table 3.1-2). The air gap volume is the product of the air gap height (0.711 m), the room width (10.06 m) and the room length (91.44 m). The backfill volume is the difference between the room volume and the sum of waste and air gap volumes. Figure 1 shows the configuration of the room contents for the baseline case.

Table 1.2 Volume of Contents in Baseline Room Configuration

Parameter	Units	Value	Reference		
			Document	Section	Page
Number of Drums	-	6804	92PAV3	3.1.6	
Volume of Room	m ³	3644.8	92PAV3	App A (Beraún, Davies 91)	p A-7
Volume of TRU Waste	m ³	1727.5	Derived		
Volume of Backfill	m ³	1263.3	Derived		
Volume of Air Gap	m ³	654.0	Derived		

Parameter Summary for the WIPP Disposal Room Model

Part I (cont) Model Geometry, Initial Stress, Boundary Conditions and Miscellaneous Constants

C. Domain Dimensions for the Numerical Model

The pillar width (i.e., the rib-to-rib distance between rooms) is specified so that a model width can be determined for multiple-room configurations and for the Infinite Array of Rooms configuration. The model width given in Table 1.3 is for the Infinite Array of Rooms configuration; this dimension is the distance from the room centerline to the pillar centerline. The analyst should choose a model height appropriate for the problem and the simulation code being used, a height which does not adversely influence the results of interest.

Table 1.3 Numerical Model Geometry

Parameter	Units	Value	Reference	
			Document	Section
Pillar	m	30.48	92PAV3	3.1.1
Width	m	20.27	Derived	
Height	m	not specified	Analyst's Discretion	

D. In Situ Stress State

The density specified in Table 1.4 is a depth-weighted average over the 107.06 m between Elevations 332.88 and 439.94 (see Part 1, Section F on Stratigraphy for discussion of Elevations); this density is calculated in Krieg (1984). The value for gravity is specified in Krieg (1984) as an elevation adjusted acceleration of gravity which, in conjunction with the density, is used to calculate the value of stress at Elevation 439.94 m; this location corresponds to the top of the (then) Reference Stratigraphy presented in Krieg (1984). Using these same constants, the value of in situ vertical stress at the depth of Clay G the local referencé -- Elevation 387.07 m -- is determined. The often cited value of 14.8 MPa as the stress level at the repository occurs at Elevation 385.3 m, based on these parameters.

Table 1.4 Initial Stress

Parameter	Units	Value	Reference		
			Document	Section	Page
Density	kg/m ³	2300.0	Krieg, 1984	IV.A	p 14
Gravity	m/s ²	9.790	Krieg, 1984	IV.A	p 14
Stress @ 439.94	MPa	-13.57	Krieg, 1984	IV.A	p 14
Stress @ 387.07	MPa	-14.76	Derived		

Parameter Summary for the WIPP Disposal Room Model

Part I (cont) Model Geometry, Initial Stress, Boundary Conditions and Miscellaneous Constants

E. Boundary Conditions for the Numerical Model

The normal stress is specified for traction boundaries at the top (52.87 m above Clay G at Elevation 387.07) and bottom (54.19 m below Clay G) of Krieg's Reference stratigraphic section. These are typical locations for the boundaries of a DRM when an Infinite Array of Rooms configuration is assumed, although the caution given in Part I, Section C above should be heeded. The values of normal stress were computed using the density and gravity from Krieg (1984) and specified in Table 1.4. The boundary conditions along the vertical boundaries of the model are specified as symmetry boundaries for the Infinite Array of Rooms configuration; the analyst should choose suitable boundary conditions at suitable distances from the rooms in multiple-room models such that the boundary effects during the length of the simulation are minimal.

Table 1.5 Boundary Conditions

Parameter	Units	Value	Reference		
			Document	Section	Page
Normal Stress @ 439.94	MPa	-13.57	Krieg, 1984	IV.A	p 14
Normal Stress @ 332.88	MPa	-15.98	Derived		
Room and Pillar Centerlines	NA	Vertical Symmetry	Assumption for Infinite Array of Rooms Configuration		

F. Stratigraphy

The stratigraphy currently recommended for disposal room modeling activities is defined by Munson, et al, 1989 and shown in Figure 2. The local or reference zero is located at Clay G (at the base of Anhydrite b); the base of this clay seam is taken to be at Elevation 387.07 m above mean sea level. In this stratigraphy, the floor of the waste disposal room is at Elevation 380.49 m, as defined in WIPP PA Vol 3 (1992). This places Clay G 6.58 m above the repository floor at Elevation 387.07 and the top of Marker Bed 139 1.38 m below the floor at Elevation 379.11. This Reference Stratigraphy identifies 12 clay seams (A, B, D, E, F, G, H, I, J, K, L and M) and 8 Marker Beds (134, 136, 138, Anhydrite a, 139, Anhydrite c, 140 and 141), but it does not include all stratigraphic details within this interval of the Salado Formation. It is anticipated that a reduced number of clay seams and marker beds can be used in DRM simulations without adverse effects on room closure behavior. An addendum to this memo will be distributed providing guidelines for simplifying the stratigraphy for DRM simulations.

Parameter Summary for the WIPP Disposal Room Model

Part 1 (cont) Model Geometry, Initial Stress, Boundary Conditions and Miscellaneous Constants

Table 1.6 Stratigraphy

Parameter	Units	Value	Reference		
			Document	Section	Figure
Revised Reference Profile	NA	Figure 2	92PAV3	App A (Munson 92)	F 2.5-1
Clay G Elevation	m	387.07	Derived		
Floor Elevation	m	380.49	92PAV3	2.2	F 2.2-3
Top of MB 139	m	379.11	Derived		

G. Miscellaneous Constants

Several constants are (have been) required for developing the DRM parameter set presented in the tables of this document. These constants include an ambient rock temperature for calculating temperature dependent properties and conversion constants for various measures. Table 1.7 contains a list of these constants.

Table 1.7 Miscellaneous Constants

Parameter	Units	Value	Reference		
			Document	Section	Table
Ambient Rock Temperature	K	300.15	92PAV3	4.1	T 4.1.1
1 Foot (exact)	m	0.3048	92PAV3	Conversion Table	T 3
1 Cubic Foot	m ³	0.02832	92PAV3	Conversion Table	T 5
1 Drum (55 gal) (internal)	m ³	0.2082	92PAV3	Conversion Table	T 5
1 Drum (55 gal) (external)	m ³	0.2539	92PAV3	3.1.5	T 3.1-2
1 Year	s	3.1557E7	92PAV3	Conversion Table	T 13

Parameter Summary for the WIPP Disposal Room Model

Part 2 Material Constants for the Host Rock

A. Munson-Dawson Parameters for Halite

The Munson-Dawson constitutive model is recommended for simulating the response of pure halite and argillaceous halite in the Salado Formation. The standard reference for the Munson-Dawson constitutive model (M-D) is Munson, et al, 1989. A summary of the model parameters

Table 2.1 Material Constants for the Host Rock

Parameter	Units	Value		Document	References ¹	
		Pure Halite	Argillaceous Halite		Section	Page
Munson-Dawson Properties for:						
						PH/AH
E	MPa	31000.	31000.	92PAV3	App A (Munson 92)	p A-110/111
v	--	0.25	0.25			p A-110/111
μ	MPa	12400.	12400.			p A-110/111
A ₁	s ⁻¹	8.386E22	1.407E23			p A-110/111
	yr ⁻¹	2.646E30	4.440E30	Derived		
A ₂	s ⁻¹	9.672E12	1.314E13			p A-110/111
	yr ⁻¹	3.052E20	4.147E20	Derived		
Q ₁	cal/mol	25000.	25000.			p A-110/111
Q ₁ /R	K	12582.	12582.	Derived		
Q ₂	cal/mol	10000.	10000.			p A-110/111
Q ₂ /R	K	5033.	5033.	Derived		
n ₁	--	5.5	5.5			p A-110/111
n ₂	--	5.0	5.0			p A-110/111
B ₁	s ⁻¹	6.086E6	8.998E6			p A-110/111
	yr ⁻¹	1.921E14	2.839E14	Derived		
B ₂	s ⁻¹	3.034E-2	4.289E-2			p A-110/111
	yr ⁻¹	9.574E5	1.353E6	Derived		
q	--	5335.	5335.			p A-110/111
σ ₀	MPa	20.57	20.57			p A-110/111
m	--	3.	3.			p A-110/111
K ₀	--	6.275E5	2.470E6			p A-110/111
c	K ⁻¹	9.198E-3	9.198E-3			p A-110/112
α	--	-17.37	-14.96			p A-110/112
β	--	-7.738	-7.738			p A-110/112
δ	--	0.58	0.58	Munson, et al, 89	2.3.4	Table 2-2 (p41)

¹ Except where noted, all parameters are from 92PAV3, Appendix A (Munson, 92) on the page cited.

Parameter Summary for the WIPP Disposal Room Model

from this report is presented by Munson (1992) in an appendix to 92PAV3. All except one parameter for the M-D model for these two materials were taken directly from this reference; parameter δ is the value cited in Munson, et. al. (1989). These parameters are listed in Table 2.1. Some additional parameters are listed as *Derived*, including the A's and the B's. Munson (1992) lists these parameters in units of s^{-1} ; the parameters are listed in these units as well as in units of yr^{-1} , derived by applying the second to year conversion given in Table 1.7. Note that in some cases the parameters listed in Table 2.1 are slightly different from previously used parameters, probably because of a difference in conversion constants, the number of significant digits, or premature roundoff. The other parameters listed as *Derived* are the Q/R terms, which were calculated from the values of Q and R (1.987 cal/mol-deg) listed in Munson (1992); these terms may also be slightly different from values published in other references. The Q and R are part of the terms in the M-D model which define a temperature-dependent creep threshold. The appropriate value of ambient rock temperature to use as a reference or to calculate the term Q/RT is given in Part 1, Miscellaneous Constants (Table 1.7). Finally, if bulk modulus and shear modulus are used to define the elastic properties of halite rather than Young's modulus and Poisson's ratio, the appropriate value of bulk modulus is 20667. MPa, while the shear modulus is given in Table 2.1.

B. Elastic Properties of Anhydrite and Polyhalite

Elastic constants for the anhydrite and polyhalite which comprise the major marker beds in the Salado Formation were obtained from Munson (1992). Shear and bulk modulus values are listed for codes which use these elastic constants. These values were derived rather than using the values from Munson (1992) directly (for the sake of avoiding differences that are important when benchmarking codes). The Munson values are identical up to the third significant figure; the additional significant digits lead to almost exact values for Young's modulus and Poisson's ratio when calculated from the bulk and shear moduli. Note that the analyst is not required to use an elastic model; plasticity parameters are available (Munson, 1992) for a Drucker-Prager Model should an elastic-plastic representation be desired for these materials.

Table 2.2 Elastic Constants for Interbeds

Parameter	Value	Value		Document	References	
		Anhydrite	Polyhalite		Section	Page
Elastic Properties for:						<u>A/P</u>
E	MPa	75100.	55300.	92PAV3	App A (Munson 92)	p A-117/A-118
ν	--	0.35	0.36	92PAV3	App A (Munson 92)	p A-117/A-118
μ	MPa	27815.	20331.	Derived		
K	MPa	83444.	65833.	Derived		

Parameter Summary for the WIPP Disposal Room Model

C. Frictional Properties of Clay Seams

Clay seams are typically modeled as frictional interfaces; the friction coefficient is specified, as well as an equivalent friction angle for models using such a formulation.

Table 2.3 Frictional Properties of Clay Seams

Parameter	Units	Value	References		
			Document	Section	Page
friction coefficient	--	0.2	92PAV3	App A (Munson 92)	p A-120
friction angle	--	11.31°	(arc tangent of friction coefficient)		

Part 3

Material Constants for Crushed Salt Backfill

The baseline backfill material for the WIPP Disposal Room is crushed salt. The recommended constitutive model for crushed salt and the standard reference is described in Sjaardema and Krieg (1987); the baseline material parameters are listed in Table 3.1. Parameter values not listed in the 92PAV3 document are taken directly from Sjaardema and Krieg (1987), except initial density (ρ_0). This value is assumed but it has been used frequently in previous Disposal Room analyses. One fundamental model assumption is the consolidation of crushed salt to an intact salt-like state. Thus, the values for final density (ρ_f), bulk modulus (K_f) and shear modulus (G_f) are values for intact halite. The value for B_0 is specified in two units of time.

Table 3.1 Material Constants for Crushed Salt Backfill

Parameter	Units	Value	Reference		
			Document	Section	Table/Page
ρ_0	kg/m ³	1300.	92PAV3	App A (Beraún, Davies 91)	p A-8
ρ_f	kg/m ³	2140.	92PAV3	2.5	T 2.5-1
K_0	MPa	0.0176	Sjaardema and Krieg, 1987	Appendix A	Eq A.1 Constant
G_0	MPa	0.0106	Sjaardema and Krieg, 1987	Appendix A	Eq A.2 Constant
K_1	m ³ /kg	0.00653	92PAV3	2.5	T 2.5-1
G_1	m ³ /kg	0.00653	92PAV3	2.5	T 2.5-1
K_f	MPa	20667.	Derived		
G_f	MPa	12400.	92PAV3	App A (Munson 92)	p A-110
B_0	kg/m ³ -s	1.3E8	92PAV3	2.5	T 2.5-1
	kg/m ³ -yr	4.102E15	Derived		
B_1	MPa ⁻¹	0.82	92PAV3	2.5	T 2.5-1
A	m ³ /kg	-0.0173	92PAV3	2.5	T 2.5-1

Parameter Summary for the WIPP Disposal Room Model

Part 4 Material Constants for TRU Waste

The constitutive model of TRU Waste is an elastic-plastic model for crushable materials developed at Sandia (R. Krieg, SC-DR-72-0883, "A Simple Constitutive Description for Soils and Crushable Foams"). Several recent references discuss the model and its parameters, including Butcher and Mendenhall (1993).

Updated information on potential waste characteristics has recently become available leading to a redefinition of the volumetric yield function for TRU Waste constitutive model. This model component has also been referred to as the waste compaction curve. A Draft version of the Baseline Inventory Report, Rev. 1 available after February 16, 1995, (CAO, Table 5-1) reported average, minimum and maximum bounds to density for various categories of waste. The grouping of the various waste types presented in the CAO table has been modified slightly (see table footnotes) to be consistent with Butcher, et. al. (1991); the average waste density (but not the maximum and minimum) information is presented in Table 4.1. With a revised inventory, the distribution of waste in each category has changed somewhat; the result is a change in the initial density, initial porosity change, and the effective waste solid density. The average initial waste density is 559.5 kg/m³, the sum of the average density of each category. The volume fraction of each category is determined from the fractional contribution of each component to the average waste density. The mass fraction is determined from the (quotient of) volume fraction and the solid density of each component. The effective solid density (1757 kg/m³) is the reciprocal of the sum of the mass fractions.

**Table 4.1 WIPP CH-TRU Waste Material Parameter Disposal Inventory
(based on Table 5-1, CAO-94-1005, available February 1995)**

Waste Category	Waste Density (kg/m ³)		Volume Fraction	Mass Fraction
	Average	Solid		
Metallic ¹	122.	7850.	0.218	2.777E-5
Sorbents ²	40.	3000.	0.071	2.367E-5
Cellulose	170.	1100.	0.304	27.636E-5
Rubber & Plastics	84.	1200.	0.150	12.500E-5
Sludges ³	<u>143.5</u>	<u>2200.</u>	<u>0.256</u>	<u>11.636E-5</u>
	559.5	1757.	0.999	56.916E-5

¹ Includes Inorganic Materials Iron, Aluminum and Other Metals.

² Other Inorganic Materials.

³ Includes Materials Soils and Solidified Inorganic and Organic Materials.

Parameter Summary for the WIPP Disposal Room Model

The model elastic constants, the von Mises yield surface parameters and the gas generation potential parameters have not changed from previous values. All can be obtained from Table 2.5-1 in the 92PA Volume 3 document (92PAV3) and are listed in Table 4.2. The revised initial waste density is the value computed from the Table 4.1 information. The initial porosity of the waste is derived from the initial density and the effective solid density ($\phi_0 = 1 - \rho_0/\rho_s$). Butcher (1995) presents a listing of axial stress-porosity data derived from the newly presented distribution of waste between the various categories using the approach described in Butcher, et. al., (1991). The stress-porosity data has been converted into a pressure-volumetric strain curve for use in mechanical simulations. (The conversion from porosity to (natural log of) volume strain is by Equation 1.)

$$\epsilon_v = \ln ((1-\phi) \rho_s / \rho_0) \quad (\text{Eqtn 1})$$

The data points defining the Volumetric Plasticity Model (Table 4.2) represent the recommended piece-wise linear definition of the volumetric yield function for TRU Waste.

Table 4.2 Material Constants for TRU Waste

Parameter	Units	Value	Reference		
			Document	Section	Table
ρ_0	kg/m ³	559.5	Derived	(see Table 4.1)	
ϕ_0	--	0.681	Butcher, 95	App B (Data)	
K	MPa	222.	92PAV3	2.5	T 2.5-1
μ	MPa	333.	92PAV3	2.5	T 2.5-1
a_0	MPa ²	0.	92PAV3	2.5	T 2.5-1
a_1	MPa	0.	92PAV3	2.5	T 2.5-1
a_2	--	3.	92PAV3	2.5	T 2.5-1
<u>Volumetric Plasticity Model</u>			(see Figure 3)		
	Pressure (MPa)	Volumetric Strain (ln ρ/ρ_0)	Derived from Data in Butcher, 95; Appendix B		
	0.00	0.00			
	0.533	0.4737			
	1.103	0.8292			
	2.031	1.1001			
	3.670	1.3198			
	10.0	1.72			
<u>Gas Generation Potential</u>					
Anoxic and Microbial	moles/drum	2.0, t: 0-550 yrs	92PAV3	2.5	T 2.5-1
Anoxic	moles/drum	1.0, t: 550-1050 yrs	92PAV3	2.5	T 2.5-1

Parameter Summary for the WIPP Disposal Room Model

References

92PAV3, Sandia WIPP Project, 1992. Preliminary Performance Assessment for the Waste Isolation Pilot Plant, December 1992, Volume 3: Model Parameters, SAND92-0700/3, prepared by Sandia National Laboratories, Albuquerque, NM

Beraún, R., and P.B. Davies, 1991. "Baseline Design Input Data Base to be Used During Calculations Effort to be Performed by Division 1514 in Determining the Mechanical Creep Closure Behavior of Waste Disposal Rooms in Bedded Salt", Sandia Internal Memorandum, September 12, in Appendix A, pp A-5 to A-14 of Preliminary Performance Assessment for the Waste Isolation Pilot Plant, December 1992, Volume 3: Model Parameters, SAND92-0700/3, prepared by Sandia National Laboratories, Albuquerque, NM

Munson, D. E., 1992. "Mechanical Parameters for Volume 3, SAND92-0700", Sandia Internal Memorandum, October 26, in Appendix A, pp A-107 to A-124 of Preliminary Performance Assessment for the Waste Isolation Pilot Plant, December 1992, Volume 3: Model Parameters, SAND92-0700/3, prepared by Sandia National Laboratories, Albuquerque, NM

Butcher, B. M., T. W. Thompson, R. G. VanBuskirk, and N. C. Patti, 1991. Mechanical Compaction of Waste Isolation Pilot Plant Simulated Waste, SAND90-1206, prepared by Sandia National Laboratories, Albuquerque, NM.

Butcher, B. M., 1995. "Waste Compressibility Curve Predictions", Memorandum of Record, Sandia National Laboratories, February 16.

Krieg, R. D., 1984. Reference Stratigraphy and Rock Properties for the Waste Isolation Pilot Plant (WIPP) Project, SAND83-1908, prepared by Sandia National Laboratories, Albuquerque, NM.

Munson, D. E., A. F. Fossum, P. E. Senseny, 1989. Advances in Resolution of Discrepancies Between Predicted and Measured In Situ WIPP Room Closures, SAND88-2948, prepared by Sandia National Laboratories, Albuquerque, NM.

Sjaardema, G. D. and R. D. Krieg, 1987. A Constitutive Model for the Consolidation of WIPP Crushed Salt and Its Use in Analyses of Backfilled Shaft and Drift Configurations, SAND87-1977, prepared by Sandia National Laboratories, Albuquerque, NM.

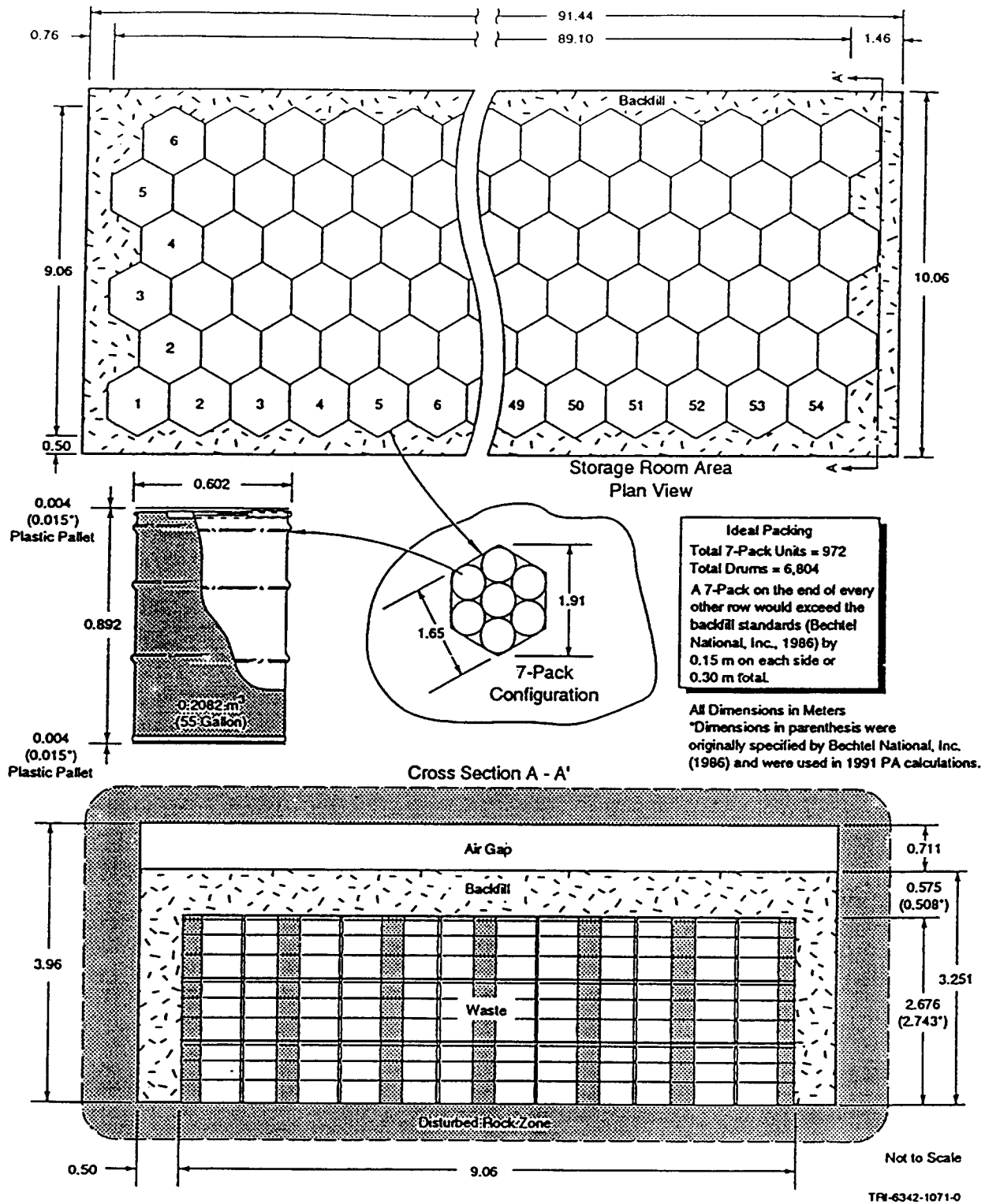


Figure 1. WIPP Disposal Room Baseline Configuration for DRM Simulations of Ideal Packing of TRU Waste in Drums (92PA V3, Figure 3.1-3)

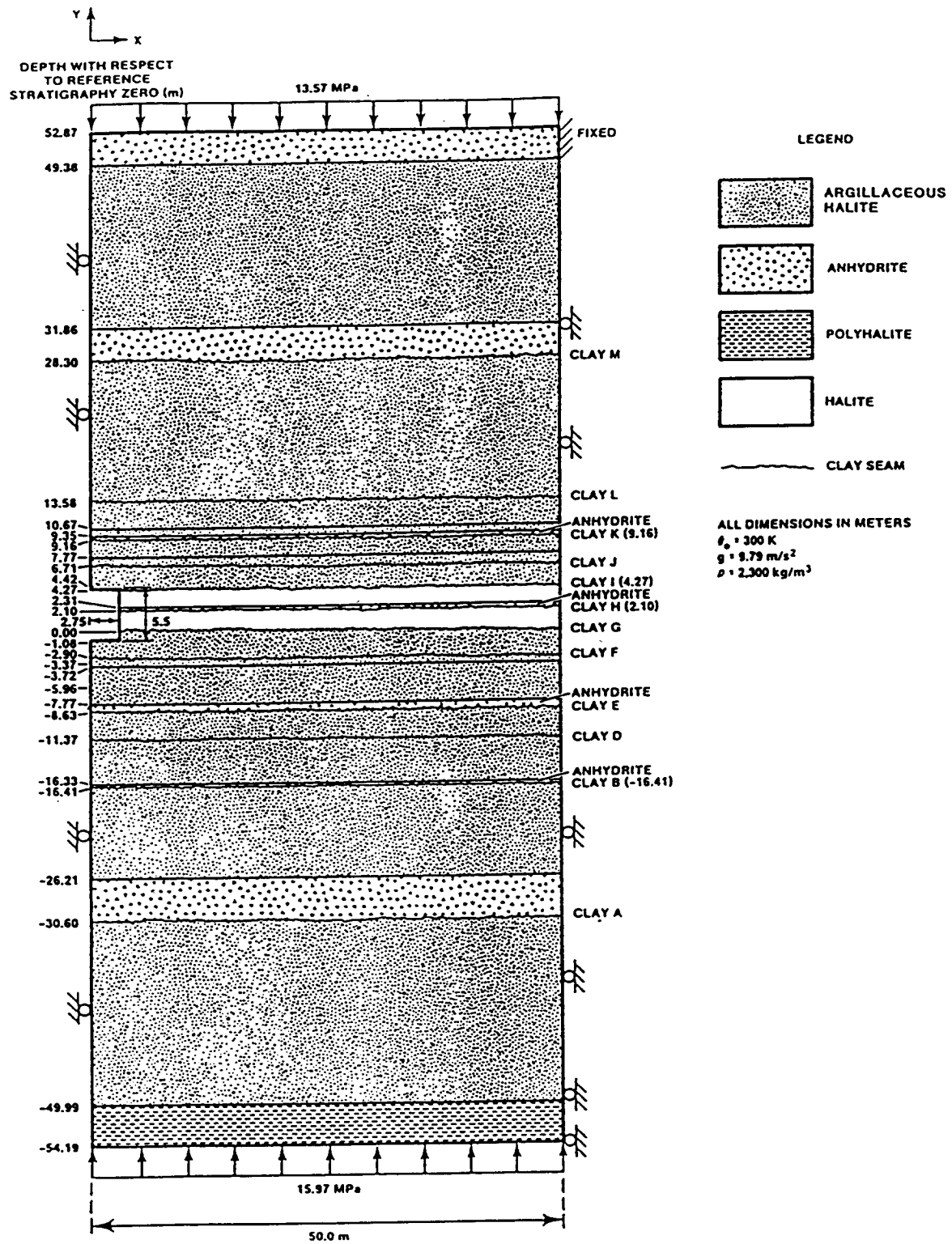


Figure 2. WIPP Revised Reference Stratigraphy for DRM Simulations (Munson, et al, 1989, Figure 3)

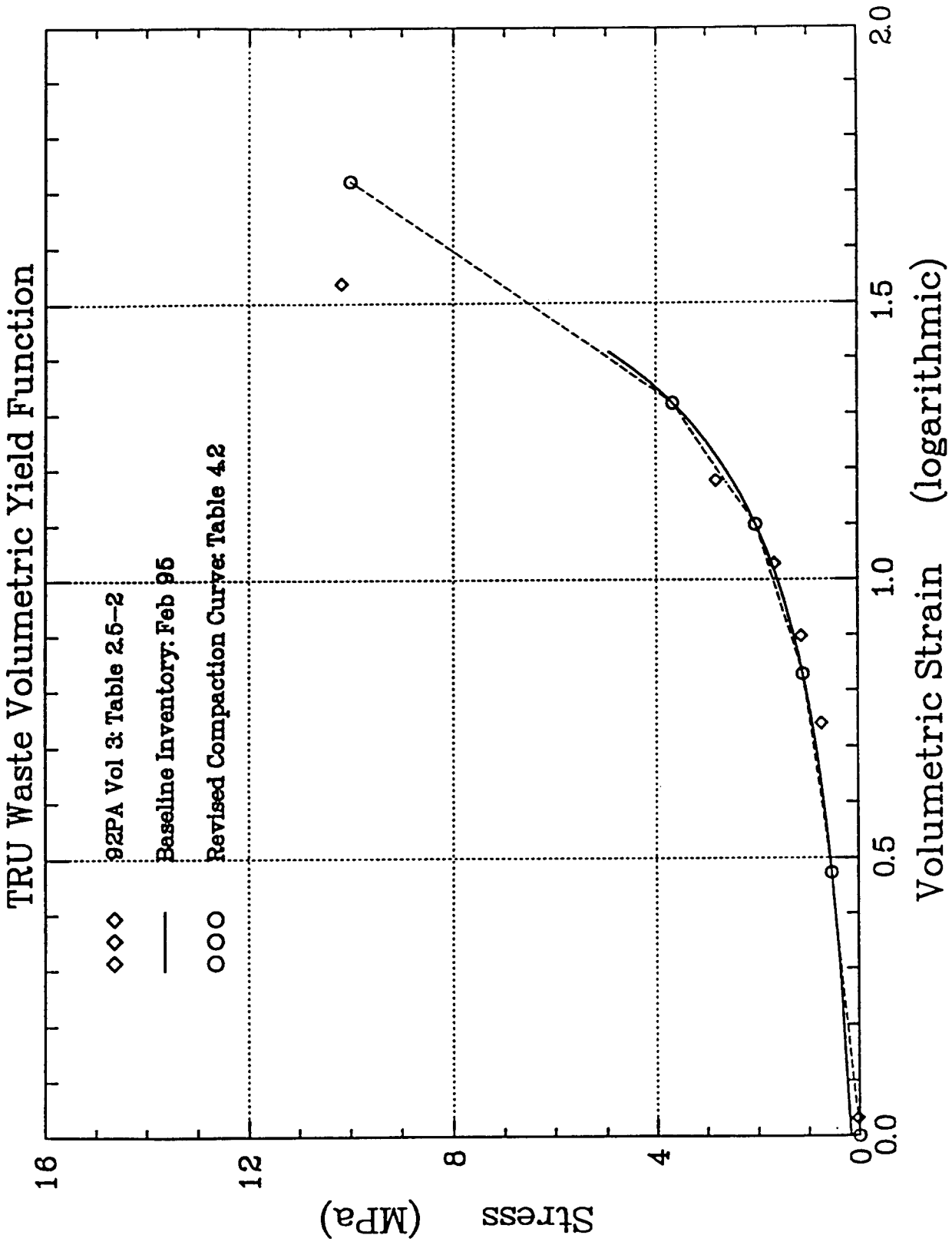


Figure 3. TRU Waste Compaction Curve Corresponding to CAO Baseline Waste Inventory (February 1995)

date: June 6, 1996

to: B. M. Butcher, 6748 (MS1341)

Charles M. Stone
from: Charles M. Stone, 9117 (MS0443)

subject: Proposed Model for the Final Porosity Surface Calculations

Introduction

This memo documents our best estimate of the configuration and constitutive property values for the final porosity surface calculations. This estimate is based on information from WIPP project documents, contractor reports, scoping analyses, and from insight gained during previous disposal room analyses. The quasi-static, large deformation finite element code SANTOS [1] will be used for the analyses. It has the capability to compute an internal room pressure and to apply the resulting forces to nodes on the deforming room boundary.

Disposal Room Model

The disposal room model consists of a rectangular room 3.96 m high by 10.06 m wide by 91.44 m in length resulting in an initial room volume of 3642.75 m³. Unlike previous calculations which included a crushed salt layer around the waste, the current analyses consider a disposal room with waste only, no backfill. The current configuration calls for 6804 drums of uniformly distributed unprocessed waste to be stored in the disposal room. The corresponding volume occupied by the waste and the drums is 1728 m³. The waste is stored in a seven-pack drum configuration with three seven-packs stacked, for a total waste height of 2.676 m, along the length of the drift. The initial porosity of the waste is 0.681 resulting in a solid volume of 551.2 m³.

Geomechanical Model

A two-dimensional plane strain disposal room model will be used for the SANTOS analyses. The model represents the room as one of an infinite number of rooms located at the repository horizon. Making use of symmetry, only half of the room needs to be modeled. The left and right boundaries are planes of symmetry with a zero-displacement boundary condition applied in the horizontal direction. The upper and lower boundaries are

located approximately 50 m from the room. Previous scoping studies have shown that locating the upper and lower boundaries at a distance of 50 m from the disposal room results in less than a 5 percent difference in room porosity when compared to room porosity calculated with the boundaries located at a distance of 100 m. It is felt that this small difference in room porosity is acceptable when compared to other uncertainties and assumptions in the model. A prescribed normal traction of 13.57 MPa is applied on the upper boundary and a normal traction of 14.76 MPa is applied at the lower boundary. A lithostatic stress ($\sigma_x = \sigma_y = \sigma_z$) that varies with depth is used as the initial stress on the configuration and gravity forces are included.

The stratigraphy is based on the WIPP Revised Reference Stratigraphy [2] shown in Figure 1. Recent work by Osnes and Labreche [3] has quantified the differences in room closure obtained by assuming different stratigraphic models incorporating different numbers of clay seams and anhydrite layers. In their study, the full stratigraphic model consisting of 12 clay seams and 7 anhydrite layers (12-Clay) is viewed as the reference analysis. Several different models were studied including models with 7, 5, and 3 clay seams. The models also included different combinations of anhydrite layers. The assumption was made *a priori* that the influence of clay seams on room closure diminishes with increasing distance between the clay seam and the disposal room. This assumption formed the basis for the development of their simplified models which eliminated the furthest clay seams from the disposal room. The room closure and room porosity results reported by Osnes and Labreche showed that the simplified models reproduced the results of the 12-Clay reference model quite well. They stated that the differences in closure predicted by the 12-Clay reference model and the 3-Clay model were relatively insignificant compared to the effects of other modeling considerations. This conclusion suggests that a simplified model may confidently be used for the disposal room response. In addition, the results showed that a disposal room located in a stratigraphy composed of all salt closed considerably faster than a disposal room located in a stratigraphic model which contained anhydrite layers. The presence of the anhydrite layers seemed to have the biggest effect on disposal room response.

Based on the results presented by Osnes and Labreche [3], we feel that a simplified stratigraphic model is justifiable for the final porosity surface calculations. The structural features in the stratigraphy shown by Osnes and Labreche to have the greatest effect on the disposal room response are the anhydrite layers. The anhydrite layers nearest the disposal room horizon will be evaluated for inclusion in the simplified model. These layers include MB 139 beneath the room and Anhydrite A above the room. MB 139 will have a large effect on the disposal room response because of its thickness and its proximity to the disposal room. The proposed stratigraphic model will also include both argillaceous and clean salt. Both types of salt must be included because of the large differences in their creep rates.

The proposed simplified stratigraphy is shown in Figure 2. Clay G is shown for reference only, it is not included in the stratigraphy. A major question regarding this stratigraphic representation is whether the clay seam beneath MB 139 is structurally important. In order

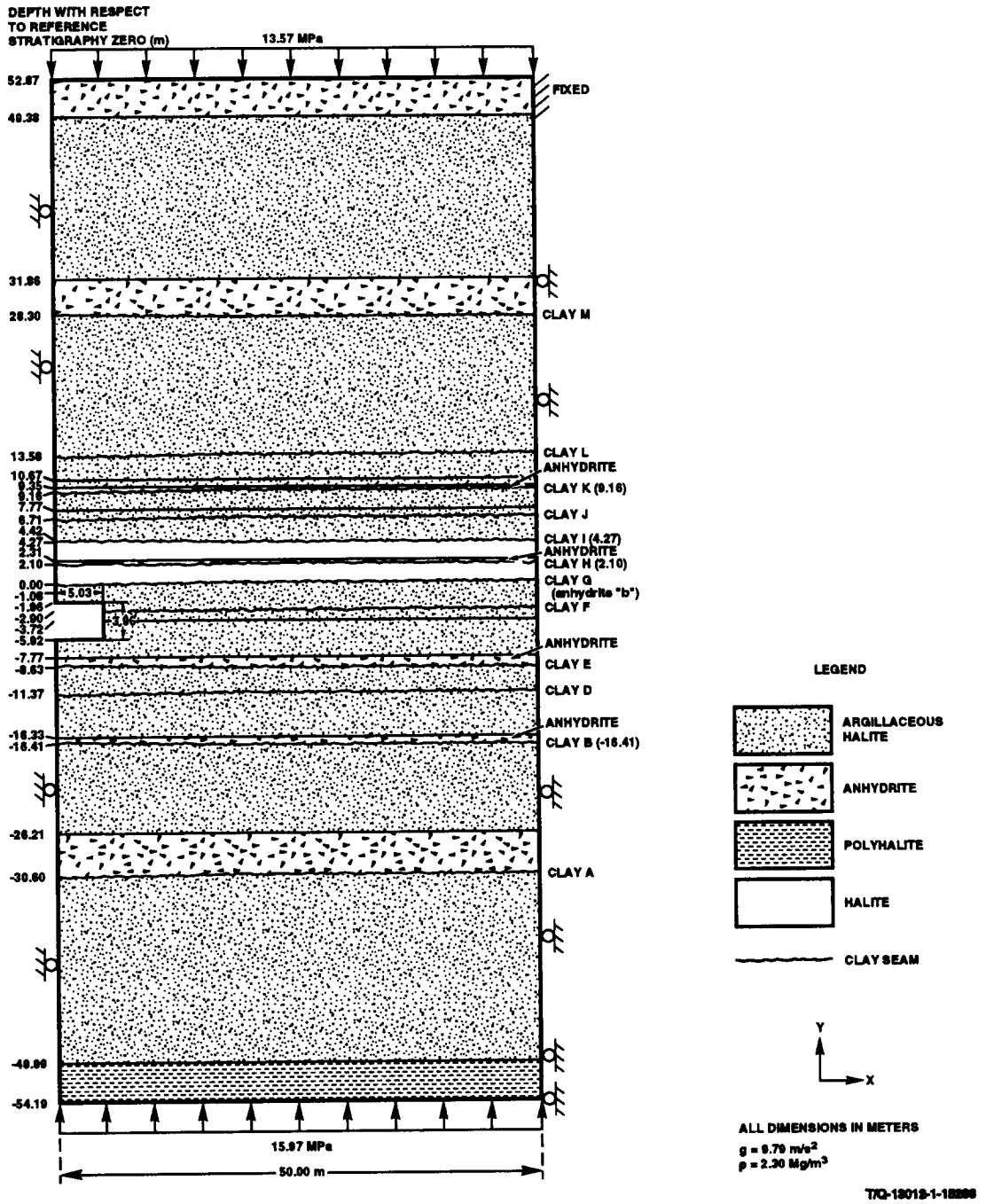


Figure 1. Idealized Stratigraphy Near the Disposal Room Horizon [2]

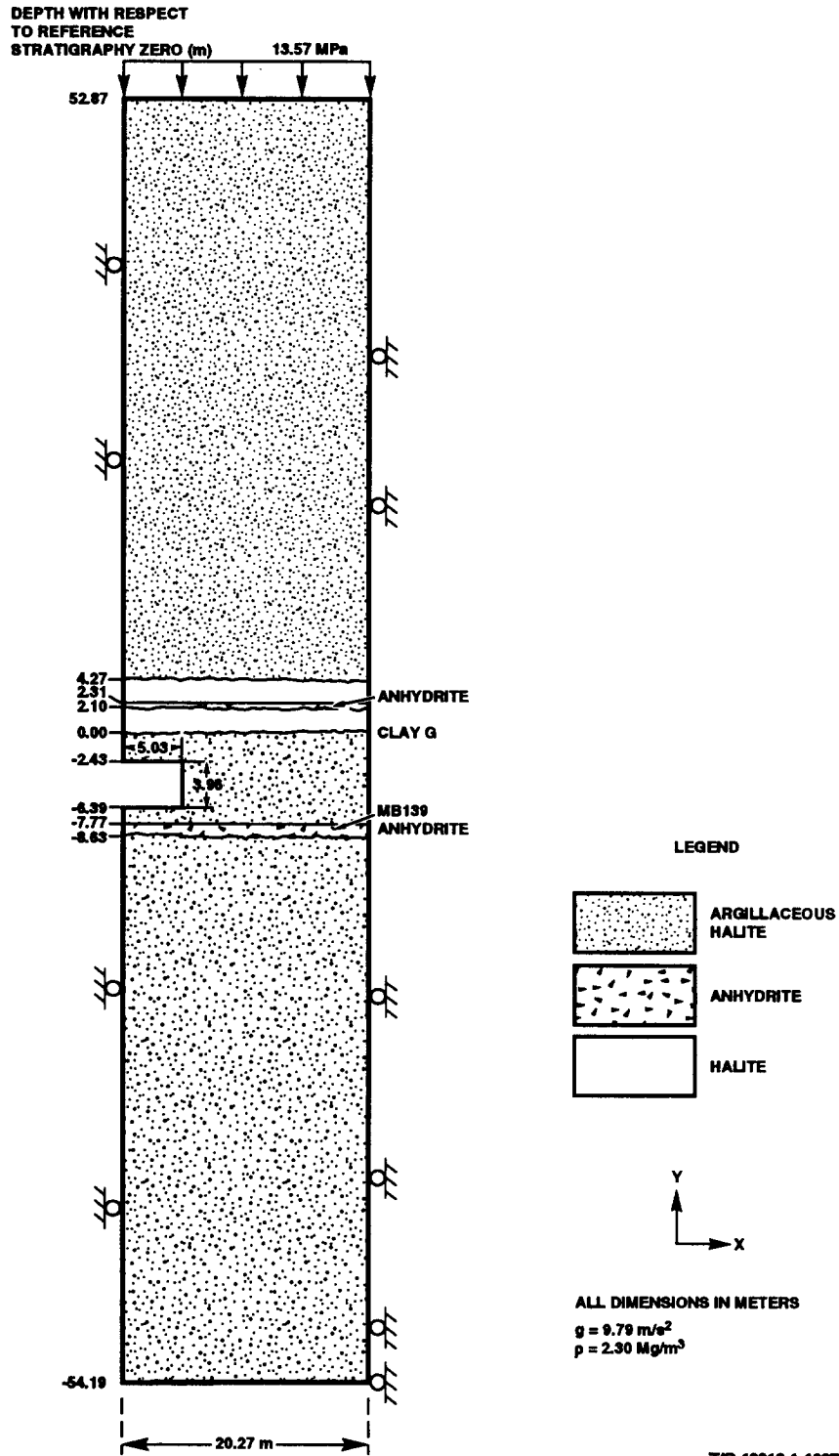


Figure 2. Proposed Stratigraphy for the Final Porosity Surface Calculations

to answer this question, several scoping analyses were run to compare disposal room closure results for a stratigraphy with and without a clay seam beneath MB 139. A second question to be answered by the study is whether the presence of the marker bed is sufficient to reduce the rate of room closure compared to an all salt stratigraphy as found by Osnes and Labreche [3]. These questions are answered by Figure 3 which shows the disposal

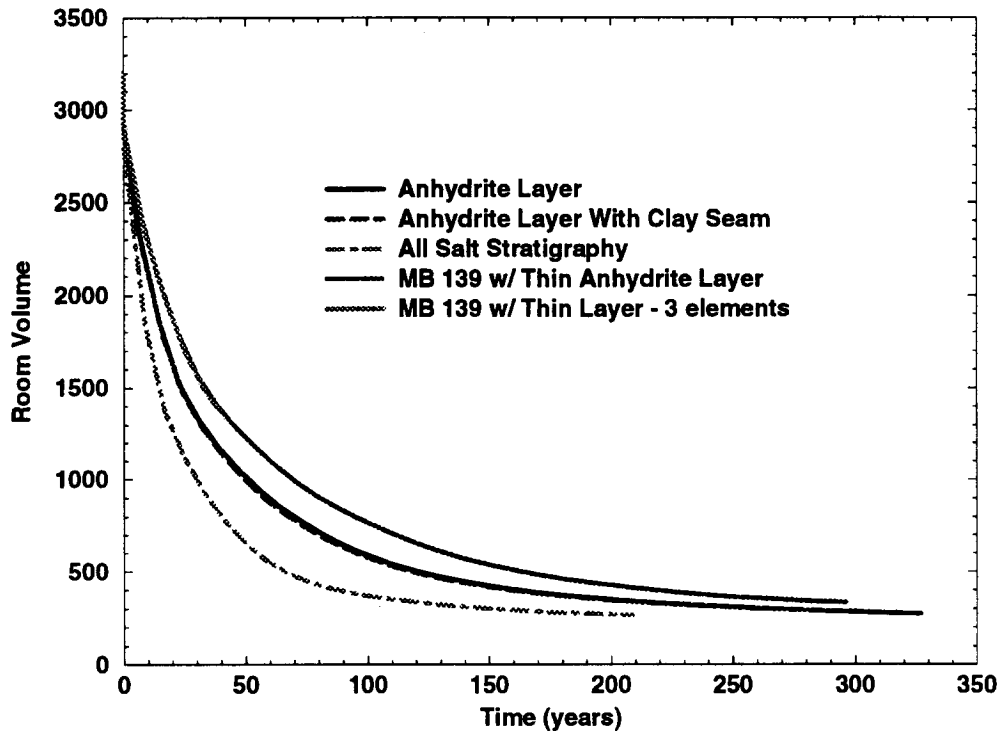


Figure 3. Disposal Room Volume History For Various Stratigraphic Assumptions.

room volume as a function of time for the scoping analyses. The analyses showed that the presence of MB 139 did slow the rate of disposal room closure when compared to the all salt stratigraphy. In addition, the presence of the clay seam beneath MB 139 did not affect the closure of the disposal room. An additional observation from this study is the fact that the horizontal closure increased when the marker bed was included in the stratigraphy. This is due to the fact that the stiff anhydrite layer forces more salt to flow horizontally into the drift rather than flowing upward at the drift floor.

An additional set of calculations was performed to assess the effects of including Anhydrite A in the stratigraphy. This thin anhydrite layer was modeled with both one and three elements through the thickness of the layer. The effect on disposal room closure is shown in Figure 3. The presence of the thin layer significantly decreased the rate of disposal room closure when compared to the stratigraphy with MB 139 only and, therefore, it should be included in the simplified stratigraphy. In addition, only a single row of elements will be used to model the thin anhydrite layer.

The proposed stratigraphy will include both argillaceous and clean salt. Two anhydrite layers, MB 139 and Anhydrite A, are also included. No clay seams will be included in the

stratigraphy. It is important to point out that all of the calculations shown above tend to approach the same disposal room volume as time proceeds. The biggest effects of the stratigraphy appear to occur early and disappear with time which agrees with the results presented in Osnes and Labreche [3]. This is an important observation because the porosity surface calculations will be run for a simulation time of 10,000 years.

The disposal room contains material representing the stored waste. The basic half-symmetry room dimensions are 3.96 m high by 5.03 m wide. The waste and drum volume of 1728 m³ is distributed along 87.96 m of the drift at a height of 2.676 m. The assumption is made that lateral deformation of a configuration of drums caused by inward movement of the walls of the disposal room is sufficient to eliminate space between the drums early in the closure process at low stress levels. Based on this assumption, the equivalent half-width of the waste is computed to be 3.735 m instead of the seven-pack width of 4.3 m. A gas pressure, p_g , will be applied around the room boundary.

Contact surfaces will be defined between the waste and room boundaries to model the contact and sliding that occurs as the room deforms and entombs the waste. Specifically, contact surfaces will be defined between the waste and floor of the room, the waste and room rib, and the waste and ceiling. All of the contacts surfaces will be allowed to separate if the forces between the surfaces reached a tensile value. This feature allows the room to reopen due to gas generation within the disposal room.

A combined transient-secondary creep constitutive model for rock salt attributed to Munson and Dawson [4] and described by Munson, et. al [5] will be used for the clean and argillaceous salt. The model can be decomposed into an elastic volumetric part defined by,

$$\varepsilon_{kk} = \frac{\sigma_{kk}}{3K} \quad (\text{EQ 1})$$

(where the ε_{ij} and the σ_{ij} are the total strain and stress components, respectively, and K is the elastic bulk modulus) and a deviatoric part defined by,

$$\dot{s}_{ij} = 2G \left(\dot{e}_{ij} - F \dot{e}_s \left[\frac{\cos 2\theta}{\cos 3\theta \sqrt{J_2}} s_{ij} - \frac{\sqrt{3} \sin \theta}{\cos 3\theta J_2} \left\{ s_{ip} s_{pj} - \frac{2J_2}{3} \delta_{ij} \right\} \right] \right), \quad (\text{EQ 2})$$

where the second term of the above equation represents the creep contribution. In the above

equation, s_{ij} is the deviatoric stress defined as $s_{ij} = \sigma_{ij} - \frac{\sigma_{kk}}{3}$, G is the elastic shear

modulus, and e_{ij} is the deviatoric strain defined by $e_{ij} = \varepsilon_{ij} - \frac{\varepsilon_{kk}}{3}$.

In the creep term of Equation 3, F is a multiplier on the steady-state creep rate to simulate the transient creep response according to the following,

$$F = \begin{cases} e^{\Delta[1-\zeta/\varepsilon_t^*]^2} & , \zeta < \varepsilon_t^* \\ 1 & , \zeta = \varepsilon_t^* \\ e^{-\delta[1-\zeta/\varepsilon_t^*]^2} & , \zeta > \varepsilon_t^* \end{cases} \quad (\text{EQ 3})$$

where Δ and δ are work-hardening and recovery parameters, respectively, and ε_t^* is the so-called transient strain limit. Finally, ζ is an internal state variable whose rate of change is determined by the following evolutionary equation,

$$\dot{\zeta} = (F - 1)\dot{\varepsilon}_s \quad (\text{EQ 4})$$

In Equation 3, the work-hardening parameter Δ is defined as $\Delta = \alpha + \beta \log(\bar{\sigma}/G)$ where α and β are constants. The variable $\bar{\sigma}$ is the equivalent Tresca stress given by

$$\bar{\sigma} = 2\sqrt{J_2} \cos \theta \quad \text{where} \quad \theta = \frac{1}{3} \arcsin \left[\frac{-3\sqrt{3}J_3}{2(J_2)^{3/2}} \right]$$

is the Lode angle and is limited to the range $-\frac{\pi}{6} \leq \theta \leq \frac{\pi}{6}$. The variables J_2 and J_3 are the second and third invariants of the stress

deviator given by $J_2 = \frac{1}{2}s_{pq}s_{qp}$ and $J_3 = \frac{1}{3}s_{pq}s_{qr}s_{rp}$, respectively. The recovery

parameter δ is held constant. The transient strain limit is given by $\varepsilon_t^* = K_o e^{cT} (\bar{\sigma}/G)^M$ where K_o , c , and M are constants.

The steady-state, or secondary creep, strain rate, $\dot{\varepsilon}_s$, is given by

$$\begin{aligned} \dot{\varepsilon}_s = & A_1 e^{-Q_1/RT} \left(\frac{\bar{\sigma}}{G}\right)^{n_1} + A_2 e^{-Q_2/RT} \left(\frac{\bar{\sigma}}{G}\right)^{n_2} \\ & + |H| [B_1 e^{-Q_1/RT} + B_2 e^{-Q_2/RT}] \sinh \left[\frac{q(\bar{\sigma} - \sigma_o)}{G} \right]; \end{aligned} \quad (\text{EQ 5})$$

where the A_i s and B_i s are constants, the Q_i s are activation energies, T is the absolute temperature, R is the universal gas constant, the n_i s are the stress exponents, q is the so-called stress constant, σ_o is the stress limit of the dislocation slip mechanism, and $|H|$ is the Heaviside step function with the argument $(\bar{\sigma} - \sigma_o)$. The material constants corresponding to the clean and argillaceous salt, used in the analyses, are given in Table 1 and Table 2.

Table 1: Elastic Properties [2]

G MPa	E MPa	ν
12,400	31,000	0.25

Table 2: Creep Properties [2]

Parameters (units)	Clean Salt	Argillaceous Salt
A_1 (/sec)	8.386E22	1.407E23
Q_1 (cal/mole)	25,000	25,000
n_1	5.5	5.5
B_1 (/sec)	6.086E6	8.998E6
A_2 (/sec)	9.672E12	1.314E13
Q_2 (cal/mole)	10,000	10,000
n_2	5.0	5.0
B_2 (/sec)	3.034E-2	4.289E-2
σ_o (MPa)	20.57	20.57
q	5,335	5,335
M	3.0	3.0
K_o	6.275E5	2.470E6
c (/T)	9.198E-3	9.198E-3
α	-17.37	-14.96
β	-7.738	-7.738
δ	0.58	0.58

The stress-strain behavior of the waste was represented by a volumetric plasticity model [1] with a piecewise linear function defining the relationship between the mean stress and the volumetric strain. Compaction experiments on simulated waste were used to develop this relationship. The deviatoric response of the waste material has not been characterized. It is anticipated that when a drum filled with loosely compacted waste is compressed axially, the drum will not undergo significant lateral expansion until most of the void space inside the drum has been eliminated.

For the volumetric plasticity model, the yield surface in principal stress space is a surface of revolution with its axis centered about the hydrostat and the open end pointing into the compression direction. The open end is capped with a plane which is at right angles to the hydrostat. The deviatoric part is elastic-perfectly plastic so the surface of revolution is stationary in stress space. The volumetric part has variable strain hardening so the end plane moves outward during volumetric yielding. The volumetric hardening is defined by a set of pressure-volumetric strain relations. A flow rule is used such that deviatoric strains produce no volume change (associated flow). The model is best broken into volumetric and deviatoric parts with the deviatoric part resembling conventional plasticity. The volumetric yield function is a product of two functions, ϕ_s and ϕ_p , describing the surface of revolution and the plane normal to the pressure axis, respectively. These are given by

$$\phi_s = \frac{1}{2}s_{ij}s_{ij} - a_0 + a_1p + a_2p^2 \quad (\text{EQ 6})$$

$$\phi_p = p - g(\epsilon_v) \quad (\text{EQ 7})$$

where a_0 , a_1 , a_2 are constants defining the deviatoric yield surface, p is the pressure, and ϵ_v is the volume strain. The form of g is defined in this problem by a set of piecewise linear segments relating pressure-volume strain. Table 3 lists the pressure-volumetric strain data used for the waste drum model. Note that the final point listed in the table is a linear extrapolation beyond the curve data given in [6]. The final pressure value of 12 MPa corresponds to an axial stress on a waste drum of 36 MPa. The elastic material parameters and constants defining the yield surface are given in Table 4.

Table 3: Pressure-Volumetric Strain Data Used in the Volumetric-Plasticity Model for the Waste Drums [6]

Pressure (MPa)	$\ln(\rho/\rho_0)$
1.530	0.5101
2.0307	0.6314
2.5321	0.7189
3.0312	0.7855
3.5301	0.8382
4.0258	0.8808
4.9333	0.9422
12.0	1.140

Table 4: Material Constants Used With the Volumetric Plasticity Model for the Waste

Parameter	Value
G	333. Mpa
K	222 Mpa
a ₀	1.0 Mpa
a ₁	3.0
a ₂	0.

The anhydrite layer beneath the disposal room is expected to experience inelastic material behavior. The MB 139 anhydrite layer is considered to be isotropic and elastic until yield occurs. Once the yield stress is reached plastic strain begins to accumulate. Yield is assumed to be governed by the Drucker-Prager criterion

$$\sqrt{J_2} = C - aJ_1 \quad (\text{EQ 8})$$

where J_2 is the second deviatoric stress invariant and J_1 is the first stress invariant (σ_{kk}). A nonassociative flow rule, Equation 9, is used to determine the plastic strain components, $\dot{\epsilon}_{ij}^p$.

$$\dot{\epsilon}_{ij}^p = \lambda s_{ij} \quad (\text{EQ 9})$$

In this equation, λ is a positive scalar function of proportionality. The elastic properties and Drucker-Prager constants, C and a, for the anhydrite are given in Table 5.

Table 5: Elastic and Drucker-Prager Constants for Anhydrite [7]

Material	Young's Modulus (GPa)	Poisson's Ratio	C (MPa)	a
Anhydrite	75.1	0.35	1.35	0.45

Gas Generation Model

The gas generation potential and gas production rate are composed of gas from two sources: anoxic corrosion and microbial activity. Reference [8] reports that the estimated gas production potential from anoxic corrosion will be 1050 *moles/drum* with a production rate of 1 *mole/drum/year*. The gas production potential from microbial activity is estimated

to be 550 *moles/drum* with a production rate of 1 *mole/drum/year*. This means that microbial activity ceases at 550 years while anoxic corrosion will continue until 1050 years after emplacement. The total amount of gas generated in a disposal room for the Baseline case was specified to be based on 6804 unprocessed waste drums per room. The total gas potential for the Baseline case is shown in Figure 3.

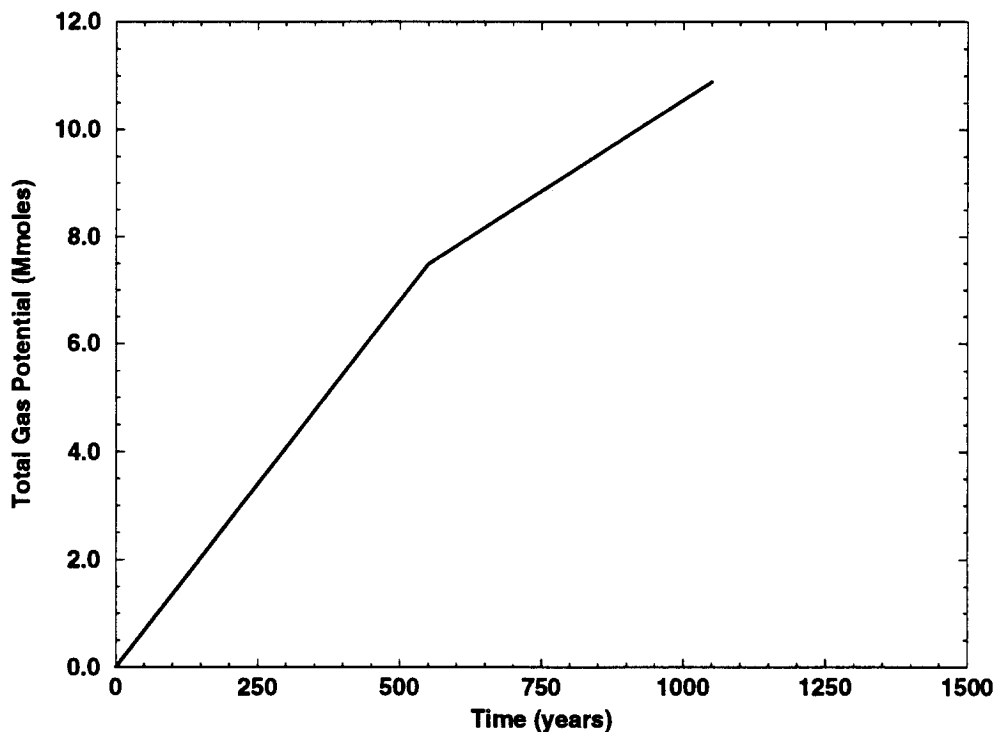


Figure 4. History of the Baseline Gas Generation Potential Used for the Disposal Room Analyses

These values for the Baseline case are considered acceptable for the calculations, even though the values for the gas generation model recommended for the final Performance Assessment BRAGFLO calculations are likely to be different. The use of the Baseline values is consistent with the porosity surface approach that compensates for the absence of detailed definition about gas generation within the repository by constructing a set of closure (void volume or porosity) curves using assumed gas generation (pressure) histories that span all of the gas generation histories that potentially might be encountered within the repository [9]. Several calculations in which the assumed rate of gas production is doubled will be made, and calculations assuming a total gas potential of 3200 *moles/drum* will also assure that the porosity surface data spans all potential gas generation histories.

The gas pressure is computed from the ideal gas law based on the current free volume in the room. Specifically, the gas pressure, p_g , is computed with the following relationship:

$$p_g = f \frac{NRT}{V}, \quad (\text{EQ 10})$$

where N , R , and T are the mass of gas in g-moles for the Baseline case, the universal gas constant, and the absolute temperature in degrees Kelvin. The variable V is the current free volume of the room. After each iteration in the analysis, the current room free volume is calculated based on the locations of the nodes on the boundary of the room. The variable f is a multiplier used in the study to scale the pressure by varying the amount of gas generation. A value of $f=1$ corresponds to an analysis with full gas generation, while a value of $f=0$ corresponds to no internal pressure increase due to gas generation.

References

1. Stone, C. M., *SANTOS – A Two-Dimensional Finite Element Program for the Quasistatic, Large Deformation, Inelastic Response of Solids*, SAND90-0543, Sandia National Laboratories, Albuquerque, New Mexico, in preparation.
2. Butcher, B. M. and J. Holmes, 'Completion of milestone DR015, definition of closure analysis input parameters, due March 31, 1995,' Sandia National Laboratories, memorandum to Les Shepard and Martin Tierney, March 31, 1995.
3. Osnes, J. D. and D. A. Labreche, 'The Effect of Clay Seams and Anhydrite Layers on the Closure of Waste Isolation Pilot Plant Disposal Rooms and Guidelines for Simplifying the Modeled Stratigraphy,' RE/SPEC External Memorandum RS(RCO)-390/7-95/58, August 29, 1995.
4. Munson, D. E. and P. R. Dawson, *A Transient Creep Model for Salt During Stress Loading and Unloading*, Sandia National Laboratories, Albuquerque, New Mexico, 1982.
5. Munson, D. E., A. E. Fossum, and P. E. Senseny, *Advances in Resolution of Discrepancies Between Predicted and Measured In Situ WIPP Room Closures*, SAND88-2948, Sandia National Laboratories, Albuquerque, New Mexico, 1989.
6. Butcher, B. M., 'Waste Compressibility Curve Predictions,' Sandia National Laboratories Memorandum of Record, February 16, 1995.
7. Munson, D. E., 'Mechanical Parameters for Volume 3, SAND92-0700', Sandia Internal Memorandum, October 26, in Appendix A, pp A-107 to A-124 of Preliminary performance Assessment for the Waste Isolation Pilot Plant, December 1992, Volume 3: Model Parameters, SAND92-0700/3, prepared by Sandia National Laboratories, Albuquerque, NM.
8. Beraun, R. and P. B. Davies, 'Baseline Design Input Data Base to be Used During Calculations Effort by Division 1514 in Determining the Mechanical Creep Closure Behavior of Waste Disposal Rooms in Bedded Salt,' Memorandum to Distribution, Sandia National Laboratories, Albuquerque, NM, September 12, 1991.

9. Butcher, B. M., S. W. Webb, and J. W. Berglund, 'Disposal Room and Cuttings Models-White Paper for Systems Prioritization and Technical Baseline,' WIPP Project Document, Section 3.2.4, 1994.

Distribution:

MS-1330		SWCF-A: 1.1.1.2.3; DRM
MS-0841	9100	P. J. Hommert
MS-0835	9102	R. D. Skocypec (Route to 9111)
MS-0833	9103	J. H. Biffle (Route to 9116)
MS-0828	9104	E. D. Gorham (Route to 9114, 9115)
MS-0834	9112	A. C. Ratzel (Route to 9113)
MS-0443	9117	H. S. Morgan (Route to Staff)
MS-0437	9118	E. P. Chen (Acting) (Route to Staff)
MS-0443	9117	C. M. Stone
MS-0443	9117	J. G. Arguello
MS-0443	9117	QA File

Appendix B: Supporting Justification Memoranda

B. M. Butcher, "Corrosion and Microbial Gas Generation Potentials," Sandia National Laboratories Memorandum of Record, March 18, 1996.	B-2
B. M. Butcher, "Baseline Inventory Assumptions for the Final Porosity Surface Calculations," Sandia National Laboratories Memorandum of Record, March 11, 1996.	B-5
C. M. Stone, "Resolution of Remaining Issues for the Final Disposal Room Calculations," Memorandum to B. M. Butcher, March 4, 1996.	B-8

Appendix B errata

p. B-3 The references should be in the following order: Beraún, R. and P.B. Davies 1992; Butcher, B. M. et al. 1994; Brush, L. H. 1991; Lappin A. R. et al. 1989; Sandia WIPP Project. 1992

p. B-8 Text reference to Munson 1989 should be reference to Munson et al. 1989.

p. B-11 Butcher and Holmes 1995 Correct spelling of Les Shephard's surname.

In addition, the following references should be added:

Butcher, B.M., and F.T. Mendenhall. 1993. *A Summary of the Models Used for the Mechanical Response of Disposal Rooms in the Waste Isolation Pilot Plant with Regard to Compliance with 40 CFR 191, Subpart B.* SAND92-0427. Albuquerque, NM: Sandia National Laboratories. The final version of this document, "Systems Prioritization Method—Iteration 2 Baseline Position Paper: Disposal Room and Cuttings Model," is dated March 28, 1995 and is on file in the Sandia WIPP Central Files as WPO#28729 (Vol. 1) and WPO#28733 (Vol. 2). This document is not available from the National Technical Information Service.

Munson, D. E., A. F. Fossum, and P. E. Senseny. 1989. "Approach to First Principles Model Prediction of Measured WIPP In Situ Room Closure in Salt," in *Rock Mechanics as a Guide for Efficient Utilization of Natural Resources, Proceedings of the 30th US Symposium on Rock Mechanics, West Virginia University, Morgantown, WV, June 19-22, 1989.* Ed. A.W. Khair. Brookfield, VT: A.A. Balkema. 673-680. The NTIS accession number and WPO# supplied at the end of this citation are the numbers for SAND88-2948 (*Advances in Resolution of Discrepancies Between Predicted and Measured In Situ WIPP Room Closures*). The title cited in this citation, "Approach to First Principles Model Prediction of Measured In Situ Room Closure in Salt," is also available as SAND88-2535C, which is available from the NTIS as DE8905777/XAB.

Sandia National Laboratories

Albuquerque, New Mexico 87185-1341

date: March 18, 1996: reissued July 10, 1996 after editorial revision

to: Memorandum of Record



from: B. M. Butcher, 6748, MS 1341

subject: Corrosion and Microbial Gas Generation Potentials

A number of values for the potential for corrosion and microbial gas generation have been used during development of the porosity surface approach (Butcher and Mendenhall, 1993, pp. 7-3 to 7-7). For example, in Lappin et. al (1989, Sec. 4.10.2) the gas generation potential was quoted as 589 moles/drum for anoxic microbial decay and 894 moles/drum for anoxic corrosion of metals.

Later, Beraún and Davies (1992) referenced Brush as recommending a gas potential of 1050 moles/drum for corrosion and 550 moles/drum for microbial decay. The source for these values was Reference 11 in Beraún and Davies (1992), which was described as "in draft," and apparently never issued. Source documentation for these values is therefore unknown, but may have been an early draft of the reference written by Brush (1991) in which the gas potential values were quoted as 900 moles/drum for corrosion and 600 moles/drum for microbial decay in the final version.

Recommended gas potentials have changed again several times since 1991. Nevertheless, use of the Beraún and Davies (1992) values of 1050 moles/drum for corrosion and 550 moles/drum for microbial decay has continued. The justification for using these values is that the porosity surface concept was adopted in order to circumvent problems related to (1) the absence of detailed definition of gas generation within the repository and (2) the realization that gas production histories typical of the repository that depend on brine inflow could not be addressed at that time as part of a mechanical closure calculation. There was no way of estimating how the brine content of the waste changes with time with structural codes such as SANTOS. To compensate for this deficiency, the porosity surface concept selects a set of gas generation histories that span all of the gas generation histories likely to be encountered within the repository. Disposal room porosities and gas pressures are calculated for each of the assumed histories as a function of time, summarized in data tables and transferred to BRAGFLO. Closure histories for specific repository conditions are then defined with the performance assessment code BRAGFLO, with which brine flow, gas generation, and gas migration are computed throughout the repository (Butcher et. al, 1994, Sections 3.2.4, 3.4.1).

In maintaining the link between SANTOS and BRAGFLO, the range of gas generation potentials for generation of the porosity surface data for the CCA exceed presently anticipated conditions for the repository. This procedure assures that BRAGFLO extrapolation outside

the data range is not needed. It also provides justification for using gas potential values that are not quite the same as values used on other performance assessment calculations. In other words, the gas model used for disposal room calculations is simply a device to enter a range of gas contents into the calculations, and should not be interpreted as having any exact significance in regard to predicted repository conditions. In other words, while it is desirable to keep these gas contents somewhat typical of parameter values used in the BRAGFLO gas model, to assist in physical intuition of the porosity surface results, the values used in SANTOS need not be exactly representative of repository conditions.

References:

- Beraún R., and P.B. Davies. 1992. "Appendix A: Baseline Design Input Data Base to be Used During Calculations Effort to be Performed by Division 1514 in Determining the Mechanical Creep Closure Behavior of Waste Disposal Rooms in Bedded Salt," *Preliminary Performance Assessment for the Waste Isolation Pilot Plant, December 1992. Volume 3: Model Parameters*. Sandia WIPP Project. SAND92-0700/3. Albuquerque, NM: Sandia National Laboratories. A-7 through A-13.
- Brush, L. H. 1991. *Current Estimates of Gas Production Rates, Gas Production Potentials, and Expected Chemical conditions Relevant to Radionuclide Chemistry for the Long-Term WIPP Performance Assessment*. Appendix A of WIPP PA (Performance Assessment) Division. 1991a. *Preliminary Comparison with 40 CFR Part 191, Subpart B for the Waste Isolation Pilot Plant, December 1991. Volume 3: Reference Data*. SAND91-0893/3. Eds. R.P. Rechard, J.D. Schreiber, H.J. Iuzzolino, M.S. Tierney, and J.S. Sandha. Albuquerque, NM: Sandia National Laboratories, Pages A-27 to A-41.
- Lappin, A.R. , R. L. Hunter, D. P. Garber, and P.B. Davies, eds. 1989. "Systems Analysis, Long-Term Radionuclide Transport, and Dose Assessments, Waste Isolation Pilot Plant (WIPP) , Southeastern New Mexico: March 1989," SAND89-0462, Sandia national Laboratories, Albuquerque, New Mexico.
- Butcher, B. M., Webb, S. W., and Berglund, J. W., 1994. "DISPOSAL ROOM AND CUTTINGS MODELS - WHITE PAPER FOR SYSTEMS PRIORITIZATION AND TECHNICAL BASELINE," WIPP Project document.
- Sandia WIPP Project. 1992. *Preliminary Performance Assessment for the Waste Isolation Pilot Plant, December 1992. Volume 3: Model Parameters*. SAND92-0700/3. Albuquerque NM: Sandia National Laboratories.

Copy to:

MS 1341 B. M. Butcher (6748) day file
MS 1330 SWCF-A: 1.1.1.2.3; DRM

Sandia National Laboratories

Albuquerque, New Mexico 87185-1341

date: March 11, 1996: reissued July 10, 1996 after revision

to: Memorandum of Record



from: B. M. Butcher

subject: Baseline Inventory Assumptions for the Final Porosity Surface Calculations

Final porosity surface calculations were started November 1, 1995, using waste compaction data derived from the February 1995 revision of the Baseline Inventory Report (BIR revision 1). The assumption was made, therefore, that future BIR adjustments would be small and have little effect on calculation results.

In contrast to the assumption, an updated draft revision, Draft B, November 1995, of the inventory was found to be quite different than the February version (Revision 1). These changes were qualified in the sense that reported values were not considered final until the document was approved. Revision 2 of the BIR was published on December 28, 1995, after the porosity surface calculations were completed. At that time, the consequences of the new values were reviewed in order to decide whether or not to scrap already completed calculations and start over again using the new inventory. The conclusion of the review was that Revision 2 did not contain sufficient information to assess the consequences of the revisions. It was observed that the compaction characteristics of the inventory described in Revision 1 represent an upper bound of the final porosity states (greatest porosity at any given time), because it takes more time to compact waste that has not been partially vitrified (discussed in a following paragraph). Therefore, more time is available for gas pressure to build up and stop closure. Less closure is considered conservative with regard to repository performance because the waste is more porous, and therefore would offer less resistance to the flow of radioactive brine.

Changes in Draft B are that vitrified waste is listed for the first time, the amount of iron-based metal has increased by over a factor of two and cellulose waste has decreased in amount by a factor of three. New inventory values taken from Table ES-1 of Draft B are compared with the Revision 1 values in Table 1.

Closer examination of the differences between Revision 1 and Draft B revealed that the increase in amount of waste was because of the presence of vitrified waste. During vitrification, combustibles are burned up, causing the drop in the combustibles inventory, but the iron-based alloys remain intact. In addition, vitrification represents a 6 fold or greater reduction in waste volume, so that more of it can be used to fill the repository to capacity. In Draft B, the total amount of iron-based metal is the amount of iron in vitrified waste, augmented by the scaling process used to fill up the repository, plus the iron-based material in unprocessed waste. The procedure accounts for the increased iron content and decreased combustibles, but does not specify quantitatively how much iron is associated with the vitrified form. We need to know how much iron is associated with iron in vitrified waste and

how much is in unprocessed waste. This information is critical because the stress-strain response of iron in vitrified waste differs greatly from that of iron in unprocessed metals waste. Iron in vitrified waste is for all practical purposes locked up in it, undergoing little consolidation because the vitrification process produces a waste form that is likely to have high enough strength to resist further large scale densification. Vitrified waste thus undergoes little further consolidation during closure, whereas unprocessed metals waste undergoes a very large amount of densification during closure.

Summary: The lack of quantitative definition of the amount of iron that is associated with the vitrified waste component in Revision 2 of the BIR prevented use of this latest information in constructing the compaction curve data input for the final porosity surface calculations. Instead, final calculations were made using waste compaction data derived from the February 1995 version of the Baseline Inventory Report (BIR Revision 1). This approach is considered to provide an upper bound of the final porosity states.

Copy to:

MS 1341 B. M. Butcher (6748) day file
MS 1330 SWCF-A: 1.1.1.2.3; DRM

Table 1: Baseline Inventory Assumptions for Disposal Room Model Calculations

	92 PA	Rev. 1: February 1995	Rev. 2: December 1995
<u>Material</u>	kg/m ³	kg/m ³	kg/m ³
Iron Base Metals		83	170
Aluminum Base Metals		12	18
Other Metals		27	72
Total Metals	110	122	260
Other Inorganic Material	32	40	33
Vitrified	0	0	50
Cellulosics	47	170	52
Rubber		21	10
Plastics		63	33
Total Rubber and Plastics	67	84	43
Solidified Inorganic Material		130	120
Solidified Organic Material		7.8	2.6
Total Sludges	171	137.8	122.6
Cement	0	0	0
Soils	0	5.7	32
Initial Waste Density	426	560	593

date: March 4, 1996 Revised May 16, 1996

to: B. M. Butcher, 6748, MS1341

Chara M. Stone
from: C. M. Stone, 9117, MS0443

subject: Resolution of remaining issues for the final disposal room calculations

Disposal Room Elevation

In Butcher and Holmes (1995), the local zero reference is defined to be Clay G which is at Elevation 387.07 m above mean sea level and the top of MB 139 is at Elevation 379.11 which results in a distance below the reference of 7.96 m. Butcher and Holmes also locates the floor of the disposal room at Elevation 380.49 m. This locates the floor 1.38 m above MB 139 and 6.58 below Clay G. The top of MB 139 is shown in Figure 2 of Butcher and Holmes (1995) and Munson (1989) to be - 7.77 m below Clay G rather than -7.96 m. It was decided to hold the top of MB 139 to be - 7.77 m as shown in the referenced figures and locate the disposal room floor 1.38 m above at -6.39 m below Clay G. It was felt that the location of the disposal room relative to MB 139 was the important dimension here. The top of the disposal room is located 3.96 m above the disposal room floor at -2.43 m relative to Clay G.

Determination of Plastic Constants for the TRU Waste

In Butcher and Holmes (1995), the inelastic deviatoric response of the TRU waste is characterized by a constitutive model of the form

$$J_2 = a_0 + a_1 p + a_2 p^2 \quad (\text{EQ 1})$$

where J_2 is the second deviatoric stress invariant, p is the pressure (positive in compression), and a_0 , a_1 , and a_2 are material constants. The material constants are defined for this particular form of deviatoric response. In SANTOS, the model for the waste is written in a different functional form

$$\bar{\sigma} = A_0 + A_1 p + A_2 p^2 \quad (\text{EQ 2})$$

where $\bar{\sigma}$ is the von Mises equivalent stress and p is the pressure (positive in compression). The material constants A_1 , A_2 , and A_3 are different from a_1 , a_2 , and a_3 .

Butcher and Holmes (1995) give the following values: $a_1 = 0.0$, $a_2 = 0.0$, and $a_3 = 3.0$. When combined with Eq. 1, the material constants define J_2 as

$$J_2 = 3p^2 \quad . \quad (\text{EQ } 3)$$

The von Mises equivalent stress is defined as $\bar{\sigma} = \sqrt{3J_2}$ and when Eq. 3 is substituted for J_2 the following result is obtained

$$\bar{\sigma} = 3p \quad . \quad (\text{EQ } 4)$$

This allows us to redefine the appropriate TRU waste material constants for SANTOS as $A_1 = 0.0$, $A_2 = 3.0$ and $A_3 = 0.0$. In order to stabilize the iterative algorithm in SANTOS, some strength is assigned to the waste at zero confining pressure. This is done by giving A_1 a value of 1.0×10^6 pa. This results in the following values used in the final porosity surface calculations; $A_1 = 1.0 \times 10^6$, $A_2 = 3.0$, and $A_3 = 0.0$.

Determination of SANTOS Input Constants for Anhydrite

The anhydrite layer beneath the disposal room is expected to experience inelastic material behavior. The MB 139 anhydrite layer is considered to be isotropic and elastic until yield occurs. Once the yield stress is reached, plastic strain begins to accumulate. Yield is assumed to be governed by the Drucker-Prager criterion

$$\sqrt{J_2} = C - aJ_1 \quad (\text{EQ } 5)$$

where J_2 is the second deviatoric stress invariant and J_1 is the first stress invariant. A nonassociative flow rule is used to determine the plastic strain components. The elastic constants and Drucker-Prager constants, C and a , as defined by Munson (1995) are given in Table 1. The input to the soil and crushable foam model in the SANTOS code requires

Table 1: Anhydrite Elastic and Drucker-Prager Constants [Munson]

Material	Young's Modulus, E, (Gpa)	Poisson's Ratio, ν	C (Mpa)	a
Anhydrite	75.1	0.35	1.35	0.45

the analyst to provide TWO MU, (2μ), and the BULK MODULUS, K . The conversion from Young's modulus, E , and Poisson's ratio, ν , to the SANTOS input parameters is given from the following relationships taken from Fung (1965):

$$2\mu = \frac{E}{(1. + \nu)} \quad (\text{EQ } 6)$$

$$K = \frac{E}{3(1. - 2\nu)}. \quad (\text{EQ 7})$$

SANTOS requires the input to the material model which describes the anhydrite nonlinear response to be given in terms of effective stress, $\bar{\sigma} = \sqrt{3J_2}$, and pressure, $p = \frac{J_1}{3}$.

Rewriting Eq. (5) in terms of $\bar{\sigma}$ and p , we obtain the following relationship

$$\bar{\sigma} = \sqrt{3}C - 3\sqrt{3}ap. \quad (\text{EQ 8})$$

The SANTOS input constant A0 is $\sqrt{3}C$ and the input constant A1 is $3\sqrt{3}a$. The set of SANTOS input parameters for the anhydrite is given in Table 2.

Table 2: SANTOS Input Parameters for the Anhydrite Layers

Material	TWO MU (Gpa)	BULK MODULUS (Gpa)	A0 (Mpa)	A1	A2
Anhydrite	55.6	83.4	2.3	2.338	0.0

Determination of SANTOS Input Elastic Constants for Halite and Argillaceous Halite

The finite element code, SANTOS, uses TWO MU and BULK MODULUS as input for the elastic parameters in the M-D creep model. The quantity, TWO MU, is twice the shear modulus, μ . The value of the shear modulus reported by Munson for halite and argillaceous halite is 12.4 Gpa. This means that TWO MU has a value of 24.8 Gpa. The value of the BULK MODULUS is not given directly by Munson (1995) but it may be calculated from the following relation given in Fung (1965):

$$K = \frac{E}{3(1. - 2\nu)} \quad (\text{EQ 9})$$

where K, E and ν are the bulk modulus, Young's modulus and Poisson's ratio, respectively. The values for Young's modulus and Poisson's ratio are given by Munson (1995). The resulting value of the bulk modulus is calculated to be 20.66 Gpa.

References

Butcher, B. M. and J. T. Holmes. 1995. "Completion of Milestone DR015, Definition of Closure Analysis Input Parameters, Due March 31, 1995," Memorandum to Les

Sheppard and Martin Tierney, Sandia National Laboratories, Albuquerque, New Mexico, March 31, 1995.

Fung, Y. C. 1965. *Foundations of Solid Mechanics*. Englewood Cliffs: NJ. Prentice Hall Inc.

Munson, D. E. 1995. "Mechanical Parameters for Update of Reference Data Report," memo to M. S. Tierney, Sandia National Laboratories, Albuquerque, New Mexico, September 26, 1995.

Munson, D. E., A. E. Fossum, and P. E. Senseny. 1989. "Advances in Resolution of Discrepancies Between Predicted and Measured In Situ WIPP Room Closures," SAND88-2948, Sandia National Laboratories, Albuquerque, New Mexico.

CMS:9117

Copy to:

MS-1330		SWCF-A: 1.1.1.2.3; DRM
MS-0841	9100	P. J. Hommert
MS-0835	9102	R. D. Skocypec (Route to 9111)
MS-0833	9103	J. H. Biffle (Route to 9116)
MS-0828	9104	E. D. Gorham (Route to 9114, 9115)
MS-0834	9112	A. C. Ratzel (Route to 9113)
MS-0443	9117	H. S. Morgan (Route to Staff)
MS-0437	9118	E. P. Chen (Acting) (Route to Staff)
MS-0443	9117	C. M. Stone
MS-0443	9117	J. G. Arguello
MS-0443	9117	QA File

This page intentionally left blank

Appendix C: Documentation of Calculations

Calculation of solid density for the inventory listed in the Baseline Inventory Report Rev 1,
February 1995 C-2

Verification of Pressure-Volumetric Strain Values Described in Table 8 of this report. April
1, 1996 C-3

Calculation of solid density for the inventory listed in the Baseline Inventory Report Rev 1, February 1995.

File C: MATHCAD STRAIN Check of Mike Stone's volume strain calculation by B. M. Butcher, April 1, 1996 using the data file C: MATHCAD BIRREV1.PRN
 This data file has the same average waste compressibility data as recommended in "Waste Compressibility Curve Predictions," Memorandum of Record by B. M. Butcher, February 16, 1995

A := READPRN(BIRREV1) RHOS := 1757 rho0 := 559.5
 i := 0 ..63

$s_i := A_{i,0}$ $\phi_i := A_{i,1}$ $\rho_i := RHOS \cdot \left[1 - \phi_i \right]$

rho0 = 559.5

$ev_i := \ln \left[\frac{\rho_i}{\rho_0} \right]$ $p_i := \frac{s_i}{3}$ (mean stress is 1/3 axial stress)

$B_{i,0} := p_i$ $B_{i,1} := ev_i$ $B_{i,2} := s_i$ $B_{i,3} := \phi_i$

WRITEPRN(EV) := B

Check Calculations

$\phi_0 := 1 - \frac{\rho_0}{RHOS}$ $\phi_0 = 0.68156$

$ev1_i := \ln \left[\frac{1 - \phi_i}{1 - \phi_0} \right]$ $delt_i := ev1_i - ev_i$

Graphing this data shows that it coincides with the curve computed by Stone

	pressure	strain	axial stress	porosity
B =	0	0.00176	0	0.681
	0.26667	-0.32536	0.8	0.77
	0.34376	-0.20106	1.03128	0.73956
	0.39185	-0.14205	1.17555	0.72373
	0.45864	-0.06795	1.37593	0.70248
	0.53331	0.00554	1.59994	0.67979
	0.6061	0.06929	1.81831	0.65871
	0.67116	0.12018	2.01348	0.6409
	0.7444	0.1714	2.23321	0.62202
	0.81993	0.21876	2.4598	0.60369
	0.89024	0.2587	2.67072	0.58754
	0.96197	0.29602	2.88592	0.57186
	1.03634	0.33145	3.10903	0.55642
	1.10346	0.36105	3.31038	0.54309
	1.17274	0.38948	3.51821	0.52991

Verification of Pressure- Volumetric Strain Values Described in Table 8 of this report.
 April 1, 1996

C:-mathcad-biroctb Calculate solid density for inventory listed in the Baseline Inventory Report, Rev 1, February 1995. Calculation made by B. M. Butcher, 12.4.95, Revised by B. M. Butcher, February 19, 1996. Solid density is calculated using the equations in Section 2.3.2 in SAND90-1206, "Mechanical Compaction of Waste Isolation Pilot Plant Simulated Waste," using the solid density values for each waste component in Table 6 of the present report ("A summary of the Sources of Input parameter Values for the Final Porosity Surface Calculations") - this last sentence was added on 4/15/96 by B. M. Butcher to reference the method of calculation

Define masses = m is metal, c is combustible, p is plastic, s is sludge/soil

wmi := 83 kg/m3 wc := 170 wim := 39 wss := 5.7
 wma := 12 wpp := 63 wsi := 130
 wmo := 27 wpr := 21 wso := 8.4

v is volume

$$vmt := \frac{wmi + wma + wmo}{7830} \qquad vmt = 0.016$$

$$vc := \frac{wc}{1100} \qquad vc = 0.155$$

$$vp := \frac{wpp + wpr}{1200} \qquad vp = 0.07$$

$$vsorb := \frac{wim}{3000} \qquad vsorb = 0.013$$

$$vslud := \frac{wsi + wso + wss}{2200} \qquad vslud = 0.066$$

$$vt := vmt + vc + vp + vsorb + vslud \qquad vt = 0.319$$

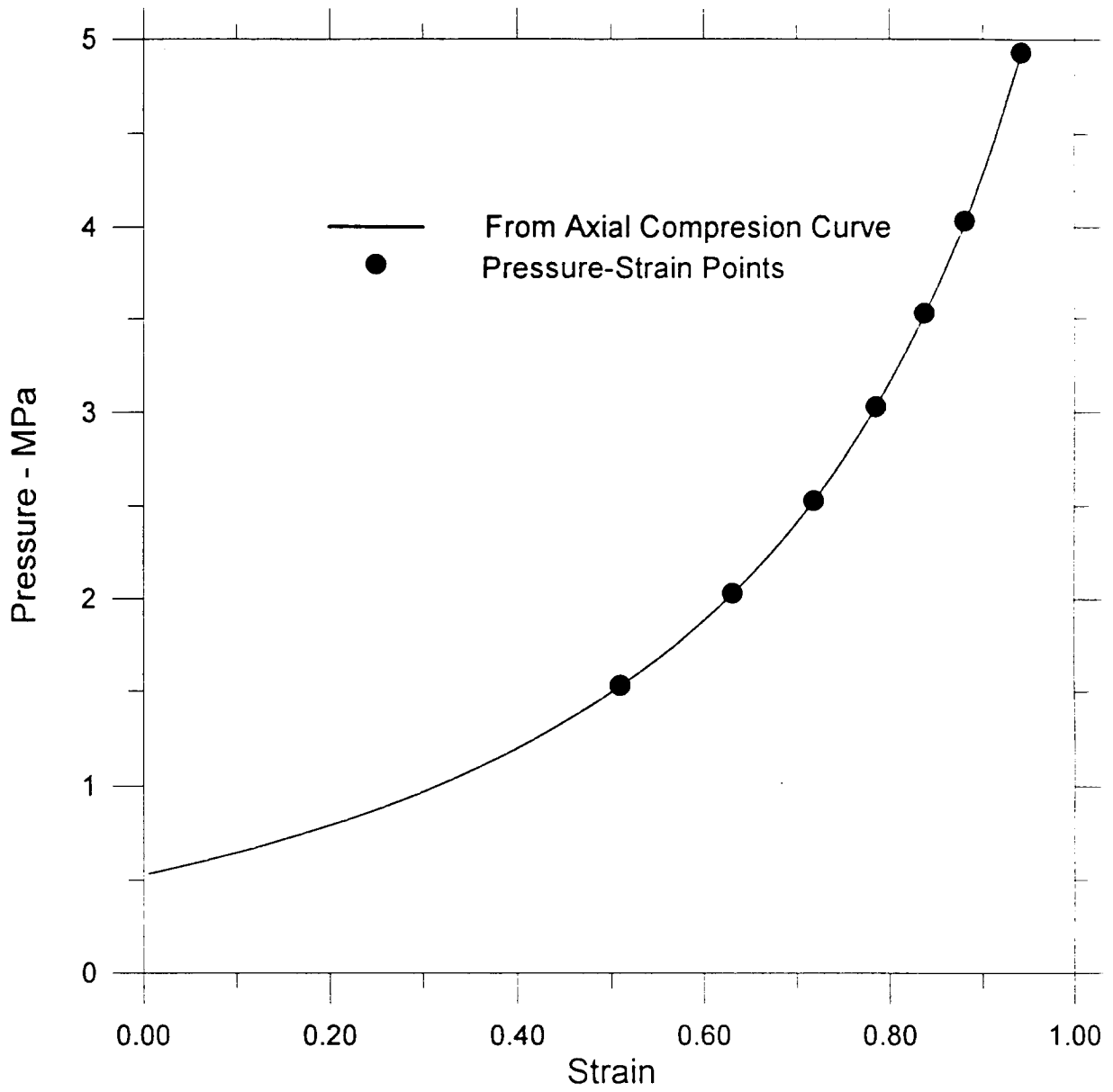
$$wt := wmi + wma + wmo + wc + wpp + wpr + wim + wsi + wso + wss \qquad wt = 559.1$$

$$rs := \frac{wt}{vt} \qquad rs = 1.755 \cdot 10^3$$

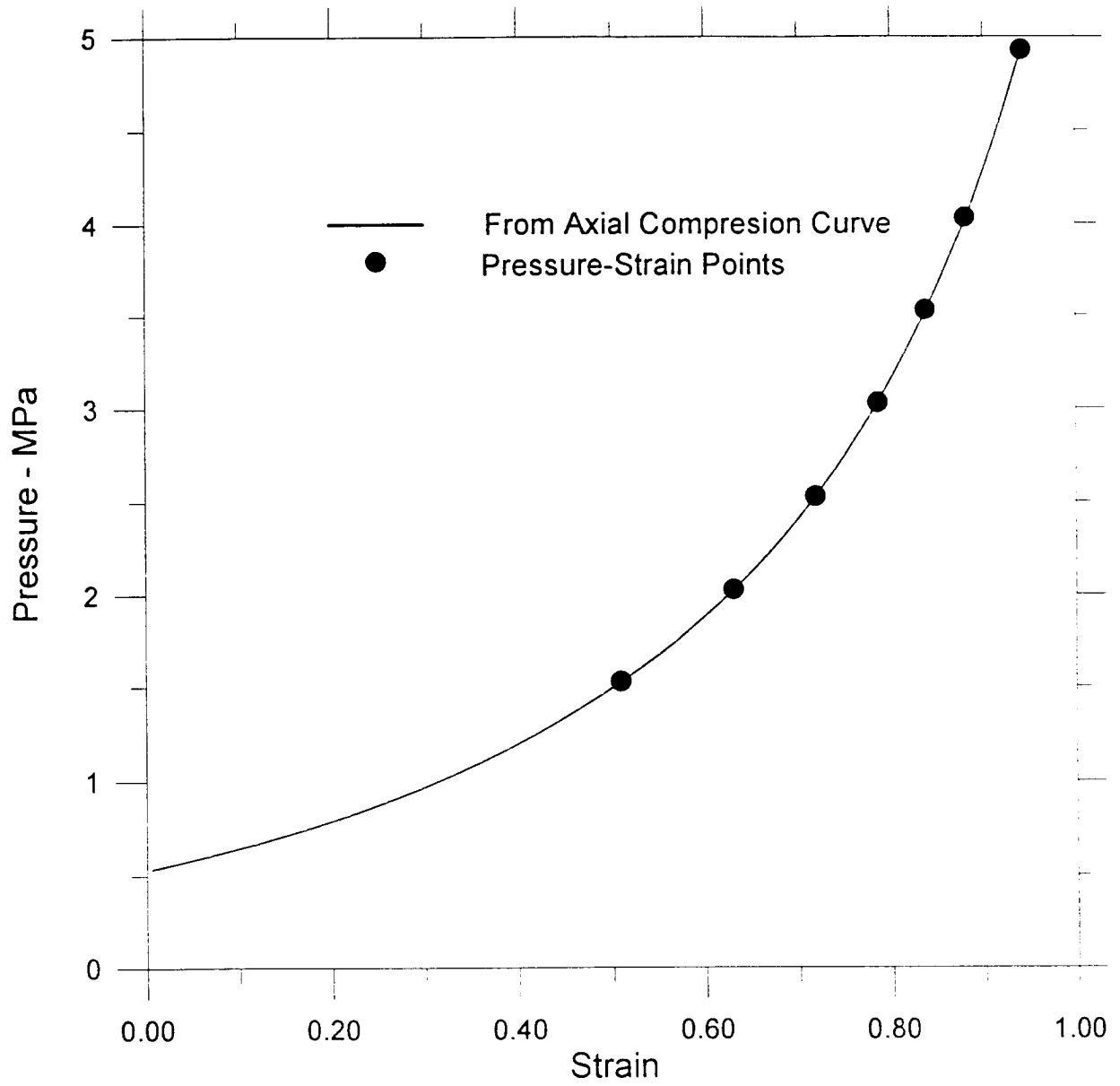
Average solid density is 1755 kg/m3

Initial porosity is $1 - \frac{vt}{1.0} = 0.681$

1.24645	0.41763	3.73935	0.51649
1.31661	0.44272	3.94982	0.50421
1.38604	0.46622	4.15811	0.49242
1.46112	0.4902	4.38335	0.4801
1.53027	0.51062	4.59081	0.46937
1.60051	0.53087	4.80154	0.45852
1.67589	0.55123	5.02766	0.44738
1.74624	0.56881	5.23872	0.43758
1.81973	0.58626	5.4592	0.42768
1.88723	0.60161	5.6617	0.41883
1.96094	0.61753	5.88281	0.4095
2.03065	0.63193	6.09195	0.40094
2.10297	0.6462	6.30891	0.39233
2.17681	0.66015	6.53043	0.38379
2.24467	0.67247	6.734	0.37615
2.3149	0.68471	6.94469	0.36847
2.38653	0.69666	7.1596	0.36088
2.45932	0.70831	7.37795	0.35339
2.5321	0.71951	7.5963	0.3461
2.60567	0.73039	7.817	0.33895
2.67416	0.74018	8.02247	0.33245
2.74508	0.74991	8.23524	0.32592
2.81782	0.75956	8.45345	0.31939
2.88619	0.76837	8.65857	0.31337
2.95721	0.77718	8.87162	0.30729
3.03123	0.78604	9.0937	0.30113
3.10064	0.79408	9.30192	0.29548
3.17464	0.80239	9.52392	0.2896
3.24331	0.80986	9.72994	0.28428
3.31715	0.81763	9.95146	0.27869
3.38493	0.82458	10.1548	0.27366
3.45557	0.83159	10.3667	0.26855
3.5301	0.83875	10.5903	0.26329
3.60177	0.84543	10.8053	0.25836
3.67023	0.85165	11.0107	0.25373
3.7436	0.85811	11.2308	0.2489
3.8162	0.86432	11.4486	0.24422
3.88753	0.87026	11.6626	0.23972
3.956	0.87582	11.868	0.23548
4.0258	0.88132	12.0774	0.23125
4.1004	0.88704	12.3012	0.22685
4.1693	0.89221	12.5079	0.22284
4.24237	0.89753	12.7271	0.21869
4.31363	0.9026	12.9409	0.21472
4.3875	0.90771	13.1625	0.2107
4.45617	0.91235	13.3685	0.20703
4.52807	0.91709	13.5842	0.20326
4.60143	0.9218	13.8043	0.1995
4.93333	0.94281	14.8	0.1825



C: Mathcad Strain.grf



C: Mathcad Strain.grf

Appendix D

Mesh Coordinates and Connectivity

List of Appendix D Tables

Table No.	Title	Page No.
D-1	Summary	D-3
D-2	Mesh Coordinates	D-5
D-3	Element Block 1 Description	D-15
D-4	Element Block 2 Description	D-25
D-5	Element Block 3 Description	D-26
D-6	Element Block 4 Description	D-28

Table D-1. Summary of Exodus File Format

Database Title:	DISPOSAL ROOM MODEL-MULTIMATERIAL STRATIGRAPHY-SLIDELINES
Conversion:	EXOTXT 3/24/94 Version 1.1 (Binary to ASCII)
Database Initial Variables:	2 Dimensions 1805 nodes 1680 elements 4 element blocks
Element Type:	4-node quad

Table D-2. Mesh Coordinates

Node			Node			Node			Node		
No.	X	Y									
1	0.0000	-54.1900	48	0.9565	-41.0373	95	1.9324	-31.5345	142	2.8667	-24.6687
2	0.9214	-54.1900	49	1.8876	-41.0373	96	2.8325	-31.5345	143	3.7072	-24.6687
3	1.8427	-54.1900	50	2.7983	-41.0373	97	3.6999	-31.5345	144	4.5085	-24.6687
4	2.7641	-54.1900	51	3.6927	-41.0373	98	4.5413	-31.5345	145	5.2786	-24.6687
5	3.6855	-54.1900	52	4.5741	-41.0373	99	5.3618	-31.5345	146	6.0237	-24.6687
6	4.6068	-54.1900	53	5.4450	-41.0373	100	6.1656	-31.5345	147	6.8125	-24.6687
7	5.5282	-54.1900	54	6.3076	-41.0373	101	6.9987	-31.5345	148	7.6158	-24.6687
8	6.4495	-54.1900	55	7.1848	-41.0373	102	7.8413	-31.5345	149	8.4348	-24.6687
9	7.3709	-54.1900	56	8.0668	-41.0373	103	8.6944	-31.5345	150	9.2713	-24.6687
10	8.2923	-54.1900	57	8.9540	-41.0373	104	9.5592	-31.5345	151	10.1270	-24.6687
11	9.2136	-54.1900	58	9.8471	-41.0373	105	10.4368	-31.5345	152	11.0037	-24.6687
12	10.1350	-54.1900	59	10.7466	-41.0373	106	11.3284	-31.5345	153	11.9036	-24.6687
13	11.0564	-54.1900	60	11.6530	-41.0373	107	12.2354	-31.5345	154	12.8289	-24.6687
14	11.9777	-54.1900	61	12.5672	-41.0373	108	13.1594	-31.5345	155	13.7823	-24.6687
15	12.8991	-54.1900	62	13.4899	-41.0373	109	14.1022	-31.5345	156	14.7666	-24.6687
16	13.8205	-54.1900	63	14.4220	-41.0373	110	15.0655	-31.5345	157	15.7848	-24.6687
17	14.7418	-54.1900	64	15.3643	-41.0373	111	16.0514	-31.5345	158	16.8403	-24.6687
18	15.6632	-54.1900	65	16.3180	-41.0373	112	17.0622	-31.5345	159	17.9369	-24.6687
19	16.5846	-54.1900	66	17.2840	-41.0373	113	18.1003	-31.5345	160	19.0786	-24.6687
20	17.5059	-54.1900	67	18.2638	-41.0373	114	19.1686	-31.5345	161	20.2700	-24.6687
21	18.4273	-54.1900	68	19.2586	-41.0373	115	20.2700	-31.5345	162	0.0000	-21.9873
22	19.3486	-54.1900	69	20.2700	-41.0373	116	0.0000	-27.8233	163	1.0444	-21.9873
23	20.2700	-54.1900	70	0.0000	-35.9007	117	1.0093	-27.8233	164	1.9997	-21.9873
24	0.0000	-47.0804	71	0.9741	-35.9007	118	1.9549	-27.8233	165	2.8838	-21.9873
25	0.9389	-47.0804	72	1.9100	-35.9007	119	2.8496	-27.8233	166	3.7108	-21.9873
26	1.8652	-47.0804	73	2.8154	-35.9007	120	3.7035	-27.8233	167	4.4921	-21.9873
27	2.7812	-47.0804	74	3.6963	-35.9007	121	4.5249	-27.8233	168	5.2370	-21.9873
28	3.6891	-47.0804	75	4.5577	-35.9007	122	5.3202	-27.8233	169	5.9527	-21.9873
29	4.5904	-47.0804	76	5.4034	-35.9006	123	6.0947	-27.8233	170	6.7195	-21.9873
30	5.4866	-47.0804	77	6.2366	-35.9007	124	6.9056	-27.8233	171	7.5030	-21.9873
31	6.3786	-47.0804	78	7.0917	-35.9007	125	7.7285	-27.8233	172	8.3051	-21.9873
32	7.2778	-47.0804	79	7.9540	-35.9007	126	8.5646	-27.8233	173	9.1274	-21.9873
33	8.1795	-47.0804	80	8.8242	-35.9007	127	9.4153	-27.8233	174	9.9721	-21.9873
34	9.0838	-47.0804	81	9.7032	-35.9006	128	10.2819	-27.8233	175	10.8413	-21.9873
35	9.9911	-47.0804	82	10.5917	-35.9007	129	11.1660	-27.8233	176	11.7376	-21.9873
36	10.9015	-47.0804	83	11.4907	-35.9007	130	12.0695	-27.8233	177	12.6637	-21.9873
37	11.8154	-47.0804	84	12.4013	-35.9007	131	12.9942	-27.8233	178	13.6224	-21.9873
38	12.7332	-47.0804	85	13.3247	-35.9006	132	13.9423	-27.8233	179	14.6172	-21.9873
39	13.6552	-47.0804	86	14.2621	-35.9006	133	14.9160	-27.8233	180	15.6515	-21.9873
40	14.5819	-47.0804	87	15.2149	-35.9007	134	15.9181	-27.8233	181	16.7294	-21.9873
41	15.5138	-47.0804	88	16.1847	-35.9007	135	16.9512	-27.8233	182	17.8551	-21.9873
42	16.4513	-47.0804	89	17.1731	-35.9007	136	18.0186	-27.8233	183	19.0336	-21.9873
43	17.3950	-47.0804	90	18.1821	-35.9007	137	19.1236	-27.8233	184	20.2700	-21.9873
44	18.3455	-47.0804	91	19.2136	-35.9007	138	20.2700	-27.8233	185	0.0000	-19.7082
45	19.3036	-47.0804	92	20.2700	-35.9007	139	0.0000	-24.6687	186	1.0620	-19.7082
46	20.2700	-47.0804	93	0.0000	-31.5345	140	1.0268	-24.6687	187	2.0222	-19.7082
47	0.0000	-41.0373	94	0.9917	-31.5345	141	1.9773	-24.6687	188	2.9009	-19.7082

Table D-2. Mesh Coordinates (continued)

Node			Node			Node			Node		
No.	X	Y									
189	3.7144	-19.7082	236	4.4430	-16.1242	283	5.0291	-13.5348	330	5.4559	-11.6639
190	4.4758	-19.7082	237	5.1122	-16.1242	284	5.5978	-13.5348	331	6.0680	-11.6639
191	5.1954	-19.7082	238	5.7398	-16.1242	285	6.2542	-13.5348	332	6.7138	-11.6639
192	5.8817	-19.7082	239	6.4403	-16.1242	286	6.9393	-13.5348	333	7.3965	-11.6639
193	6.6264	-19.7082	240	7.1648	-16.1242	287	7.6561	-13.5348	334	8.1198	-11.6639
194	7.3903	-19.7082	241	7.9157	-16.1242	288	8.4077	-13.5348	335	8.8878	-11.6639
195	8.1753	-19.7082	242	8.6956	-16.1242	289	9.1976	-13.5348	336	9.7049	-11.6639
196	8.9834	-19.7082	243	9.5074	-16.1242	290	10.0296	-13.5348	337	10.5762	-11.6639
197	9.8172	-19.7082	244	10.3543	-16.1242	291	10.9080	-13.5348	338	11.5069	-11.6639
198	10.6790	-19.7082	245	11.2399	-16.1242	292	11.8374	-13.5348	339	12.5030	-11.6639
199	11.5717	-19.7082	246	12.1679	-16.1242	293	12.8229	-13.5348	340	13.5711	-11.6639
200	12.4984	-19.7082	247	13.1427	-16.1242	294	13.8700	-13.5348	341	14.7184	-11.6639
201	13.4625	-19.7082	248	14.1689	-16.1242	295	14.9850	-13.5348	342	15.9528	-11.6639
202	14.4677	-19.7082	249	15.2516	-16.1242	296	16.1747	-13.5348	343	17.2830	-11.6639
203	15.5182	-19.7082	250	16.3966	-16.1242	297	17.4465	-13.5348	344	18.7185	-11.6639
204	16.6184	-19.7082	251	17.6099	-16.1242	298	18.8086	-13.5348	345	20.2700	-11.6639
205	17.7734	-19.7082	252	18.8986	-16.1242	299	20.2700	-13.5348	346	0.0000	-10.9333
206	18.9886	-19.7082	253	20.2700	-16.1242	300	0.0000	-12.5235	347	1.1851	-10.9333
207	20.2700	-19.7082	254	0.0000	-14.7245	301	1.1499	-12.5235	348	2.1792	-10.9332
208	0.0000	-17.7709	255	1.1147	-14.7245	302	2.1343	-12.5235	349	3.0205	-10.9333
209	1.0796	-17.7709	256	2.0895	-14.7245	303	2.9863	-12.5235	350	3.7397	-10.9333
210	2.0446	-17.7709	257	2.9522	-14.7245	304	3.7325	-12.5235	351	4.3611	-10.9333
211	2.9180	-17.7709	258	3.7252	-14.7245	305	4.3939	-12.5235	352	4.9043	-10.9333
212	3.7180	-17.7709	259	4.4266	-14.7245	306	4.9875	-12.5235	353	5.3849	-10.9333
213	4.4594	-17.7709	260	5.0706	-14.7245	307	5.5268	-12.5235	354	5.9750	-10.9333
214	5.1538	-17.7709	261	5.6688	-14.7245	308	6.1611	-12.5235	355	6.6010	-10.9333
215	5.8108	-17.7709	262	6.3472	-14.7245	309	6.8265	-12.5235	356	7.2667	-10.9333
216	6.5333	-17.7709	263	7.0520	-14.7245	310	7.5263	-12.5235	357	7.9758	-10.9333
217	7.2775	-17.7709	264	7.7859	-14.7245	311	8.2637	-12.5235	358	8.7329	-10.9333
218	8.0455	-17.7709	265	8.5516	-14.7245	312	9.0427	-12.5235	359	9.5426	-10.9332
219	8.8395	-17.7709	266	9.3525	-14.7245	313	9.8673	-12.5235	360	10.4102	-10.9333
220	9.6623	-17.7709	267	10.1920	-14.7245	314	10.7421	-12.5235	361	11.3416	-10.9333
221	10.5166	-17.7709	268	11.0739	-14.7245	315	11.6721	-12.5235	362	12.3431	-10.9333
222	11.4058	-17.7709	269	12.0026	-14.7245	316	12.6629	-12.5235	363	13.4217	-10.9333
223	12.3332	-17.7709	270	12.9828	-14.7245	317	13.7206	-12.5235	364	14.5851	-10.9333
224	13.3026	-17.7709	271	14.0194	-14.7245	318	14.8517	-12.5235	365	15.8419	-10.9333
225	14.3183	-17.7709	272	15.1183	-14.7245	319	16.0637	-12.5235	366	17.2013	-10.9333
226	15.3849	-17.7709	273	16.2856	-14.7245	320	17.3647	-12.5235	367	18.6735	-10.9332
227	16.5075	-17.7709	274	17.5282	-14.7245	321	18.7635	-12.5235	368	20.2700	-10.9333
228	17.6917	-17.7709	275	18.8536	-14.7245	322	20.2700	-12.5235	369	0.0000	-10.3122
229	18.9436	-17.7709	276	20.2700	-14.7245	323	0.0000	-11.6639	370	1.2026	-10.3122
230	20.2700	-17.7709	277	0.0000	-13.5348	324	1.1675	-11.6639	371	2.2016	-10.3122
231	0.0000	-16.1242	278	1.1323	-13.5348	325	2.1567	-11.6639	372	3.0376	-10.3122
232	1.0972	-16.1242	279	2.1119	-13.5348	326	3.0034	-11.6639	373	3.7433	-10.3122
233	2.0670	-16.1242	280	2.9692	-13.5348	327	3.7361	-11.6639	374	4.3447	-10.3122
234	2.9351	-16.1242	281	3.7288	-13.5348	328	4.3775	-11.6639	375	4.8627	-10.3122
235	3.7216	-16.1242	282	4.4102	-13.5348	329	4.9459	-11.6639	376	5.3139	-10.3122

Table D-2. Mesh Coordinates (continued)

Node			Node			Node			Node		
No.	X	Y	No.	X	Y	No.	X	Y	No.	X	Y
377	5.8819	-10.3122	425	6.8773	-9.3356	473	7.9584	-8.6300	521	9.5806	-8.2000
378	6.4883	-10.3122	426	7.5440	-9.3356	474	8.7309	-8.6300	522	10.5153	-8.2000
379	7.1369	-10.3122	427	8.2682	-9.3356	475	9.5806	-8.6300	523	11.5435	-8.2000
380	7.8319	-10.3122	428	9.0556	-9.3356	476	10.5153	-8.6300	524	12.6746	-8.2000
381	8.5780	-10.3122	429	9.9125	-9.3356	477	11.5435	-8.6300	525	13.9187	-8.2000
382	9.3802	-10.3122	430	10.8459	-9.3356	478	12.6746	-8.6300	526	15.2872	-8.2000
383	10.2443	-10.3122	431	11.8634	-9.3356	479	13.9187	-8.6300	527	16.7926	-8.2000
384	11.1764	-10.3122	432	12.9734	-9.3356	480	15.2872	-8.6300	528	18.4485	-8.2000
385	12.1832	-10.3122	433	14.1853	-9.3356	481	16.7926	-8.6300	529	20.2700	-8.2000
386	13.2723	-10.3122	434	15.5091	-9.3356	482	18.4485	-8.6300	530	0.0000	-7.9850
387	14.4518	-10.3122	435	16.9560	-9.3356	483	20.2700	-8.6300	531	1.2730	-7.9850
388	15.7309	-10.3122	436	18.5385	-9.3356	484	0.0000	-8.4150	532	2.2913	-7.9850
389	17.1195	-10.3122	437	20.2700	-9.3356	485	1.2730	-8.4150	533	3.1060	-7.9850
390	18.6285	-10.3122	438	0.0000	-8.9542	486	2.2913	-8.4150	534	3.7578	-7.9850
391	20.2700	-10.3122	439	1.2554	-8.9542	487	3.1060	-8.4150	535	4.2792	-7.9850
392	0.0000	-9.7843	440	2.2689	-8.9542	488	3.7578	-8.4150	536	4.6963	-7.9850
393	1.2202	-9.7843	441	3.0889	-8.9542	489	4.2792	-8.4150	537	5.0300	-7.9850
394	2.2240	-9.7843	442	3.7542	-8.9542	490	4.6963	-8.4150	538	5.5097	-7.9850
395	3.0547	-9.7843	443	4.2956	-8.9542	491	5.0300	-8.4150	539	6.0373	-7.9850
396	3.7469	-9.7843	444	4.7379	-8.9542	492	5.5097	-8.4150	540	6.6177	-7.9850
397	4.3283	-9.7843	445	5.1010	-8.9542	493	6.0373	-8.4150	541	7.2561	-7.9850
398	4.8211	-9.7843	446	5.6027	-8.9542	494	6.6177	-8.4150	542	7.9584	-7.9850
399	5.2429	-9.7843	447	6.1500	-8.9542	495	7.2561	-8.4150	543	8.7309	-7.9850
400	5.7888	-9.7843	448	6.7475	-8.9542	496	7.9584	-8.4150	544	9.5806	-7.9850
401	6.3755	-9.7843	449	7.4000	-8.9542	497	8.7309	-8.4150	545	10.5153	-7.9850
402	7.0071	-9.7843	450	8.1133	-8.9542	498	9.5806	-8.4150	546	11.5435	-7.9850
403	7.6879	-9.7843	451	8.8932	-8.9542	499	10.5153	-8.4150	547	12.6746	-7.9850
404	8.4231	-9.7843	452	9.7465	-8.9542	500	11.5435	-8.4150	548	13.9187	-7.9850
405	9.2179	-9.7843	453	10.6806	-8.9542	501	12.6746	-8.4150	549	15.2872	-7.9850
406	10.0784	-9.7843	454	11.7035	-8.9542	502	13.9187	-8.4150	550	16.7926	-7.9850
407	11.0111	-9.7843	455	12.8240	-8.9542	503	15.2872	-8.4150	551	18.4485	-7.9850
408	12.0233	-9.7843	456	14.0520	-8.9542	504	16.7926	-8.4150	552	20.2700	-7.9850
409	13.1228	-9.7843	457	15.3981	-8.9542	505	18.4485	-8.4150	553	0.0000	-7.7700
410	14.3185	-9.7843	458	16.8743	-8.9542	506	20.2700	-8.4150	554	1.2730	-7.7700
411	15.6200	-9.7843	459	18.4935	-8.9542	507	0.0000	-8.2000	555	2.2913	-7.7700
412	17.0378	-9.7843	460	20.2700	-8.9542	508	1.2730	-8.2000	556	3.1060	-7.7700
413	18.5835	-9.7843	461	0.0000	-8.6300	509	2.2913	-8.2000	557	3.7578	-7.7700
414	20.2700	-9.7843	462	1.2730	-8.6300	510	3.1060	-8.2000	558	4.2792	-7.7700
415	0.0000	-9.3356	463	2.2913	-8.6300	511	3.7578	-8.2000	559	4.6963	-7.7700
416	1.2378	-9.3356	464	3.1060	-8.6300	512	4.2792	-8.2000	560	5.0300	-7.7700
417	2.2465	-9.3356	465	3.7578	-8.6300	513	4.6963	-8.2000	561	5.5097	-7.7700
418	3.0718	-9.3356	466	4.2792	-8.6300	514	5.0300	-8.2000	562	6.0373	-7.7700
419	3.7505	-9.3356	467	4.6963	-8.6300	515	5.5097	-8.2000	563	6.6177	-7.7700
420	4.3119	-9.3356	468	5.0300	-8.6300	516	6.0373	-8.2000	564	7.2561	-7.7700
421	4.7795	-9.3356	469	5.5097	-8.6300	517	6.6177	-8.2000	565	7.9584	-7.7700
422	5.1720	-9.3356	470	6.0373	-8.6300	518	7.2561	-8.2000	566	8.7309	-7.7700
423	5.6958	-9.3356	471	6.6177	-8.6300	519	7.9584	-8.2000	567	9.5806	-7.7700
424	6.2628	-9.3356	472	7.2561	-8.6300	520	8.7309	-8.2000	568	10.5153	-7.7700

Table D-2. Mesh Coordinates (continued)

Node			Node			Node			Node		
No.	X	Y									
569	11.5435	-7.7700	617	13.9187	-7.2180	665	16.7926	-6.6660	713	8.7309	-5.7300
570	12.6746	-7.7700	618	15.2872	-7.2180	666	18.4485	-6.6660	714	9.5806	-5.7300
571	13.9187	-7.7700	619	16.7926	-7.2180	667	20.2700	-6.6660	715	10.5153	-5.7300
572	15.2872	-7.7700	620	18.4485	-7.2180	668	0.0000	-6.3900	716	11.5435	-5.7300
573	16.7926	-7.7700	621	20.2700	-7.2180	669	1.2730	-6.3900	717	12.6746	-5.7300
574	18.4485	-7.7700	622	0.0000	-6.9420	670	2.2913	-6.3900	718	13.9187	-5.7300
575	20.2700	-7.7700	623	1.2730	-6.9420	671	3.1060	-6.3900	719	15.2872	-5.7300
576	0.0000	-7.4940	624	2.2913	-6.9420	672	3.7578	-6.3900	720	16.7926	-5.7300
577	1.2730	-7.4940	625	3.1060	-6.9420	673	4.2792	-6.3900	721	18.4485	-5.7300
578	2.2913	-7.4940	626	3.7578	-6.9420	674	4.6963	-6.3900	722	20.2700	-5.7300
579	3.1060	-7.4940	627	4.2792	-6.9420	675	5.0300	-6.3900	723	5.0300	-5.4000
580	3.7578	-7.4940	628	4.6963	-6.9420	676	5.5097	-6.3900	724	5.5097	-5.4000
581	4.2792	-7.4940	629	5.0300	-6.9420	677	6.0373	-6.3900	725	6.0373	-5.4000
582	4.6963	-7.4940	630	5.5097	-6.9420	678	6.6177	-6.3900	726	6.6177	-5.4000
583	5.0300	-7.4940	631	6.0373	-6.9420	679	7.2561	-6.3900	727	7.2561	-5.4000
584	5.5097	-7.4940	632	6.6177	-6.9420	680	7.9584	-6.3900	728	7.9584	-5.4000
585	6.0373	-7.4940	633	7.2561	-6.9420	681	8.7309	-6.3900	729	8.7309	-5.4000
586	6.6177	-7.4940	634	7.9584	-6.9420	682	9.5806	-6.3900	730	9.5806	-5.4000
587	7.2561	-7.4940	635	8.7309	-6.9420	683	10.5153	-6.3900	731	10.5153	-5.4000
588	7.9584	-7.4940	636	9.5806	-6.9420	684	11.5435	-6.3900	732	11.5435	-5.4000
589	8.7309	-7.4940	637	10.5153	-6.9420	685	12.6746	-6.3900	733	12.6746	-5.4000
590	9.5806	-7.4940	638	11.5435	-6.9420	686	13.9187	-6.3900	734	13.9187	-5.4000
591	10.5153	-7.4940	639	12.6746	-6.9420	687	15.2872	-6.3900	735	15.2872	-5.4000
592	11.5435	-7.4940	640	13.9187	-6.9420	688	16.7926	-6.3900	736	16.7926	-5.4000
593	12.6746	-7.4940	641	15.2872	-6.9420	689	18.4485	-6.3900	737	18.4485	-5.4000
594	13.9187	-7.4940	642	16.7926	-6.9420	690	20.2700	-6.3900	738	20.2700	-5.4000
595	15.2872	-7.4940	643	18.4485	-6.9420	691	5.0300	-6.0600	739	5.0300	-5.0700
596	16.7926	-7.4940	644	20.2700	-6.9420	692	5.5097	-6.0600	740	5.5097	-5.0700
597	18.4485	-7.4940	645	0.0000	-6.6660	693	6.0373	-6.0600	741	6.0373	-5.0700
598	20.2700	-7.4940	646	1.2730	-6.6660	694	6.6177	-6.0600	742	6.6177	-5.0700
599	0.0000	-7.2180	647	2.2913	-6.6660	695	7.2561	-6.0600	743	7.2561	-5.0700
600	1.2730	-7.2180	648	3.1060	-6.6660	696	7.9584	-6.0600	744	7.9584	-5.0700
601	2.2913	-7.2180	649	3.7578	-6.6660	697	8.7309	-6.0600	745	8.7309	-5.0700
602	3.1060	-7.2180	650	4.2792	-6.6660	698	9.5806	-6.0600	746	9.5806	-5.0700
603	3.7578	-7.2180	651	4.6963	-6.6660	699	10.5153	-6.0600	747	10.5153	-5.0700
604	4.2792	-7.2180	652	5.0300	-6.6660	700	11.5435	-6.0600	748	11.5435	-5.0700
605	4.6963	-7.2180	653	5.5097	-6.6660	701	12.6746	-6.0600	749	12.6746	-5.0700
606	5.0300	-7.2180	654	6.0373	-6.6660	702	13.9187	-6.0600	750	13.9187	-5.0700
607	5.5097	-7.2180	655	6.6177	-6.6660	703	15.2872	-6.0600	751	15.2872	-5.0700
608	6.0373	-7.2180	656	7.2561	-6.6660	704	16.7926	-6.0600	752	16.7926	-5.0700
609	6.6177	-7.2180	657	7.9584	-6.6660	705	18.4485	-6.0600	753	18.4485	-5.0700
610	7.2561	-7.2180	658	8.7309	-6.6660	706	20.2700	-6.0600	754	20.2700	-5.0700
611	7.9584	-7.2180	659	9.5806	-6.6660	707	5.0300	-5.7300	755	5.0300	-4.7400
612	8.7309	-7.2180	660	10.5153	-6.6660	708	5.5097	-5.7300	756	5.5097	-4.7400
613	9.5806	-7.2180	661	11.5435	-6.6660	709	6.0373	-5.7300	757	6.0373	-4.7400
614	10.5153	-7.2180	662	12.6746	-6.6660	710	6.6177	-5.7300	758	6.6177	-4.7400
615	11.5435	-7.2180	663	13.9187	-6.6660	711	7.2561	-5.7300	759	7.2561	-4.7400
616	12.6746	-7.2180	664	15.2872	-6.6660	712	7.9584	-5.7300	760	7.9584	-4.7400

Table D-2. Mesh Coordinates (continued)

Node No.	X	Y									
761	8.7309	-4.7400	809	8.7309	-3.7500	857	8.7309	-2.7600	905	10.5153	-2.0829
762	9.5806	-4.7400	810	9.5806	-3.7500	858	9.5806	-2.7600	906	11.5435	-2.0829
763	10.5153	-4.7400	811	10.5153	-3.7500	859	10.5153	-2.7600	907	12.6746	-2.0829
764	11.5435	-4.7400	812	11.5435	-3.7500	860	11.5435	-2.7600	908	13.9187	-2.0829
765	12.6746	-4.7400	813	12.6746	-3.7500	861	12.6746	-2.7600	909	15.2872	-2.0829
766	13.9187	-4.7400	814	13.9187	-3.7500	862	13.9187	-2.7600	910	16.7926	-2.0829
767	15.2872	-4.7400	815	15.2872	-3.7500	863	15.2872	-2.7600	911	18.4485	-2.0829
768	16.7926	-4.7400	816	16.7926	-3.7500	864	16.7926	-2.7600	912	20.2700	-2.0829
769	18.4485	-4.7400	817	18.4485	-3.7500	865	18.4485	-2.7600	913	0.0000	-1.7357
770	20.2700	-4.7400	818	20.2700	-3.7500	866	20.2700	-2.7600	914	1.2730	-1.7357
771	5.0300	-4.4100	819	5.0300	-3.4200	867	5.0300	-2.4300	915	2.2913	-1.7357
772	5.5097	-4.4100	820	5.5097	-3.4200	868	5.5097	-2.4300	916	3.1060	-1.7357
773	6.0373	-4.4100	821	6.0373	-3.4200	869	6.0373	-2.4300	917	3.7578	-1.7357
774	6.6177	-4.4100	822	6.6177	-3.4200	870	6.6177	-2.4300	918	4.2792	-1.7357
775	7.2561	-4.4100	823	7.2561	-3.4200	871	7.2561	-2.4300	919	4.6963	-1.7357
776	7.9584	-4.4100	824	7.9584	-3.4200	872	7.9584	-2.4300	920	5.0300	-1.7357
777	8.7309	-4.4100	825	8.7309	-3.4200	873	8.7309	-2.4300	921	5.5097	-1.7357
778	9.5806	-4.4100	826	9.5806	-3.4200	874	9.5806	-2.4300	922	6.0373	-1.7357
779	10.5153	-4.4100	827	10.5153	-3.4200	875	10.5153	-2.4300	923	6.6177	-1.7357
780	11.5435	-4.4100	828	11.5435	-3.4200	876	11.5435	-2.4300	924	7.2561	-1.7357
781	12.6746	-4.4100	829	12.6746	-3.4200	877	12.6746	-2.4300	925	7.9584	-1.7357
782	13.9187	-4.4100	830	13.9187	-3.4200	878	13.9187	-2.4300	926	8.7309	-1.7357
783	15.2872	-4.4100	831	15.2872	-3.4200	879	15.2872	-2.4300	927	9.5806	-1.7357
784	16.7926	-4.4100	832	16.7926	-3.4200	880	16.7926	-2.4300	928	10.5153	-1.7357
785	18.4485	-4.4100	833	18.4485	-3.4200	881	18.4485	-2.4300	929	11.5435	-1.7357
786	20.2700	-4.4100	834	20.2700	-3.4200	882	20.2700	-2.4300	930	12.6746	-1.7357
787	5.0300	-4.0800	835	5.0300	-3.0900	883	0.0000	-2.4300	931	13.9187	-1.7357
788	5.5097	-4.0800	836	5.5097	-3.0900	884	1.2730	-2.4300	932	15.2872	-1.7357
789	6.0373	-4.0800	837	6.0373	-3.0900	885	2.2913	-2.4300	933	16.7926	-1.7357
790	6.6177	-4.0800	838	6.6177	-3.0900	886	3.1060	-2.4300	934	18.4485	-1.7357
791	7.2561	-4.0800	839	7.2561	-3.0900	887	3.7578	-2.4300	935	20.2700	-1.7357
792	7.9584	-4.0800	840	7.9584	-3.0900	888	4.2792	-2.4300	936	0.0000	-1.3886
793	8.7309	-4.0800	841	8.7309	-3.0900	889	4.6963	-2.4300	937	1.2730	-1.3886
794	9.5806	-4.0800	842	9.5806	-3.0900	890	0.0000	-2.0829	938	2.2913	-1.3886
795	10.5153	-4.0800	843	10.5153	-3.0900	891	1.2730	-2.0829	939	3.1060	-1.3886
796	11.5435	-4.0800	844	11.5435	-3.0900	892	2.2913	-2.0829	940	3.7578	-1.3886
797	12.6746	-4.0800	845	12.6746	-3.0900	893	3.1060	-2.0829	941	4.2792	-1.3886
798	13.9187	-4.0800	846	13.9187	-3.0900	894	3.7578	-2.0829	942	4.6963	-1.3886
799	15.2872	-4.0800	847	15.2872	-3.0900	895	4.2792	-2.0829	943	5.0300	-1.3886
800	16.7926	-4.0800	848	16.7926	-3.0900	896	4.6963	-2.0829	944	5.5097	-1.3886
801	18.4485	-4.0800	849	18.4485	-3.0900	897	5.0300	-2.0829	945	6.0373	-1.3886
802	20.2700	-4.0800	850	20.2700	-3.0900	898	5.5097	-2.0829	946	6.6177	-1.3886
803	5.0300	-3.7500	851	5.0300	-2.7600	899	6.0373	-2.0829	947	7.2561	-1.3886
804	5.5097	-3.7500	852	5.5097	-2.7600	900	6.6177	-2.0829	948	7.9584	-1.3886
805	6.0373	-3.7500	853	6.0373	-2.7600	901	7.2561	-2.0829	949	8.7309	-1.3886
806	6.6177	-3.7500	854	6.6177	-2.7600	902	7.9584	-2.0829	950	9.5806	-1.3886
807	7.2561	-3.7500	855	7.2561	-2.7600	903	8.7309	-2.0829	951	10.5153	-1.3886
808	7.9584	-3.7500	856	7.9584	-2.7600	904	9.5806	-2.0829	952	11.5435	-1.3886

Table D-2. Mesh Coordinates (continued)

Node			Node			Node			Node		
No.	X	Y	No.	X	Y	No.	X	Y	No.	X	Y
953	12.6746	-1.3886	1001	15.2872	-0.6943	1049	18.4485	0.0000	1097	0.0000	1.5750
954	13.9187	-1.3886	1002	16.7926	-0.6943	1050	20.2700	0.0000	1098	1.2730	1.5750
955	15.2872	-1.3886	1003	18.4485	-0.6943	1051	0.0000	0.5250	1099	2.2913	1.5750
956	16.7926	-1.3886	1004	20.2700	-0.6943	1052	1.2730	0.5250	1100	3.1060	1.5750
957	18.4485	-1.3886	1005	0.0000	-0.3471	1053	2.2913	0.5250	1101	3.7578	1.5750
958	20.2700	-1.3886	1006	1.2730	-0.3471	1054	3.1060	0.5250	1102	4.2792	1.5750
959	0.0000	-1.0414	1007	2.2913	-0.3471	1055	3.7578	0.5250	1103	4.6963	1.5750
960	1.2730	-1.0414	1008	3.1060	-0.3471	1056	4.2792	0.5250	1104	5.0300	1.5750
961	2.2913	-1.0414	1009	3.7578	-0.3471	1057	4.6963	0.5250	1105	5.5097	1.5750
962	3.1060	-1.0414	1010	4.2792	-0.3471	1058	5.0300	0.5250	1106	6.0373	1.5750
963	3.7578	-1.0414	1011	4.6963	-0.3471	1059	5.5097	0.5250	1107	6.6177	1.5750
964	4.2792	-1.0414	1012	5.0300	-0.3471	1060	6.0373	0.5250	1108	7.2561	1.5750
965	4.6963	-1.0414	1013	5.5097	-0.3471	1061	6.6177	0.5250	1109	7.9584	1.5750
966	5.0300	-1.0414	1014	6.0373	-0.3471	1062	7.2561	0.5250	1110	8.7309	1.5750
967	5.5097	-1.0414	1015	6.6177	-0.3471	1063	7.9584	0.5250	1111	9.5806	1.5750
968	6.0373	-1.0414	1016	7.2561	-0.3471	1064	8.7309	0.5250	1112	10.5153	1.5750
969	6.6177	-1.0414	1017	7.9584	-0.3471	1065	9.5806	0.5250	1113	11.5435	1.5750
970	7.2561	-1.0414	1018	8.7309	-0.3471	1066	10.5153	0.5250	1114	12.6746	1.5750
971	7.9584	-1.0414	1019	9.5806	-0.3471	1067	11.5435	0.5250	1115	13.9187	1.5750
972	8.7309	-1.0414	1020	10.5153	-0.3471	1068	12.6746	0.5250	1116	15.2872	1.5750
973	9.5806	-1.0414	1021	11.5435	-0.3471	1069	13.9187	0.5250	1117	16.7926	1.5750
974	10.5153	-1.0414	1022	12.6746	-0.3471	1070	15.2872	0.5250	1118	18.4485	1.5750
975	11.5435	-1.0414	1023	13.9187	-0.3471	1071	16.7926	0.5250	1119	20.2700	1.5750
976	12.6746	-1.0414	1024	15.2872	-0.3471	1072	18.4485	0.5250	1120	0.0000	2.1000
977	13.9187	-1.0414	1025	16.7926	-0.3471	1073	20.2700	0.5250	1121	1.2730	2.1000
978	15.2872	-1.0414	1026	18.4485	-0.3471	1074	0.0000	1.0500	1122	2.2913	2.1000
979	16.7926	-1.0414	1027	20.2700	-0.3471	1075	1.2730	1.0500	1123	3.1060	2.1000
980	18.4485	-1.0414	1028	0.0000	0.0000	1076	2.2913	1.0500	1124	3.7578	2.1000
981	20.2700	-1.0414	1029	1.2730	0.0000	1077	3.1060	1.0500	1125	4.2792	2.1000
982	0.0000	-0.6943	1030	2.2913	0.0000	1078	3.7578	1.0500	1126	4.6963	2.1000
983	1.2730	-0.6943	1031	3.1060	0.0000	1079	4.2792	1.0500	1127	5.0300	2.1000
984	2.2913	-0.6943	1032	3.7578	0.0000	1080	4.6963	1.0500	1128	5.5097	2.1000
985	3.1060	-0.6943	1033	4.2792	0.0000	1081	5.0300	1.0500	1129	6.0373	2.1000
986	3.7578	-0.6943	1034	4.6963	0.0000	1082	5.5097	1.0500	1130	6.6177	2.1000
987	4.2792	-0.6943	1035	5.0300	0.0000	1083	6.0373	1.0500	1131	7.2561	2.1000
988	4.6963	-0.6943	1036	5.5097	0.0000	1084	6.6177	1.0500	1132	7.9584	2.1000
989	5.0300	-0.6943	1037	6.0373	0.0000	1085	7.2561	1.0500	1133	8.7309	2.1000
990	5.5097	-0.6943	1038	6.6177	0.0000	1086	7.9584	1.0500	1134	9.5806	2.1000
991	6.0373	-0.6943	1039	7.2561	0.0000	1087	8.7309	1.0500	1135	10.5153	2.1000
992	6.6177	-0.6943	1040	7.9584	0.0000	1088	9.5806	1.0500	1136	11.5435	2.1000
993	7.2561	-0.6943	1041	8.7309	0.0000	1089	10.5153	1.0500	1137	12.6746	2.1000
994	7.9584	-0.6943	1042	9.5806	0.0000	1090	11.5435	1.0500	1138	13.9187	2.1000
995	8.7309	-0.6943	1043	10.5153	0.0000	1091	12.6746	1.0500	1139	15.2872	2.1000
996	9.5806	-0.6943	1044	11.5435	0.0000	1092	13.9187	1.0500	1140	16.7926	2.1000
997	10.5153	-0.6943	1045	12.6746	0.0000	1093	15.2872	1.0500	1141	18.4485	2.1000
998	11.5435	-0.6943	1046	13.9187	0.0000	1094	16.7926	1.0500	1142	20.2700	2.1000
999	12.6746	-0.6943	1047	15.2872	0.0000	1095	18.4485	1.0500	1143	0.0000	4.2700
1000	13.9187	-0.6943	1048	16.7926	0.0000	1096	20.2700	1.0500	1144	1.2730	4.2700

Table D-2. Mesh Coordinates (continued)

Node			Node			Node			Node		
No.	X	Y									
1145	2.2913	4.2700	1193	3.7505	5.2900	1241	4.8627	6.6389	1289	6.0680	8.4228
1146	3.1060	4.2700	1194	4.3119	5.2900	1242	5.3139	6.6389	1290	6.7138	8.4228
1147	3.7578	4.2700	1195	4.7795	5.2900	1243	5.8819	6.6389	1291	7.3965	8.4228
1148	4.2792	4.2700	1196	5.1720	5.2900	1244	6.4883	6.6389	1292	8.1198	8.4228
1149	4.6963	4.2700	1197	5.6958	5.2900	1245	7.1369	6.6389	1293	8.8878	8.4228
1150	5.0300	4.2700	1198	6.2628	5.2900	1246	7.8319	6.6389	1294	9.7049	8.4228
1151	5.5097	4.2700	1199	6.8773	5.2900	1247	8.5780	6.6389	1295	10.5762	8.4228
1152	6.0373	4.2700	1200	7.5440	5.2900	1248	9.3802	6.6389	1296	11.5069	8.4228
1153	6.6177	4.2700	1201	8.2682	5.2900	1249	10.2443	6.6389	1297	12.5030	8.4228
1154	7.2561	4.2700	1202	9.0556	5.2900	1250	11.1764	6.6389	1298	13.5711	8.4228
1155	7.9584	4.2700	1203	9.9125	5.2900	1251	12.1832	6.6389	1299	14.7184	8.4228
1156	8.7309	4.2700	1204	10.8459	5.2900	1252	13.2723	6.6389	1300	15.9528	8.4228
1157	9.5806	4.2700	1205	11.8634	5.2900	1253	14.4518	6.6389	1301	17.2830	8.4228
1158	10.5153	4.2700	1206	12.9734	5.2900	1254	15.7309	6.6389	1302	18.7185	8.4228
1159	11.5435	4.2700	1207	14.1853	5.2900	1255	17.1195	6.6389	1303	20.2700	8.4228
1160	12.6746	4.2700	1208	15.5091	5.2900	1256	18.6285	6.6389	1304	0.0000	9.5202
1161	13.9187	4.2700	1209	16.9560	5.2900	1257	20.2700	6.6389	1305	1.1499	9.5202
1162	15.2872	4.2700	1210	18.5385	5.2900	1258	0.0000	7.4686	1306	2.1343	9.5202
1163	16.7926	4.2700	1211	20.2700	5.2900	1259	1.1851	7.4686	1307	2.9863	9.5202
1164	18.4485	4.2700	1212	0.0000	5.9174	1260	2.1792	7.4686	1308	3.7325	9.5202
1165	20.2700	4.2700	1213	1.2202	5.9174	1261	3.0205	7.4686	1309	4.3939	9.5202
1166	0.0000	4.7444	1214	2.2240	5.9174	1262	3.7397	7.4686	1310	4.9875	9.5202
1167	1.2554	4.7444	1215	3.0547	5.9174	1263	4.3611	7.4686	1311	5.5268	9.5202
1168	2.2689	4.7444	1216	3.7469	5.9174	1264	4.9043	7.4686	1312	6.1611	9.5202
1169	3.0889	4.7444	1217	4.3283	5.9174	1265	5.3849	7.4686	1313	6.8265	9.5202
1170	3.7542	4.7444	1218	4.8211	5.9174	1266	5.9750	7.4686	1314	7.5263	9.5202
1171	4.2956	4.7444	1219	5.2429	5.9174	1267	6.6010	7.4686	1315	8.2637	9.5202
1172	4.7379	4.7444	1220	5.7888	5.9174	1268	7.2667	7.4686	1316	9.0427	9.5202
1173	5.1010	4.7444	1221	6.3755	5.9174	1269	7.9758	7.4686	1317	9.8673	9.5202
1174	5.6027	4.7444	1222	7.0071	5.9174	1270	8.7329	7.4686	1318	10.7421	9.5202
1175	6.1500	4.7444	1223	7.6879	5.9174	1271	9.5426	7.4686	1319	11.6721	9.5202
1176	6.7475	4.7444	1224	8.4231	5.9174	1272	10.4102	7.4686	1320	12.6629	9.5202
1177	7.4000	4.7444	1225	9.2179	5.9174	1273	11.3416	7.4686	1321	13.7206	9.5202
1178	8.1133	4.7444	1226	10.0784	5.9174	1274	12.3431	7.4686	1322	14.8517	9.5202
1179	8.8932	4.7444	1227	11.0111	5.9174	1275	13.4217	7.4686	1323	16.0637	9.5202
1180	9.7465	4.7444	1228	12.0233	5.9174	1276	14.5851	7.4686	1324	17.3647	9.5202
1181	10.6806	4.7444	1229	13.1228	5.9174	1277	15.8419	7.4686	1325	18.7635	9.5202
1182	11.7035	4.7444	1230	14.3186	5.9174	1278	17.2013	7.4686	1326	20.2700	9.5202
1183	12.8240	4.7444	1231	15.6200	5.9174	1279	18.6735	7.4686	1327	0.0000	10.7821
1184	14.0520	4.7444	1232	17.0378	5.9174	1280	20.2700	7.4686	1328	1.1323	10.7821
1185	15.3981	4.7444	1233	18.5835	5.9174	1281	0.0000	8.4228	1329	2.1119	10.7821
1186	16.8743	4.7444	1234	20.2700	5.9174	1282	1.1675	8.4228	1330	2.9692	10.7821
1187	18.4935	4.7444	1235	0.0000	6.6389	1283	2.1567	8.4228	1331	3.7288	10.7821
1188	20.2700	4.7444	1236	1.2026	6.6389	1284	3.0034	8.4228	1332	4.4102	10.7821
1189	0.0000	5.2900	1237	2.2016	6.6389	1285	3.7361	8.4228	1333	5.0291	10.7821
1190	1.2378	5.2900	1238	3.0376	6.6389	1286	4.3775	8.4228	1334	5.5978	10.7821
1191	2.2465	5.2900	1239	3.7433	6.6389	1287	4.9459	8.4228	1335	6.2542	10.7821
1192	3.0718	5.2900	1240	4.3447	6.6389	1288	5.4559	8.4228	1336	6.9393	10.7821

Table D-2. Mesh Coordinates (continued)

Node			Node			Node			Node		
No.	X	Y									
1337	7.6561	10.7821	1385	9.5074	13.9022	1433	11.5717	18.0286	1481	13.7823	23.4857
1338	8.4077	10.7821	1386	10.3543	13.9022	1434	12.4984	18.0286	1482	14.7666	23.4857
1339	9.1976	10.7821	1387	11.2399	13.9022	1435	13.4625	18.0286	1483	15.7848	23.4857
1340	10.0296	10.7821	1388	12.1679	13.9022	1436	14.4677	18.0286	1484	16.8403	23.4857
1341	10.9080	10.7821	1389	13.1427	13.9022	1437	15.5182	18.0286	1485	17.9369	23.4857
1342	11.8374	10.7821	1390	14.1689	13.9022	1438	16.6184	18.0286	1486	19.0786	23.4857
1343	12.8229	10.7821	1391	15.2516	13.9022	1439	17.7734	18.0286	1487	20.2700	23.4857
1344	13.8700	10.7821	1392	16.3966	13.9022	1440	18.9886	18.0286	1488	0.0000	26.8425
1345	14.9850	10.7821	1393	17.6099	13.9022	1441	20.2700	18.0286	1489	1.0093	26.8425
1346	16.1747	10.7821	1394	18.8986	13.9022	1442	0.0000	20.5668	1490	1.9549	26.8425
1347	17.4465	10.7821	1395	20.2700	13.9022	1443	1.0444	20.5668	1491	2.8496	26.8425
1348	18.8086	10.7821	1396	0.0000	15.8215	1444	1.9997	20.5668	1492	3.7035	26.8425
1349	20.2700	10.7821	1397	1.0796	15.8215	1445	2.8838	20.5668	1493	4.5249	26.8425
1350	0.0000	12.2333	1398	2.0446	15.8215	1446	3.7108	20.5668	1494	5.3202	26.8425
1351	1.1147	12.2333	1399	2.9180	15.8215	1447	4.4921	20.5668	1495	6.0947	26.8425
1352	2.0895	12.2333	1400	3.7180	15.8215	1448	5.2370	20.5668	1496	6.9056	26.8425
1353	2.9522	12.2333	1401	4.4594	15.8215	1449	5.9527	20.5668	1497	7.7285	26.8425
1354	3.7252	12.2333	1402	5.1538	15.8215	1450	6.7195	20.5668	1498	8.5646	26.8425
1355	4.4266	12.2333	1403	5.8108	15.8215	1451	7.5030	20.5668	1499	9.4153	26.8425
1356	5.0706	12.2333	1404	6.5333	15.8215	1452	8.3051	20.5668	1500	10.2819	26.8425
1357	5.6688	12.2333	1405	7.2775	15.8215	1453	9.1274	20.5668	1501	11.1660	26.8425
1358	6.3472	12.2333	1406	8.0455	15.8215	1454	9.9721	20.5668	1502	12.0695	26.8425
1359	7.0520	12.2333	1407	8.8395	15.8215	1455	10.8413	20.5668	1503	12.9942	26.8425
1360	7.7859	12.2333	1408	9.6623	15.8215	1456	11.7376	20.5668	1504	13.9423	26.8425
1361	8.5516	12.2333	1409	10.5166	15.8215	1457	12.6637	20.5668	1505	14.9160	26.8425
1362	9.3525	12.2333	1410	11.4058	15.8215	1458	13.6224	20.5668	1506	15.9181	26.8425
1363	10.1920	12.2333	1411	12.3332	15.8215	1459	14.6172	20.5668	1507	16.9512	26.8425
1364	11.0739	12.2333	1412	13.3026	15.8215	1460	15.6515	20.5668	1508	18.0186	26.8425
1365	12.0026	12.2333	1413	14.3183	15.8215	1461	16.7294	20.5668	1509	19.1236	26.8425
1366	12.9828	12.2333	1414	15.3849	15.8215	1462	17.8551	20.5668	1510	20.2700	26.8425
1367	14.0194	12.2333	1415	16.5075	15.8215	1463	19.0336	20.5668	1511	0.0000	30.7028
1368	15.1183	12.2333	1416	17.6917	15.8215	1464	20.2700	20.5668	1512	0.9917	30.7028
1369	16.2856	12.2333	1417	18.9436	15.8215	1465	0.0000	23.4857	1513	1.9324	30.7028
1370	17.5282	12.2333	1418	20.2700	15.8215	1466	1.0268	23.4857	1514	2.8325	30.7028
1371	18.8536	12.2333	1419	0.0000	18.0286	1467	1.9773	23.4857	1515	3.6999	30.7028
1372	20.2700	12.2333	1420	1.0620	18.0286	1468	2.8667	23.4857	1516	4.5413	30.7028
1373	0.0000	13.9022	1421	2.0222	18.0286	1469	3.7072	23.4857	1517	5.3618	30.7028
1374	1.0972	13.9022	1422	2.9009	18.0286	1470	4.5085	23.4857	1518	6.1656	30.7028
1375	2.0670	13.9022	1423	3.7144	18.0286	1471	5.2786	23.4857	1519	6.9987	30.7028
1376	2.9351	13.9022	1424	4.4758	18.0286	1472	6.0237	23.4857	1520	7.8413	30.7028
1377	3.7216	13.9022	1425	5.1954	18.0286	1473	6.8125	23.4857	1521	8.6944	30.7028
1378	4.4430	13.9022	1426	5.8817	18.0286	1474	7.6158	23.4857	1522	9.5592	30.7028
1379	5.1122	13.9022	1427	6.6264	18.0286	1475	8.4348	23.4857	1523	10.4368	30.7028
1380	5.7398	13.9022	1428	7.3903	18.0286	1476	9.2713	23.4857	1524	11.3284	30.7028
1381	6.4403	13.9022	1429	8.1753	18.0286	1477	10.1270	23.4857	1525	12.2354	30.7028
1382	7.1648	13.9022	1430	8.9834	18.0286	1478	11.0037	23.4857	1526	13.1594	30.7028
1383	7.9157	13.9022	1431	9.8172	18.0286	1479	11.9036	23.4857	1527	14.1022	30.7028
1384	8.6956	13.9022	1432	10.6790	18.0286	1480	12.8289	23.4857	1528	15.0655	30.7028

Table D-2. Mesh Coordinates (continued)

Node No.	X	Y	Node No.	X	Y	Node No.	X	Y	Node No.	X	Y
1529	16.0514	30.7028	1577	18.2638	40.2473	1625	20.2700	52.8700	1673	1.1025	-4.8586
1530	17.0622	30.7028	1578	19.2586	40.2473	1626	0.0000	-6.3900	1674	1.4700	-4.8586
1531	18.1003	30.7028	1579	20.2700	40.2473	1627	0.3675	-6.3900	1675	1.8375	-4.8586
1532	19.1686	30.7028	1580	0.0000	46.1183	1628	0.7350	-6.3900	1676	2.2050	-4.8586
1533	20.2700	30.7028	1581	0.9389	46.1183	1629	1.1025	-6.3900	1677	2.5725	-4.8586
1534	0.0000	35.1421	1582	1.8652	46.1183	1630	1.4700	-6.3900	1678	2.9400	-4.8586
1535	0.9741	35.1421	1583	2.7812	46.1183	1631	1.8375	-6.3900	1679	3.3075	-4.8586
1536	1.9100	35.1421	1584	3.6891	46.1183	1632	2.2050	-6.3900	1680	3.6750	-4.8586
1537	2.8154	35.1421	1585	4.5904	46.1183	1633	2.5725	-6.3900	1681	0.0000	-4.4757
1538	3.6963	35.1421	1586	5.4866	46.1183	1634	2.9400	-6.3900	1682	0.3675	-4.4757
1539	4.5577	35.1421	1587	6.3786	46.1183	1635	3.3075	-6.3900	1683	0.7350	-4.4757
1540	5.4034	35.1421	1588	7.2778	46.1183	1636	3.6750	-6.3900	1684	1.1025	-4.4757
1541	6.2366	35.1421	1589	8.1795	46.1183	1637	0.0000	-6.0071	1685	1.4700	-4.4757
1542	7.0917	35.1421	1590	9.0838	46.1183	1638	0.3675	-6.0071	1686	1.8375	-4.4757
1543	7.9540	35.1421	1591	9.9911	46.1183	1639	0.7350	-6.0071	1687	2.2050	-4.4757
1544	8.8242	35.1421	1592	10.9015	46.1183	1640	1.1025	-6.0071	1688	2.5725	-4.4757
1545	9.7032	35.1421	1593	11.8154	46.1183	1641	1.4700	-6.0071	1689	2.9400	-4.4757
1546	10.5917	35.1421	1594	12.7332	46.1183	1642	1.8375	-6.0071	1690	3.3075	-4.4757
1547	11.4907	35.1421	1595	13.6552	46.1183	1643	2.2050	-6.0071	1691	3.6750	-4.4757
1548	12.4013	35.1421	1596	14.5819	46.1183	1644	2.5725	-6.0071	1692	0.0000	-4.0929
1549	13.3247	35.1421	1597	15.5138	46.1183	1645	2.9400	-6.0071	1693	0.3675	-4.0929
1550	14.2621	35.1421	1598	16.4513	46.1183	1646	3.3075	-6.0071	1694	0.7350	-4.0929
1551	15.2149	35.1421	1599	17.3950	46.1183	1647	3.6750	-6.0071	1695	1.1025	-4.0929
1552	16.1847	35.1421	1600	18.3455	46.1183	1648	0.0000	-5.6243	1696	1.4700	-4.0929
1553	17.1731	35.1421	1601	19.3036	46.1183	1649	0.3675	-5.6243	1697	1.8375	-4.0929
1554	18.1821	35.1421	1602	20.2700	46.1183	1650	0.7350	-5.6243	1698	2.2050	-4.0929
1555	19.2136	35.1421	1603	0.0000	52.8700	1651	1.1025	-5.6243	1699	2.5725	-4.0929
1556	20.2700	35.1421	1604	0.9214	52.8700	1652	1.4700	-5.6243	1700	2.9400	-4.0929
1557	0.0000	40.2473	1605	1.8427	52.8700	1653	1.8375	-5.6243	1701	3.3075	-4.0929
1558	0.9565	40.2473	1606	2.7641	52.8700	1654	2.2050	-5.6243	1702	3.6750	-4.0929
1559	1.8876	40.2473	1607	3.6855	52.8700	1655	2.5725	-5.6243	1703	0.0000	-3.7100
1560	2.7983	40.2473	1608	4.6068	52.8700	1656	2.9400	-5.6243	1704	0.3675	-3.7100
1561	3.6927	40.2473	1609	5.5282	52.8700	1657	3.3075	-5.6243	1705	0.7350	-3.7100
1562	4.5741	40.2473	1610	6.4495	52.8700	1658	3.6750	-5.6243	1706	1.1025	-3.7100
1563	5.4450	40.2473	1611	7.3709	52.8700	1659	0.0000	-5.2414	1707	1.4700	-3.7100
1564	6.3076	40.2473	1612	8.2923	52.8700	1660	0.3675	-5.2414	1708	1.8375	-3.7100
1565	7.1848	40.2473	1613	9.2136	52.8700	1661	0.7350	-5.2414	1709	2.2050	-3.7100
1566	8.0668	40.2473	1614	10.1350	52.8700	1662	1.1025	-5.2414	1710	2.5725	-3.7100
1567	8.9540	40.2473	1615	11.0564	52.8700	1663	1.4700	-5.2414	1711	2.9400	-3.7100
1568	9.8471	40.2473	1616	11.9777	52.8700	1664	1.8375	-5.2414	1712	3.3075	-3.7100
1569	10.7466	40.2473	1617	12.8991	52.8700	1665	2.2050	-5.2414	1713	3.6750	-3.7100
1570	11.6530	40.2473	1618	13.8205	52.8700	1666	2.5725	-5.2414	1714	0.0000	2.3100
1571	12.5672	40.2473	1619	14.7418	52.8700	1667	2.9400	-5.2414	1715	1.2730	2.3100
1572	13.4900	40.2473	1620	15.6632	52.8700	1668	3.3075	-5.2414	1716	2.2913	2.3100
1573	14.4220	40.2473	1621	16.5846	52.8700	1669	3.6750	-5.2414	1717	3.1060	2.3100
1574	15.3643	40.2473	1622	17.5059	52.8700	1670	0.0000	-4.8586	1718	3.7578	2.3100
1575	16.3180	40.2473	1623	18.4273	52.8700	1671	0.3675	-4.8586	1719	4.2792	2.3100
1576	17.2840	40.2473	1624	19.3486	52.8700	1672	0.7350	-4.8586	1720	4.6963	2.3100

Table D-2. Mesh Coordinates (continued)

Node			Node			Node			Node		
No.	X	Y									
1721	5.0300	2.3100	1743	4.6963	2.8000	1765	4.2792	3.2900	1787	3.7578	3.7800
1722	5.5097	2.3100	1744	5.0300	2.8000	1766	4.6963	3.2900	1788	4.2792	3.7800
1723	6.0373	2.3100	1745	5.5097	2.8000	1767	5.0300	3.2900	1789	4.6963	3.7800
1724	6.6177	2.3100	1746	6.0373	2.8000	1768	5.5097	3.2900	1790	5.0300	3.7800
1725	7.2561	2.3100	1747	6.6177	2.8000	1769	6.0373	3.2900	1791	5.5097	3.7800
1726	7.9584	2.3100	1748	7.2561	2.8000	1770	6.6177	3.2900	1792	6.0373	3.7800
1727	8.7309	2.3100	1749	7.9584	2.8000	1771	7.2561	3.2900	1793	6.6177	3.7800
1728	9.5806	2.3100	1750	8.7309	2.8000	1772	7.9584	3.2900	1794	7.2561	3.7800
1729	10.5153	2.3100	1751	9.5806	2.8000	1773	8.7309	3.2900	1795	7.9584	3.7800
1730	11.5435	2.3100	1752	10.5153	2.8000	1774	9.5806	3.2900	1796	8.7309	3.7800
1731	12.6746	2.3100	1753	11.5435	2.8000	1775	10.5153	3.2900	1797	9.5806	3.7800
1732	13.9187	2.3100	1754	12.6746	2.8000	1776	11.5435	3.2900	1798	10.5153	3.7800
1733	15.2872	2.3100	1755	13.9187	2.8000	1777	12.6746	3.2900	1799	11.5435	3.7800
1734	16.7926	2.3100	1756	15.2872	2.8000	1778	13.9187	3.2900	1800	12.6746	3.7800
1735	18.4485	2.3100	1757	16.7926	2.8000	1779	15.2872	3.2900	1801	13.9187	3.7800
1736	20.2700	2.3100	1758	18.4485	2.8000	1780	16.7926	3.2900	1802	15.2872	3.7800
1737	0.0000	2.8000	1759	20.2700	2.8000	1781	18.4485	3.2900	1803	16.7926	3.7800
1738	1.2730	2.8000	1760	0.0000	3.2900	1782	20.2700	3.2900	1804	18.4485	3.7800
1739	2.2913	2.8000	1761	1.2730	3.2900	1783	0.0000	3.7800	1805	20.2700	3.7800
1740	3.1060	2.8000	1762	2.2913	3.2900	1784	1.2730	3.7800			
1741	3.7578	2.8000	1763	3.1060	3.2900	1785	2.2913	3.7800			
1742	4.2792	2.8000	1764	3.7578	3.2900	1786	3.1060	3.7800			

Table D-3. Element Block 1 Description

1324 Elements, 4 Nodes per Element

Element No.	Connectivity			
1	1	2	25	24
2	2	3	26	25
3	3	4	27	26
4	4	5	28	27
5	5	6	29	28
6	6	7	30	29
7	7	8	31	30
8	8	9	32	31
9	9	10	33	32
10	10	11	34	33
11	11	12	35	34
12	12	13	36	35
13	13	14	37	36
14	14	15	38	37
15	15	16	39	38
16	16	17	40	39
17	17	18	41	40
18	18	19	42	41
19	19	20	43	42
20	20	21	44	43
21	21	22	45	44
22	22	23	46	45
23	24	25	48	47
24	25	26	49	48
25	26	27	50	49
26	27	28	51	50
27	28	29	52	51
28	29	30	53	52
29	30	31	54	53
30	31	32	55	54
31	32	33	56	55
32	33	34	57	56
33	34	35	58	57
34	35	36	59	58
35	36	37	60	59
36	37	38	61	60
37	38	39	62	61
38	39	40	63	62
39	40	41	64	63
40	41	42	65	64
41	42	43	66	65
42	43	44	67	66
43	44	45	68	67
44	45	46	69	68
45	47	48	71	70
46	48	49	72	71
47	49	50	73	72
48	50	51	74	73

Element No.	Connectivity			
49	51	52	75	74
50	52	53	76	75
51	53	54	77	76
52	54	55	78	77
53	55	56	79	78
54	56	57	80	79
55	57	58	81	80
56	58	59	82	81
57	59	60	83	82
58	60	61	84	83
59	61	62	85	84
60	62	63	86	85
61	63	64	87	86
62	64	65	88	87
63	65	66	89	88
64	66	67	90	89
65	67	68	91	90
66	68	69	92	91
67	70	71	94	93
68	71	72	95	94
69	72	73	96	95
70	73	74	97	96
71	74	75	98	97
72	75	76	99	98
73	76	77	100	99
74	77	78	101	100
75	78	79	102	101
76	79	80	103	102
77	80	81	104	103
78	81	82	105	104
79	82	83	106	105
80	83	84	107	106
81	84	85	108	107
82	85	86	109	108
83	86	87	110	109
84	87	88	111	110
85	88	89	112	111
86	89	90	113	112
87	90	91	114	113
88	91	92	115	114
89	93	94	117	116
90	94	95	118	117
91	95	96	119	118
92	96	97	120	119
93	97	98	121	120
94	98	99	122	121
95	99	100	123	122
96	100	101	124	123

Element No.	Connectivity			
97	101	102	125	124
98	102	103	126	125
99	103	104	127	126
100	104	105	128	127
101	105	106	129	128
102	106	107	130	129
103	107	108	131	130
104	108	109	132	131
105	109	110	133	132
106	110	111	134	133
107	111	112	135	134
108	112	113	136	135
109	113	114	137	136
110	114	115	138	137
111	116	117	140	139
112	117	118	141	140
113	118	119	142	141
114	119	120	143	142
115	120	121	144	143
116	121	122	145	144
117	122	123	146	145
118	123	124	147	146
119	124	125	148	147
120	125	126	149	148
121	126	127	150	149
122	127	128	151	150
123	128	129	152	151
124	129	130	153	152
125	130	131	154	153
126	131	132	155	154
127	132	133	156	155
128	133	134	157	156
129	134	135	158	157
130	135	136	159	158
131	136	137	160	159
132	137	138	161	160
133	139	140	163	162
134	140	141	164	163
135	141	142	165	164
136	142	143	166	165
137	143	144	167	166
138	144	145	168	167
139	145	146	169	168
140	146	147	170	169
141	147	148	171	170
142	148	149	172	171
143	149	150	173	172
144	150	151	174	173

Table D-3. Element Block 1 Description (continued)

Element No.	Connectivity				
145	151	152	175	174	
146	152	153	176	175	
147	153	154	177	176	
148	154	155	178	177	
149	155	156	179	178	
150	156	157	180	179	
151	157	158	181	180	
152	158	159	182	181	
153	159	160	183	182	
154	160	161	184	183	
155	162	163	186	185	
156	163	164	187	186	
157	164	165	188	187	
158	165	166	189	188	
159	166	167	190	189	
160	167	168	191	190	
161	168	169	192	191	
162	169	170	193	192	
163	170	171	194	193	
164	171	172	195	194	
165	172	173	196	195	
166	173	174	197	196	
167	174	175	198	197	
168	175	176	199	198	
169	176	177	200	199	
170	177	178	201	200	
171	178	179	202	201	
172	179	180	203	202	
173	180	181	204	203	
174	181	182	205	204	
175	182	183	206	205	
176	183	184	207	206	
177	185	186	209	208	
178	186	187	210	209	
179	187	188	211	210	
180	188	189	212	211	
181	189	190	213	212	
182	190	191	214	213	
183	191	192	215	214	
184	192	193	216	215	
185	193	194	217	216	
186	194	195	218	217	
187	195	196	219	218	
188	196	197	220	219	
189	197	198	221	220	
190	198	199	222	221	
191	199	200	223	222	
192	200	201	224	223	

Element No.	Connectivity				
193	201	202	225	224	
194	202	203	226	225	
195	203	204	227	226	
196	204	205	228	227	
197	205	206	229	228	
198	206	207	230	229	
199	208	209	232	231	
200	209	210	233	232	
201	210	211	234	233	
202	211	212	235	234	
203	212	213	236	235	
204	213	214	237	236	
205	214	215	238	237	
206	215	216	239	238	
207	216	217	240	239	
208	217	218	241	240	
209	218	219	242	241	
210	219	220	243	242	
211	220	221	244	243	
212	221	222	245	244	
213	222	223	246	245	
214	223	224	247	246	
215	224	225	248	247	
216	225	226	249	248	
217	226	227	250	249	
218	227	228	251	250	
219	228	229	252	251	
220	229	230	253	252	
221	231	232	255	254	
222	232	233	256	255	
223	233	234	257	256	
224	234	235	258	257	
225	235	236	259	258	
226	236	237	260	259	
227	237	238	261	260	
228	238	239	262	261	
229	239	240	263	262	
230	240	241	264	263	
231	241	242	265	264	
232	242	243	266	265	
233	243	244	267	266	
234	244	245	268	267	
235	245	246	269	268	
236	246	247	270	269	
237	247	248	271	270	
238	248	249	272	271	
239	249	250	273	272	
240	250	251	274	273	

Element No.	Connectivity				
241	251	252	275	274	
242	252	253	276	275	
243	254	255	278	277	
244	255	256	279	278	
245	256	257	280	279	
246	257	258	281	280	
247	258	259	282	281	
248	259	260	283	282	
249	260	261	284	283	
250	261	262	285	284	
251	262	263	286	285	
252	263	264	287	286	
253	264	265	288	287	
254	265	266	289	288	
255	266	267	290	289	
256	267	268	291	290	
257	268	269	292	291	
258	269	270	293	292	
259	270	271	294	293	
260	271	272	295	294	
261	272	273	296	295	
262	273	274	297	296	
263	274	275	298	297	
264	275	276	299	298	
265	277	278	301	300	
266	278	279	302	301	
267	279	280	303	302	
268	280	281	304	303	
269	281	282	305	304	
270	282	283	306	305	
271	283	284	307	306	
272	284	285	308	307	
273	285	286	309	308	
274	286	287	310	309	
275	287	288	311	310	
276	288	289	312	311	
277	289	290	313	312	
278	290	291	314	313	
279	291	292	315	314	
280	292	293	316	315	
281	293	294	317	316	
282	294	295	318	317	
283	295	296	319	318	
284	296	297	320	319	
285	297	298	321	320	
286	298	299	322	321	
287	300	301	324	323	

Table D-3. Element Block 1 Description (continued)

Element No.	Connectivity			
288	301	302	325	324
289	302	303	326	325
290	303	304	327	326
291	304	305	328	327
292	305	306	329	328
293	306	307	330	329
294	307	308	331	330
295	308	309	332	331
296	309	310	333	332
297	310	311	334	333
298	311	312	335	334
299	312	313	336	335
300	313	314	337	336
301	314	315	338	337
302	315	316	339	338
303	316	317	340	339
304	317	318	341	340
305	318	319	342	341
306	319	320	343	342
307	320	321	344	343
308	321	322	345	344
309	323	324	347	346
310	324	325	348	347
311	325	326	349	348
312	326	327	350	349
313	327	328	351	350
314	328	329	352	351
315	329	330	353	352
316	330	331	354	353
317	331	332	355	354
318	332	333	356	355
319	333	334	357	356
320	334	335	358	357
321	335	336	359	358
322	336	337	360	359
323	337	338	361	360
324	338	339	362	361
325	339	340	363	362
326	340	341	364	363
327	341	342	365	364
328	342	343	366	365
329	343	344	367	366
330	344	345	368	367
331	346	347	370	369
332	347	348	371	370
333	348	349	372	371
334	349	350	373	372
335	350	351	374	373

Element No.	Connectivity			
336	351	352	375	374
337	352	353	376	375
338	353	354	377	376
339	354	355	378	377
340	355	356	379	378
341	356	357	380	379
342	357	358	381	380
343	358	359	382	381
344	359	360	383	382
345	360	361	384	383
346	361	362	385	384
347	362	363	386	385
348	363	364	387	386
349	364	365	388	387
350	365	366	389	388
351	366	367	390	389
352	367	368	391	390
353	369	370	393	392
354	370	371	394	393
355	371	372	395	394
356	372	373	396	395
357	373	374	397	396
358	374	375	398	397
359	375	376	399	398
360	376	377	400	399
361	377	378	401	400
362	378	379	402	401
363	379	380	403	402
364	380	381	404	403
365	381	382	405	404
366	382	383	406	405
367	383	384	407	406
368	384	385	408	407
369	385	386	409	408
370	386	387	410	409
371	387	388	411	410
372	388	389	412	411
373	389	390	413	412
374	390	391	414	413
375	392	393	416	415
376	393	394	417	416
377	394	395	418	417
378	395	396	419	418
379	396	397	420	419
380	397	398	421	420
381	398	399	422	421
382	399	400	423	422
383	400	401	424	423

Element No.	Connectivity			
384	401	402	425	424
385	402	403	426	425
386	403	404	427	426
387	404	405	428	427
388	405	406	429	428
389	406	407	430	429
390	407	408	431	430
391	408	409	432	431
392	409	410	433	432
393	410	411	434	433
394	411	412	435	434
395	412	413	436	435
396	413	414	437	436
397	415	416	439	438
398	416	417	440	439
399	417	418	441	440
400	418	419	442	441
401	419	420	443	442
402	420	421	444	443
403	421	422	445	444
404	422	423	446	445
405	423	424	447	446
406	424	425	448	447
407	425	426	449	448
408	426	427	450	449
409	427	428	451	450
410	428	429	452	451
411	429	430	453	452
412	430	431	454	453
413	431	432	455	454
414	432	433	456	455
415	433	434	457	456
416	434	435	458	457
417	435	436	459	458
418	436	437	460	459
419	438	439	462	461
420	439	440	463	462
421	440	441	464	463
422	441	442	465	464
423	442	443	466	465
424	443	444	467	466
425	444	445	468	467
426	445	446	469	468
427	446	447	470	469
428	447	448	471	470
429	448	449	472	471
430	449	450	473	472
431	450	451	474	473

Table D-3. Element Block 1 Description (continued)

Element No.	Connectivity				Element No.	Connectivity				Element No.	Connectivity			
432	451	452	475	474	481	594	595	618	617	530	646	647	670	669
433	452	453	476	475	482	595	596	619	618	531	647	648	671	670
434	453	454	477	476	483	596	597	620	619	532	648	649	672	671
435	454	455	478	477	484	597	598	621	620	533	649	650	673	672
436	455	456	479	478	485	599	600	623	622	534	650	651	674	673
437	456	457	480	479	486	600	601	624	623	535	651	652	675	674
438	457	458	481	480	487	601	602	625	624	536	652	653	676	675
439	458	459	482	481	488	602	603	626	625	537	653	654	677	676
440	459	460	483	482	489	603	604	627	626	538	654	655	678	677
441	553	554	577	576	490	604	605	628	627	539	655	656	679	678
442	554	555	578	577	491	605	606	629	628	540	656	657	680	679
443	555	556	579	578	492	606	607	630	629	541	657	658	681	680
444	556	557	580	579	493	607	608	631	630	542	658	659	682	681
445	557	558	581	580	494	608	609	632	631	543	659	660	683	682
446	558	559	582	581	495	609	610	633	632	544	660	661	684	683
447	559	560	583	582	496	610	611	634	633	545	661	662	685	684
448	560	561	584	583	497	611	612	635	634	546	662	663	686	685
449	561	562	585	584	498	612	613	636	635	547	663	664	687	686
450	562	563	586	585	499	613	614	637	636	548	664	665	688	687
451	563	564	587	586	500	614	615	638	637	549	665	666	689	688
452	564	565	588	587	501	615	616	639	638	550	666	667	690	689
453	565	566	589	588	502	616	617	640	639	551	675	676	692	691
454	566	567	590	589	503	617	618	641	640	552	676	677	693	692
455	567	568	591	590	504	618	619	642	641	553	677	678	694	693
456	568	569	592	591	505	619	620	643	642	554	678	679	695	694
457	569	570	593	592	506	620	621	644	643	555	679	680	696	695
458	570	571	594	593	507	622	623	646	645	556	680	681	697	696
459	571	572	595	594	508	623	624	647	646	557	681	682	698	697
460	572	573	596	595	509	624	625	648	647	558	682	683	699	698
461	573	574	597	596	510	625	626	649	648	559	683	684	700	699
462	574	575	598	597	511	626	627	650	649	560	684	685	701	700
463	576	577	600	599	512	627	628	651	650	561	685	686	702	701
464	577	578	601	600	513	628	629	652	651	562	686	687	703	702
465	578	579	602	601	514	629	630	653	652	563	687	688	704	703
466	579	580	603	602	515	630	631	654	653	564	688	689	705	704
467	580	581	604	603	516	631	632	655	654	565	689	690	706	705
468	581	582	605	604	517	632	633	656	655	566	691	692	708	707
469	582	583	606	605	518	633	634	657	656	567	692	693	709	708
470	583	584	607	606	519	634	635	658	657	568	693	694	710	709
471	584	585	608	607	520	635	636	659	658	569	694	695	711	710
472	585	586	609	608	521	636	637	660	659	570	695	696	712	711
473	586	587	610	609	522	637	638	661	660	571	696	697	713	712
474	587	588	611	610	523	638	639	662	661	572	697	698	714	713
475	588	589	612	611	524	639	640	663	662	573	698	699	715	714
476	589	590	613	612	525	640	641	664	663	574	699	700	716	715
477	590	591	614	613	526	641	642	665	664	575	700	701	717	716
478	591	592	615	614	527	642	643	666	665	576	701	702	718	717
479	592	593	616	615	528	643	644	667	666	577	702	703	719	718
480	593	594	617	616	529	645	646	669	668	578	703	704	720	719

Table D-3. Element Block 1 Description (continued)

Element No.	Connectivity			
579	704	705	721	720
580	705	706	722	721
581	707	708	724	723
582	708	709	725	724
583	709	710	726	725
584	710	711	727	726
585	711	712	728	727
586	712	713	729	728
587	713	714	730	729
588	714	715	731	730
589	715	716	732	731
590	716	717	733	732
591	717	718	734	733
592	718	719	735	734
593	719	720	736	735
594	720	721	737	736
595	721	722	738	737
596	723	724	740	739
597	724	725	741	740
598	725	726	742	741
599	726	727	743	742
600	727	728	744	743
601	728	729	745	744
602	729	730	746	745
603	730	731	747	746
604	731	732	748	747
605	732	733	749	748
606	733	734	750	749
607	734	735	751	750
608	735	736	752	751
609	736	737	753	752
610	737	738	754	753
611	739	740	756	755
612	740	741	757	756
613	741	742	758	757
614	742	743	759	758
615	743	744	760	759
616	744	745	761	760
617	745	746	762	761
618	746	747	763	762
619	747	748	764	763
620	748	749	765	764
621	749	750	766	765
622	750	751	767	766
623	751	752	768	767
624	752	753	769	768
625	753	754	770	769
626	755	756	772	771
627	756	757	773	772

Element No.	Connectivity			
628	757	758	774	773
629	758	759	775	774
630	759	760	776	775
631	760	761	777	776
632	761	762	778	777
633	762	763	779	778
634	763	764	780	779
635	764	765	781	780
636	765	766	782	781
637	766	767	783	782
638	767	768	784	783
639	768	769	785	784
640	769	770	786	785
641	771	772	788	787
642	772	773	789	788
643	773	774	790	789
644	774	775	791	790
645	775	776	792	791
646	776	777	793	792
647	777	778	794	793
648	778	779	795	794
649	779	780	796	795
650	780	781	797	796
651	781	782	798	797
652	782	783	799	798
653	783	784	800	799
654	784	785	801	800
655	785	786	802	801
656	787	788	804	803
657	788	789	805	804
658	789	790	806	805
659	790	791	807	806
660	791	792	808	807
661	792	793	809	808
662	793	794	810	809
663	794	795	811	810
664	795	796	812	811
665	796	797	813	812
666	797	798	814	813
667	798	799	815	814
668	799	800	816	815
669	800	801	817	816
670	801	802	818	817
671	803	804	820	819
672	804	805	821	820
673	805	806	822	821
674	806	807	823	822
675	807	808	824	823
676	808	809	825	824

Element No.	Connectivity			
677	809	810	826	825
678	810	811	827	826
679	811	812	828	827
680	812	813	829	828
681	813	814	830	829
682	814	815	831	830
683	815	816	832	831
684	816	817	833	832
685	817	818	834	833
686	819	820	836	835
687	820	821	837	836
688	821	822	838	837
689	822	823	839	838
690	823	824	840	839
691	824	825	841	840
692	825	826	842	841
693	826	827	843	842
694	827	828	844	843
695	828	829	845	844
696	829	830	846	845
697	830	831	847	846
698	831	832	848	847
699	832	833	849	848
700	833	834	850	849
701	835	836	852	851
702	836	837	853	852
703	837	838	854	853
704	838	839	855	854
705	839	840	856	855
706	840	841	857	856
707	841	842	858	857
708	842	843	859	858
709	843	844	860	859
710	844	845	861	860
711	845	846	862	861
712	846	847	863	862
713	847	848	864	863
714	848	849	865	864
715	849	850	866	865
716	851	852	868	867
717	852	853	869	868
718	853	854	870	869
719	854	855	871	870
720	855	856	872	871
721	856	857	873	872
722	857	858	874	873
723	858	859	875	874
724	859	860	876	875
725	860	861	877	876

Table D-3. Element Block 1 Description (continued)

Element No.	Connectivity			
726	861	862	878	877
727	862	863	879	878
728	863	864	880	879
729	864	865	881	880
730	865	866	882	881
731	883	884	891	890
732	884	885	892	891
733	885	886	893	892
734	886	887	894	893
735	887	888	895	894
736	888	889	896	895
737	889	867	897	896
738	867	868	898	897
739	868	869	899	898
740	869	870	900	899
741	870	871	901	900
742	871	872	902	901
743	872	873	903	902
744	873	874	904	903
745	874	875	905	904
746	875	876	906	905
747	876	877	907	906
748	877	878	908	907
749	878	879	909	908
750	879	880	910	909
751	880	881	911	910
752	881	882	912	911
753	890	891	914	913
754	891	892	915	914
755	892	893	916	915
756	893	894	917	916
757	894	895	918	917
758	895	896	919	918
759	896	897	920	919
760	897	898	921	920
761	898	899	922	921
762	899	900	923	922
763	900	901	924	923
764	901	902	925	924
765	902	903	926	925
766	903	904	927	926
767	904	905	928	927
768	905	906	929	928
769	906	907	930	929
770	907	908	931	930
771	908	909	932	931
772	909	910	933	932
773	910	911	934	933
774	911	912	935	934

Element No.	Connectivity			
775	913	914	937	936
776	914	915	938	937
777	915	916	939	938
778	916	917	940	939
779	917	918	941	940
780	918	919	942	941
781	919	920	943	942
782	920	921	944	943
783	921	922	945	944
784	922	923	946	945
785	923	924	947	946
786	924	925	948	947
787	925	926	949	948
788	926	927	950	949
789	927	928	951	950
790	928	929	952	951
791	929	930	953	952
792	930	931	954	953
793	931	932	955	954
794	932	933	956	955
795	933	934	957	956
796	934	935	958	957
797	936	937	960	959
798	937	938	961	960
799	938	939	962	961
800	939	940	963	962
801	940	941	964	963
802	941	942	965	964
803	942	943	966	965
804	943	944	967	966
805	944	945	968	967
806	945	946	969	968
807	946	947	970	969
808	947	948	971	970
809	948	949	972	971
810	949	950	973	972
811	950	951	974	973
812	951	952	975	974
813	952	953	976	975
814	953	954	977	976
815	954	955	978	977
816	955	956	979	978
817	956	957	980	979
818	957	958	981	980
819	959	960	983	982
820	960	961	984	983
821	961	962	985	984
822	962	963	986	985
823	963	964	987	986

Element No.	Connectivity			
824	964	965	988	987
825	965	966	989	988
826	966	967	990	989
827	967	968	991	990
828	968	969	992	991
829	969	970	993	992
830	970	971	994	993
831	971	972	995	994
832	972	973	996	995
833	973	974	997	996
834	974	975	998	997
835	975	976	999	998
836	976	977	1000	999
837	977	978	1001	1000
838	978	979	1002	1001
839	979	980	1003	1002
840	980	981	1004	1003
841	982	983	1006	1005
842	983	984	1007	1006
843	984	985	1008	1007
844	985	986	1009	1008
845	986	987	1010	1009
846	987	988	1011	1010
847	988	989	1012	1011
848	989	990	1013	1012
849	990	991	1014	1013
850	991	992	1015	1014
851	992	993	1016	1015
852	993	994	1017	1016
853	994	995	1018	1017
854	995	996	1019	1018
855	996	997	1020	1019
856	997	998	1021	1020
857	998	999	1022	1021
858	999	1000	1023	1022
859	1000	1001	1024	1023
860	1001	1002	1025	1024
861	1002	1003	1026	1025
862	1003	1004	1027	1026
863	1005	1006	1029	1028
864	1006	1007	1030	1029
865	1007	1008	1031	1030
866	1008	1009	1032	1031
867	1009	1010	1033	1032
868	1010	1011	1034	1033
869	1011	1012	1035	1034
870	1012	1013	1036	1035
871	1013	1014	1037	1036
872	1014	1015	1038	1037

Table D-3. Element Block 1 Description (continued)

Element No.	Connectivity				Element No.	Connectivity				Element No.	Connectivity			
873	1015	1016	1039	1038	922	1181	1182	1205	1204	971	1232	1233	1256	1255
874	1016	1017	1040	1039	923	1182	1183	1206	1205	972	1233	1234	1257	1256
875	1017	1018	1041	1040	924	1183	1184	1207	1206	973	1235	1236	1259	1258
876	1018	1019	1042	1041	925	1184	1185	1208	1207	974	1236	1237	1260	1259
877	1019	1020	1043	1042	926	1185	1186	1209	1208	975	1237	1238	1261	1260
878	1020	1021	1044	1043	927	1186	1187	1210	1209	976	1238	1239	1262	1261
879	1021	1022	1045	1044	928	1187	1188	1211	1210	977	1239	1240	1263	1262
880	1022	1023	1046	1045	929	1189	1190	1213	1212	978	1240	1241	1264	1263
881	1023	1024	1047	1046	930	1190	1191	1214	1213	979	1241	1242	1265	1264
882	1024	1025	1048	1047	931	1191	1192	1215	1214	980	1242	1243	1266	1265
883	1025	1026	1049	1048	932	1192	1193	1216	1215	981	1243	1244	1267	1266
884	1026	1027	1050	1049	933	1193	1194	1217	1216	982	1244	1245	1268	1267
885	1143	1144	1167	1166	934	1194	1195	1218	1217	983	1245	1246	1269	1268
886	1144	1145	1168	1167	935	1195	1196	1219	1218	984	1246	1247	1270	1269
887	1145	1146	1169	1168	936	1196	1197	1220	1219	985	1247	1248	1271	1270
888	1146	1147	1170	1169	937	1197	1198	1221	1220	986	1248	1249	1272	1271
889	1147	1148	1171	1170	938	1198	1199	1222	1221	987	1249	1250	1273	1272
890	1148	1149	1172	1171	939	1199	1200	1223	1222	988	1250	1251	1274	1273
891	1149	1150	1173	1172	940	1200	1201	1224	1223	989	1251	1252	1275	1274
892	1150	1151	1174	1173	941	1201	1202	1225	1224	990	1252	1253	1276	1275
893	1151	1152	1175	1174	942	1202	1203	1226	1225	991	1253	1254	1277	1276
894	1152	1153	1176	1175	943	1203	1204	1227	1226	992	1254	1255	1278	1277
895	1153	1154	1177	1176	944	1204	1205	1228	1227	993	1255	1256	1279	1278
896	1154	1155	1178	1177	945	1205	1206	1229	1228	994	1256	1257	1280	1279
897	1155	1156	1179	1178	946	1206	1207	1230	1229	995	1258	1259	1282	1281
898	1156	1157	1180	1179	947	1207	1208	1231	1230	996	1259	1260	1283	1282
899	1157	1158	1181	1180	948	1208	1209	1232	1231	997	1260	1261	1284	1283
900	1158	1159	1182	1181	949	1209	1210	1233	1232	998	1261	1262	1285	1284
901	1159	1160	1183	1182	950	1210	1211	1234	1233	999	1262	1263	1286	1285
902	1160	1161	1184	1183	951	1212	1213	1236	1235	1000	1263	1264	1287	1286
903	1161	1162	1185	1184	952	1213	1214	1237	1236	1001	1264	1265	1288	1287
904	1162	1163	1186	1185	953	1214	1215	1238	1237	1002	1265	1266	1289	1288
905	1163	1164	1187	1186	954	1215	1216	1239	1238	1003	1266	1267	1290	1289
906	1164	1165	1188	1187	955	1216	1217	1240	1239	1004	1267	1268	1291	1290
907	1166	1167	1190	1189	956	1217	1218	1241	1240	1005	1268	1269	1292	1291
908	1167	1168	1191	1190	957	1218	1219	1242	1241	1006	1269	1270	1293	1292
909	1168	1169	1192	1191	958	1219	1220	1243	1242	1007	1270	1271	1294	1293
910	1169	1170	1193	1192	959	1220	1221	1244	1243	1008	1271	1272	1295	1294
911	1170	1171	1194	1193	960	1221	1222	1245	1244	1009	1272	1273	1296	1295
912	1171	1172	1195	1194	961	1222	1223	1246	1245	1010	1273	1274	1297	1296
913	1172	1173	1196	1195	962	1223	1224	1247	1246	1011	1274	1275	1298	1297
914	1173	1174	1197	1196	963	1224	1225	1248	1247	1012	1275	1276	1299	1298
915	1174	1175	1198	1197	964	1225	1226	1249	1248	1013	1276	1277	1300	1299
916	1175	1176	1199	1198	965	1226	1227	1250	1249	1014	1277	1278	1301	1300
917	1176	1177	1200	1199	966	1227	1228	1251	1250	1015	1278	1279	1302	1301
918	1177	1178	1201	1200	967	1228	1229	1252	1251	1016	1279	1280	1303	1302
919	1178	1179	1202	1201	968	1229	1230	1253	1252	1017	1281	1282	1305	1304
920	1179	1180	1203	1202	969	1230	1231	1254	1253	1018	1282	1283	1306	1305
921	1180	1181	1204	1203	970	1231	1232	1255	1254	1019	1283	1284	1307	1306

Table D-3. Element Block 1 Description (continued)

Element No.	Connectivity			
1020	1284	1285	1308	1307
1021	1285	1286	1309	1308
1022	1286	1287	1310	1309
1023	1287	1288	1311	1310
1024	1288	1289	1312	1311
1025	1289	1290	1313	1312
1026	1290	1291	1314	1313
1027	1291	1292	1315	1314
1028	1292	1293	1316	1315
1029	1293	1294	1317	1316
1030	1294	1295	1318	1317
1031	1295	1296	1319	1318
1032	1296	1297	1320	1319
1033	1297	1298	1321	1320
1034	1298	1299	1322	1321
1035	1299	1300	1323	1322
1036	1300	1301	1324	1323
1037	1301	1302	1325	1324
1038	1302	1303	1326	1325
1039	1304	1305	1328	1327
1040	1305	1306	1329	1328
1041	1306	1307	1330	1329
1042	1307	1308	1331	1330
1043	1308	1309	1332	1331
1044	1309	1310	1333	1332
1045	1310	1311	1334	1333
1046	1311	1312	1335	1334
1047	1312	1313	1336	1335
1048	1313	1314	1337	1336
1049	1314	1315	1338	1337
1050	1315	1316	1339	1338
1051	1316	1317	1340	1339
1052	1317	1318	1341	1340
1053	1318	1319	1342	1341
1054	1319	1320	1343	1342
1055	1320	1321	1344	1343
1056	1321	1322	1345	1344
1057	1322	1323	1346	1345
1058	1323	1324	1347	1346
1059	1324	1325	1348	1347
1060	1325	1326	1349	1348
1061	1327	1328	1351	1350
1062	1328	1329	1352	1351
1063	1329	1330	1353	1352
1064	1330	1331	1354	1353
1065	1331	1332	1355	1354
1066	1332	1333	1356	1355
1067	1333	1334	1357	1356
1068	1334	1335	1358	1357

Element No.	Connectivity			
1069	1335	1336	1359	1358
1070	1336	1337	1360	1359
1071	1337	1338	1361	1360
1072	1338	1339	1362	1361
1073	1339	1340	1363	1362
1074	1340	1341	1364	1363
1075	1341	1342	1365	1364
1076	1342	1343	1366	1365
1077	1343	1344	1367	1366
1078	1344	1345	1368	1367
1079	1345	1346	1369	1368
1080	1346	1347	1370	1369
1081	1347	1348	1371	1370
1082	1348	1349	1372	1371
1083	1350	1351	1374	1373
1084	1351	1352	1375	1374
1085	1352	1353	1376	1375
1086	1353	1354	1377	1376
1087	1354	1355	1378	1377
1088	1355	1356	1379	1378
1089	1356	1357	1380	1379
1090	1357	1358	1381	1380
1091	1358	1359	1382	1381
1092	1359	1360	1383	1382
1093	1360	1361	1384	1383
1094	1361	1362	1385	1384
1095	1362	1363	1386	1385
1096	1363	1364	1387	1386
1097	1364	1365	1388	1387
1098	1365	1366	1389	1388
1099	1366	1367	1390	1389
1100	1367	1368	1391	1390
1101	1368	1369	1392	1391
1102	1369	1370	1393	1392
1103	1370	1371	1394	1393
1104	1371	1372	1395	1394
1105	1373	1374	1397	1396
1106	1374	1375	1398	1397
1107	1375	1376	1399	1398
1108	1376	1377	1400	1399
1109	1377	1378	1401	1400
1110	1378	1379	1402	1401
1111	1379	1380	1403	1402
1112	1380	1381	1404	1403
1113	1381	1382	1405	1404
1114	1382	1383	1406	1405
1115	1383	1384	1407	1406
1116	1384	1385	1408	1407
1117	1385	1386	1409	1408

Element No.	Connectivity			
1118	1386	1387	1410	1409
1119	1387	1388	1411	1410
1120	1388	1389	1412	1411
1121	1389	1390	1413	1412
1122	1390	1391	1414	1413
1123	1391	1392	1415	1414
1124	1392	1393	1416	1415
1125	1393	1394	1417	1416
1126	1394	1395	1418	1417
1127	1396	1397	1420	1419
1128	1397	1398	1421	1420
1129	1398	1399	1422	1421
1130	1399	1400	1423	1422
1131	1400	1401	1424	1423
1132	1401	1402	1425	1424
1133	1402	1403	1426	1425
1134	1403	1404	1427	1426
1135	1404	1405	1428	1427
1136	1405	1406	1429	1428
1137	1406	1407	1430	1429
1138	1407	1408	1431	1430
1139	1408	1409	1432	1431
1140	1409	1410	1433	1432
1141	1410	1411	1434	1433
1142	1411	1412	1435	1434
1143	1412	1413	1436	1435
1144	1413	1414	1437	1436
1145	1414	1415	1438	1437
1146	1415	1416	1439	1438
1147	1416	1417	1440	1439
1148	1417	1418	1441	1440
1149	1419	1420	1443	1442
1150	1420	1421	1444	1443
1151	1421	1422	1445	1444
1152	1422	1423	1446	1445
1153	1423	1424	1447	1446
1154	1424	1425	1448	1447
1155	1425	1426	1449	1448
1156	1426	1427	1450	1449
1157	1427	1428	1451	1450
1158	1428	1429	1452	1451
1159	1429	1430	1453	1452
1160	1430	1431	1454	1453
1161	1431	1432	1455	1454
1162	1432	1433	1456	1455
1163	1433	1434	1457	1456
1164	1434	1435	1458	1457
1165	1435	1436	1459	1458
1166	1436	1437	1460	1459

Table D-3. Element Block 1 Description (continued)

Element No.	Connectivity				
1167	1437	1438	1461	1460	
1168	1438	1439	1462	1461	
1169	1439	1440	1463	1462	
1170	1440	1441	1464	1463	
1171	1442	1443	1466	1465	
1172	1443	1444	1467	1466	
1173	1444	1445	1468	1467	
1174	1445	1446	1469	1468	
1175	1446	1447	1470	1469	
1176	1447	1448	1471	1470	
1177	1448	1449	1472	1471	
1178	1449	1450	1473	1472	
1179	1450	1451	1474	1473	
1180	1451	1452	1475	1474	
1181	1452	1453	1476	1475	
1182	1453	1454	1477	1476	
1183	1454	1455	1478	1477	
1184	1455	1456	1479	1478	
1185	1456	1457	1480	1479	
1186	1457	1458	1481	1480	
1187	1458	1459	1482	1481	
1188	1459	1460	1483	1482	
1189	1460	1461	1484	1483	
1190	1461	1462	1485	1484	
1191	1462	1463	1486	1485	
1192	1463	1464	1487	1486	
1193	1465	1466	1489	1488	
1194	1466	1467	1490	1489	
1195	1467	1468	1491	1490	
1196	1468	1469	1492	1491	
1197	1469	1470	1493	1492	
1198	1470	1471	1494	1493	
1199	1471	1472	1495	1494	
1200	1472	1473	1496	1495	
1201	1473	1474	1497	1496	
1202	1474	1475	1498	1497	
1203	1475	1476	1499	1498	
1204	1476	1477	1500	1499	
1205	1477	1478	1501	1500	
1206	1478	1479	1502	1501	
1207	1479	1480	1503	1502	
1208	1480	1481	1504	1503	
1209	1481	1482	1505	1504	
1210	1482	1483	1506	1505	
1211	1483	1484	1507	1506	
1212	1484	1485	1508	1507	
1213	1485	1486	1509	1508	
1214	1486	1487	1510	1509	
1215	1488	1489	1512	1511	

Element No.	Connectivity				
1216	1489	1490	1513	1512	
1217	1490	1491	1514	1513	
1218	1491	1492	1515	1514	
1219	1492	1493	1516	1515	
1220	1493	1494	1517	1516	
1221	1494	1495	1518	1517	
1222	1495	1496	1519	1518	
1223	1496	1497	1520	1519	
1224	1497	1498	1521	1520	
1225	1498	1499	1522	1521	
1226	1499	1500	1523	1522	
1227	1500	1501	1524	1523	
1228	1501	1502	1525	1524	
1229	1502	1503	1526	1525	
1230	1503	1504	1527	1526	
1231	1504	1505	1528	1527	
1232	1505	1506	1529	1528	
1233	1506	1507	1530	1529	
1234	1507	1508	1531	1530	
1235	1508	1509	1532	1531	
1236	1509	1510	1533	1532	
1237	1511	1512	1535	1534	
1238	1512	1513	1536	1535	
1239	1513	1514	1537	1536	
1240	1514	1515	1538	1537	
1241	1515	1516	1539	1538	
1242	1516	1517	1540	1539	
1243	1517	1518	1541	1540	
1244	1518	1519	1542	1541	
1245	1519	1520	1543	1542	
1246	1520	1521	1544	1543	
1247	1521	1522	1545	1544	
1248	1522	1523	1546	1545	
1249	1523	1524	1547	1546	
1250	1524	1525	1548	1547	
1251	1525	1526	1549	1548	
1252	1526	1527	1550	1549	
1253	1527	1528	1551	1550	
1254	1528	1529	1552	1551	
1255	1529	1530	1553	1552	
1256	1530	1531	1554	1553	
1257	1531	1532	1555	1554	
1258	1532	1533	1556	1555	
1259	1534	1535	1558	1557	
1260	1535	1536	1559	1558	
1261	1536	1537	1560	1559	
1262	1537	1538	1561	1560	
1263	1538	1539	1562	1561	
1264	1539	1540	1563	1562	

Element No.	Connectivity				
1265	1540	1541	1564	1563	
1266	1541	1542	1565	1564	
1267	1542	1543	1566	1565	
1268	1543	1544	1567	1566	
1269	1544	1545	1568	1567	
1270	1545	1546	1569	1568	
1271	1546	1547	1570	1569	
1272	1547	1548	1571	1570	
1273	1548	1549	1572	1571	
1274	1549	1550	1573	1572	
1275	1550	1551	1574	1573	
1276	1551	1552	1575	1574	
1277	1552	1553	1576	1575	
1278	1553	1554	1577	1576	
1279	1554	1555	1578	1577	
1280	1555	1556	1579	1578	
1281	1557	1558	1581	1580	
1282	1558	1559	1582	1581	
1283	1559	1560	1583	1582	
1284	1560	1561	1584	1583	
1285	1561	1562	1585	1584	
1286	1562	1563	1586	1585	
1287	1563	1564	1587	1586	
1288	1564	1565	1588	1587	
1289	1565	1566	1589	1588	
1290	1566	1567	1590	1589	
1291	1567	1568	1591	1590	
1292	1568	1569	1592	1591	
1293	1569	1570	1593	1592	
1294	1570	1571	1594	1593	
1295	1571	1572	1595	1594	
1296	1572	1573	1596	1595	
1297	1573	1574	1597	1596	
1298	1574	1575	1598	1597	
1299	1575	1576	1599	1598	
1300	1576	1577	1600	1599	
1301	1577	1578	1601	1600	
1302	1578	1579	1602	1601	
1303	1580	1581	1604	1603	
1304	1581	1582	1605	1604	
1305	1582	1583	1606	1605	
1306	1583	1584	1607	1606	
1307	1584	1585	1608	1607	
1308	1585	1586	1609	1608	
1309	1586	1587	1610	1609	
1310	1587	1588	1611	1610	
1311	1588	1589	1612	1611	
1312	1589	1590	1613	1612	
1313	1590	1591	1614	1613	

Table D-3. Element Block 1 Description (continued)

Element No.	Connectivity				
1314	1591	1592	1615	1614	
1315	1592	1593	1616	1615	
1316	1593	1594	1617	1616	
1317	1594	1595	1618	1617	

Element No.	Connectivity				
1318	1595	1596	1619	1618	
1319	1596	1597	1620	1619	
1320	1597	1598	1621	1620	
1321	1598	1599	1622	1621	

Element No.	Connectivity				
1322	1599	1600	1623	1622	
1323	1600	1601	1624	1623	
1324	1601	1602	1625	1624	

Table D-4. Element Block 2 Description

110 Elements, 4 Nodes per Element

Element No.	Connectivity			
1325	461	462	485	484
1326	462	463	486	485
1327	463	464	487	486
1328	464	465	488	487
1329	465	466	489	488
1330	466	467	490	489
1331	467	468	491	490
1332	468	469	492	491
1333	469	470	493	492
1334	470	471	494	493
1335	471	472	495	494
1336	472	473	496	495
1337	473	474	497	496
1338	474	475	498	497
1339	475	476	499	498
1340	476	477	500	499
1341	477	478	501	500
1342	478	479	502	501
1343	479	480	503	502
1344	480	481	504	503
1345	481	482	505	504
1346	482	483	506	505
1347	484	485	508	507
1348	485	486	509	508
1349	486	487	510	509
1350	487	488	511	510
1351	488	489	512	511
1352	489	490	513	512
1353	490	491	514	513
1354	491	492	515	514
1355	492	493	516	515
1356	493	494	517	516
1357	494	495	518	517
1358	495	496	519	518
1359	496	497	520	519
1360	497	498	521	520
1361	498	499	522	521
1362	499	500	523	522
1363	500	501	524	523
1364	501	502	525	524
1365	502	503	526	525
1366	503	504	527	526
1367	504	505	528	527
1368	505	506	529	528
1369	507	508	531	530
1370	508	509	532	531
1371	509	510	533	532
1372	510	511	534	533

Element No.	Connectivity			
1373	511	512	535	534
1374	512	513	536	535
1375	513	514	537	536
1376	514	515	538	537
1377	515	516	539	538
1378	516	517	540	539
1379	517	518	541	540
1380	518	519	542	541
1381	519	520	543	542
1382	520	521	544	543
1383	521	522	545	544
1384	522	523	546	545
1385	523	524	547	546
1386	524	525	548	547
1387	525	526	549	548
1388	526	527	550	549
1389	527	528	551	550
1390	528	529	552	551
1391	530	531	554	553
1392	531	532	555	554
1393	532	533	556	555
1394	533	534	557	556
1395	534	535	558	557
1396	535	536	559	558
1397	536	537	560	559
1398	537	538	561	560
1399	538	539	562	561
1400	539	540	563	562
1401	540	541	564	563
1402	541	542	565	564
1403	542	543	566	565
1404	543	544	567	566
1405	544	545	568	567
1406	545	546	569	568
1407	546	547	570	569
1408	547	548	571	570
1409	548	549	572	571
1410	549	550	573	572
1411	550	551	574	573
1412	551	552	575	574
1413	1120	1121	1715	1714
1414	1121	1122	1716	1715
1415	1122	1123	1717	1716
1416	1123	1124	1718	1717
1417	1124	1125	1719	1718
1418	1125	1126	1720	1719
1419	1126	1127	1721	1720
1420	1127	1128	1722	1721

Element No.	Connectivity			
1421	1128	1129	1723	1722
1422	1129	1130	1724	1723
1423	1130	1131	1725	1724
1424	1131	1132	1726	1725
1425	1132	1133	1727	1726
1426	1133	1134	1728	1727
1427	1134	1135	1729	1728
1428	1135	1136	1730	1729
1429	1136	1137	1731	1730
1430	1137	1138	1732	1731
1431	1138	1139	1733	1732
1432	1139	1140	1734	1733
1433	1140	1141	1735	1734
1434	1141	1142	1736	1735

Table D-5. Element Block 3 Description

176 Elements, 4 Nodes per Element

Element No.	Connectivity			
1435	1028	1029	1052	1051
1436	1029	1030	1053	1052
1437	1030	1031	1054	1053
1438	1031	1032	1055	1054
1439	1032	1033	1056	1055
1440	1033	1034	1057	1056
1441	1034	1035	1058	1057
1442	1035	1036	1059	1058
1443	1036	1037	1060	1059
1444	1037	1038	1061	1060
1445	1038	1039	1062	1061
1446	1039	1040	1063	1062
1447	1040	1041	1064	1063
1448	1041	1042	1065	1064
1449	1042	1043	1066	1065
1450	1043	1044	1067	1066
1451	1044	1045	1068	1067
1452	1045	1046	1069	1068
1453	1046	1047	1070	1069
1454	1047	1048	1071	1070
1455	1048	1049	1072	1071
1456	1049	1050	1073	1072
1457	1051	1052	1075	1074
1458	1052	1053	1076	1075
1459	1053	1054	1077	1076
1460	1054	1055	1078	1077
1461	1055	1056	1079	1078
1462	1056	1057	1080	1079
1463	1057	1058	1081	1080
1464	1058	1059	1082	1081
1465	1059	1060	1083	1082
1466	1060	1061	1084	1083
1467	1061	1062	1085	1084
1468	1062	1063	1086	1085
1469	1063	1064	1087	1086
1470	1064	1065	1088	1087
1471	1065	1066	1089	1088
1472	1066	1067	1090	1089
1473	1067	1068	1091	1090
1474	1068	1069	1092	1091
1475	1069	1070	1093	1092
1476	1070	1071	1094	1093
1477	1071	1072	1095	1094
1478	1072	1073	1096	1095
1479	1074	1075	1098	1097
1480	1075	1076	1099	1098
1481	1076	1077	1100	1099
1482	1077	1078	1101	1100

Element No.	Connectivity			
1483	1078	1079	1102	1101
1484	1079	1080	1103	1102
1485	1080	1081	1104	1103
1486	1081	1082	1105	1104
1487	1082	1083	1106	1105
1488	1083	1084	1107	1106
1489	1084	1085	1108	1107
1490	1085	1086	1109	1108
1491	1086	1087	1110	1109
1492	1087	1088	1111	1110
1493	1088	1089	1112	1111
1494	1089	1090	1113	1112
1495	1090	1091	1114	1113
1496	1091	1092	1115	1114
1497	1092	1093	1116	1115
1498	1093	1094	1117	1116
1499	1094	1095	1118	1117
1500	1095	1096	1119	1118
1501	1097	1098	1121	1120
1502	1098	1099	1122	1121
1503	1099	1100	1123	1122
1504	1100	1101	1124	1123
1505	1101	1102	1125	1124
1506	1102	1103	1126	1125
1507	1103	1104	1127	1126
1508	1104	1105	1128	1127
1509	1105	1106	1129	1128
1510	1106	1107	1130	1129
1511	1107	1108	1131	1130
1512	1108	1109	1132	1131
1513	1109	1110	1133	1132
1514	1110	1111	1134	1133
1515	1111	1112	1135	1134
1516	1112	1113	1136	1135
1517	1113	1114	1137	1136
1518	1114	1115	1138	1137
1519	1115	1116	1139	1138
1520	1116	1117	1140	1139
1521	1117	1118	1141	1140
1522	1118	1119	1142	1141
1523	1714	1715	1738	1737
1524	1715	1716	1739	1738
1525	1716	1717	1740	1739
1526	1717	1718	1741	1740
1527	1718	1719	1742	1741
1528	1719	1720	1743	1742
1529	1720	1721	1744	1743
1530	1721	1722	1745	1744

Element No.	Connectivity			
1531	1722	1723	1746	1745
1532	1723	1724	1747	1746
1533	1724	1725	1748	1747
1534	1725	1726	1749	1748
1535	1726	1727	1750	1749
1536	1727	1728	1751	1750
1537	1728	1729	1752	1751
1538	1729	1730	1753	1752
1539	1730	1731	1754	1753
1540	1731	1732	1755	1754
1541	1732	1733	1756	1755
1542	1733	1734	1757	1756
1543	1734	1735	1758	1757
1544	1735	1736	1759	1758
1545	1737	1738	1761	1760
1546	1738	1739	1762	1761
1547	1739	1740	1763	1762
1548	1740	1741	1764	1763
1549	1741	1742	1765	1764
1550	1742	1743	1766	1765
1551	1743	1744	1767	1766
1552	1744	1745	1768	1767
1553	1745	1746	1769	1768
1554	1746	1747	1770	1769
1555	1747	1748	1771	1770
1556	1748	1749	1772	1771
1557	1749	1750	1773	1772
1558	1750	1751	1774	1773
1559	1751	1752	1775	1774
1560	1752	1753	1776	1775
1561	1753	1754	1777	1776
1562	1754	1755	1778	1777
1563	1755	1756	1779	1778
1564	1756	1757	1780	1779
1565	1757	1758	1781	1780
1566	1758	1759	1782	1781
1567	1760	1761	1784	1783
1568	1761	1762	1785	1784
1569	1762	1763	1786	1785
1570	1763	1764	1787	1786
1571	1764	1765	1788	1787
1572	1765	1766	1789	1788
1573	1766	1767	1790	1789
1574	1767	1768	1791	1790
1575	1768	1769	1792	1791
1576	1769	1770	1793	1792
1577	1770	1771	1794	1793
1578	1771	1772	1795	1794

Table D-5. Element Block 3 Description (continued)

Element No.	Connectivity				
1579	1772	1773	1796	1795	
1580	1773	1774	1797	1796	
1581	1774	1775	1798	1797	
1582	1775	1776	1799	1798	
1583	1776	1777	1800	1799	
1584	1777	1778	1801	1800	
1585	1778	1779	1802	1801	
1586	1779	1780	1803	1802	
1587	1780	1781	1804	1803	
1588	1781	1782	1805	1804	
1589	1783	1784	1144	1143	

Element No.	Connectivity				
1590	1784	1785	1145	1144	
1591	1785	1786	1146	1145	
1592	1786	1787	1147	1146	
1593	1787	1788	1148	1147	
1594	1788	1789	1149	1148	
1595	1789	1790	1150	1149	
1596	1790	1791	1151	1150	
1597	1791	1792	1152	1151	
1598	1792	1793	1153	1152	
1599	1793	1794	1154	1153	
1600	1794	1795	1155	1154	

Element No.	Connectivity				
1601	1795	1796	1156	1155	
1602	1796	1797	1157	1156	
1603	1797	1798	1158	1157	
1604	1798	1799	1159	1158	
1605	1799	1800	1160	1159	
1606	1800	1801	1161	1160	
1607	1801	1802	1162	1161	
1608	1802	1803	1163	1162	
1609	1803	1804	1164	1163	
1610	1804	1805	1165	1164	

Table D-6. Element Block 4 Description

70 Elements, 4 Nodes per Element

Element No.	Connectivity			
1611	1626	1627	1638	1637
1612	1627	1628	1639	1638
1613	1628	1629	1640	1639
1614	1629	1630	1641	1640
1615	1630	1631	1642	1641
1616	1631	1632	1643	1642
1617	1632	1633	1644	1643
1618	1633	1634	1645	1644
1619	1634	1635	1646	1645
1620	1635	1636	1647	1646
1621	1637	1638	1649	1648
1622	1638	1639	1650	1649
1623	1639	1640	1651	1650
1624	1640	1641	1652	1651
1625	1641	1642	1653	1652
1626	1642	1643	1654	1653
1627	1643	1644	1655	1654
1628	1644	1645	1656	1655
1629	1645	1646	1657	1656
1630	1646	1647	1658	1657
1631	1648	1649	1660	1659
1632	1649	1650	1661	1660
1633	1650	1651	1662	1661
1634	1651	1652	1663	1662
1635	1652	1653	1664	1663
1636	1653	1654	1665	1664
1637	1654	1655	1666	1665
1638	1655	1656	1667	1666
1639	1656	1657	1668	1667
1640	1657	1658	1669	1668
1641	1659	1660	1671	1670
1642	1660	1661	1672	1671
1643	1661	1662	1673	1672
1644	1662	1663	1674	1673
1645	1663	1664	1675	1674
1646	1664	1665	1676	1675
1647	1665	1666	1677	1676
1648	1666	1667	1678	1677
1649	1667	1668	1679	1678
1650	1668	1669	1680	1679
1651	1670	1671	1682	1681
1652	1671	1672	1683	1682
1653	1672	1673	1684	1683
1654	1673	1674	1685	1684
1655	1674	1675	1686	1685
1656	1675	1676	1687	1686
1657	1676	1677	1688	1687
1658	1677	1678	1689	1688

Element No.	Connectivity			
1659	1678	1679	1690	1689
1660	1679	1680	1691	1690
1661	1681	1682	1693	1692
1662	1682	1683	1694	1693
1663	1683	1684	1695	1694
1664	1684	1685	1696	1695
1665	1685	1686	1697	1696
1666	1686	1687	1698	1697
1667	1687	1688	1699	1698
1668	1688	1689	1700	1699
1669	1689	1690	1701	1700
1670	1690	1691	1702	1701
1671	1692	1693	1704	1703
1672	1693	1694	1705	1704
1673	1694	1695	1706	1705
1674	1695	1696	1707	1706
1675	1696	1697	1708	1707
1676	1697	1698	1709	1708
1677	1698	1699	1710	1709
1678	1699	1700	1711	1710
1679	1700	1701	1712	1711
1680	1701	1702	1713	1712

WIPP
UC721 - DISTRIBUTION LIST
SAND97-0796

Federal Agencies

US Department of Energy (4)
Office of Civilian Radioactive Waste Mgmt.
Attn: Deputy Director, RW-2
Acting Director, RW-10
Office of Human Resources & Admin.
Director, RW-30
Office of Program Mgmt. & Integ.
Director, RW-40
Office of Waste Accept., Stor., & Tran.
Forrestal Building
Washington, DC 20585

Attn: Project Director
Yucca Mountain Site Characterization Office
Director, RW-3
Office of Quality Assurance
P.O. Box 30307
Las Vegas, NV 89036-0307

US Department of Energy
Albuquerque Operations Office
Attn: National Atomic Museum Library
P.O. Box 5400
Albuquerque, NM 87185-5400

US Department of Energy
Research & Waste Management Division
Attn: Director
P.O. Box E
Oak Ridge, TN 37831

US Department of Energy (5)
Carlsbad Area Office
Attn: G. Dials
D. Galbraith
M. McFadden
R. Lark
J. A. Mewhinney
P.O. Box 3090
Carlsbad, NM 88221-3090

US Department of Energy
Office of Environmental Restoration and
Waste Management
Attn: M Frei, EM-30
Forrestal Building
Washington, DC 20585-0002

US Department of Energy (3)
Office of Environmental Restoration and
Waste Management
Attn: J. Juri, EM-34, Trevion II
Washington, DC 20585-0002

US Department of Energy
Office of Environmental Restoration and
Waste Management
Attn: S. Schneider, EM-342, Trevion II
Washington, DC 20585-0002

US Department of Energy (2)
Office of Environment, Safety & Health
Attn: C. Borgstrom, EH-25
R. Pelletier, EH-231
Washington, DC 20585

US Department of Energy (2)
Idaho Operations Office
Fuel Processing & Waste Mgmt. Division
785 DOE Place
Idaho Falls, ID 83402

US Environmental Protection Agency (2)
Radiation Protection Programs
Attn: M. Oge
ANR-460
Washington, DC 20460

Boards

Defense Nuclear Facilities Safety Board
Attn: D. Winters
625 Indiana Ave. NW, Suite 700
Washington, DC 20004

Nuclear Waste Technical Review Board (2)
Attn: Chairman
J. L. Cohon
1100 Wilson Blvd., Suite 910
Arlington, VA 22209-2297

State Agencies

Attorney General of New Mexico
P.O. Drawer 1508
Santa Fe, NM 87504-1508

Environmental Evaluation Group (3)
Attn: Library
7007 Wyoming NE
Suite F-2
Albuquerque, NM 87109

NM Energy, Minerals, and Natural
Resources Department
Attn: Library
2040 S. Pacheco
Santa Fe, NM 87505

NM Environment Department (3)
Secretary of the Environment
Attn: Mark Weidler
1190 St. Francis Drive
Santa Fe, NM 87503-0968

NM Bureau of Mines & Mineral Resources
Socorro, NM 87801

Laboratories/Corporations

Battelle Pacific Northwest Laboratories
Battelle Blvd.
Richland, WA 99352

Los Alamos National Laboratory
Attn: B. Erdal, INC-12
P.O. Box 1663
Los Alamos, NM 87544

Tech Repts, Inc. (3)
Attn: J. Chapman (1)
Loretta Robledo (2)
5000 Marble NE, Suite 222
Albuquerque, NM 87110

Westinghouse Electric Corporation (5)
Attn: Library
J. Epstein
J. Lee
B. A. Howard
R. Kehrman
P.O. Box 2078
Carlsbad, NM 88221

S. Cohen & Associates
Attn: Bill Thurber
1355 Beverly Road
McLean, VA 22101

National Academy of Sciences, WIPP Panel

Howard Adler
Oxyrase, Incorporated
7327 Oak Ridge Highway
Knoxville, TN 37931

Tom Kiess
Board of Radioactive Waste Management
GF456
2101 Constitution Ave.
Washington, DC 20418

Rodney C. Ewing
Department of Geology
University of New Mexico
Albuquerque, NM 87131

Charles Fairhurst
Department of Civil and Mineral Engineering
University of Minnesota
500 Pillsbury Dr. SE
Minneapolis, MN 55455-0220

B. John Garrick
PLG Incorporated
4590 MacArthur Blvd., Suite 400
Newport Beach, CA 92660-2027

Leonard F. Konikow
US Geological Survey
431 National Center
Reston, VA 22092

Carl A. Anderson, Director
Board of Radioactive Waste Management
National Research Council
HA 456
2101 Constitution Ave. NW
Washington, DC 20418

Christopher G. Whipple
ICF Kaiser Engineers
1800 Harrison St., 7th Floor
Oakland, CA 94612-3430

John O. Blomeke
720 Clubhouse Way
Knoxville, TN 37909

Sue B. Clark
University of Georgia
Savannah River Ecology Lab
P.O. Drawer E
Aiken, SC 29802

Konrad B. Krauskopf
Department of Geology
Stanford University
Stanford, CA 94305-2115

Della Roy
Pennsylvania State University
217 Materials Research Lab
Hastings Road
University Park, PA 16802

David A. Waite
CH₂ M Hill
P.O. Box 91500
Bellevue, WA 98009-2050

Thomas A. Zordon
Zordan Associates, Inc.
3807 Edinburg Drive
Murrysville, PA 15668

Universities

University of New Mexico
Geology Department
Attn: Library
141 Northrop Hall
Albuquerque, NM 87131

University of Washington
College of Ocean & Fishery Sciences
Attn: G. R. Heath
583 Henderson Hall, HN-15
Seattle, WA 98195

Libraries

Thomas Brannigan Library
Attn: D. Dresp
106 W. Hadley St.
Las Cruces, NM 88001

Government Publications Department
Zimmerman Library
University of New Mexico
Albuquerque, NM 87131

New Mexico Junior College
Pannell Library
Attn: R. Hill
Lovington Highway
Hobbs, NM 88240

New Mexico State Library
Attn: N. McCallan
325 Don Gaspar
Santa Fe, NM 87503

New Mexico Tech
Martin Speere Memorial Library
Campus Street
Socorro, NM 87810

WIPP Public Reading Room
Carlsbad Public Library
101 S. Halagueno St.
Carlsbad, NM 88220

Foreign Addresses

Atomic Energy of Canada, Ltd.
Whiteshell Laboratories
Attn: B. Goodwin
Pinawa, Manitoba, CANADA R0E 1L0

Francois Chenevier (2)
ANDRA
Route de Panorama Robert Schumann
B. P. 38
92266 Fontenay-aux-Roses, Cedex
FRANCE

Claude Sombret
Centre d'Etudes Nucleaires de la Vallee Rhone
CEN/VALRHO
S.D.H.A. B.P. 171
30205 Bagnols-Sur-Ceze
FRANCE

Commissariat a L'Energie Atomique
Attn: D. Alexandre
Centre d'Etudes de Cadarache
13108 Saint Paul Lez Durance Cedex
FRANCE

Bundesanstalt für Geowissenschaften und
Rohstoffe
Attn: M. Langer
Postfach 510 153
D-30631 Hannover
GERMANY

Bundesministerium für Forschung und
Technologie
Postfach 200 706
5300 Bonn 2
GERMANY

Institut für Tieflagerung
Attn: K. Kuhn
Theodor-Heuss-Strasse 4
D-3300 Braunschweig
GERMANY

Gesellschaft für Anlagen und Reaktorsicherheit
(GRS)
Attn: B. Baltes
Schwertnergasse 1
D-50667 Cologne
GERMANY

Shingo Tashiro
Japan Atomic Energy Research Institute
Tokai-Mura, Ibaraki-Ken, 319-11
JAPAN

Netherlands Energy Research Foundation ECN
Attn: J. Prij
3 Westerduinweg
P.O. Box 1
1755 ZG Petten
THE NETHERLANDS

Svensk Kärnbränsleforsörjning AB
Attn: F. Karlsson
Project KBS (Kärnbränslesakerhet)
Box 5864
S-102 48 Stockholm
SWEDEN

Nationale Genossenschaft für die Lagerung
Radioaktiver Abfälle (2)
Attn: S. Vomvoris
P. Zuidema
Hardstrasse 73
CH-5430 Wettingen
SWITZERLAND

AEA Technology
Attn: J. H. Rees
D5W/29 Culham Laboratory
Abington, Oxfordshire OX14 3DB
UNITED KINGDOM

AEA Technology
Attn: W. R. Rodwell
044/A31 Winfrith Technical Centre
Dorchester, Dorset DT2 8DH
UNITED KINGDOM

AEA Technology
Attn: J. E. Tinson
B4244 Harwell Laboratory
Didcot, Oxfordshire OX11 0RA
UNITED KINGDOM

Internal

<u>MS</u>	<u>Org.</u>	
1324	6115	P. B. Davies
1320	6831	E. J. Nowak
1322	6121	J. R. Tillerson
1328	6849	D. R. Anderson
1328	6848	H. N. Jow
1335	6801	M. Chu
1341	6832	J. T. Holmes
1395	6800	L. Shephard
1395	6821	M. Marietta
0443	9117	J. G. Arguello
0443	9117	C. M. Stone
0443	9117	A. Fossum
0443	9117	G. D. Sjaardema
0815	5932	F. T. Mendenhall
0425	5932	R. C. Lincoln
0716	6113	D. E. Munson
1341	6822	K. W. Larson
1395	6801	P. Swift
1341	6832	L. H. Brush
3128	6848	D. M. Stoelzel
1328	6849	P. Vaughn
1324	6115	A. R. Lappin
1324	6115	S. W. Webb
1345	6832	B. M. Butcher (5)
1330	6811	K. Hart (2)
1330	4415	NWM Library (20)
9018	8940-2	Central Technical Files
0899	4916	Technical Library (5)
0619	12690	Review and Approval Desk (2), For DOE/OSTI

